ACCESSIBILITY: OPEN

OsloMet – Oslo Metropolitan University

Department of Built Environment

Section of Civil Engineering

Master Program in Structural Engineering & Building Technology

MASTER THESIS

TITLE OF REPORT	DATE
Finite Element Analysis and field investigation of a deteriorated RC bridge: A case study of Øvre Kvamme bridge	25.05.2023
	PAGES / ATTACHMENTS 147 / 11
AUTHOR(S) Mjahed Babawat Per Henrik Ellefsen	**SUPERVISOR(S)** Mahdi Kioumarsi Amirhosein Shabani

IN COLLABORATION WITH	CONTACT PERSON
Vestland County Municipality	Øyvind Sætra

SUMMARY / SYNOPSIS

Øvre Kvamme concrete bridge is approaching the end of its design life due to significant deterioration. To address this, a collaboration with the Vestland County Municipality was established to rehabilitate and strengthen the reinforced concrete bridge. Subsequently, A comprehensive field investigation using Non-Destructive Tests (NDT) and Structural Health Monitoring (SHM) instruments was performed. The collected data from the field investigation was processed with a wide range of softwares, including Operational Modal Analysis (OMA) and Building Information Modeling (BIM) techniques. The final assessment was utilized and implemented into Finite Element Analysis (FEA) in Abaqus to examine the proposed strengthening methods, including Carbon Fiber Reinforced Polymers (CFRP) and Ultra-High Performance Fiber-Reinforced Concrete (UHPFRC) retrofitting.

KEYWORDS
Condition Assessment
Finite Element Analysis
Model updating
Rehabilitation

Foreword

This master's thesis has been written as the final part of the two-year master's program in Structural Engineering & Building Technology Program at Oslo Metropolitan University. The thesis was written during the Spring semester of 2023 and constituted 30 credits per student. Its topic and scope were established in collaboration with OsloMet and Vestland County Municipality.

This thesis offers a thorough study on the Øvre Kvamme bridge, providing insight into its condition as well as challenges associated with ageing concrete bridges in Nordic environments and increasing traffic load. Furthermore, rehabilitation techniques used to extend its lifespan are discussed.

We would like to extend our profound thanks to Mahdi Kioumarsi and Amirhosein Shabani for their commitment and guidance throughout this thesis. Additionally, we would like to express our thanks to Øyvind Sætra from Vestland County Municipality who assisted with planning an excursion to Øvre Kvamme bridge as well as providing vital information regarding this thesis. Finally, Dr. Farhood Shahidi for his professional consultation with finite element modeling in Abaqus and ETABS.

We wish for this thesis to serve as an invaluable reference for engineers, researchers, and professionals working in bridge maintenance and rehabilitation. By drawing attention to the unique challenges that concrete bridges in demanding environments face, we hope to raise awareness and encourage proactive measures when designing future infrastructure. A comprehensive field investigation coupled with advanced techniques and software provides a basis for assessing aging reinforced concrete bridges' as well as devising effective repair and strengthening methods.

Oslo Metropolitan University, 25.05.2023

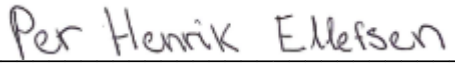

Mjahed Babawat Per Henrik Ellefsen

Abstract

A significant number of concrete bridges in Norway are currently approaching the end of their anticipated design life due to deterioration and poor condition. Over the years, these bridges have been subjected to various environmental factors, heavy traffic loads, and limited maintenance, leading to significant wear and structural degradation. The Øvre Kvamme bridge situated in Lærdal municipality, is an aged reinforced concrete structure that has experienced significant deterioration.

In response to this, the Vestland County Municipality has initiated a collaboration to assess the bridge and explore rehabilitation options aimed at improving its mechanical strength and durability. To effectively adress these challenges, a comprehensive field investigation was conducted, emplying various Non-Destructive Testing (NDT) and Structural Health Monitoring (SHM) instruments. The extracted results was processed with a comprehensive condition assessment of the bridge, and through a wide range of softwares with the help of Building Information Modeling (BIM). Subsequently, the findings are complemented by structural analysis using Operational Modal Analysis (OMA), Finite Element Modeling (FEM) and Nonlinear Finite Element Analysis (NFEA) to analyze and assess the behavior of Øvre Kvamme bridge with and without retrofitting.

The results from the field investigation on the bridge revealed significant deterioration mainly due to corroded reinforcement likely from carbonation. The severe detected degradation is impacting its serviceability and load-bearing capacity, necessitating urgent repair and strengthening. Adhering to standard and regulations, measures such as removing damaged concrete, addressing corrosion, and ensuring strong material bonds are crucial for rehabilitation of the bridge.

An feasable finite element model was developed to replicate the behavior of the bridge, and various configurations of two strengthening materials were tested using FEM software Abaqus. The objective was to assess their impact on the flexural behavior of the bridge and determine the most effective approach to enhance its load-bearing capacity and durability. The use of Carbon Fiber Reinforced Polmyers (CFRP) and Ultra-High Performance Fiber-Reinforced Concrete (UHPFRC) was found effective in achieving this. Specifically, the simulations demonstrated that UHPFRC performed superior under realistic traffic loads, whereas retrofitting with CFRP provided the greatest flexural resistance at a much higher loads.

Sammendrag

Et betydelig antall betongbroer i Norge nærmer seg nå slutten av sin forventede levetid på grunn av dårlig forfatning. Gjennom tidene har disse broene blitt påvirket av ulike miljøfaktorer, tung trafikkbelastning og begrenset vedlikehold, noe som har ført til betydelig slitasje og strukturell nedbrytning. Øvre Kvamme bro lokalisert i Lærdal kommune, er en gammel armert betongkonstruksjon som har opplevd betydelig degradering over tid.

Som svar på dette, har Vestland fylkeskommune engasjert et samarbeid med mål om å evaluere broens tilstand og utforske rehabiliteringsmuligheter for å forbedre dens bæreevne og holdbarhet. For å effektivt håndtere disse utfordringene ble det gjennomført en omfattende feltundersøkelse av broen ved hjelp av ulike ikke-destruktive tester (NDT)- og strukturelle helseovervåkingsinstrumenter (SHM)-. Resultatene fra undersøkelsene ble behandlet for en grundig tilstandsvurdering av broen og ved bruk av ulike programvareverktøy som bygningsinformasjonsmodellering (BIM). Deretter ble funnene supplert med konstruksjonsanalyser ved hjelp av operativ modalanalyse (OMA), endelig elementmodellering og ikke-lineær endelig elementanalyse for å analysere og vurdere oppførselen til Øvre Kvamme broen både med og uten forsterkning.

Resultatene fra feltundersøkelsen av broen avdekket betydelig degradering, hovedsakelig på grunn av korrosjon av armeringsjern, mest sannsynlig fra karbonisering. Den alvorlige degraderingen som ble påvist, påvirker broens bruk og bæreevne, og det er derfor nødvendig med umiddelbar reparasjon og forsterkning. I tråd med standarder og forskrifter er tiltak som fjerning av skadet betong, behandling av korrosjon og sikring av sterke materialesammensetninger avgjørende for rehabiliteringen av broen.

Det ble utviklet en håndterlig endelig elementmodell for å så nøyaktig som mulig gjenskape broens oppførsel. Flere konfigurasjoner av to ulike forsterkningsmaterialer ble testet i FEM-programvaren Abaqus for å vurdere deres innvirkning på broens oppførsel under bøyning, og for å identifisere den mest effektive metoden for å styrke broens bæreevne og holdbarhet. Bruken av karbonfiberarmerte polymer og høyfast fiberarmert betong viste seg å være effektive metoder for å oppnå dette målet. Resultatene viste at høyfast fiberarmert betong var bedre i under trafikkbelastning, mens forsterkning med karbonfiberarmerte polymer ga størst bøyemotstand ved en mye høyere vertikal belastning og forskyvning.

Table of Contents

List of Figures

List of Tables

List of Abbreviations & symbols

BIM	Building information Modeling
CAE	Computer Aided Engineering
CDP	Concrete Damage Plasticity
CFRP	Carbon Fiber Reinforced Polymer
DT	Destructive Test
EC2	Eurocode 2
EMA	Experimental Modal Analysis
EMA	Experimental Modal Analysis
FDD	Frequency Domain Decomposition
FEA	Finite Element Analysis
FEM	Finite Element Model
FFT	Fast Fourier Transform
FRC	Fiber Reinforced Concrete
FRP	Fiber Reinforced Polymer
ISMA	Impact Synchronous Modal Analysis
ISO	International Organization for Standardization
LiDAR	Light Detection and Ranging
MLS	Mobile Laser Scanning
MRS	Maintenance, Repair & Strengthening
NDT	Non-Destructive Test
NFEA	Non-linear Finite Element Analysis
NPRA	Norwegian Public Road Administration
OMA	Operational Modal Analysis
PP	Peak Picking
PRISMA	Preferred Reporting Items for Systematic Reviews and Meta-Analyses
RC	Reinforced Concrete
SHM	Structural Health Monitoring
TLS	Terrestrial Laser Scanning
UHPFRC	Ultra-High Performance Fiber-Reinforced Concrete
A_0	Initial cross-section area
E_{cm}	Elastic modulus for concrete
G_X^C	Fracture energy of longitudinal compression

G_X^T	Fracture energy of longitudinal tension
G_Y^C	Fracture energy of transverse compression
G_Y^T	Fracture energy of transverse tension
L_0	Initial length
S^L	Longitudinal shear
S^T	Transverse shear
X^C	Longitudinal compression
X^T	Longitudinal tension
Y^C	Transverse compression
Y^T	Transverse tension
f_c	Compressive strength
f_{ck}	Concrete's characteristic cylinder compressive strength after 28 days
f_{cm}	Mean value of concrete's cylinder compressive strength
ε_{0t}^{el}	Initial elastic tensile strain
ε_E	Engineering strain
ε_T	True strain
ε_c	Compressive strain
ε_{c1}	Strain at maximum stress
ε_t	Tensile strain
ε_t^{ck}	Cracking strain
σ_E	Engineering stress
σ_T	True stress
σ_c	Compressive stress
σ_t	Tensile stress
A	Cross-section area
F	Force
G	Shear modulus
L	Length
T	Period
f	Frequency
v	Poisson's ratio

1 Introduction

The infrastructure of transportation is critical for all societies, and bridges play a vital role in connecting communities and enabling movement of goods and people. However, a large sum of the existing infrastructure, especially concrete bridges in Norway and the world are reaching the end of their expected design life, primarily because many of these bridges were constructed after World War II [1-2]. As of today, numerous concrete bridges in Norway have exceeded 60 years of age, and the majority of the older concrete bridges were not built to meet the newer standards for a design life of 100 years. Additionally, the construction quality of these bridges did not comply with the present-day strict standard requirements to shield itself from the harsh Nordic environment and the heavy traffic loads, leading to a greater risk of degradation. Consequently, the awareness and interest in repairing, maintaining, and strengthening concrete bridges has been increasing annually to ensure safe operation and prolong the service life in a safe and eco-friendly manner [3-4].

According to Brutus, a classified bridge management tool-system by Norwegian Public Road Administration (NPRA), reports that there are nearly 17,000 registered bridges in Norway, where approximately 13,700 are identified as concrete bridges. Each year, between 15,000 and 18,000 bridge inspections are meant to conducted[1][2] and in 2019, the NPRA identified 271 bridges that were in urgent need of strengthening and maintenance[3]. Furthermore, Brutus has documented roughly 5,600 bridges with load capacity damage. The main cause of degradation of concrete bridges are due to increased traffic load, harsh environmental conditions, aging infrastructure, insufficient project design and lack of maintenance and repair [5]. Hence, performing a comprehensive field investigation and a structural analysis of these bridges will allow specialists to identify the specific areas that require attention, so the repair process can be as targeted and effective as possible. This is essential to keep Norway's bridges in optimal condition, benefitting both the public and the environment. Figure 1 visually represents two groups of identified bridges in Norway: a) bridges with severe damage, and b) bridges that have not been inspected, as displayed by VG[4] in 2017

[1] https://www.nrk.no/nordland/betongbruer-far-forlenget-levetid-og-sparer-staten-for-milliarder-1.15743249
[2] https://bil24.no/i-ar-sjekkes-17-000-norske-bruer/
[3] https://www.nrk.no/nyheter/vedlikehold-av-broer-1.14455266
[4] https://www.vg.no/spesial/2017/de-forsomte-broene/kart/index-eng.php#skade

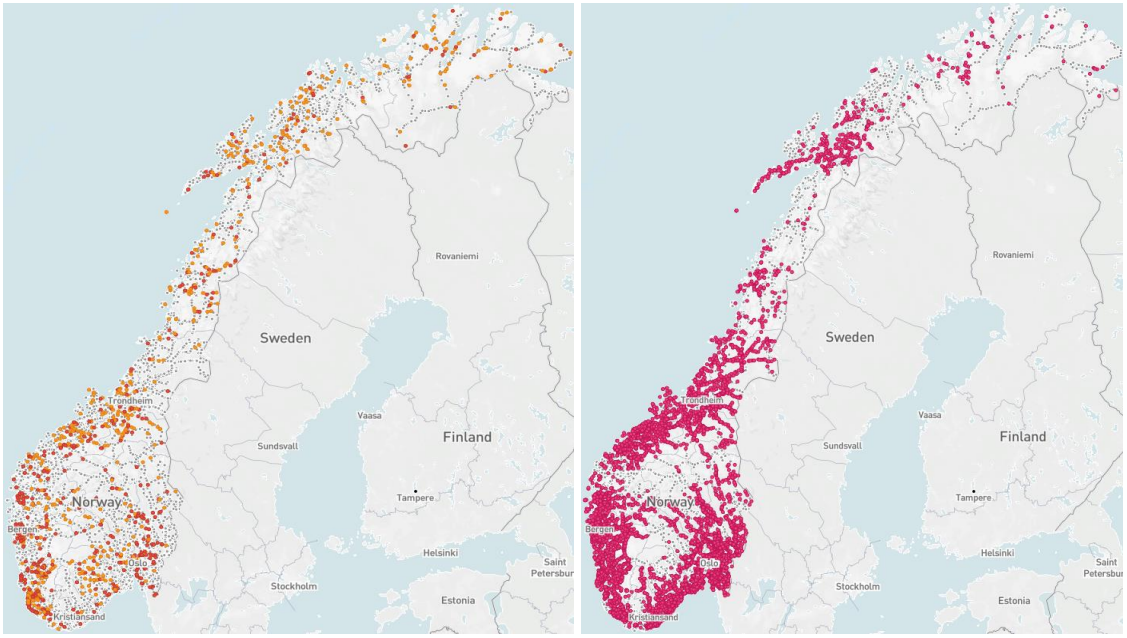

a) b)

Figure 1: a) Severe damage bridges; b) lack of required bridge inspections[5]

An aged, Reinforced Concrete (RC) bridge – Øvre Kvamme, located in Lærdal municipality, has been in service for many years and has experienced significant deterioration. The ongoing deterioration has brought the bridge closer to the end of its expected lifespan. As a response, the Vestland County Municipality has initiated a collaborative effort to analyze the structure's condition and evaluate potential maintenance options to improve its mechanical strength and durability. To accomplish this, a comprehensive examination of the bridge's structure will be conducted. This will involve the use of numerical simulation analyses, as well as a condition assessment of the bridge that will be carried out to identify the extent of the deterioration and any structural vulnerabilities that require attention. Figure 2 below shows the Øvre Kvamme bridge during the inspection conducted in November 2022.

Figure 2: Øvre Kvamme bridge in Lærdal at time of inspection

[5] https://www.vg.no/spesial/2017/de-forsomte-broene/kart/index-eng.php#inspeksjon

1.1 Background

RC bridges have been an important component of transportation infrastructure for over a century. When engineers first introduced reinforced concrete in the early 1900s, it quickly gained popularity in the industry. This allowed design of structures capable of supporting higher loads and spanning larger distances than traditional masonry or timber bridges [6]. The durability, resistance to fire, and low maintenance properties of RC bridges made them the ideal choice of bridge constructions [6].

During the early stages of reinforced concrete bridge construction, the knowledge of concrete behavior and its long-term durability was not yet fully developed. Thus, many bridges built had deficiencies in design, materials, and construction. Over time it was showcased that despite the reputation for high durability properties, reinforced concrete was susceptible to degradation. This is due to concrete being a porous material, making it highly vulnerable to the harmful effects of water and freeze-thaw cycles. These factors contribute to the formation of cracks, spalling, and corrosion among other things.

Corrosion is a chemical reaction that develops when steel is exposed to oxygen and water, which results in the formation of rust. Due to the larger volume of the reaction product compared to its initial state, the concrete undergoes cracking and spalling. Corrosion is considered to be the main cause of deterioration of reinforced concrete structures, as it heavily weakens the structural integrity of the structure [4]. Even though there are other types of damage mechanisms, corrosion stands out as the primary cause of concrete failure that has a significant impact on the service life. Consequently, comprehending corrosion becomes crucial since it ultimately renders bridges unsafe. The most common causes of bridge failure and collapse are due to design and construction defects, corrosion, design and supervision errors, accidental overloading, and shocks, and lack of maintenance or inspection [7].

In recent years, there has been an increased interest in rehabilitation and strengthening of deteriorated concrete bridges. This involves the use of many different methods, products, and techniques such as patching, overlays, epoxies, and other protective coatings to better assist the structures. Additionally, advancements in technology have led to the development of innovative Maintenance, Repair and Strengthening (MRS) methods such as, Non-Destructive Tests (NDT), Structural Health Monitoring (SHM), structural adhesive systems or the use of composite materials as a repair and strengthening method. Using composite materials as a

strengthening technique has proven excellent results, providing a longer service life and a higher load-bearing capacity for the structure [8].

Over the years, a number of numerical analysis methods have been developed to solve diverse problems. Among these methods, the Finite Element Method (FEM) has been widely employed to solve partial differential equations and determine approximate solutions [9]. Its origins can be traced back to the 1940s, where it was initially used to address complex elasticity and structural problems. Today, it stands as the mathematical foundation of modern Finite Element Analysis (FEA). By the use of FEM, engineering design in various industries, such as automotive, aviation, marine, as well as the construction industry, has been significantly revolutionized [10]. FEA is a powerful method that allows the analysis of structural behavior in clear details under different loads and conditions. It involves diving a complex geometry into much smaller and more simple elements, and then applying complex mathematical equations to each element to calculate its realistic behavior. By combining the results from all of the elements, the overall behavior of the structural system can be assessed. It is very important to note that the results from FEAs are only as strong as the quality of the input. Hence, it is very important to ensure that inputs such as material properties, boundary conditions, contact definitions, units, and other variables are all consistent, connected and correspond with the highest possible accuracy to the real problem.

1.2 Objectives

The main objective of this thesis is to introduce a methodological framework for analyzing the structural behavior of Øvre Kvamme RC bridge under current operational conditions and propose the optimum strengthening methodology. To further support the primary objective, the following additional secondary objectives will also be undertaken to:

- Conduct a comprehensive systematic literature review on the topic of interest, emphasizing the structural performance evaluation of RC bridges.
- Perform a field investigation of the Øvre Kvamme RC bridge with the assistance of multiple NDTs and SHM techniques, in order to identify any existing damage or deterioration and evaluate the current condition of the bridge, specifically focusing on areas of deterioration and assessing the level of impact on the structural integrity of the bridge.

- Propose the most suitable repair and reinforcement techniques for the bridge, emphasizing the use of composite materials as a strengthening method, and analyze their effectiveness using FEA and other advanced techniques.

1.3 Research significance

The research significance of this thesis is manifold. Not only will it address the knowledge gaps, safety, and structural integrity of the existing bridge but it will also function as a potential proposition to Vestland County Municipality and NPRA for a solution to the on-going conditions on the deteriorated existing RC bridge. It will address and provide a solution to its durability and structural issues but also strengthen the sustainability of the project. Additionally, the thesis can be beneficial for future structural analyses, field investigation, and preliminary assessment of other similar existing structures in comparable Nordic environment. The findings of this thesis can be used to inform future MRS strategies for similar bridges, potentially saving municipalities and governments significant costs in the long term. Furthermore, this thesis can serve as a valuable resource for researchers and professionals in the field of civil engineering, especially those interested in bridge safety, durability, and sustainability.

1.4 Scope & limitations

The scope of this thesis consists of performing a condition assessment and FEM-analyses on an existing RC bridge to simulate the behavior of the structure under different loads and conditions before, and after applying the proposed repairs and strengthening techniques. This will be supported by a thorough literature review and a field investigation of the bridge. The scope of this thesis is constrained by its high level of intricacy and given time frame. As a result, in order to complete the research in the specific time frame, several presumptions and limitations will be presented:

- The thesis will be limited to only one bridge in a specific geographic region, and thus the proposed solutions of repair and maintenance methods may not be generalizable to all other types of bridges or regions with similar or different conditions or characteristics.
- The thesis will not include a detailed analysis of the environmental impact of the repair and strengthening process, and thus the long-term performance of the proposed

techniques and methods of repair may not take all environmental and maintenance factors into account.

- The thesis is limited to the availability and quality of technical and design documentations as well as data regarding the case study, such as material properties, material models, boundary conditions, loads, geometrical and rebar measurements.
- The thesis will be limited to numerical models and simulations from software.
- The thesis will be constrained by the accessibility to efficient instruments and software required to collect and provide high-quality data for the numerical simulations and analyses.
- This thesis will be restricted to only non-destructive testing, which could influence the accuracy of the conducted structural health assessment and its proposal for rehabilitation techniques.

1.5 Thesis structure

The structure of this thesis contains a total of 9 chapters and 4 appendices. The following sections will provide a short insight into the organization of each chapter:

Chapter 1. Introduction: The first chapter will introduce the thesis topic, background, objectives, research significance, scope, and limitations of the thesis as well as research questions.

Chapter 2. Literature review: The second chapter will include an overview of the process behind discovering the existing research reviewed, the search process and a systematic review with a showcase of general trends, keywords, and publications by year and country. Additionally, a summary of some key findings will be presented.

Chapter 3. Research methodology: The third chapter will describe the methods used in this thesis to achieve its mentioned objectives, including field investigation, numerical simulation, and analyses.

Chapter 4. Field investigation of Øvre Kvamme bridge: The fourth chapter introduces the case study that represents the basis of this thesis and provides an in-depth insight into the current condition and health of the bridge as it stands today, with a close look at its condition and properties. Additionally, non-destructive testing and structural health monitoring instruments were utilized to get a more comprehensive bridge assessment.

Chapter 5. Modeling of Øvre Kvamme bridge**:** The fifth chapter includes an overview of the creation of the FEM model and an experimental insight on updating the FE-model to match its up-to-date condition and the health of the bridge.

Chapter 6. Finite element analyses: The sixth chapter will include all the Finite element analyses performed on the Øvre Kvamme bridge as it stands in its current condition with the final updated model of the FEM-model.

Chapter 7. Rehabilitation and strengthening proposal for Øvre Kvamme bridge: The seventh chapter will include a proposal for strengthening methods with the introduction, background, and mechanical properties of the selected composite material chosen as a strengthening measure. Additionally, it will discuss standard practices for maintaining and repairing concrete structures. The retrofitting process of these strengthening methods will undergo finite element analyses to assess the behavior of the bridge after retrofitting.

Chapter 8. Results & discussions: In this chapter the results from the field investigation, numerical simulations and analysis are presented. Additionally, it will present summarized discussions and results related to the findings from the previous chapters.

Chapter 9. Conclusion: The ninth chapter. This chapter will summarize the main findings of the thesis, answer the objectives of this study, and provide recommendation for future work on the topic.

Appendix A: Concrete damage plasticity parameters for concrete, supports, and ultra-high performance fiber-reinforced concrete.

Appendix B: Brutus document – Design drawing of the Øvre Kvamme bridge

Appendix C: Brutus document – Rebar bending schedule of mid-span, Øvre Kvamme bridge

Appendix D: A comprehensive literature review

2 Literature review

This chapter will provide an overview of the approach used for the systematic literature review, a bibliometric analysis, as well as a summary of the results and findings obtained from the collected literature.

2.1 Search strategy

The main objective of conducting a systematic literature review is to establish a solid framework and get a more comprehensive understanding of the existing research on the topic of interest [11]. The idea is to systematically map out the collected information and identify knowledge gaps, keywords, and trends in the relevant studies that address the objectives of this thesis [11]. To accomplish this, multiple sources were chosen for the collection of literature, including a search engine and an academic database. In this thesis, the documents were collected using Oria as the academic search engine, Web of Science[6] and Scopus[7] as the selected databases. These were chosen due to their large and diverse collection of sources and libraries in the same field of interest as the thesis. Furthermore, using these source tools allowed for the retrieval of high-quality and relevant documents from trusted sources.

The search process involved a combination of multiple search techniques to strengthen the search string to collect the relevant documents. This includes a specific set of keywords, truncations, phrase searching, and a set of boolean operators to enhance the search string criteria and improve the relevance of the results. See Table 1 below for an overview of the search techniques used to enhance the search string.

Table 1: Overview of used search techniques in the search string

Search techniques	Description
Keywords	Specific words or phrases which is relevant to the studies.
Truncations	Visualized as an asterisk symbol * to replace the rest of the word with other meanings to broaden the search.
Phrase searching	Visualized as quotation marks to make the search result in exact or very identical fields.
Boolean operators	(AND, OR and NOT) words that are used to refine the search.

[6] https://clarivate.com/products/scientific-and-academic-research/research-discovery-and-workflow-solutions/webofscience-platform/
[7] https://www.scopus.com/

The complete search string criteria consisted of three distinct methods: a search only within the article title, a search within all fields, and an exclusion search. The keywords used only for the article title were “Reinforc* Concrete bridg*” and “RC bridg*”. The all-fields search utilized the following keywords: (1) Repair*; (2) Strength*; (3) Rebuild*; (4) Reconstruct*; (5) Fix*; (6) Reinforc*; (7) FEM*; (8) Finite Element* and (9) Finite*. The selected search string was carefully designed to only retrieve specific area of interest studies related to the thesis objectives while excluding any irrelevant or unrelated material. And lastly, it was important for the search string to exclude everything related to seismic studies, as it provided a vast diverse collection of irrelevant studies to the main objectives and motive of the thesis.

Once the initial search was completed, a large number of academic documents were retrieved. More specifically, 40 documents were returned from Oria, 78 from Web of Science, and 188 from Scopus, resulting in 306 academic papers. While the initial search was broad and comprehensive, it was necessary to further refine the search results to narrow it down even further. To accomplish this, a set of filters were applied to the search engine post-initial search results. The filters were selected to further assist in eliminating the less relevant academic papers and focusing more on specific subject areas.

The first applied filter was *Publication date*, which restricted the results to papers published within a specific timeframe (From the year 2000 to 2022). The second applied filter was based on *Language* (Norwegian & English), and the last filter applied was *Subject area* (Engineering & Building technology) to better assist the field relevance of the search results. Due to this, 82 articles were eliminated, leaving 224 relevant academic documents for data review. Although this still represented a considerable number of articles, due to time constraints and impending deadlines, only a total of 40 academic papers were manually selected from the databases and recommendations from supervisors for a full manual review, while still conducting a bibliometric analysis of the 224 documents. These 40 documents were selected by title and abstract relevance to create a strong enough foundation for the objectives of the thesis. It is also worth mentioning that some of the academic papers that appeared in the search results after applying filters, may be duplicates. As they could be provided by more than one of the used databases.

Figure 3 below displays a Preferred Reporting Items for Systematic Reviews and Meta-Analyses (PRISMA) flow diagram which provides a graphical presentation of the search process utilized in this thesis. The diagram follows a standardized format outlined by PRISMA guidelines [12].

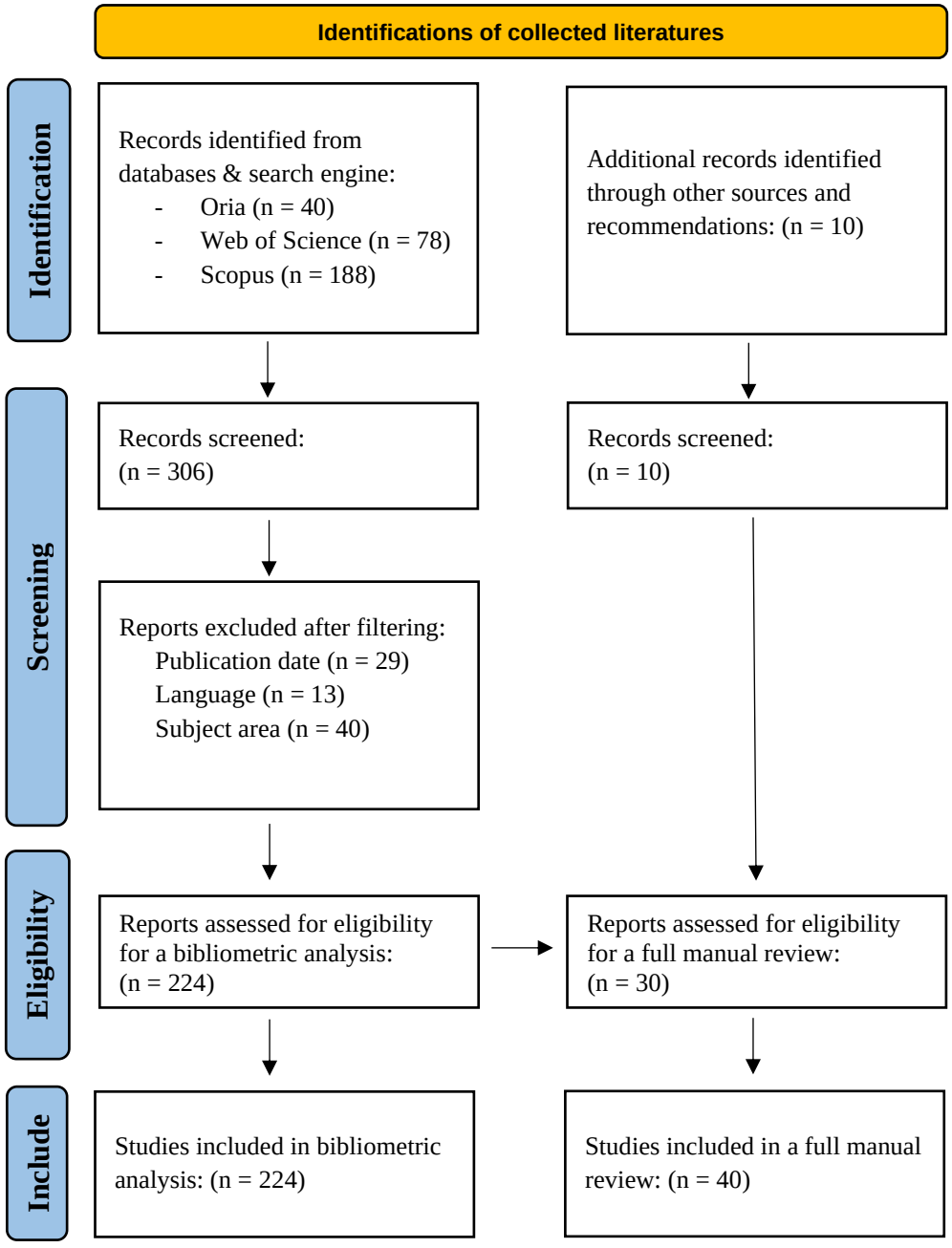

Figure 3: PRSIMA flow diagram of collected literatures – Retrieved from [12]

2.2 Bibliometric analysis

A bibliometric analysis of the search string post filtering is important to the thesis as it will provide valuable insights into the current state of research in this field. A total of 224 documents were analyzed post-filtering from Oria, Web of Science, and Scopus. Figure 4 below displays the total number of documents published from 2000 to 2022 in filtered languages. The x-axis represents the years, and the y-axis represents the number of documents published. The chart indicates that attention and interest in the field had a slow start in the earlier years but significantly accelerated in 2016 and beyond. The number of documents published peaked in 2021, with a total of 31 released, followed by a slight decline in the subsequent year.

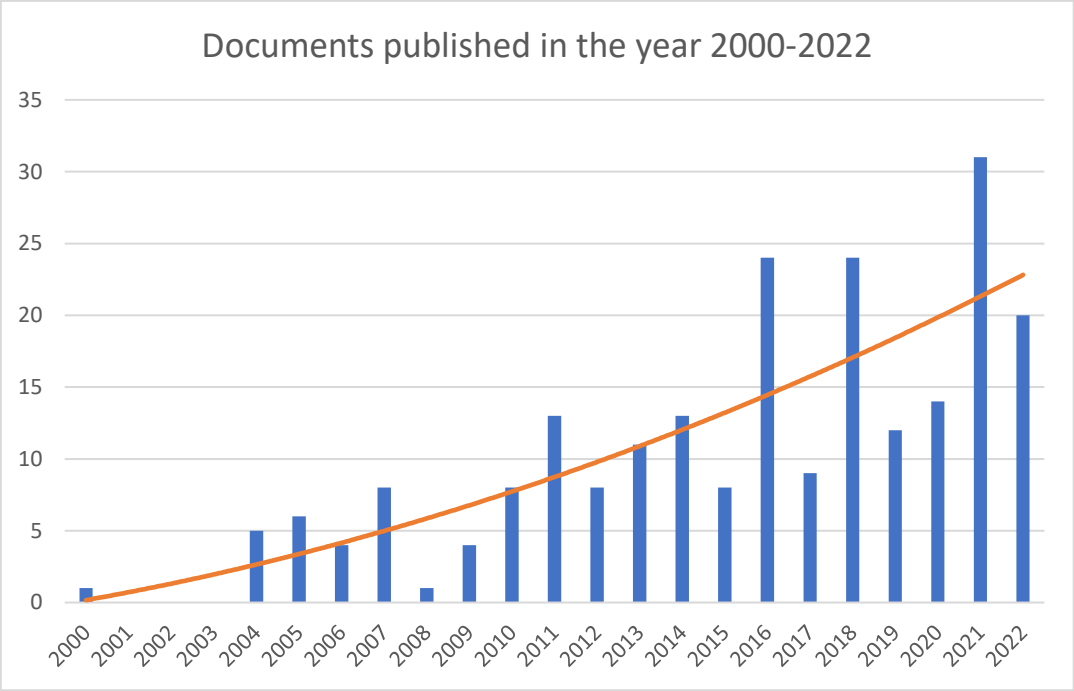

Figure 4: Total published documents from 2000-2022 based on the search string

Figure 5 showcases the number of documents published by the top 15 countries from the year 2000 to 2022, in addition to filtered language. The bar graph ranks the countries on the x-axis from the highest on the left to the lowest on the right, and the number of documents published on the y-axis. The data presented in Figure 5 highlights China and USA as the dominant players in this field by a large margin, with Canada as next in line. The data also reveals interesting patterns, such as the potential growth in non-English speaking countries like China, Japan, and Italy. This suggests that there may be opportunities for international collaboration and expansion in this field.

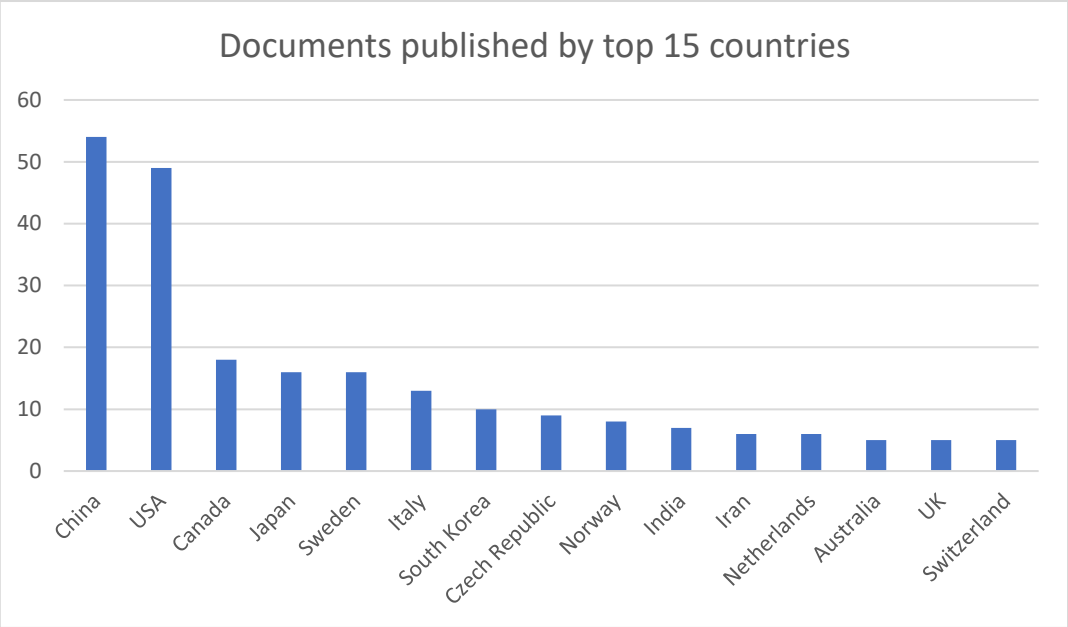

Figure 5: Total documents published by country based on the search string

In order to efficiently map out the network of trends and keywords found in the retrieved documents, VOSviewer software was utilized [13]. The frequency of the keywords in the documents was set to a minimum of 10 times in order to appear as a relevant keyword. See Figure 6 below for a generated visualization map of the keywords most frequently used.

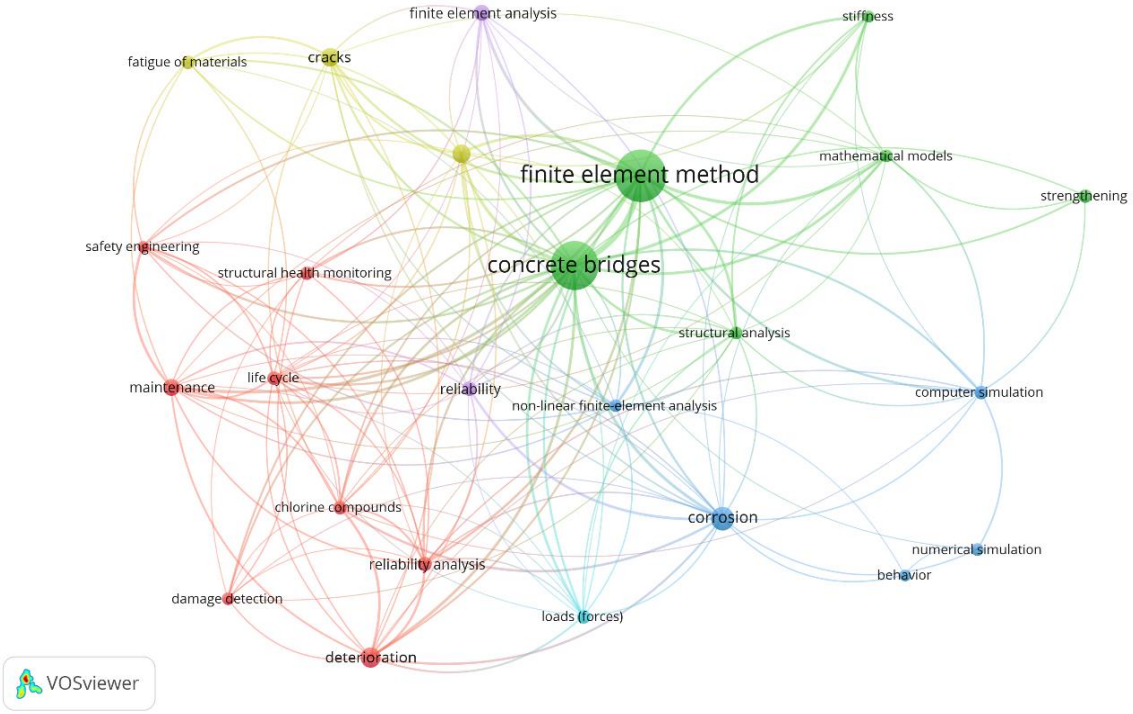

Figure 6: Frequency of keywords created in VOSviewer [13]

The size of the bubbles corresponds to the frequency of the word's occurrence in the documents. The larger the bubble, the more the word is repeated in the documents, and the lines between the bubbles illustrate the level of connectivity between the keywords. The thicker the lines, the stronger the connection. It is also important to note that the closer the bubbles are to each other, the more related they are to each other. Furthermore, Figure 6 identifies six main research topics represented by different colors, Finite Element Method (green), Corrosion (blue), Loads (cyan), Deterioration (red), Cracks (yellow), and Finite Element Analysis (purple) with "Concrete bridges" in the center of these crucial topics. This confirms that the search string used for the systematic literature review was appropriate for the objectives and motives of the thesis.

Figure 7 below indicates the trending research topics based on the time of publication. Yellow color presents more recent studies while dark purple indicates older studies. Figure 7 highlights a notable trend in research that indicates an increasing focus on numerical simulation and analysis, along with concrete bridge maintenance. It is also important to highlight that the absence of links between some of the keywords in the network map indicates a potential knowledge gap and an opportunity for future investigation.

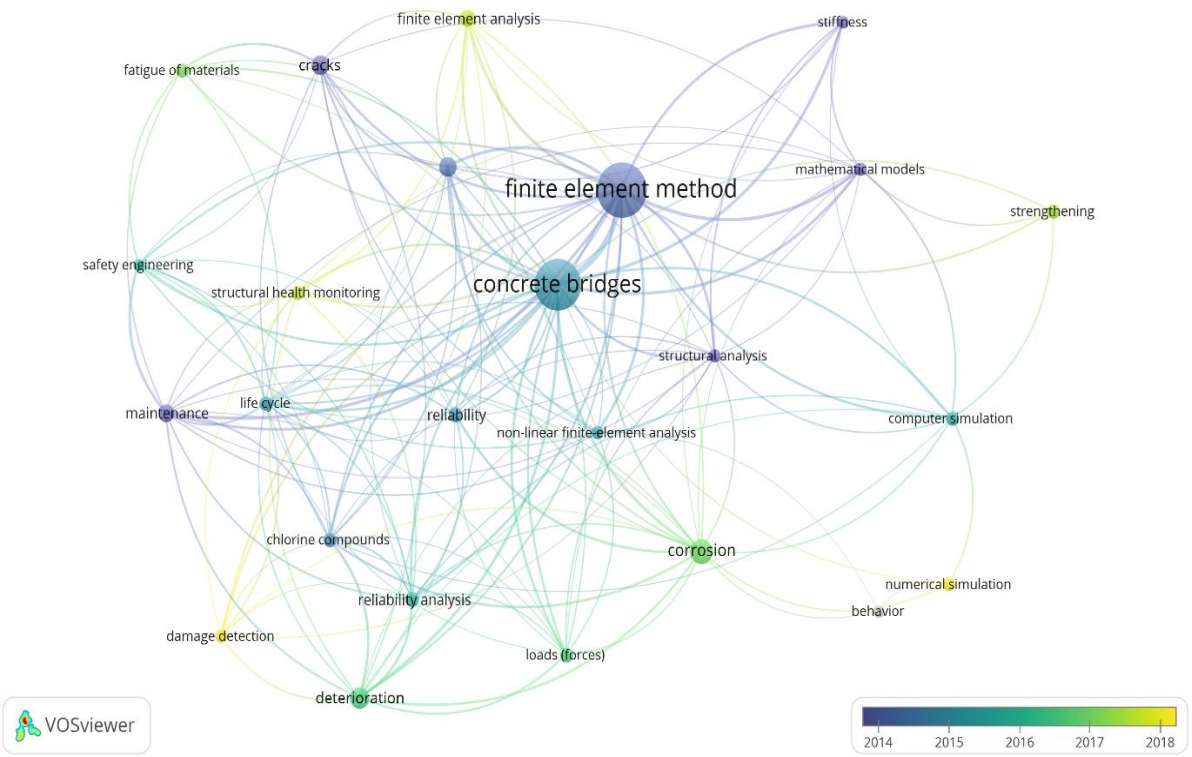

Figure 7: Network of trends created in VOSviewer [13]

2.3 Research findings

Following a careful selection process of 40 academic literature sources, the subsequent phase involved a detailed manual review of each source, as part of a systematic review. An efficient review system was established using Microsoft Excel spreadsheet to better organize and summarize the information obtained. All the handpicked literatures from the sources will be listed in an external Excel file, where the review will be conducted, see Appendix D. By using Excel as an overview of the papers, it was easy to sort and filter the data according to specific criteria quickly. This allowed for a more efficient analysis of the papers and identifications of common themes and trends in the industry, but also a reliable foundation and a general understanding of the subject. The full manual review process will include the following:

- The identification of the literature (DOI, Title, Authors, Publication date, the country the research was performed from, and the type of research)
- Software used for simulation or FEM-analyses
- A simplified research question of the literature
- A summary of the method and research methodology used in the paper
- Results and findings that will be relevant to this thesis's objectives
- A conclusion of what was concluded with relevance to this thesis's objectives

It is important to note that in some of the cells in the Manual Review Excel file, there are only " – " written inside. This is due to the information not being relevant to this thesis or its non-existent. These hand-selected documents underwent a full manual review and were used as the basis for the objectives of this thesis. Some of the relevant findings and research of these studies are summarized in the following sub-sections.

2.3.1 Condition assessment of RC bridges

Conducting a systematic condition assessment can provide significant advantages for the health of bridges, such as efficiently reducing repair costs and increasing the service life of reinforced concrete structures. Proper evaluation and inspection of deterioration, along with an appropriate repair, maintenance, and strengthening plan, can greatly prevent bridge collapse. Each of these factors plays a critical role in ensuring the success and long-term durability of an RC structure [3-5]. Various types of assessments were conducted using similar or different methods and techniques to achieve satisfactory results in the studies.

In an attempt to identify common patterns of deteriorations among RC bridges, Yavuz et al. [5] conducted a study utilizing a combination of visual inspection and Non-Destructive Tests (NDT). The researchers investigated in detail 104 concrete bridges in Albania and evaluated the condition of each one using a rating system ranging from 1 to 5. A rating of 1 indicated "*No Risk"*, while the rating of 5 indicated "*Very High Risk"*. At the end of the study, Yavuz et al. [5] revealed that the investigated bridges were in very poor condition due to traffic loads, lack of maintenance, and lack of proper design, among other factors. Thus, Yavuz et al. recommended to utilizing various NDT methods such as visual inspections, cover meters, vibration instruments, rebound hammer tests, half-cell potentiometer test, carbonation tests, and the use of digital image processing for a more comprehensive and precise assessment during field investigation [5]. A maintenance plan schedule was highly advisable by Yavuz et al. [5] and it is crucial to effectively address the challenges posed by deteriorated concrete bridges and ensure that the structure remains safe and healthy.

In a study by Mohammed et al. [4], traditional approaches in condition assessment of RC bridges were explored. The study identified two methods of condition assessment: Destructive Tests (DT) and Non-Destructive Tests. While DTs such as coring tests are highly effective in detecting chemical attacks like carbonization, they are often problematic due to their potential to damage the bridge, their time-consuming nature, and their high cost. Thus, the study suggested a greater reliance on NDTs, which offer more benefits but require interpretation. The researchers investigated six NDT instruments in more detail, assessing their capabilities and limitations, and concluded that Ground Penetrating Radar as the most effective option. Mohammed et al. [4] also noted that the current practices indicate visual inspection as the most commonly employed method for condition assessment as it is very effective to detect surface defects. This approach is often performed with a simple NDT tool like hammer sounding or chain dragging to identify defects such as delamination. However, visual inspection has received criticism for relying heavily on the expertise and knowledge of the investigator [4].

Tarek & Moncef [3] investigated current practices of condition assessment of RC bridges in North America and its research challenges. The researchers classified the current practices into five main categories, visual inspection, load testing, non-destructive evaluation, SHM, and finite element modeling. Each practice is described in detail with its advantages, limitations, and application. However, it is important to note the value of integrating the extracted data from SHM and NDTs to FEM to improve the accuracy of the condition assessment greatly. All in all, Tarek & Moncef [3] recommended caution before using any of these practices, as a cost-

benefit analysis should be carried out first to determine its value in both the short- and long-term. Additionally, the authors highlighted the importance of integrating the enormous amount of information and knowledge that has already been produced in the bridge condition assessment field into a data-stored system, which could be used anytime by various participants in the field for quality management and structural assessment purposes.

Giovanna et al. [14] investigated the condition of a four-span RC bridge through analytical results with field observations and dynamic testing before, and after strengthening with the application of Carbon Fiber Reinforced Polymers (CFRP). The researchers initiated a vibration-based assessment by installing sensors on the bridge and recording the frequencies in different locations. These frequencies were further used in model updating of the FE-model to obtain a more realistic behavior of the current state of the bridge for a thorough analysis. The application of CFRP on the bridge resulted in higher frequencies, and the change in the frequency before and post application of CFRP indicates increased structural stiffness. Giovanna et al. [14] later concludes that dynamic-based assessment procedures are a powerful technique to calibrate and optimize the design of these strengthening interventions [14].

Gunawan & Narciso [15] assessed the condition of a deteriorated bridge located in Brunei Darussalam. The main aim of the study was to evaluate the current state of the bridge and identify the reasons behind the deterioration of its concrete. Gunawan & Narciso [15] performed a field investigation with a combination of destructive tests and non-destructive tests. This consisted of Visual Inspection, Acoustic Impact testing, Ferroscan Pachometer survey, Rebound Hammer testing, Ultrasonic Pulse Velocity, measurements in concrete dimensions, and a collection of concrete core and concrete powder samples [15]. Through destructive tests it was revealed that carbonation was one of the leading causes of concrete degradation in the bridge. The columns of the bridge were found to be in the most severe condition, and it was determined that carbonation-induced corrosion in the reinforcement was the primary reason for the deterioration.

2.3.2 Numerical simulation and analyses of RC bridges

Using finite element modeling and analyses enables the evaluation of the structural system performance and behavior without the need for physical instruments, making it a very cost-effective approach. Additionally, collecting data from field instruments for bridge inspection can be used for model updating in the numerical simulations to further calibrate the finite element model for more precise and accurate results as discussed by Tarek & Moncef [3].

When performing a numerical simulation and analysis, several systems and factors must be considered. These may include the bond between concrete and steel, the impact of deterioration, chemical defects, material properties, mesh configurations, non-linear models, and other related variables.

A study performed by Mohammad & Mohsen [16], was conducted to investigate how reinforcement parameters affect the punching shear strength of bridge slabs made of concrete reinforced with FRP and laterally restrained. The bridge was modelled in FEA software Abaqus with an 8-noded hexahedral element, reduced integration (C3D8R), mesh sensitivity of 25mm, and with the application of Concrete Damaged Plasticity (CDP) model for the Non-Linear Finite Element Analysis (NFEA). It was assumed to be a perfect bond between concrete and all other materials included in the bridge. Mohammad & Mohsen [16] later revealed through numerical simulation and analysis that the spacing between bars has more impact on punching shear strength compared to the bar area. Additionally, the researchers found that enhancing the transverse reinforcement will greatly improve the serviceability of the bridge slab. It would be noted, however, that the longitudinal reinforcement had minimal impact on the serviceability of the structure.

Arto et al. [17] developed a 3D non-linear FE-model of a reinforced concrete bridge and loaded it to failure. The bridge was monitored and strengthened with FRP on the bottom of the deck to improve its bending capacity. The 3D model was created using Abaqus software, assuming a perfect bond between the composite material, steel, and concrete. The measurements were extracted from the monitoring instruments and implemented in Abaqus to further calibrate the model. The FE-model of the concrete bridge was modelled with solid elements of type C3D8R, while the reinforcement was modelled as wires of type 2-node linear 3D truss element. The supports were modelled using the shell element of type S4R. Overall, the model consisted of 152,460 elements, and the application of CDP-model for the NFEA was used. It was revealed by Arto et al. [17] that the maximum load it could tolerate was a mid-span load of 11.7 MN, and the additional load from the failure condition was carried by the FRP bars which enhanced the bond stress between the epoxy adhesive and the surrounding concrete. A bond failure was also observed and caused by a combined action of shear, torsion and bending. It was discovered that the developed 3D NFEA-model can accurately predict the behavior of the bridge as the load increases, up to the point of bond failure [17].

Micheal et al. [18] researched investigating a reliable methodology for structural analyzing RC bridge decks and thus performed FEA in the software Abaqus. The RC deck was modelled with shell and rebar elements of type S4R, the steel girders were modelled with beam elements, and a total of 5,211 elements were created from the whole FE-model. This resulted in 40,000 total degrees of freedom. The overall results from the FEM analysis performed by Micheal et al. [18] revealed that the FEA software Abaqus provided a very precise and accurate measurement of its behavior during loading. The software successfully simulated the interaction between concrete and steel, applied loads, and, most significantly, predicted the realistic structure behavior of the bridge that would otherwise not be typically obtained through experimentations. Abaqus was able to predict deflections, strains, and stresses while minimizing unnecessary complexities [18].

Sujata [19] initiated an investigation on performing nonlinear finite element analysis in Abaqus on a bridge approach slab. Sujata employed a smeared crack model to represent the nonlinear behavior of the FE-model. The entire concrete bridge approach slab was modelled, resulting in 600 elements of type S4R and reduced integration, while the reinforcements were modelled using the rebar layer option. Sujata established that Abaqus is more than suitable for performing nonlinear finite element analyses of reinforced concrete structures to predict the structural behavior, specifically, the stress and strain behavior and defects. Additionally, tension stiffening must be employed to model the interaction behavior of concrete and steel after the cracking stage more accurately [19]. In the study, a value of $20\varepsilon_{cr}$ was appropriate and used for tension stiffening of the finite element model.

2.3.3 Repairing and strengthening methods of RC bridges

The exposure of concrete bridge slabs to harsh environmental and mechanical conditions requires the development of innovative techniques to enhance their durability and augment their load-bearing capacity [8, 20-23]. Most of the severe degradation on concrete bridges comes from corrosion of reinforcement. Recently, the trend for extension of life cycle, repair, and strengthening have shifted towards utilizing composite materials as the preferred choice of rehabilitation and reinforcement with retrofitting.

In a study conducted by Masoud et al. [21], the behavior of corrosion-damaged reinforced concrete beams with and without CFRP retrofit was investigated. Masoud et al. [21] performed a numerical simulation of the concrete structure in Abaqus [24], utilizing the concrete damage plasticity to predict the nonlinear behavior of the beam. The model was created using solid

elements and the rebars were modelled using wire elements. The corroded rebars, however, were modelled with spring element for the bond between concrete and corroded steel. The composite material CFRP was installed on the beam in three different retrofit cases and two different levels of corrosion:

- Case A: CFRP strips along the bottom of the beam, at 20% and 40% corrosion level
- Case B: CFRP strips along the bottom of the beam and three vertical CFRP plates on both sides for shear strengthening (c/c 150mm), at 20% and 40% corrosion level
- Case C: CFRP strips along the bottom of the beam and three CFRP plates installed for shear strengthening at an angle of 45° (c/c 150mm), at 20% and 40% corrosion level

According to Masoud et al. [21], the structure's moment capacity may be reduced by corrosion, resulting in the development of concentrated crack patterns. Furthermore, CFRP was identified as an effective technique to retrofit corrosion-damaged RC-structures as it greatly enhances the capacity of the structure element. However, the researchers cautioned against excessive use of the composite material and recommended a maximum limit of 40% capacity gain. Based on the results from the finite element analysis, Case B was the most beneficial, as it yielded the highest moment capacity values.

An investigation conducted by Ayesha et al. [22] explored the overall properties of FRP concrete strengthening. The study aimed to provide an up-to-date overview of the use of FRP in strengthening RC structures, focusing on their performance, failure modes, modeling, challenges, and opportunities. The most common failure modes were found to be debonding for side-wrap and u-wrap strengthened systems and rupture of the FRP for full-wrapping systems. The researchers suggested that further research is needed to establish design guidelines for strengthening RC structures using FRPs under different loading conditions. Additionally, the use of FRP in strengthening RC structures will increase with the development of new techniques that reduces brittleness, energy consumption, carbon emissions, and initial costs. Ayesha et al. [22] have pointed out that while numerous studies have been conducted on FRP strengthening, they have mostly focused on short-term performance under specific conditions. The long-term behavior and performance of FRP strengthening under extreme conditions have not been widely investigated.

An investigation conducted by Ayesha et al. [22] explored the overall properties of FRP concrete strengthening. The study aimed to provide an up-to-date overview of the use of FRP in strengthening RC structures, with a focus on their performance, failure modes, modeling,

challenges, and opportunities. The most common failure modes were found to be debonding for side-wrap and u-wrap strengthened systems, and rupture of the FRP for full-wrapping systems. The researchers suggested that further research is needed to establish design guidelines for strengthening RC structures using FRPs under different loading conditions. Additionally, the use of FRP in strengthening RC structures will increase with the development of new techniques that reduce brittleness, energy consumption, carbon emissions, and initial costs. Ayesha et al. [22] have pointed out that while numerous studies have been conducted on FRP strengthening, they have mostly focused on short-term performance under specific conditions. The long-term behavior and performance of FRP strengthening under extreme conditions have not been widely investigated.

Fahmy et al. [23] explored the structural properties of applying carbon fiber-reinforced polymer sheets on RC bridge slabs through an analytical study. A finite element model in a FEA software called ANSYS was developed and four application cases of CFRP sheets were analyzed. The study revealed that CFRP strengthening can enable many structures to meet today's standard requirements while being cost-effective compared to conventional methods. The researchers observed a significant increase in the ultimate load capacity of the structure (43.2% for 3 sheets with 100 mm width and 54.8% for three sheets with 200 mm width) [23]. Moreover, Fahmy et al. [23] discussed that even better capacity could be achieved by using more comprehensive sheets, closer sheet spacing, and positioning along the longitudinal axis of the slab.

Research conducted by Nicholas & Hira [25] reports on experimental investigations of the performance of two CFRP-based repair and strengthening schemes on severely damaged 40% scale model flat slab bridges, which represent a large class of multi-span RC flat slab bridges in Australia that are over 60 years old. Both static and dynamic tests were conducted, and the researchers found out that both CFRP-based strengthening systems are viable remedial strengthening strategies for flat slab bridge deck applications. However, the ultimate performance of both schemes was somewhat brittle. The dynamic testing technique used in the study can be valuable for condition monitoring applications by calibrating FEA models of bridge structures.

Hsuan-Teh et al. [8] performed a non-linear finite element analysis on various methods of FRP strengthening on a reinforced concrete beam. The method included FRP application methods on a long, and short beam length, as well as low and high reinforcement ratios. The beam was modelled in Abaqus using 8-node solid elements, the FRP was modelled using shell elements,

and it was assumed perfect bonding between the concrete and the composite material. According to the study, it was found that incorporating FRP on the underside of the concrete yielded a higher stiffness value for the beam compared to the sides. The length of the beam with a high reinforcement ratio did not affect the impact of FRP on the bottom. However, the research also showed that the combination of high reinforcement ratio and FRP applied on the underside of the beam resulted in more cracks in the central region as opposed to the beam with a low reinforcement ratio. But the beams with a low reinforcement ratio and FRP applied at the bottom of the beam resulted in more cracks at the support region [8]. Hsuan-Teh et al. [8] concluded that correct appliance of FRP-reinforcing on the bottom of the structure element will result in higher ultimate strength values.

Malena et al. [20] explored the use of Ultra-High Performance Fiber-Reinforced Concrete (UHPFRC) as a composite material for repairing and strengthening the reinforced concrete deck slabs in bridges. The researchers applied an additional layer of UHPFRC to the concrete bridge deck and conducted both experimental and analytical studies to investigate the behavior of the structure under various types of loads and identify failure modes. The experimental tests including bending, punching, and cantilever tests, as well as the analytical approach revealed that UHPFRC composite material significantly improved the structure's load-bearing capacity and enhanced the durability of the bridge deck. This was also confirmed by Lionel & Philippe [26] in similar research. The researchers, Lionel & Philippe [26] investigated on various application cases of the composite material UHPFRC on different RC bridges. Their research and the study conducted by Malena et al. [20] concluded that UHPFRC possesses effective traits such as waterproof membranes and extending the life cycle at a limited cost. Furthermore, adding reinforcement to the UHPFRC layer can further enhance the flexural and shear strength of the structure.

2.4 Standards and regulations

Before conducting any type of work or research on Øvre Kvamme, it is critical to understand the regulation and requirements of the Norwegian government as it is the foundation of the following work process in the thesis. Following these laws, guidelines, and standards guarantees that the proposed solutions, techniques, and FEM analyses are based on the most up-to-date technical information. This ensures that the results of the thesis are relevant and applicable to a real-world scenario of condition assessment, structural analyses, repairing

techniques, and maintaining concrete bridges in Norway. The following sub-sections will present a description of each relevant code and standard.

2.4.1 Eurocode 2 and handbooks

Eurocode 2 (EC2) [27] is a European standard series for the design of concrete structures and was first published in 1992. It has been revised several times to ensure the information it provides stays up to date on the newest developments in research findings and changes in construction practices.

Handbooks from the NPRA are a series of technical manuals and guidelines that provides relevant information and details regarding the design, construction, and maintenance of roads and bridges in Norway. These handbooks are regularly updated to the latest advances in technology and practices in road and bridge engineering. See Table 2 below for a summarized overview of relevant papers from each series:

Table 2: Overview of relevant Eurocodes and Handbooks

Identification	**Description**
NS-EN 1992-1-1: Eurocode 2 [28]	Design of concrete structures - Part 1-1: General rules and rules for buildings
NS-EN 1992-2: Eurocode 2 [29]	Design of concrete structures - Part 2: Bridges
Handbook N400 [30]	Bridge design
Handbook V412 [31]	Load-bearing capacity classification of bridges, loads
Handbook V413 [32]	Load-bearing capacity classification of bridges, materials
Handbook N-441 [33]	Bridge inspection

2.4.2 ISO 16311 series

International Organization for Standardization (ISO) 16311 is a series of standards that provides guidelines for assessment, repairment, and strengthening of concrete structures. This code series of standards covers different aspects of the systematic process of condition assessment and MRS in-depth, including:

1. ISO 16311-1: defines the general principles and a framework for the assessment, repair, and strengthening of concrete and masonry structures [34].

2. ISO 16311-2: provides guidance on the selection of appropriate repair and strengthening methods and materials [35].
3. ISO 16311-3: provides guidance on the assessment of the structural safety of concrete and masonry structures [36].
4. ISO 16311-4: provides guidance on the design and execution of the repair and strengthening of concrete and masonry structures [37].

3 Research methodology

This chapter presents the methods used in this thesis to achieve the research objectives and serves as a foundation coupled with the literature review for the subsequent chapters. It employs a mixed-methods research design and a case study approach to efficiently reach the thesis aims, but also the conducted literature review implements a framework for the thesis. The following sub-chapters will provide a more comprehensive understanding of how the research will be conducted in detail and what methods were used to collect, calibrate, and analyze the data. Figure 8 below displays a flow chart for a systematic insight on the performed methodologies in this thesis:

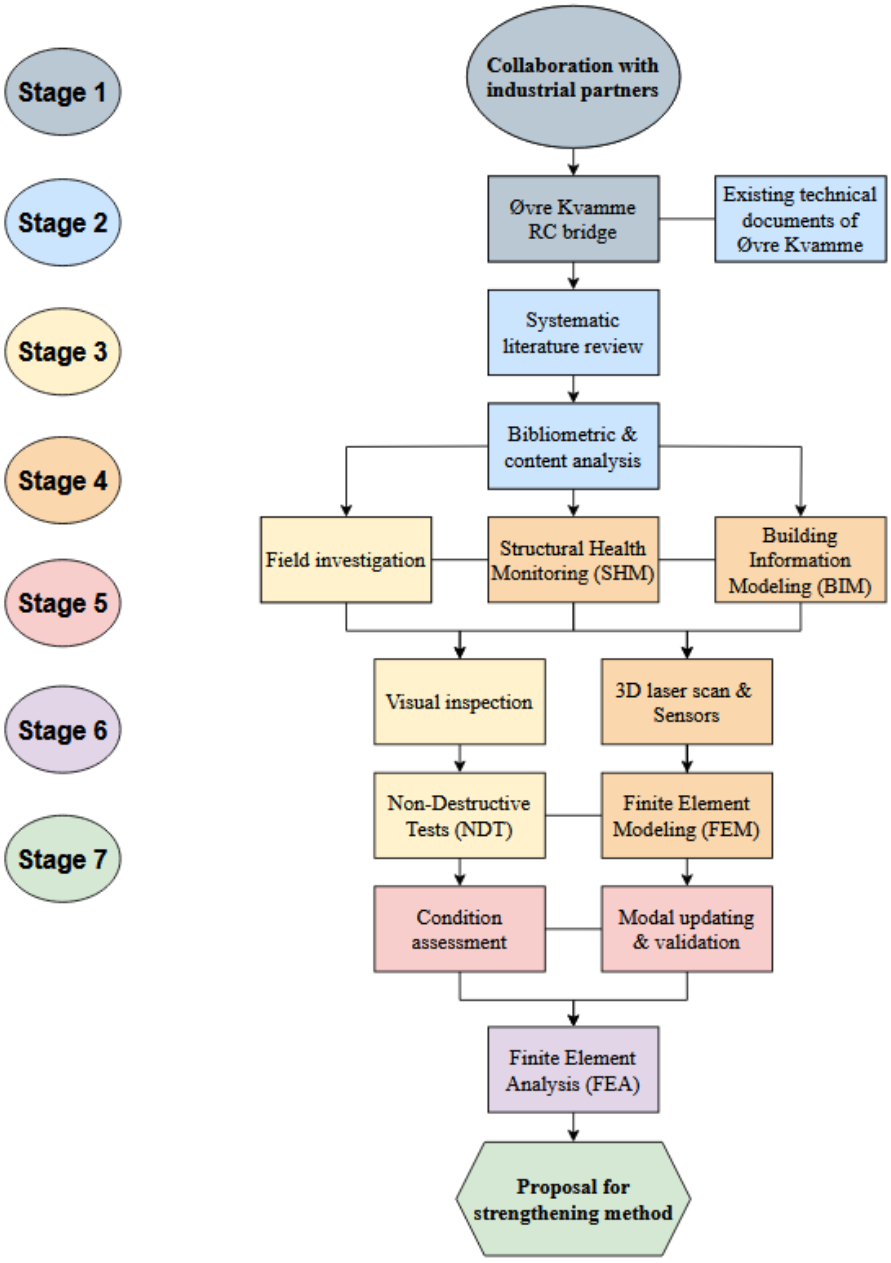

Figure 8: Methodology process of this thesis

3.1 Systematic review

Chapter 2's literature review was conducted as the primary work and laid the foundation for further research in this thesis. The review employed a systematic approach, a thorough manual review, and a bibliometric analysis of the collected documents. This comprehensive approach provided essential information for the thesis objectives, furnishing a complete perspective on the critical aspects. The review provided a comprehensive understanding of the condition assessment methods, repair and strengthening methods, as well as numerical simulation and analyses, presenting relevant findings on each of these topics. See Chapter 2 for a more detailed overview.

3.2 Field investigation

A field investigation on Øvre Kvamme holds significant importance in this thesis for multiple reasons. By performing a visual inspection, and conducting tests with NDT instruments, the current state of the concrete bridge can be more accurately assessed. This information can then be further analyzed and evaluated for the level of maintenance and strengthening procedures required for the bridge. See Chapter 4 for a more detailed description and a conducted field investigation on the bridge.

Additionally, structural health monitoring will be utilized in the field investigation to gather data for both numerical simulation and model updating. This will involve various techniques, such as using OMAway sensors and a laser scanning system such as LiDAR (Light Detection and Ranging), to obtain precise data on the behavior and performance of the structure. The data collected will then be utilized for model updating, which involves adjusting the structural model parameters to better represent the actual behavior of the system. By refining the numerical simulations in this way, the system's structural response can be improved [3].

3.3 Numerical simulation

Conducting a numerical simulation and analysis is a highly important tool for an in-depth investigation and structural examination of the case study. This is highly beneficial for modeling and studying complex systems, such as the behavior of the bridge in various loads and conditions, which would normally be very difficult to observe directly. This thesis will include performing a numerical simulation and analysis utilizing the FEM software Abaqus.

Initially, a point cloud from the data gathered during the field investigation will be generated. Following, it will be transferred to Revit for modeling, and finally, it will be imported to Abaqus. Subsequently, the model will be calibrated through the application of the model updating method with results extracted from the OMAway sensors and other potential NDT's instruments used in the field investigation. See Chapter 5 for a more detailed description and a performed numerical bridge simulation.

3.4 Software

Several software tools will be utilized in the data calibration and analysis phase of the thesis. The following is an overview of each used software tool, their features, and why they were chosen.

3.4.1 Proceq software

Proceq is a company specializing in developing Non-Destructive Testing (NDT) instruments and software. Proceq software is designed to be user-friendly, real-time data collecting of its NDT instrument, mapping, and allows for generating custom reports with the software's built-in reporting tool. The collected data can be exported into Excel for further analysis [38].

The Proceq software of relevance are:

- **ProfometerLink**: This software is used to analyze data collected by the Proceq Profometer instrument, Profometer 650 AI [39].
- **HammerLink**: A software used for analyzing the test results obtained from Schmidt Hammer [40].
- **ResipodLink:** This software is used for real-time data analysis of the electrical resistivity readings provided by Proceq Resipod instrument [41].

3.4.2 Leica Cyclone

Cyclone REGISTER 360 is a laser scanning registration computer software developed by Leica which allows users to register, merge, and align multiple 3D point cloud scans. The scans are captured with the Leica Cyclone FIELD 360 mobile application and integrated into a unified coordinate system. The mobile application facilitates use in situ, providing the ability to review captured scans and ensure it is correct. Both software include tools such as registering and georeferencing scans, filtering and editing the data, and then exporting the finished calibrated data for use to other software [42].

Leica Cyclone software will be utilized to capture, merge, align, and generate the point cloud of the reinforced concrete bridge. Subsequently, the point cloud data will be exported to a *.rcp* file for further processing in Autodesk Revit.

3.4.3 Autodesk Revit

Autodesk Revit is a powerful Building Information Modeling (BIM) software tool that is widely used by engineers, architects, and construction professionals in the building industry. It serves as a comprehensive tool for planning, developing, and managing building and infrastructure projects. Revit offers a vast collection of simple and efficient architectural, MEP, and construction design tools. It allows users to create highly detailed 3D models of buildings and other structures and generate professional 2D drawings and documentation [43].

Revit will be used to develop a 3D model based on the point cloud generated from the laser scanning software, Cyclone REGISTER 360. This includes incorporating the coordinates of the concrete slabs and supports, ensuring accurate dimensional modeling of Øvre Kvamme bridge in its current state.

3.4.4 Abaqus

Abaqus is a versatile, user-friendly, and powerful finite element analysis software that allows users to simulate and analyze the behavior of a wide range of materials and complex structures. The software is also incredibly useful for studying linear and nonlinear response of structures subjected to static and dynamic loading. Additionally, the Abaqus/CAE (Computer-Aided-Engineering) software tool, which will benefit in this thesis, further provides a more comprehensive set of tools for creating, editing, and analyzing constructions. Tools such as mesh generation, geometrical creation, loads and boundary conditions [19, 44-45].

The geometric properties modelled in Revit will be imported into Abaqus as an ACIS file in the *.sat* format for further detailing of model parameters, loads, boundary conditions and mesh generation.

3.4.5 UnquakeOMAway

UnquakeOMAway, developed by Unquake, is a specialized software designed for Operational Modal Analyses (OMA) to monitor the vibrations of construction elements and structures. The software provides immediate results from each installed sensor, obtaining data in triaxial dimensions, x-, y- and z-axis. The data can be used to assess the structure's condition and the geographical location of each installed sensor. The obtained data can be utilized to conduct further analysis and model updating using its simple tools [46]. The results from the software

will be important in the model updating process in Abaqus, allowing adjustments of the stiffness in the model to align with the actual behavior of the bridge.

3.5 Numerical analysis

After the initial numerical simulation of the bridge, the model is updated with the relevant data acquired from the field investigation to ensure higher accuracy and reflect the current state of the bridge. This is followed by different structural analyses using the finite element software Abaqus.

3.6 Proposal for strengthening method

Upon completion of the comprehensive condition assessment, which involves field investigation and structural analyses, the results will be evaluated. Afterward, a proposal is presented, outlining appropriate strengthening and repair methods for the concrete bridge. The proposal considers the relevant guidelines provided in ISO 16311 Part 3 [36] and 4 [37]. The comprehensive approach used in the analysis ensures that the proposal is tailored to address the specific needs of the bridge.

4 Field investigation of Øvre Kvamme bridge

It was desirable to select an existing bridge in Norway that exhibited poor condition and required repair and strengthening. In order to identify a fitting choice, a collaboration was established with an internal supervisor and an external supervisor from Vestland County Municipality. The selection process involved a thorough evaluation of several potential bridges, considering their structural integrity, age, and condition. After thorough consideration, Øvre Kvamme, a short three-span reinforced concrete bridge, was considered an appropriate option for the thesis.

With Handbook V441 [33], ISO 16311 Part 1 [34], and Part 2 [35] standards as a foundation for this chapter, a field investigation of Øvre Kvamme can be conducted in a professional manner. A reverse engineering process was necessary since the structure under investigation already exists. This entails employing non-destructive testing tools to examine the bridge and gather information about its characteristics, material properties, and design. Hence, a systematic approach is essential, encompassing data collection, processing, analysis, and interpretation stages. This approach is necessary because of the limited information available and the lack of detailed documentation about the entire bridge.

When carrying out a field investigation, it is crucial to have an assessment plan prepared beforehand [34]. The assessment plan will outline the procedures and methodologies that will be employed to gather and evaluate data. The assessment plan will serve as a blueprint for the entire field investigation and will ensure that the investigation is organized and structured. According to ISO 16311-1 [34], the assessment category is classified as an initial assessment. Furthermore, for this thesis, a preliminary level of assessment was selected, as defined by ISO 16311-1 [34] and more in detail by ISO 16311-2 [35], with the addition of structural analysis. This decision was influenced by several factors, including time constraints, resource availability, and the limitation of not being able to use destructive tests, which made a detailed level of assessment impractical.

A field investigation was performed on Øvre Kvamme on November 9th, 2022, with the assistance of various non-destructive test instruments. During the field investigation, adherence to established safety protocols was ensured by incorporating the use of reflex vests and a blinking object to alert both passing vehicles and pedestrians for caution of on-going work on the concrete bridge. The excursion and implementation were conducted alongside bridge manager Øyvind Sætra from Vestland County Municipality and according to inspection

regulations from NPRA. Despite good initial weather conditions, it eventually changed into heavy rain and strong winds, impeding the successful administration of non-destructive testing tools, particularly the OMA sensors. Given the inconveniences it entailed, in the field investigation, it is crucial to acknowledge the possible influence this has on the reliability of the results. It is imperative to take these considerations into account to ensure accurate assessment.

It's worth mentioning that even though core sampling is a reliable technique for evaluating the state and degradation of bridge structures, conducting destructive tests was prohibited, as stated earlier. This decision was probably due to a variety of factors, including safety concerns, budgetary limitations, and the possibility of significant harm to the bridge's integrity. The limitation imposed by the prohibition of destructive testing methods highlights the importance of carefully considering the available non-destructive testing methods and interpreting the results obtained from such tests with caution. While non-destructive testing is undoubtedly valuable, the results are often less comprehensive than through destructive testing [4].

The instruments employed for the field investigation were borrowed from OsloMet University and consisted of a rebound hammer, 3D laser scanner, OMA-sensors, Covermeter, and concrete resistivity meter. Figure 9 below illustrates a flow chart that outlines the systematic approach for the assessment plan of the field investigation, incorporating the methods and instruments used.

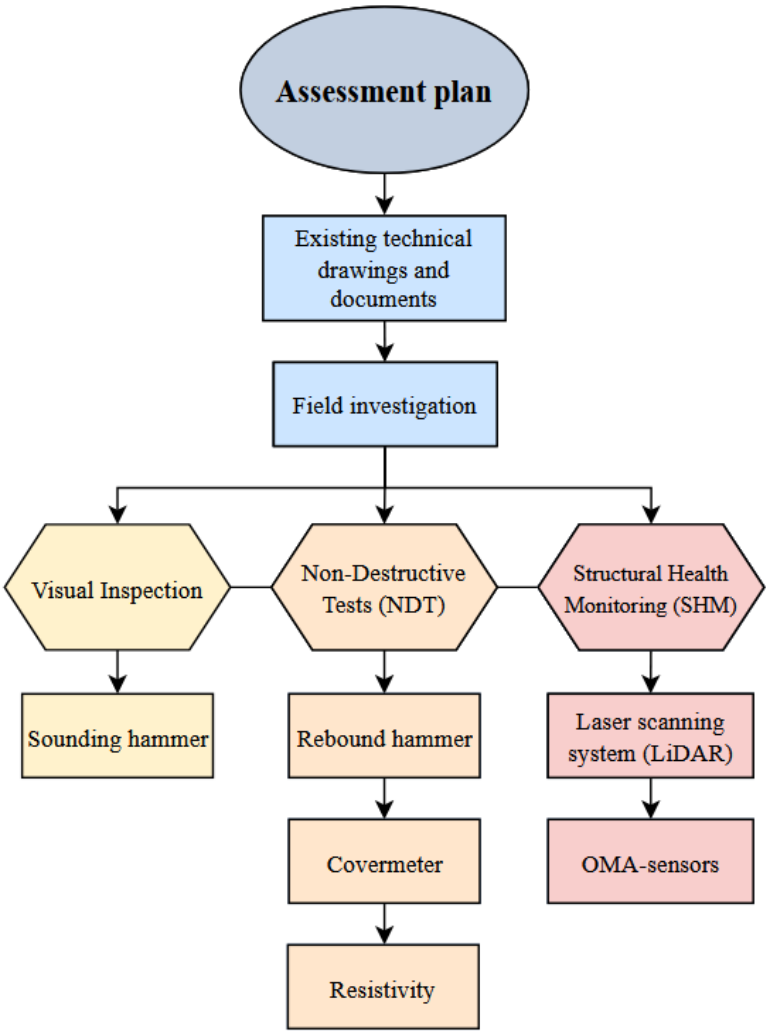

Figure 9: Assessment plan for Øvre Kvamme bridge

Each investigation method will be described in detail in the following sub-chapters, along with its advantages, limitations, and results from the field investigation.

4.1 Project description – Øvre Kvamme bridge

The selected concrete bridge, Øvre Kvamme , is located in Borgund within Lærdal Municipality and was built in 1927. As of 2023, the bridge is 96 years old and is located on fylkesvei 630, connecting Lærdal in the west with Borlaug in the east. The road is relatively quiet, with an annual average traffic volume of approximately 160 vehicles per day, as reported by Brutus. Formerly, this road was a European road – E16, which was rebuilt, and now runs parallel to fylkesvei 630. Despite the road experiencing low traffic, the bridge holds significant importance to the local community and residents. Figure 10 shows the location of the bridge in Norway.

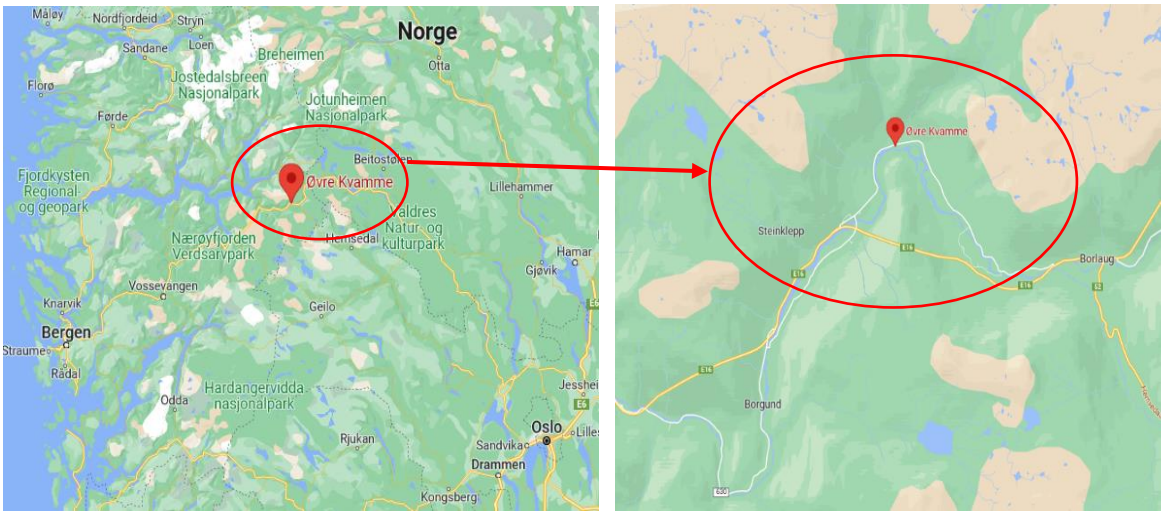

Figure 10: Location of the concrete bridge in Lærdal from Google Maps

The bridge is composed of three concrete slabs spanning approximately 6 meters, resulting in a total length of 18 meters. According to the initial technical drawings provided by Brutus (Appendix B), the bridge exhibits a width of 6.76 meters. It features a single carriageway measuring 6 meters, allowing for two-way traffic. The concrete slabs are 0.36 meters thick, with 0.52-meter-high parapets to ensure the safety of vehicles crossing the bridge. The four supports are built of dry stacked stone with a thin concrete cover coating. The height is approximately 2.6 meters measured from the seabed. However, an additional height has been accounted for to accommodate the foundation depth. Due to the bridge's location on a sloping hill with freshwater flowing from the mountains, the supports vary in height. See Figure 2 for reference.

It should be emphasized that the three concrete slabs display clear indications of cast-in-place concrete and have been reinforced with Ks 40 and St. 00 grade steel. The concrete quality has been specified as B300 in the rebar bending schedule document (Appendix C). In contemporary terms, this is equivalent to a concrete quality of B20, with a compressive strength (cylinder) of 28 MPa. Table 3 provides an overview of the characteristic compressive strength history of concrete, retrieved from Handbook V413 [32].

Table 3: Evolution of concrete strength classifications – Retrieved from [32]

Building year	**NS 427 (1939)**	**NS 427A (1962)**	**NS 3473 (1973-2003)**	**NS 3473 (2003-2010)**		**NS-EN 1992-1-1 (NA 3.1.2)**	
	Concrete quality	Concrete quality	Strength classes	Strength classes	f_{ck} (N/mm^2)	Strength classes	f_{ck} (N/mm^2)
Before 1920	C-concrete	B200	C15	B10	11,2	B12	12
1920-1945	B-concrete	B250	C20	B16	14,0	B16	16
After 1945	A-concrete	B300	C25	B20	16,8	B20	20
		B350	C30	B25	20,3	B25	25
		B400	C35	B28	22,4	B28	28
		B450	C40	B32	25,2	B32	32
			C45	B35	27,3	B35	35
		B600	C55	B45	34,3	B45	45

The bridge underwent rehabilitation around 50 years after its original construction in the 1970s. During this rehabilitation, the middle span of the bridge was strengthened, although the reason for this remains unknown. The available information on the rehabilitation is limited to drawings and a rebar bending schedule prepared at the time. Given the proximity of the strengthening to the age of the bridge, it can be inferred that the outer spans are likely the most crucial. For the dimensions of the bridge, refer to Figure 11 below, retrieved from a technical drawing in Brutus. Additional information on the dimensions and rebar bending schedule can be found in Appendix B and Appendix C.

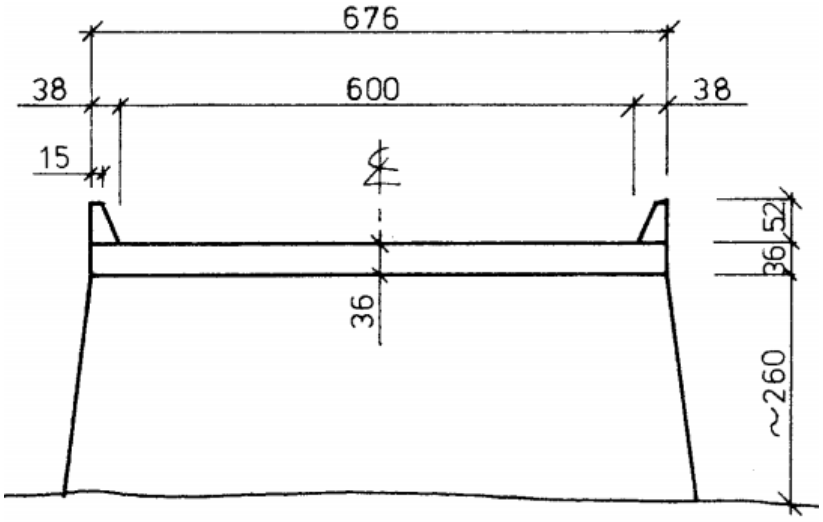

Figure 11: Dimensions of Øvre Kvamme bridge - Retrieved from Brutus

On September 16 and 17, 2021, BruKon AS conducted a special inspection of the Øvre Kvamme bridge, and an accompanying report with the findings from the inspection was made. [47]. The inspection revealed that the bridge was in very bad condition, and most of the severe degradation was found on the bottom surface of the concrete slabs. Corrosion and carbonatization were identified as the predominant issues affecting the three slabs. Based on the findings, a strong recommendation was made to reduce the bridge from two-way to one-way centric driving [47]. This decision was based on the extensive damage observed, particularly on the sides of the slabs beneath the parapets. By implementing one-way centric driving, the most critical areas would be subjected to lower loads and stresses. It was concluded that the concrete bridge condition falls under the category of *3B – Major damage/deficiency, and measures need to be taken within 1-3 years* [33].

4.2 Visual inspection

An accurate assessment of a bridge's structural condition requires in situ investigations and information about its construction and operation history. Visual inspection is the most common and highly important technique used in such assessments which is invaluable and typically conducted early in the evaluation process [3]. Visual inspection typically involves closely examining the surface and internal features to identify any visible flaws, defects, or irregularities that could compromise safety, functionality, or aesthetics of a structure [3]. These tools are selected based on the type of structure or product being examined and the specific details that need to be evaluated [3]. Visual inspections are typically conducted with some simple tools like a hammer, ruler, and camera.

A camera can be a useful tool for capturing images of the area of concern, allowing for analysis of any indications of degradation. Additionally, these images can be used for comparative purposes, to monitor any changes over time, or to assess the effectiveness of any repair work that has been carried out. The sounding hammer is another highly valuable tool, it is mostly utilized to tap on concrete surfaces to assess the condition of the underlying material. It is used to examine the density, strength, and consistency of the concrete element. The hammer’s impact generates vibrations that are perceptible to an experienced inspector, providing important details about the concrete’s quality and identifying potential defects that may require further examination. The measuring tool is another indispensable instrument for visual inspection. This tool is utilized to measure the width and length of cracks, as well as the thickness of the concrete cover. Such measurements are important in evaluating the extent of damage [48].

However, it is important to remember that performing visual inspections without the use of NDT and/or DTs has received considerable criticism for being unreliable [3-4]. The effectiveness of this method depends a lot on the expertise, experience, and quality of equipment utilized, all of which significantly impact the results. Table 4 summarizes the advantages and limitations of performing visual inspection.

Table 4: Advantages and limitations of visual inspection

Advantages	**Limitations**
- Cost-effective	- Limited accuracy & depth
- Quick and efficient	- Limited scope & accessibility
- Broad coverage	- Human error

As described in Sub-chapter 4.1, the bridge consists of three slabs and four supports, each assigned a letter and a number for easy orientation throughout the field investigation. Figure 12 provides an orientation map that showcases the labeling system, with the supports designated as B1-B4 and the slabs denoted as A1-A3. This mapping is essential to identify the key types of deterioration and their corresponding locations throughout the investigation.

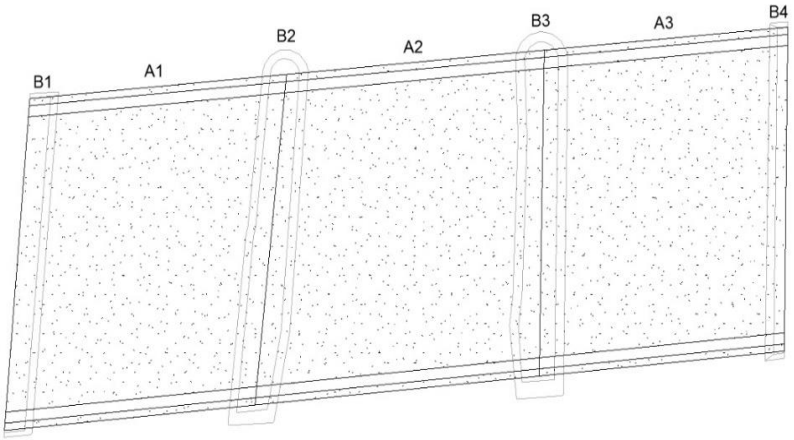

Figure 12: Top-down view of the orientation map of Øvre Kvamme from Revit

When performing a visual inspection of the Øvre Kvamme bridge, it was observed that the top surface of the bridge was in good condition, exhibiting a solid asphalt coating without any signs of damage, openings, or deterioration. It should be noted that the bridge is situated in a Nordic environment characterized by severe rain, snow, and wind, in addition to water flowing from the mountains beneath it. These factors could play a significant role in the observed deterioration during the visual investigation. With that being noted, many traces of efflorescence, moss, and small cracks were detected on the sides of the concrete bridge on the parapets. These findings are unlikely to result in a reduction of the bridge's structural load capacity or overall lifespan.

Upon inspecting the bridge, it was identified some efflorescence, especially on the bottom of the concrete slabs and on the supports, see Figure 13 for reference. Efflorescence on concrete is the result of lime-rich water penetrating through cracks, dissolving calcium hydroxide. Over time, this dissolved calcium hydroxide can form calcium carbonate, forming white or grey areas on the concrete surface. While efflorescence is a cosmetic issue, it may also indicate the presence of underlying problems of greater severity [49].

Figure 13: Efflorescence & small cracks detected on supports

Additionally, it was recorded that the concrete bridge exhibited considerable degradation beneath the bridge, with spalling and exposed corroded reinforcement bars being a prominent issue. The extent of the damage was particularly evident along the outer edges of the bridge structure and heavily concentrated on the underside of the bridge slabs. All three slabs showed significant signs of spalling, with the exposed reinforcement bars exhibiting noticeable corrosion. This corrosion could be a sign of long-term exposure to moisture and oxygen, which can lead to further deterioration of the steel reinforcement and ultimately compromise the structural integrity of the bridge. The corrosion of steel leads to the formation of rust, which occupies a larger volume than the original steel. As a result, the expansion causes tensile stresses within the concrete, eventually leading to further cracking, spalling, and delamination [50]. Figure 14 displays the different deterioration mechanisms of cracking, spalling and delamination.

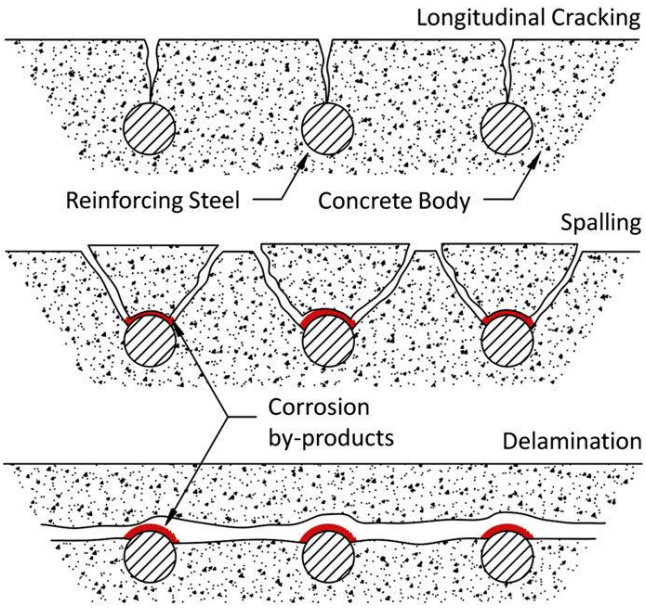

Figure 14: Deterioration type due to reinforcement corrosion – Retrieved from [51]

The spalling observed on the bridge structure indicates that the concrete has suffered significant deterioration mechanisms such as exposure to freeze-thaw cycles, chloride, or carbonation [52]. The absence of indications of freeze-thaw cycles and minimal evidence of chloride exposure suggest that carbonation is the most probable cause. Carbonation is the leading factor for reinforcement corrosion and, thus, spalling. The location of the spalling with exposed rebars, particularly along the edges and underneath the slabs, suggests that moisture and water infiltration have played a significant role in the deterioration of the concrete. When carbon dioxide from the air enters the concrete and reacts with calcium hydroxide, it results in carbonation, which produces carbonates [50]. This reaction decreases the pH of the pore solution to a point where the passive film on the steel becomes unstable [50]. The carbonation front penetrates the concrete gradually, and in well-made concrete, it may increase at a rate of up to 1.0 mm per year [50].

Figure 15 displays some of the identified areas of spalling with exposed corroded rebars, as well as indication of small cracks in the surroundings of the spalling areas most likely developed by reinforcement corrosion.

Figure 15: Spalling with exposed rebars on the sides & bottom of the bridge slabs

It was detected both uniform corrosion and pitting on the bridge. Furthermore, the notable corrosion observed beneath the concrete bridge slabs is likely to play a critical role in the progression of other detected deteriorations during the field investigation. Corrosion that occurs in reinforcing steel is the most dominant factor contributing to the deterioration of steel as it heavily weakens the structural integrity of concrete over time, both in structural load capacity and its durability [50]. Moreover, if the reinforcement is positioned with a small concrete cover, it can potentially result in early damage [5].

Analyzing the cracks present in a reinforced concrete structure is vital to comprehending their behavior and identifying any potential defects. Special emphasis must be placed on examining structural cracks to ensure their proper evaluation [5]. The major cracks detected through visual inspection were identified as plastic shear cracks and longitudinal cracks. Figure 16 below displays some of the identified cracks, including plastic shear crack that was identified on abutments B1 and B4, with the addition of a longitudinal crack on the nearest slab. Furthermore, the identification of smaller cracks on Øvre Kvamme was also made, however, the longitudinal cracks that were parallel to the reinforcement and considered the largest and most critical were found on slabs A1 and A3. These cracks result from drying shrinkage, reinforcement corrosion, or structural overloading in this case. Figure 17 displays a critical longitudinal crack detected throughout the entire slab A3.

Figure 16: Efflorescence, plastic shear & longitudinal crack detected on A1 and B1

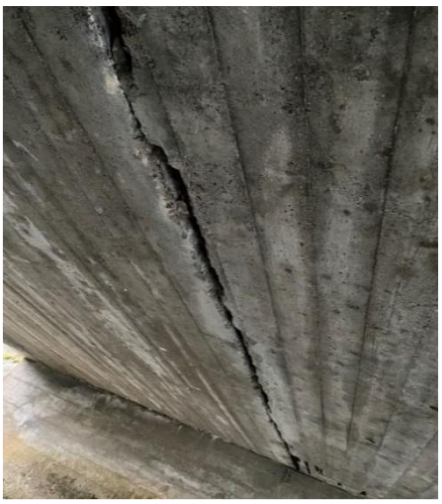

Figure 17: Longitudinal crack and spalling observed on slab A3

During the visual inspection, the cracks detected in the structure were measured using a ruler. It was observed that there were cracks of various sizes, ranging from a few millimeters to the largest crack identified on slab A3, which was a combination of a longitudinal crack with exposed reinforcing rebar and spalling, as displayed in Figure 18. The width of it was approximately 60 millimeters. The identified longitudinal crack may have occurred as a consequence of reinforcement corrosion caused by carbonation. These forms of detected deterioration were likely happening simultaneously and were progressively expanding throughout slab A3.

Figure 18: Longitudinal crack measured with exposing rebar

The supports, particularly B1, B2 and B4, exhibited noticeable deterioration, with erosion being the most probable cause. The continuous exposure to running water and wind-borne particles

over time likely contributed to this erosion [50]. Figure 19 highlights the loss of the concrete layer on B2, potentially due to erosion.

Figure 19: Potential erosion detected on support pier B2

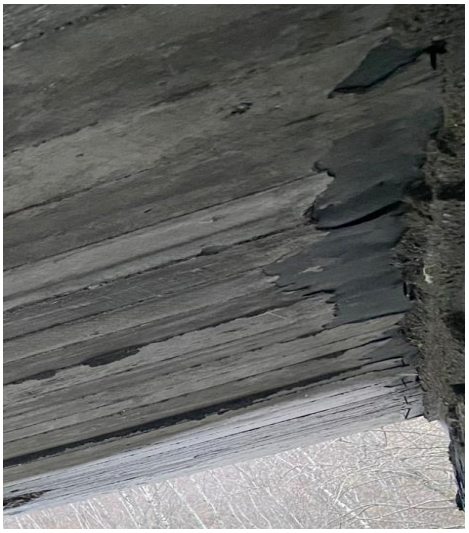

Figure 20: Delamination on the bottom of slab A2 on support pier B3

It was observed that parts of concrete on slab A1 had separated, indicating delamination as shown in Figure 20. Delamination may be caused by air and running water becoming trapped beneath a prematurely closed or densified mortar surface, typically leading to the separation of some millimeter of the top layer of mortar from the underlying concrete [50] [51]. These voids create weakened areas just beneath the surface, which can lead to detachment during loading. Delamination of concrete can also be caused by factors such as freeze-thaw of trapped water, insufficient vibration during casting, improper troweling, excessive water-cement ratio, and excessive loading. The delamination was confirmed with the sounding technique by tapping on the structure with a heavy object on the concrete. The process includes striking its surface and the resulting sound is analyzed. The sound can give an indication of an ongoing deterioration; a solid concrete surface will produce a clear, ringing sound when struck, while a surface with spalling, delamination, or voids will produce a more hollow or flat sound [53].

The visual inspection has revealed significant deteriorations that require further attention and examination. These deteriorations are crucial as they can greatly impact the overall performance and functionality of the concrete bridge. A mapping figure including the size and location was created and shown in Figure 21 to present the findings from the visual inspection. The findings depicted reveal that most of the severe damage primarily affects the bottom surface of the bridge slabs, except for erosion observed on the supports B1, B2, and B4. Furthermore, the figure illustrates multiple damaged and deteriorated areas across all spans, each exhibiting approximately the same degree of severity.

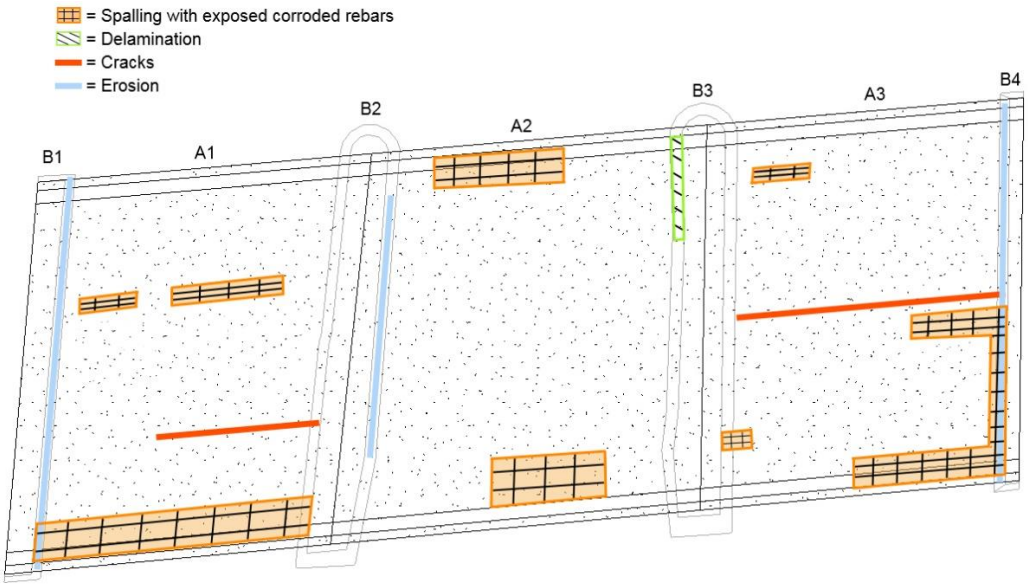

Figure 21: Mapping of detected deteriorated areas

4.3 Non-destructive testing

Conducting a comprehensive examination of existing infrastructure is a persistent challenge. As it is often impeded by several factors that can hinder the acquisition of accurate and realistic analyses. Overcoming challenges requires addressing factors such as geometry, uncertainties in material properties, unfamiliar construction techniques, and limited relevant information such as drawings. Non-destructive tests are a promising solution when the condition of a structure is unknown [3]. Various NDT tools are available for assessing the condition of concrete structures, with each tool's effectiveness depending on the specific problem observed [3]. However, due to limited access and financial means, only five NDTs have been utilized as previously mentioned. Table 5 presents some of the advantages and limitations of conducting non-destructive tests [3].

Table 5: Advantages & limitations of NDTs

Advantages	**Limitations**
- Effective & accurate condition assessment - Does not harm the structural integrity of the structure - Quick & easy to perform	- The appliance of multiple NDT is often required to assess correctly - No "best" instrument to detect all types of deterioration - Trained personnel for data collection & analysis are required

4.3.1 Rebound hammer

Ernst O. Schmidt developed the rebound hammer during the 1950s, and has since been refined and updated by Proceq SA [54]. This non-destructive testing method is classified as a miscellaneous method of non-destructive testing and is intended to evaluate the in situ compressive strength of concrete while preserving the structure's properties or aesthetics. The rebound hammer testing method utilizes the rebound of an elastic mass, where a plunger rod is pressed against a hardened concrete base, which triggers a spring mechanism to apply a specific level of impact energy. The responding rebound of the mass during the impact is measured and recorded as a rebound number. This rebound value depends on the quality of the concrete and provides a valuable indication of the compressive strength [54-55]. Figure 22 depicts the mentioned mechanism of the rebound hammer.

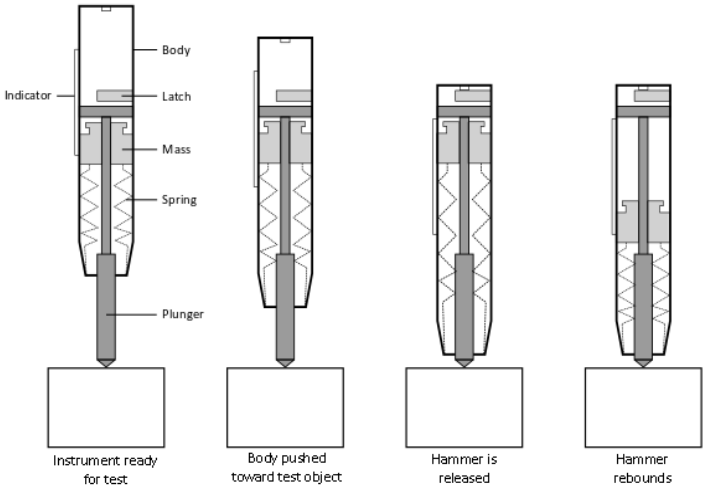

Figure 22: Mechanism of rebound hammer - Retrieved from [56]

While the rebound hammer tool is a highly reliable and robust non-destructive testing instrument, caution should be exercised when used. The results obtained from the instrument can be influenced by numerous factors [54]. Carbonation may be one of the main contributors to significant influence on the rebound hammer results. The carbonation of concrete causes the interior region of concrete to become harder than the surface region. As a result, there is a potential for overestimation of the concrete strength. This is because the hardening of the interior region is not detectable, resulting in higher strength readings when compared to non-carbonated concrete [54-55]. Other important affecting factors include the concrete mix, concrete age, surface- and environmental conditions [54-55].

The rebound hammer SilverSchmidt produced by Proceq was utilized on the Øvre Kvamme bridge, and a total of 12 compressive strength tests were recorded and collected in HammerLink software. For each obtained compressive strength value, ten impacts were performed, with each impact point spaced at least 25 mm apart [15, 40]. The results obtained from these ten impacts were recorded, averaged, and displayed on the instrument. The recorded compressive strength values ranged from 34 MPa to 80 MPa. The results obtained from the HammerLink software and chosen settings for the software and instrument can be seen in Figure 24 [40].

Figure 23: Rebound hammer performed in situ

Name	Date & Time	Mean val...	Averaging mode	Valid/Total	Conv. curve	Form factor	Carbonation factor
Test 1	11/09/2022 8:18 PM	34.5 MPa	Mean	10/10	Curve EU	Cylinder (81%)	1.00
Test 2	11/09/2022 8:24 PM	74.5 MPa	Mean	10/10	Curve EU	Cylinder (82%)	1.00
Test 3	11/09/2022 8:31 PM	34.0 MPa	Mean	10/10	Curve EU	Cylinder (81%)	1.00
Test 4	11/09/2022 8:39 PM	53.5 MPa	Mean	10/10	Curve EU	Cylinder (83%)	1.00
Test 5	11/09/2022 8:45 PM	46.0 MPa	Mean	10/10	Curve EU	Cylinder (82%)	1.00
Test 6	11/09/2022 8:56 PM	60.0 MPa	Mean	10/10	Curve EU	Cylinder (82%)	1.00
Test 7	11/09/2022 9:05 PM	46.0 MPa	Mean	10/10	Curve EU	Cylinder (82%)	1.00
Test 8	11/09/2022 9:13 PM	80.0 MPa	Mean	10/10	Curve EU	Cylinder (84%)	1.00
Test 9	11/09/2022 9:21 PM	34.0 MPa	Mean	10/10	Curve EU	Cylinder (81%)	1.00
Test 10	11/09/2022 9:26 PM	38.0 MPa	Mean	10/10	Curve EU	Cylinder (78%)	1.00
Test 11	11/09/2022 9:32 PM	75.5 MPa	Mean	10/10	Curve EU	Cylinder (82%)	1.00
Test 12	11/09/2022 9:39 PM	66.0 MPa	Mean	10/10	Curve EU	Cylinder (80%)	1.00

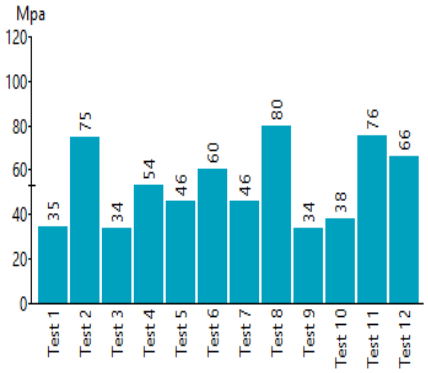

Figure 24: Rebound hammer tests - Retrieved from HammerLink [40]

The overall mean value of the 12 readings was registered as f_{ck} = 53.5 MPa, while the median value was f_{ck} = 50 MPa. The mean value was found to be identical to the measurements conducted in the special inspection by BruKon AS [47]. However, it should be noted that the lowest reading of 34 MPa was measured in two different locations, while the highest impact reading was recorded as 80 MPa. The results collected from the rebound hammer gives an indication that the Øvre Kvamme bridge was constructed with a higher concrete quality than anticipated, as it was documented to be of concrete class B20. The bridges remarkable ability to withstand the various stresses over these past 96 years is evident to its construction. However, it is important to acknowledge that the data obtained from the hammer test may have been compromised due to detected carbonation. Resulting in far less accurate measurements.

The highest and lowest recorded compressive strength from the testing can be seen in Figure 25. Despite these results, it needs to be emphasized that the moisture levels in the concrete slabs

due to heavy rain and strong winds could have significantly impacted the readings. Additionally, it is important to note that the concrete cover is small, and it's crucial to do the measurements in areas without reinforcement bars directly above. Some of the measurements may have been impacted by this, as the spacing between the reinforcement was found to be very inconsistent, and thus challenging to determine the optimal locations for testing.

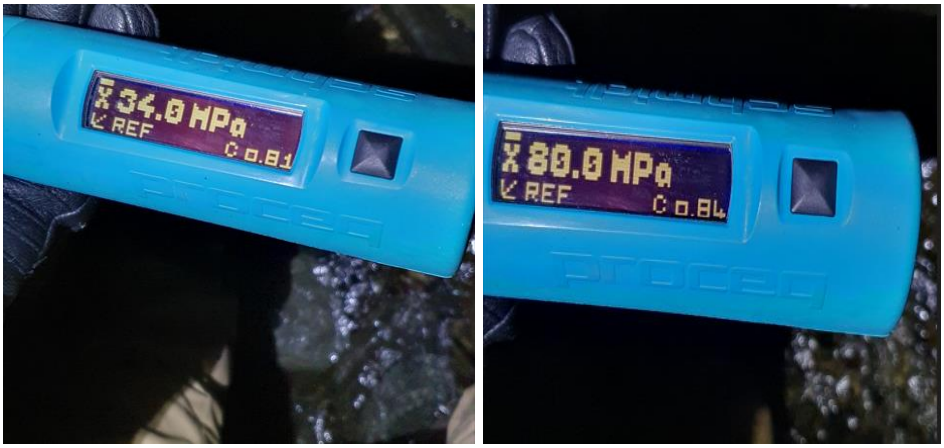

Figure 25: Lowest and highest recorded compressive strength

The rebound hammer was performed on four different locations per slab, each location is on the outer edges of the concrete slabs. These locations were carefully selected to represent the locations where the strength of the concrete is typically lower compared to the center of the slab. All the rebound hammer test results and locations are shown in Figure 26 and were performed in the numbered order.

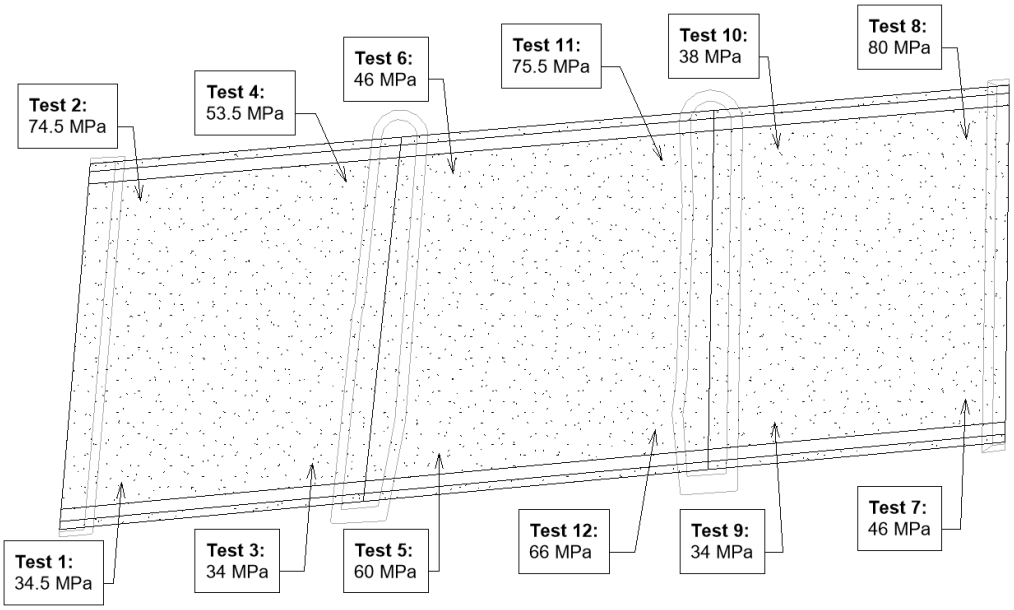

Figure 26: Mapping of performed rebound hammer tests – Developed in Revit

4.3.2 Covermeter

The depth of the concrete cover is a crucial consideration in the design and construction of concrete structures, particularly for ensuring its minimum service life [57]. Alongside the quality of the concrete mix, the concrete cover plays a significant role in determining the duration before aggressive mechanisms such as chlorides and carbonation can penetrate the concrete and reach the steel reinforcement bars [57]. The recommendations for the concrete cover are provided by all the major standards series based on the environmental exposure class that the structure is subjected to. The two most frequently used NDT instruments to identify the existing concrete covers are the magnetic eddy current technique, which is also known as the covermeter, and ground penetrating radar [57]. In this thesis, the covermeter was used to obtain information about the reinforcement.

The covermeter is an electromagnetic technique utilized to locate steel reinforcement, measure the rebar diameter, and determine the thickness of the concrete cover [39, 58]. It operates through the use of electromagnetic pulse induction technology, where the coils in the probe are periodically charged with current pulses to generate a magnetic field [39, 58]. As the magnetic field interacts with any electrically conductive material present in the concrete, such as the reinforcing steel bars, it generates eddy currents in the opposite direction, which produce a magnetic field. By analyzing the changes in the electromagnetic field, the instrument can determine the presence, diameter, spacing and concrete cover of the reinforcement bars [39, 58]. Figure 27 illustrates the concept of the covermeter testing method.

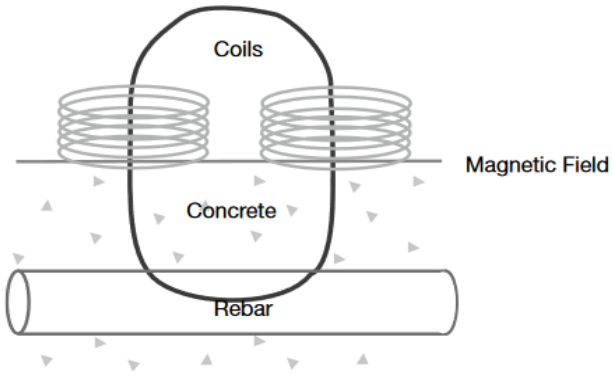

Figure 27: Covermeter mechanism - Retrieved from [39]

However, the use of covermeter is limited when the reinforcement intersects with installed grids, anchors, and other metals, aggregates with magnetic properties are present in the concrete, and when the concrete cover is large [39]. Additionally, the covermeter is vulnerable to the influence of moisture level, temperature, oxygen content, and carbonation [39]. The pH level of the concrete decreases once the concrete structure carbonates, and as a result, it causes

a change in the magnetic properties of the reinforcing steel bars. Consequently, this alteration in magnetic properties can influence the precision of the covermeter readings.

A Profometer 650 AI was used for the covermeter tests performed during the field investigation. The absence of reinforcement drawings of the entire bridge was found to be critical for the modeling purposes, making it crucial to perform a covermeter test. The only available reinforcement drawings are found in Appendix C and are obtained from Brutus. The reinforcement drawing includes a rebar bending schedule for the middle span from when it was supposedly reinforced in the 1970s. By conducting a covermeter test, a more accurate understanding of the structure and its composition can be obtained, improving the accuracy in the FEM software.

Proceq manufactures Profometer 650 AI and consists of a touch screen device and a universal probe with a ruggedized scan cart connected to the touch screen device for registering the readings. The measurements are performed by dragging the device along a line perpendicular to the reinforcement to prevent overlapping results from the different reinforcement layers. Therefore, in most cases, inspection involves multiple line checks forming a network to ensure accurate measurements [58]. Additionally, the Profometer has a depth limitation of approximately 80 mm, making it suitable for mainly detecting the placement of steel reinforcement [58]. Given the low concrete cover in the bridge, this feature provided successful results.

During the assessment of Øvre Kvamme bridge, the Profometer 650 AI was utilized to obtain readings on the concrete structure. The longitudinal reinforcement of two spans was examined specifically because these reinforcement bars were considered the most critical, displayed significant corrosion, and were located closest to the surface. The instrument was used in both the single-line mode and locating mode to detect the concrete cover depth and identify the reinforcement bars. The single-line mode was employed to assess the concrete cover depth and spacing along a single line, while the locating mode was utilized to locate and identify the diameter [39].

Figure 28: Profometer performed in situ

Once the rebars were identified, they were marked on the bottom surface of the concrete slabs using chalk to provide a visual representation of the arrangement, as shown in Figure 28. This marking process facilitated the conduction of other potential non-destructive testing on the slabs. The measurements were only conducted on slabs A1 and A3 as the middle slab properties were already known from the drawings provided in Brutus. Furthermore, there was insufficient time to conduct a more extensive investigation. The results obtained from slab A1 and A3 were useful references to be compared with the existing drawings of slab A2. All of the readings were recorded on the Profometer device, and later imported to the ProfometerLink software for further analysis.

The results obtained from slab A1 can be seen in Figure 29 with a total of 81 readings. The x-axis showcases the bridge width measured with the scanning cart, and the y-axis illustrates the concrete cover depth. The lowest reading recorded was measured to be 16 mm, and the highest at 63 mm. Upon further analysis, it was determined that the concrete cover depth measured a mean value of 29.1 mm, nearly identical to the 30 mm described in the existing drawings.

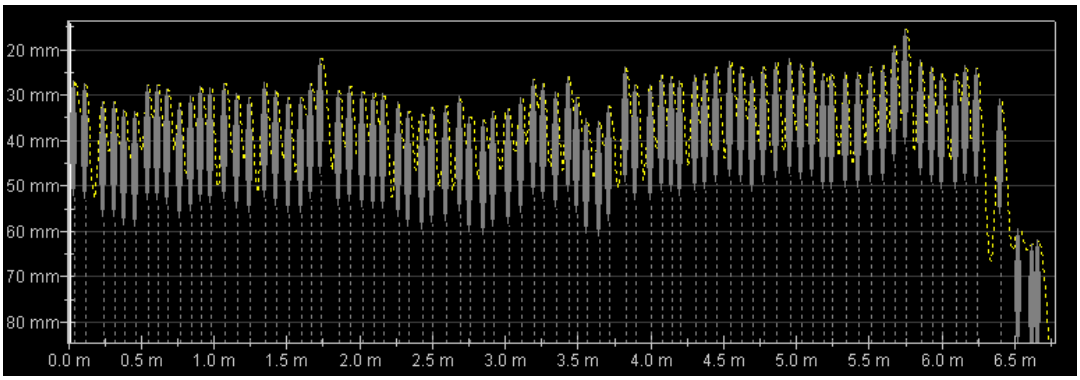

Figure 29: Detected cover depth on slab A1 from ProfometerLink [39]

The results obtained from slab A3 were found to be quite similar to A1. Figure 30 presents the data collected from the Profometer, which was later exported from the ProfometerLink software. A total of 78 readings were measured, ranging from a minimum of 19 mm to a maximum of 66 mm, and these readings were similar to those recorded on slab A1. The mean value of the readings on slab A3 was found to be 28.1 mm, which is nearly consistent with the readings on slab A1. Thus, these results reveal that the side slabs has appriximately the same concrete cover as documented of the middle span.

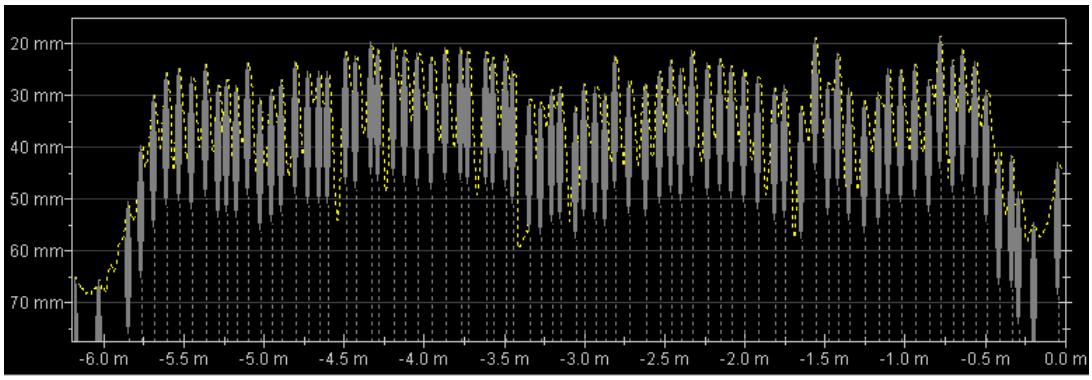

Figure 30: Detected cover depth on slab A3 from ProfometerLink [39]

Due to time constraints, measurements using locating mode on the Profometer were only conducted on slab A1 to determine the location and diameter of the rebars. It was assumed that slab A3 yielded the same results. The results, shown in Figure 31, include a total of 82 readings and a calculated mean value of 24.90 mm using the software. However, to simplify the presentation, the figure provides a concise representation of the results in Excel. The mean diameter value of 24.90 mm aligns pretty well with the bending schedule of 25 mm for the middle span, indicating that the reinforcement of the reinforcement arrangement is likely identical to slab A1 and A3.

Number	1	2	3	4	5	6	7	8	9	10	11	12	13	14	15	16	17	18	19	20	21
Diameter	26	28	27	26	24	24	22	26	25	25	27	28	27	27	26	25	25	24	23	24	23
Number	22	23	24	25	26	27	28	29	30	31	32	33	34	35	36	37	38	39	40	41	42
Diameter	25	26	26	26	28	26	27	26	24	25	25	24	24	27	25	24	24	27	29	25	25
Number	43	44	45	46	47	48	49	50	51	52	53	54	55	56	57	58	59	60	61	62	63
Diameter	30	26	27	24	24	20	23	24	24	22	24	27	26	24	24	23	23	29	23	22	23
Number	64	65	66	67	68	69	70	71	72	73	74	75	76	77	78	79	80	81	82		
Diameter	22	23	23	25	24	22	23	25	27	40	22	20	30	22	24	18	22	23	25		
Mean	24,90																				
Median	25																				

Figure 31: Locating mode data on slab A1 retrieved from ProfometerLink

Despite obtaining consistent results for rebar diameter and concrete cover, the measurements of reinforcement spacing yielded contrasting findings. According to the drawings, a spacing of 150 mm is specified. However, the actual measurements showed significant variation, ranging from a minimum of 66 mm to a maximum of 165 mm, with a mean value of 84 mm. This inconsistency was also observed in the measurements of concrete cover. Over a length of 6.5 m, a total of 81 measurements were taken, suggesting that the spacing in the side spans are lower than specified in the drawings. It is important to acknowledge that the results obtained from the Profometer tests may have been influenced by factors such as presence of other

metallic objects, improper and outdated calibration, surface conditions and the proficiency of the user. However, despite the possibility for errors, the measured results from slab A1 and A3 showed reasonable results of diameter and concrete cover when compared to existing information on the concrete and reinforcement arrangement of slab A2. The documented spacing is found to be considerably higher than the actual measurements obtained from two Profometer tests and measurements conducted with a ruler on visible reinforcement. These findings will enable a more accurate and correct model assembly in the finite element analyses.

4.3.3 Electrical resistivity

The electrical resistance of a material is a useful metric for a diverse range of applications, as it reflects the material's capacity to impede the movement of ions when subjected to an electric field [59]. Among the methods for testing electrical resistance is the *Wenner* method, which employs a four-probe approach. Originally developed by Wenner at the National Bureau of Standards in the 1910s to identify soil strata in geological fieldwork, this method has since been adapted for concrete applications over time [59]. The Wenner four-probe test for measuring the electrical resistivity of concrete involves the placement of four uniformly spaced electrodes on the material [59]. Corrosion occurs through the exchange of electrons and ions between metals and the solution, and the rate of this reaction depends on the variance in potential [59]. By employing four equally spaced linear electrodes in this technique, the surface electrical resistivity of the concrete can be measured, with the two outer electrodes applying the AC current and the inner probes recording the electrical potential [59]. Measuring the concrete's resistance allows estimation of the speed at which this exchange occurs. Due to the better electrical conductivity of steel, measurement must be conducted in areas with no reinforcement [59]. Figure 32 displays the principles of electrical resistivity, more specifically on the product Resipod from Proceq, utilizing the Wenner method.

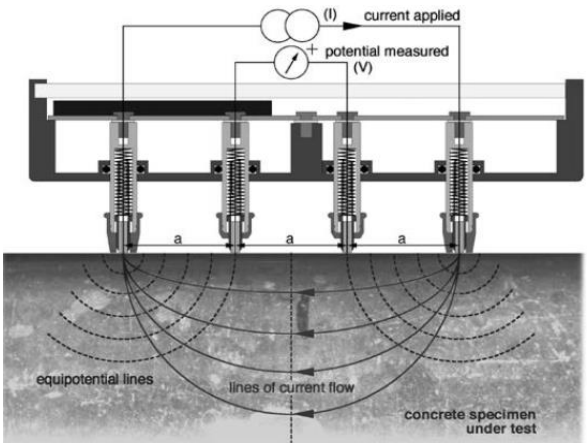

Figure 32: Mechanism of the Resipod - Retrieved from [41]

To perform the Resipod, it is important to establish a solid connection between the NDT-instrument and the concrete surface for accurate and dependable measurements. To ensure a reliable reading, it was recommended to dip the Resipod contacts into water multiple times before taking the measurement [41]. Additionally, it is advised to utilize a shallow container that can be pressed against the bottom to fill the reservoirs adequately. To obtain stable and accurate measurements, it is important to firmly press the Resipod down until the outer two rubber caps contacts the tested surface [41]. After successful completion of the measurement, a resistance value will be displayed, which can be categorized into four different groups. Table 6 displays the resistivity measurement groups with a description of each range of value.

Table 6: Estimation of potential corrosion [41]

When ≥ 100 kΩcm	Negligible risk of corrosion
When = 50-100 kΩcm	Low risk of corrosion
When = 10-50 kΩcm	Moderate risk of corrosion
When ≤ 10 kΩcm	High risk of corrosion

Furthermore, when measuring electrical resistivity, the presence of rebars can disrupt the readings due to their superior current conductivity in comparison to the surrounding concrete. This issue is especially prominent when the covering depth is below 30 mm [41]. To minimize this effect, it's important to avoid placing the probe directly above the reinforcement bars or in parallel with them. The most suitable measurement orientation should be determined based on the spacing of the rebars relative to the probe spacing [41]. Figure 33 illustrates the most preferred orientation when measuring with the Resipod on reinforced concrete structures. The most optimal method involves placing it diagonally as seen to the left. However, if the reinforcement spacing is narrow, the optimal placement is parallel to the reinforcement, as depicted to the right.

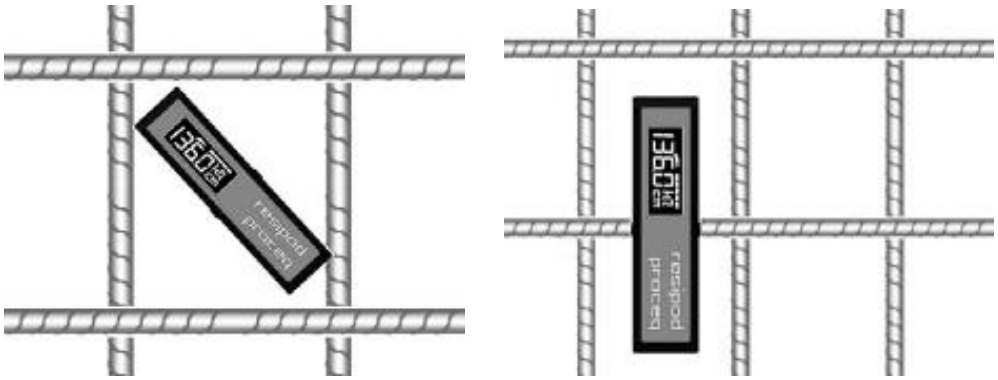

Figure 33: The optimal orientation of Resipod - Retrieved from [41]

Using a Proceq Resipod, measurements were conducted to assess the probability of corrosion and corrosion rate on areas without any visible signs of corrosion. The objective was to identify any potential ongoing corrosion in locations other than what has been identified. The presence of moisture on the concrete during the measurements may have influenced the results, as moist materials tend to be more conductive compared to dry ones. Figure 34 shows the test carried out with Resipod on the Øvre Kvamme bridge during the inspection. To prevent placing the Resipod directly under the reinforcement bars, it was positioned between specific areas of the concrete marked with chalk from the Profometer tests.

Figure 34: Concrete resistivity instrument performed in situ

The recorded data collected on site were further analyzed with the ResipodLink software [41]. Given the limited time available, only ten readings were measured on the bridge, four on slab A1, three on slab A2, and three on slab A3. The measurements were taken on areas with no visible signs of corrosion to detect potential internal damage. Figure 35 presents the results obtained when importing the data to the ResipodLink software, and its calibrated settings.

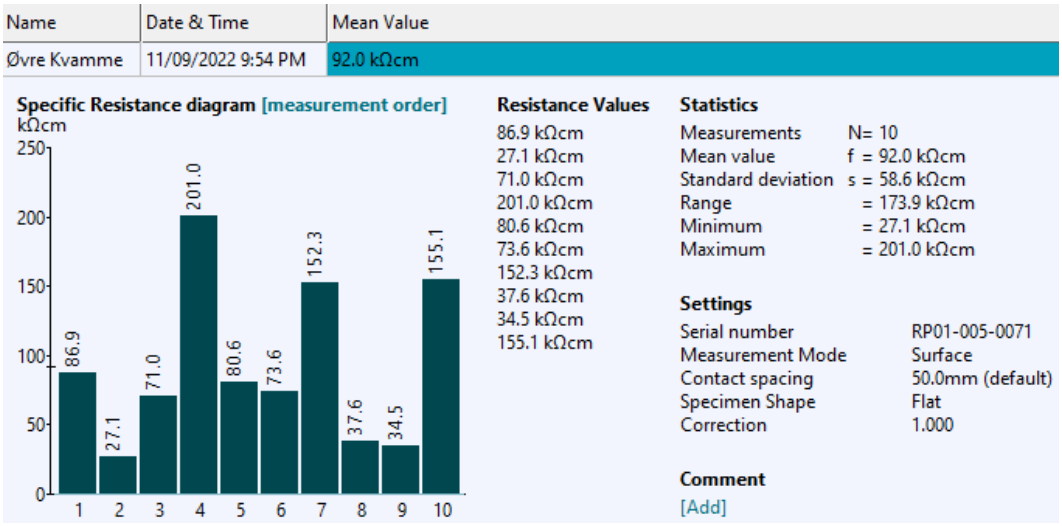

Figure 35: Resipod resistivity results – Retrieved from ResipodLink [41]

Measurements were taken on the three different slabs: slab A3 (readings 1-4), slab A2 (readings 5-7), and slab A1 (readings 8-10). The resistivity measurements were ranging a lot with the lowest recorded value of 27.1 kΩcm, and the highest value 201 kΩcm, both obtained from slab A3 as shown in Figure 36 below. The collected resistivity results indicate large discrepancies,

suggesting the presence of potential hidden corrosion beneath the concrete surface. This is particularly evident in results 2, 8 and 9, which show a moderate risk of corrosion according to Table 6. The findings highlight that slabs A1 and A3 are at highest risk of corrosion, as expected since the bridge's middle slab was reinforced in the 1970s. Furthermore, results 5 and 6 taken on the middle slab suggests a low risk of corrosion.

Figure 36: Highest & lowest resistivity measured in situ

However, it is important to note that electrical resistivity measurements can be significantly influenced by factors such as carbonation, concrete mix, temperature, and moisture levels [41, 59]. Consequently, it is essential to interpret the findings obtained from the Resipod with caution. The results are best interpreted in conjunction with other complementary test methods in order to obtain a comprehensive assessment of the bridge's condition. A destructive test for carbonation, which assesses the penetration depth, is another method that can effectively be used in conjunction with concrete resistivity measurements.

4.4 Structural health monitoring

Structural health monitoring is a non-destructive testing method that traditionally employs one or multiple sensors installed on a structure to monitor and evaluate its response, with the aim of detecting any abnormal behavior and predicting potential deterioration. This technique is highly beneficial as it offers reliable insights into a structure's response, capacity, and expected lifespan, as well as enabling reverse engineering [3, 60]. Furthermore, employing LiDAR tools for 3D scanning and measurements of deteriorated existing structures is a valuable method for gathering data to increase the accuracy of modeling and structural analyses [60].

In recent years, numerous SHM systems have been developed and utilized to enhance bridge maintenance strategies. The majority of these systems employ similar fundamental components, including sensor and laser scanning instrumentation for geometric calibrations,

and structural assessment through model analysis [3]. Table 7 displays some of the important advantages and limitations of conducting structural health monitoring on a concrete bridge.

Table 7: Advantages and limitations of SHM applications [3, 60]

Advantages	Limitations
- Accurate and precise measurements - Real-time bridge assessment - Reliable for both short-term and long-term assessment	- Costly and expensive to maintain - Wireless sensors rely on battery power - Data interpretation requires trained personnel for analysis - Weather conditions can heavily affect the instrument if it's in the open field

4.4.1 3D laser scanning

In recent years, LiDAR systems has found several applications in health monitoring and damage detection of structures [3, 60]. The ability of laser scanning to create texture-mapped 3D point clouds makes it an effective tool for documenting quantitative information about the current conditions of bridges as well as its precise geometry [3, 60]. By capturing individual laser scans of a scene from various viewpoints, a complete 3D record of a damaged bridge can be created, making it a very valuable optical non-destructive testing method [3, 60]. LiDAR devices can be categorized into two main groups, stationary devices, also known as Terrestrial Laser Scanners (TLS), and mobile devices like drones, which are referred to as Mobile Laser Scanners (MLS) [60]. It is important to note, however, that TLS is limited in terms of accessibility, but it generally captures more detailed and precise point clouds than MLS, despite requiring more manual labor and time [60]. Figure 37 showcases the various applications of LiDAR systems and devices for structural health monitoring.

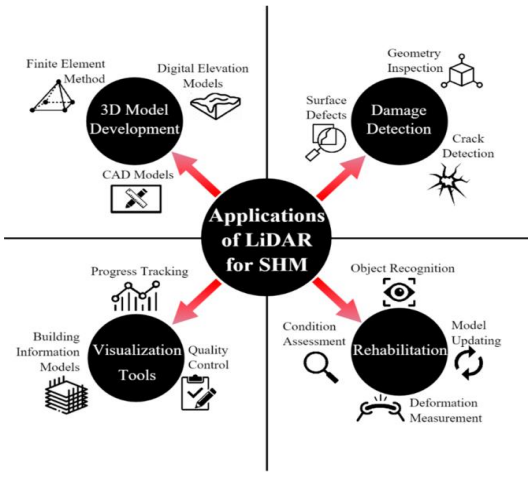

Figure 37: Applications of LiDAR for SHM - Retrieved from [60]

In the field investigation, a terrestrial laser scanning device named BLK360 produced by Leica Geosystems, a manufacturer from Switzerland, was utilized [61]. The Leica BLK360 is a highly compact laser scanner that can collect two different types of image data. The HDR 13-megapixel camera can generate colored point clouds and 360° panorama images at a rate of up to 680,000 points per second using its three cameras. It also features an infrared camera for thermographic imaging [62]. The scanner has a range of up to 60 m and offers high ranging accuracy, with measurements accurate to within 4 mm at a distance of 10 meters from the scanner, and 7 mm at a distance of 20 meters [63]. In addition, the scanner is relatively fast, with a measuring time from 40 seconds to a few minutes depending on desired quality and settings [63].

The beneficial aspect of the device is its remotely controllable options via the Leica Cyclone FIELD 360 application that can be installed and utilized on phones or tablets. The app enables setups of real-time measurements to be registered directly in the field. The registered data from the phone or tablet are saved automatically in folders and can be accessed at any given point. This allows for point cloud preprocessing before going through the advanced options and calibrations on the computer software. Figure 39 shows the Leica BLK360 in action, conducting a 3D scanning of the Øvre Kvamme bridge.

Figure 38: In situ 3D laser scan with Leica BLK360

Because of the limited amount of daylight, careful planning was necessary for scanning the bridge on site. It was essential to ensure that overlapping surfaces between objects were captured accurately during the scans, as this would allow the software to establish necessary connections between the various captured surfaces. The scanning process was conducted systematically, and a total of 18 scans were captured to ensure a comprehensive and complete scan of the bridge. Following the scans, the resulting files were divided into three distinct projects, each containing scans associated with one of the bridge's spans.

The first project consisted of six captured scans, more specifically, three scans were carried out in the vicinity of the bridge of slab A1, whereas the other three were performed beneath the concrete bridge of the same slab. The second project entailed an equal capturing process, whereby six scans were conducted. In this project, three scans were performed beneath slab A2, while the other three were performed on the top of the bridge on the asphalt layer. Lastly, the third project included six scans on slab A3, with identical configuration as slab A1.

Figure 39: 3D scanning performed in situ

In order to merge and refine all of the captured scans, they were all saved within the mobile application, Leica Cyclone Field 360, and later intended to be exported into the Leica Cyclone Register 360 software. Further details on this process will be provided in Sub-chapter 5.1.

4.4.2 OMAway sensors

Six sensors with the use of OMA technology from Unquake [64] was provided by the OsloMet, and each one was assigned a number from 1 to 6 to systemize each configuration. Unfortunately, sensor number 2 was not working at all, resulting in installation of only five sensors on Øvre Kvamme bridge to measure the natural frequencies. The sensors consisted of an accelerometer and a datalogger, with the accelerometer connected to the data loggers to store the output data. Figure 40 below displays the OMAway sensors utilized in the field investigation.

a) b)

Figure 40: a) Datalogger; b) accelerometer - Retrieved from [64]

The datalogger has an integrated storage system via a microSD card and can utilize a GPS antenna to timestamp each reading in real-time. Furthermore, the accelerometer can measure the frequency of the structure in three different axes, X, Y, and Z, respectively. The accelerometer's orientation is shown on the face of the accelerometer as presented in Figure 40, b). It is important to note that the sensors had an issue with the readings of Z-axis, which meant only X- and Y-axis were fully operational. In order to measure the Z-axis, the accelerometers X- and Y-axes had to be reoriented. This involved positioning the X-axis to measure the Z-axis, while the Y-axis would either remain or be repositioned to measure the X-axis. To address this challenge, it was crucial to determine the orientation of the bridge prior to installing the sensors. A system was devised in collaboration with a PhD student from OsloMet to determine the optimal configurations for the best results.

Additionally, to ensure higher quality and reliable data, it is recommended to install sensors for an extended period. However, due to constraints such as time, deadlines, and financial support, only one site visit was feasible. Consequently, two different configurations setups were deployed strategically in critical areas for four hours to gather the frequency data during that one trip. Figure 41 below showcases the location and orientation, as well as the global axis of the five installed sensors in both setups.

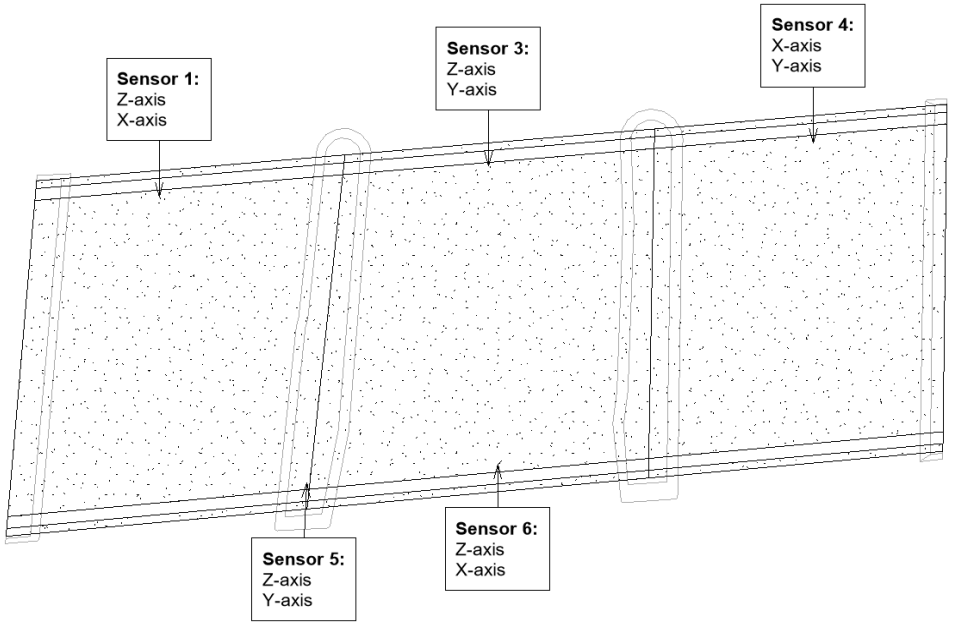

a)

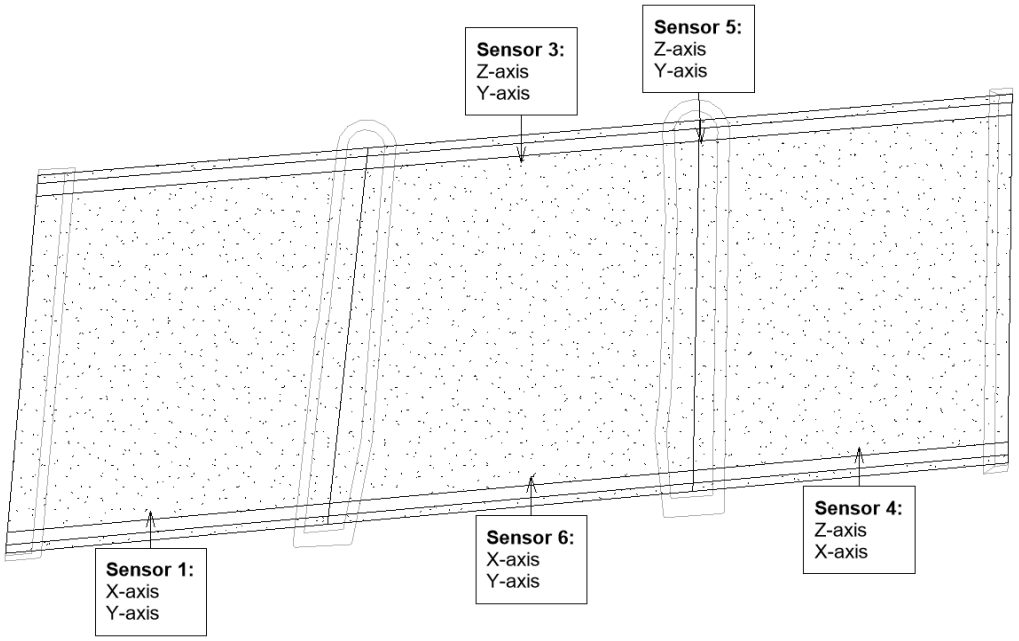

b)

Figure 41: OMAway sensor installed - a) Setup 1; b) Setup 2

Sensor 3 was installed as the reference sensor in order to compare and understand the data from the other sensors. Additionally, sensor 6 was unstable in the tests carried out before the trip, which posed a challenge in obtaining the necessary data. As a solution, sensor number 6 was intended to serve as a secondary reference to the other sensors. To guarantee the accuracy and reliability of the gathered data, two reference sensors were deliberately positioned on opposite sides of the mid-span in both setups. This arrangement allowed for backup in case of a malfunction, such as sensor 6 failing to collect any data.

The accelerometers, with its powerful magnetic capabilities were installed on a steel plate and positioned correctly following the configurations consultet with supervisor. To ensure reliable results and a great bond between the steel plates and the asphalt, sticky tacks were attached to hold the accelormeter in place. This was done to prevent the accelormeters from dislodging of the asphalt during the data acquisition. The accelerormeters were then installed on specific locations on the bridge as presented in Figure 41. Additionally, it should adressed that the sensors have a limited battery life, and to ensure continious operation for eight hours, power banks were employed. Figure 42 displays the sensors installed on each side of the bridge close to the parapets.

Figure 42: OMAway sensors installed on each side of the concrete bridge

During the last hour of the first setup, it started raining heavily followed by strong winds. These weather conditions posed a significant risk to the sensors, as they could potentially compromise the reliability of the collected data and introduce unwanted noise in the data recordings. To address this, plastic bags were used to protect the sensors from the water. However, the effectiveness of this solution remains uncertain, and the possibility of the weather conditions impacting the results cannot be entirely ruled out. Although the data loggers and accelerometers were covered, the presence of significant amount of water may have affected the bond between the sticky tacks and the asphalt. Furthermore, due to damage and missing screws from previous use, the dataloggers and their corresponding cables were at a risk of being damaged by rain. It is important to consider the potential impact of these environmental factors in the analysis of the bridge. Chapter 5.4 explores the theoretical basis of the OMA technology and sensor measurements, providing a comprehensive examination of the results.

4.5 Assessment of the field investigation

After examining the available documents, conducting visual inspection, and utilizing a variety of non-destructive tests, it has become evident that the structure has undergone significant deterioration. Several forms of degradation have been observed on the concrete bridge, with corroded reinforcement being the primary cause and most critical factor. Both uniform corrosion and pitting were detected. Determining precisely what is causing the corrosion and its expansion without carrying out destructive testing is challenging. However, the investigation findings suggest that carbonation is the contributing factor, which was confirmed by the special inspection conducted by BruKon AS. Despite the initial good quality and design of the bridge, it has now reached 96 years of age, making such deterioration expected. The sides of the bridge have been most severely affected, resulting in a higher load-bearing capacity in the center of the slabs and the need for restrictions to centric one-way driving.

Despite the high moisture level in the concrete, challenging conditions during the investigations, and the carbonation degradation heavily affecting the results, it was revealed by SilverSchmidt rebound hammer that the obtained data displayed a higher concrete quality than what was documented in the original construction and designs records. Additionally, the compressive strength of the concrete had a very similar mean value in the investigation conducted by BruKon AS compared to the investigation conducted on November 9th, 2022. However, there was a significant difference in the highest recorded compressive strength. While the highest compressive strength recorded by BruKon AS was 64.5 MPa [47], the readings taken on November 9th, 2022, showed a substantially higher compressive strength of 80 MPa. This considerable difference and the high compressive strength values can strongly indicate the significant expansion of carbonation during the testing periods of both investigations, affecting the rebound hammer test more aggressively in the most recent investigation.

The results obtained from the Profometer indicated that the reinforcement diameter and concrete cover depth are identical throughout the bridge. Thus, allowing the use of the existing documents for the middle span as a basis for modeling the whole bridge. It turned out to be large discrepancies between measured and the documented rebar spacing. Based on two profometer measurements conducted on the side spans, and the assessment of corroded reinforcement using a ruler, it is determined that a spacing of 85 mm will be used for the longitudinal reinforcement in subsequent work. Furthermore, the electrical resistivity testing results indicated potential active corrosion taking place inside the concrete slabs in areas that showed no visible signs of corrosion. This discovery is particularly concerning, as it may suggest that the corrosion could be more extensive than can be observed visually.

A summary of the survey that was carried out through visual inspection and non-destructive testing tools is presented in Table 8 below. The table outlines the existing and potential defect and deteriorations identified.

Table 8: Survey of recorded conditions and possible deteriorations

Deterioration type	Description
Efflorescence	Identified areas exposed to efflorescence
Spalling	Identified the location of the spalling areas, depth, width, and condition of the spall
Exposed steel	Identified extend and condition of exposed steel
Corrosion	Identified symptoms leading to potential corrosion
Crack/voids	Identified type and width of crack/voids
Delamination	Identified the areas of delamination and the depth of areas
Erosion	Identified the areas of potential erosion
Carbonation	Identified symptoms potentially caused by carbonation

In summary, it can be concluded that the bridge is severely damaged, and undergoes significant deterioration, affecting both its serviceability and load-bearing capacity. This means that the bridge's remaining lifespan is diminishing rapidly, emphasizing the need for immediate repair, and strengthening to ensure future safety. Based on annex B.1 from ISO 16311-2 [35] and B.2 [35], the structure can be defined as *Condition level 3 – Severe deterioration* and *Consequence level 3 – Large consequences*.

5 Modeling of Øvre Kvamme bridge

This chapter presents the methodology used to develop a finite element model of Øvre Kvamme bridge, starting from the 3D laser scanning. The purpose of this methodology is to provide a clear and thorough explanation of the necessary steps undertaken to achieve the final model used in structural analyses. The following sub-chapters will provide a more detailed comprehension of the settings and choices made during the process for each software and technique used. Figure 43 illustrates a flow chart that outlines the methodology used to model the selected case study from start to finish.

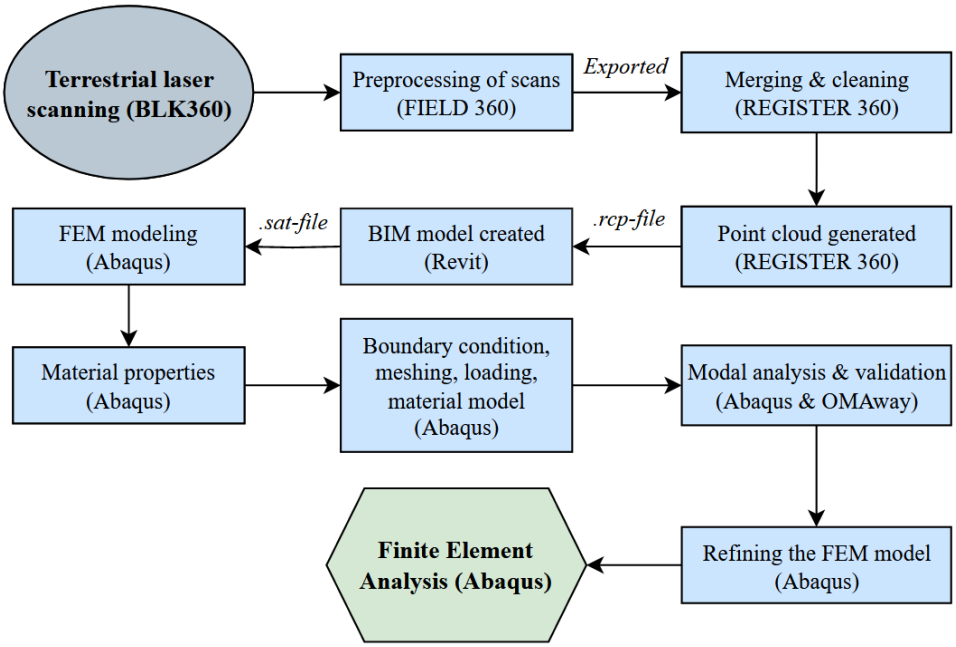

Figure 43: Modeling process of Øvre Kvamme bridge

5.1 Documentation of 3D geometry of Øvre Kvamme bridge

After completing the 3D scanning of the concrete bridge using the BLK360, the resulting 18 scans were exported from the mobile app and imported into its software, Cyclone REGISTER 360. This software allows for the merging and alignment of all scans to create a complete point cloud of the entire bridge. The alignment process in Cyclone REGISTER 360 requires precision and attention to detail. It involves selecting corresponding points in different scans and using them to create a common coordinate system between all scans. This process ensures that the final point cloud accurately represents the entire structure of the concrete bridge as it is today. In Figure 44 the properly merged and aligned point cloud generated from Cyclone REGISTER 360 software of all 18 scans can be seen.

Figure 44: Point cloud generated from all the scans

Once all of the scans are properly aligned, the next step involves removing unwanted noise and elements from the point cloud. This includes elements such as trees, grass, stones, and other irrelevant objects captured during the scanning process which are not relevant to the model. This is performed so the final point cloud can be modelled in a BIM software to accurately represent the real dimensions of each structural element. The software provides various editing tools to remove these unwanted elements and leave only the concrete bridge in the point cloud. The final refined point cloud in Leica Cyclone Register 360 can be seen in Figure 45.

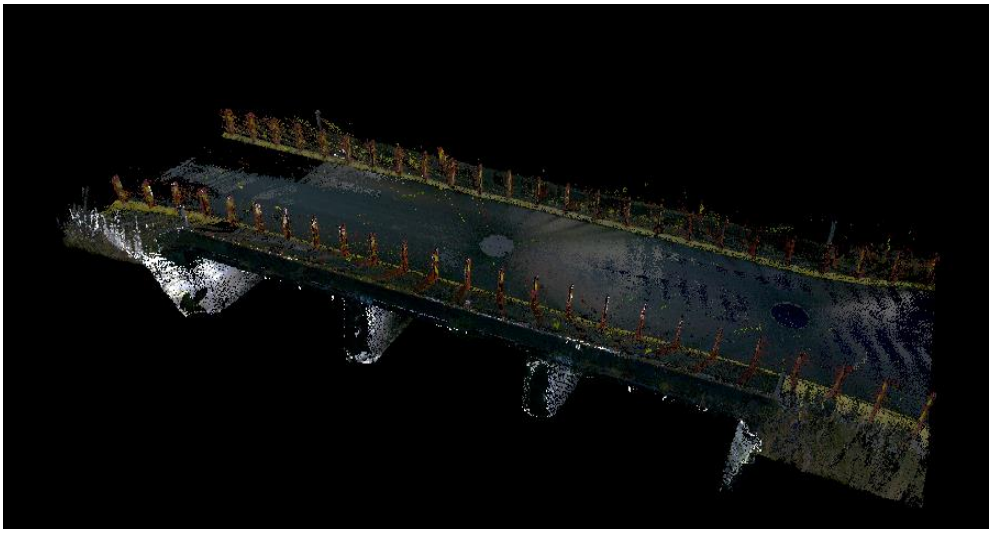

Figure 45: Final point cloud model of Øvre Kvamme bridge

The final refined point cloud is exported to a .rcp file format, which can be imported into Revit software for BIM-modeling. This step involves using the software's import function to bring in the point cloud data and create a 3D concrete bridge model.

In Revit, the model is refined and cleaned up by removing remaining noise and adding necessary details such as textures, materials, and structural element dimensions. This ensures that the final model accurately represents the real-world structure of the bridge and utilizing only the structural elements for the finite element modeling and analyses. Figure 46 shows the complete Revit model with a) pointcloud overlapping and b) the final Revit model, which will be used in FEM.

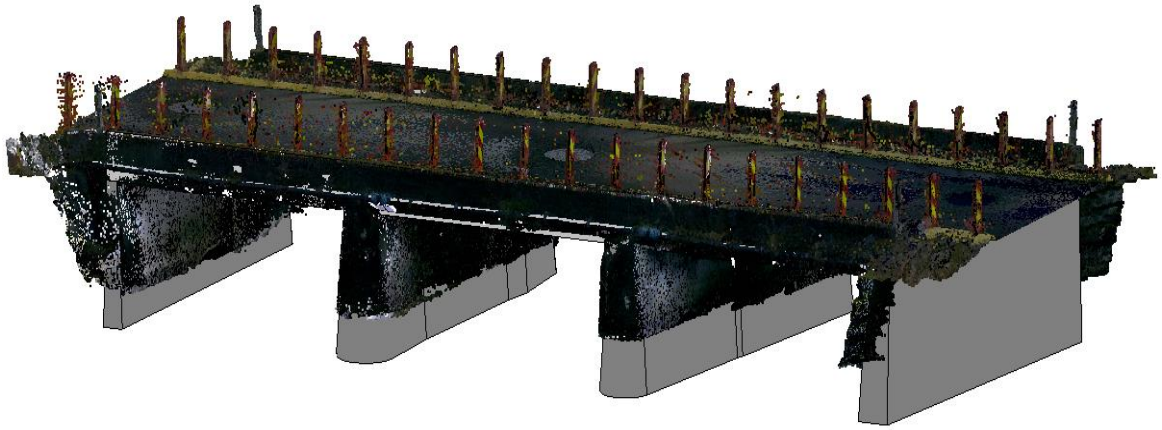

a)

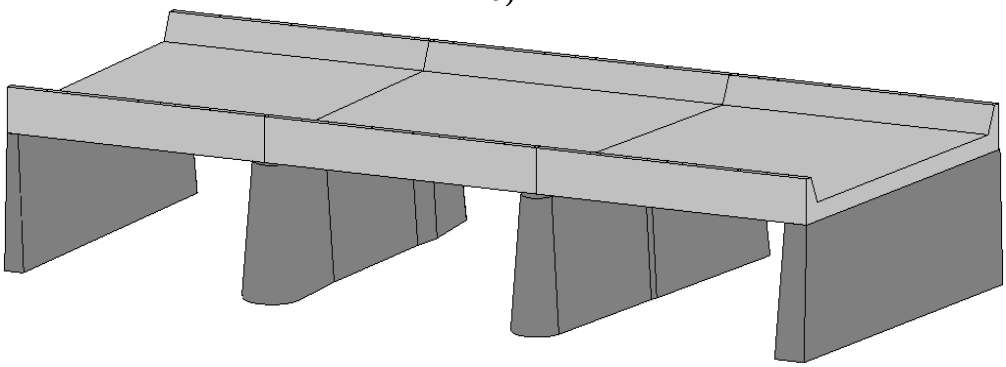

b)

Figure 46: a) Point cloud overlap with the Revit model; b) Final Revit model

The BIM model accurately represents the generated point cloud as seen in Figure 46. However, the height of the supports in the point cloud appears to be too low, due to water reflection that interfered with the laser scanning. Laser scanning is highly vulnerable to reflections as it can heavily interfere with the points measured. To address this issue, the affected area of the point cloud, including the ground where there was running water, was removed for the sake of simplicity. It is worth noting that the geometry of the point cloud obtained differed from the technical drawings from the 1970s, such as the center span being 6 cm wider in reality. A cross-sectional profile of the middle span was created and is presented in Figure 47.

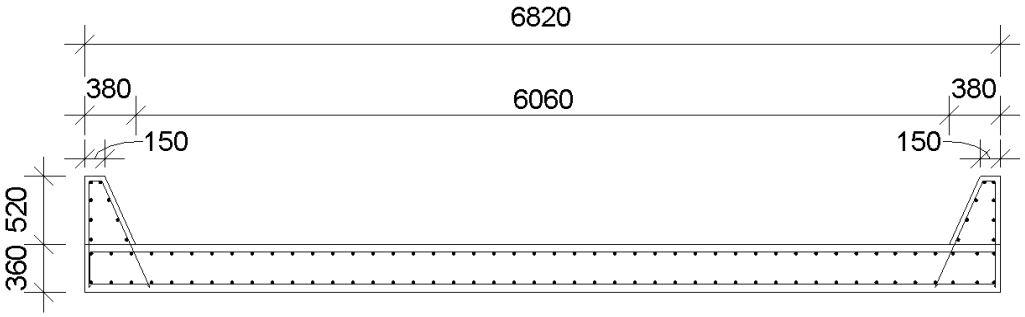

Figure 47: Illustration of the concrete slab of Øvre Kvamme from Revit

The figure illustrates the geometric measurements obtained from the 3D laser scan, represented in millimeters, along with the positioning of the rebars. Moreover, a floor plan has been created in Revit, which shows an overhead illustration of how the bridge is modelled. The floor plan is shown in Figure 48, incorporating all relevant measurements.

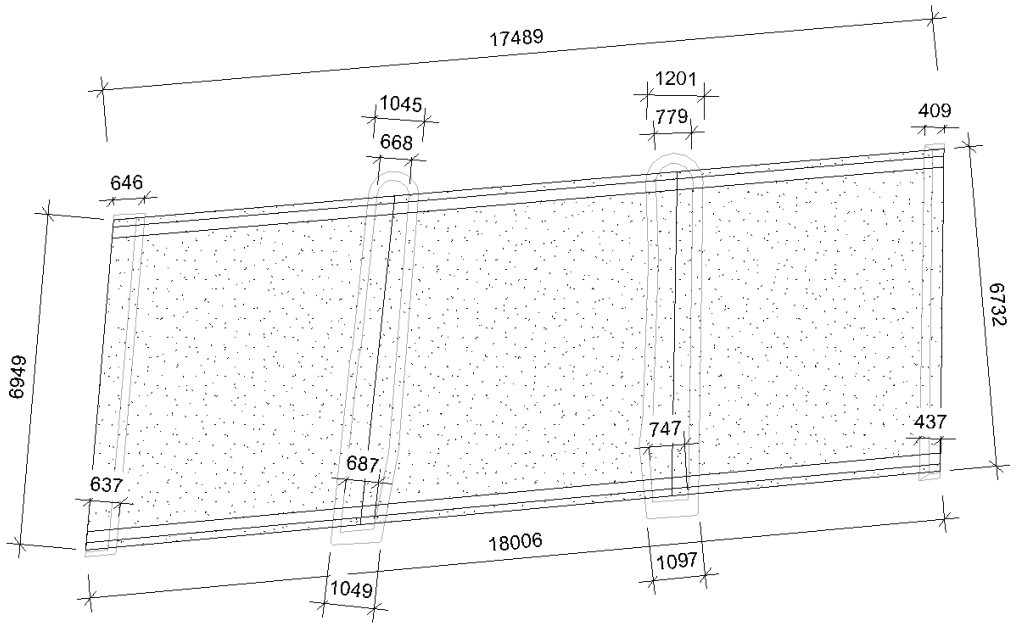

Figure 48: Floor plan dimensions of Øvre Kvamme bridge from Revit

Creating a finite element model of the bridge modeled Revit involved importing the model into Abaqus. Although Abaqus accepts a number of file formats for importing parts, none of the default files available in Revit are compatible. Therefore, the Revit file of the bridge was exported as an ACIS SAT file. A ACIS SAT file contains three-dimensional geometry information about the project in a text format and can be read by various of softwares. To optimize the model, it was decided to import the model as individual parts, allowing for assignation of different properties to the slabs and supports.

By default, Abaqus placed the imported parts at the origin of its datum coordinate system when instances were created. For the various components to lie correctly, they were rotated and translated as necessary. Figure 49 below shows the final model assembly in Abaqus after

importing and moving the various elements. The geometry in the Abaqus model is preserved during the import, remaining indistinguishable to the Revit model.

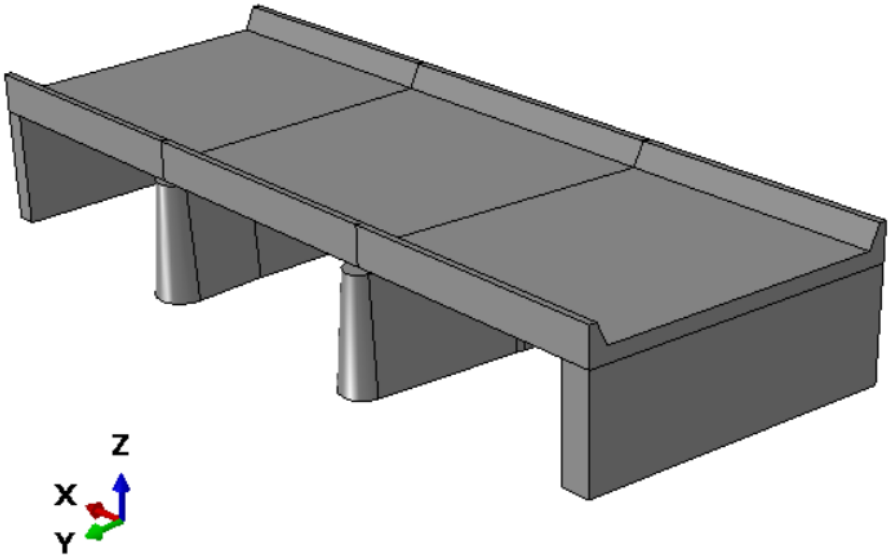

Figure 49: Initial FEM-model of Øvre Kvamme imported in Abaqus

It is important to acknowledge that Abaqus lacks a pre-established unit system. Consequently, the units utilized as input in the software will directly influence the output results. Therefore, it is crucial to select the appropriate units for each parameter and ensure that they remain consistent across the whole model. By maintaining consistency in the unit system through the simulations, it can be ensured that the results from finite element analyses will be reliable and eliminate the confusion of potentially unrealistic values. In this finite element model, the mm SI-unit system was chosen and utilized throughout the simulations. Table 9 displays the relevant mm SI-units used in Abaqus [65].

Table 9: Selected units in Abaqus

Quantity	**SI (mm)**
Length	mm
Force	N
Mass	tons
Time	s
Stress	MPa
Energy	mJ
Density	tons/mm^3

5.2 Material behavior

Performing a nonlinear analysis of structures is important since it enables a more accurate simulation of the structure's behavior under real-life loading conditions. Materials of the structures exhibit unique behavior in terms of their response to loads and stresses. This behavior includes the way in which the material deforms and reacts to external forces. When a material is subjected to stress, it can exhibit either linear behavior (elasticity) or nonlinear behavior (plasticity) [66]. The reversible and time-dependent deformation defines the linear behavior of a material. In other words, once the external force is removed, the material body will revert to its original configuration. At the same time, the irreversible and permanent deformation characterizes the nonlinear behavior of a material. This can be displayed in a simplified curve by illustrating the relationship between the force and displacement throughout load cycling. See Figure 50 for a review of the linear and nonlinear behavior concept.

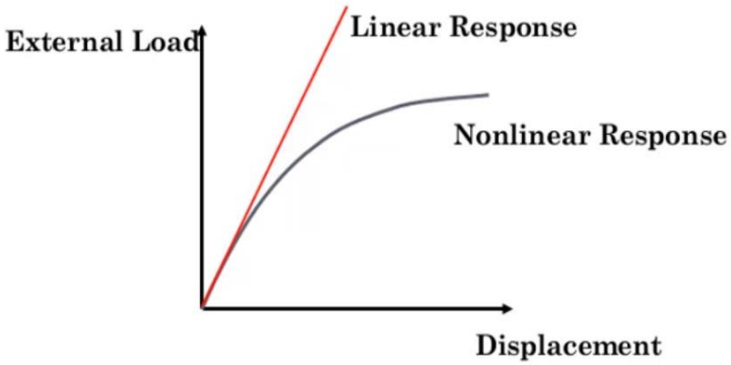

Figure 50: Linear and nonlinear behavior - Retrieved from [66]

Abaqus divides the source of nonlinearity behavior in structural mechanics in three [24]:

- Material nonlinearity: The material properties are functions of stress and strain.
- Boundary nonlinearity: Both applied forces and contact behavior relationship.
- Geometric nonlinearity: Large deformation and changes of the materials' structure.

It is important to note that these sources of nonlinearity may also occur in combination with each other. It is, therefore, crucial to make good considerations in FEM to provide realistic NFEA. Furthermore, every material exhibits a range of mechanical properties, such as yield strength, ultimate strength, and failure behavior, which govern the behavior during FEA. A thorough understanding of the material behavior of the structural system being analyzed can lead to a more comprehensive reading of the finite element analyses and their results. Before utilizing FEM modeling and analysis on Øvre Kvamme bridge, it is crucial to understand the behavior of concrete and steel.

5.2.1 Steel

Steel is a ductile material and consists primarily of iron and carbon. Ductile materials are characterized by withstanding a considerable amount of plastic deformation before eventually failing. This is due to the ability of the material to undergo large plastic deformations without fracturing, which makes it a suitable choice for the construction industry when the applications require strength and high flexibility. Furthermore, steel responds very similarly to both tension and compression stresses. A typical stress-strain behavior of a ductile material is displayed in Figure 51. The figure exhibits an engineering stress-strain curve, showcased from O to E, as well as a true stress-strain curve, depicted from O to E'. Furthermore, the figure illustrates some of the most common terms used in describing material behavior, which will be valuable to know and understand when performing structural analyses and extracting results from FEA-software.

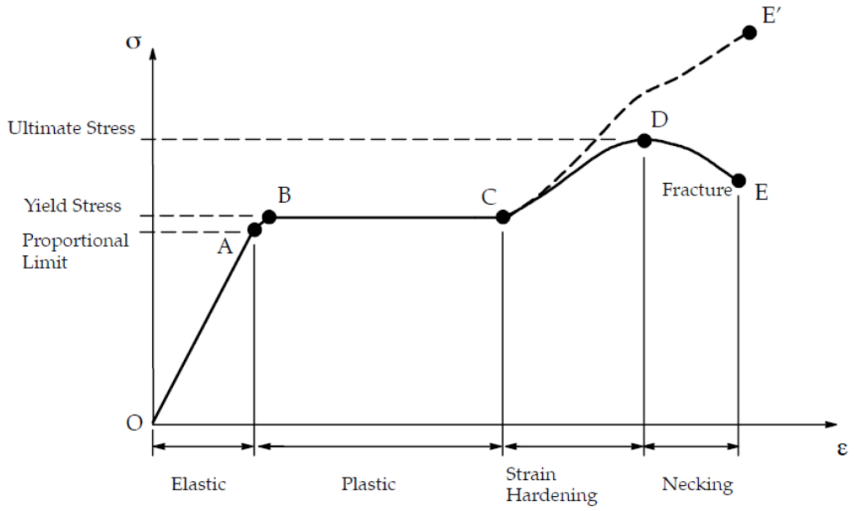

Figure 51: Typical stress-strain relationship for ductile materials - Retrieved from [67]

From point O to A, the ductile material experiences elastic deformation as stress and strain maintains an equilibrium until the proportional limit point. Beyond this point, the material's stress and strain are no longer proportional, and no longer follows Hooke's law. The limit of elastic deformation occurs at the highest point before yielding to plastic deformation, which is also known as the yield stress and can be observed at point B in Figure 51. Furthermore, the line between point B and C is referred to as perfect plasticity, indicating that the material can undergo irreversible deformation without an increase in stresses or loads. Furthermore, as the material is further deformed, it begins to harden and eventually reaches its maximum stress capacity. At this point, known as the ultimate stress, the material can no longer withstand higher stresses and starts necking in point D, before failure at point E.

Additionally, the figure includes a curve that extends to a point E', representing the true stress-strain behavior. Unlike engineering stress-strain, the true stress-strain behavior accounts for the

changes in cross-sectional area during loading. As a result, the stresses continuously increase until failure. True stress-strain provides a more realistic depiction of how the material responds to deformations.

5.2.2 Concrete

Concrete is a brittle and non-homogenous composite material composed of cement, water, aggregates, and other potential additives. Brittle materials are defined by their ability to withstand mostly elastic deformations before failure at maximum load. The nonlinear behavior of the composite material combined with reinforcing steel has proven to be difficult to predict. Although concrete exhibits high compressive strength, it possesses limited tensile strength, which is why it is commonly reinforced with steel.

Concrete exhibits elastic behavior up to around 30% of its compressive strength when subjected to pressure [68]. Beyond this, it undergoes permanent deformations before reaching its ultimate capacity. Additionally, once the concrete has reached its maximum stress, it loses its capacity before reaching failure. When subjected to tensile stress, concrete behaves differently than it does under compression. A linear relationship exists between stress and strain until the concrete reaches its maximum tensile strength, before cracking and losing all its capacity. The behavior of concrete is nonlinear under a wide range of loading conditions due to its complexity. Figure 52 illustrates a typical stress-strain of concrete in both compression and tension.

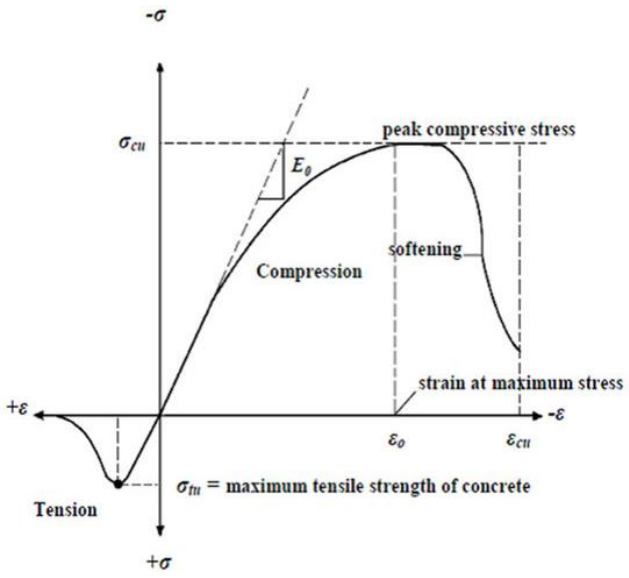

Figure 52: Typical stress-strain curve for concrete - Retrieved from [68]

In order to accurately model reinforced concrete and account for its nonlinear response, it is crucial to understand the material's behavior in a nonlinear context. This includes factors such as concrete's ultimate strength in both tension and compression, plastic strains, ultimate strain,

as well as the interaction between the concrete and reinforcement. Masoud & Chunwel [69] described that modeling the behavior of reinforced concrete is challenging due to the significant obstacle of accurately capturing the observable behavior of the physical system through realistic material models [69]. Due to the intricate nature of the material's nonlinear response, a variety of material models have been developed to aid in predicting more realistic behavior in finite element modeling and analysis. Some of these models include Drucker-Prager, Mohr-Coulomb, and Concrete Damage Plasticity (CDP). The selected material model for this thesis will be described further in section 5.3.5.

5.3 Finite element modeling

The idea behind the finite element method is to discretize complex systems and structures, including those with nonlinear behavior and complex geometry. A finite element discretization procedure is used to simplify problems by dividing systems into a finite number of smaller elements. Unknown field variables are expressed within each elements using assumed approximate functions [9]. An important aspect of the finite element method is that it incorporates the concept of piecewise polynomial interpolation. As elements are connected together, the field quantity is interpolated across the entire structure bit by bit. By summing up the stiffness contributions of each element, a stiffness matrix can be derived to describe the overall system [70].

FEA has the advantage of being very versatile, as various problems, including complex geometries, can be solved effectively. It is also capable of dealing with irregular geometries, complex boundary conditions, and contact problems, which makes it well suited for a wide range of applications. In cases where hand calculations would be impossible or inefficient due to the complexity of the problem, FEA proves to be a valuable tool. It can also serve as a cost-effective alternative to experimental testing. Even though finite element analysis is a powerful tool, it also poses a number of challenges. As the model approximates a real structure, inherent errors are likely. The results obtained in FEA relies on the assumptions that are taken during the modeling process, meaning that the validity of these assumptions directly affects the accuracy [70].

ANSYS, ETABS, COMSOL, Abaqus and Diana are some examples of the many FEA software’s available. Software choice depends on the type of analysis, specific needs, and the individual’s preferences. It is also important to use software that you are familiar with, as these

are often complicated and time-consuming to learn. In this study, Abaqus /CAE was chosen as software for the modeling of Øvre Kvamme bridge. This decision was based on previous experience with the software, and its suitability for solving the problem. This software allows advanced analysis to be efficiently created, visualized, and diagnosed. Additionally, nonlinear analyses are available, which are necessary to obtain accurate results for structures such as reinforced concrete bridges.

A complete analysis in Abaqus requires geometric definition, material description, boundary conditions, loading, mesh, and various settings to define the type of analysis to be performed [18]. The steps and choices made to finalize the Abaqus model are described below.

5.3.1 Material properties

The geometry of the concrete was imported to Abaqus in order to improve the accuracy of the simulations. The concrete sections of the bridge exhibit unsymmetrical geometries, with varying slab widths and significantly different lengths. There are a number of different types of elements available in the Abaqus library, and it is important to select the appropriate element type for the specific application. The various elements have distinct behaviors that depend on factors such as the degrees of freedom, number of nodes, integration, and formulation of the problem, which affects the results. Upon import into Abaqus, the various concrete parts were defined as three-dimensional deformable solid elements. Figure 53 illustrates the most common elements in the Abaqus library.

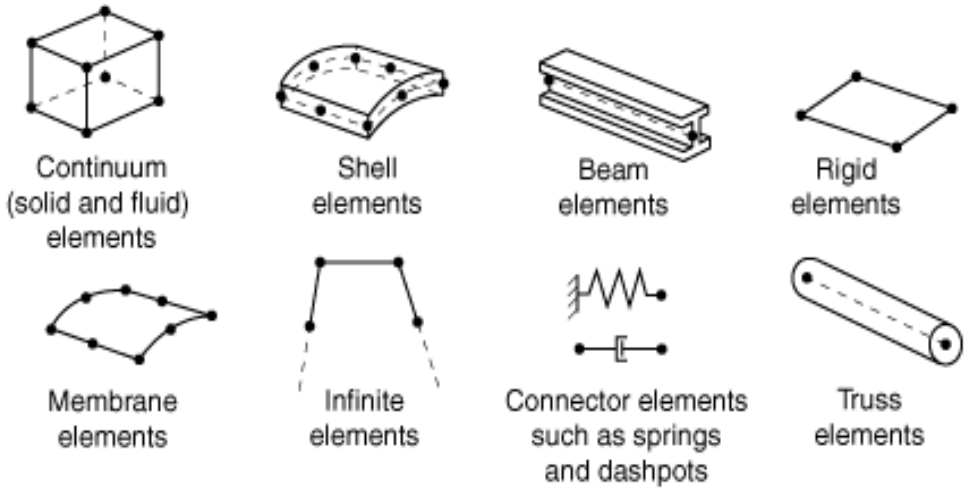

Figure 53: Common element types in Abaqus [71]

In Abaqus, it is essential to assign material properties to the imported parts of the bridge, which is defined in its own module. Initially, only the elastic material properties were necessary for

the preliminary analyses, such as the frequency analyses. The elastic properties that must be defined in Abaqus are density, Young's modulus, and Poisson's ratio.

As mentioned in Sub-chapter 4.1, the concrete used in the bridge is equivalent to today's B20 class concrete. This concrete class possesses a characteristic cylinder compressive strength of 20 MPa and tensile strength of 2.2 MPa, according to Eurocode 2 [28]. The Young's modulus of concrete is calculated using the following formula:

$$E_{cm} = 22 * (\frac{f_{cm}}{10})^{0,3} \qquad Eq(1)$$

By solving this equation for class B20 concrete, a Young's modulus of approximately 30 GPa is obtained, which was assumed for the initial model. As the bridge is so old, it is likely that phenomena such as creep have greatly reduced its strength. When concrete is subjected to sustained loading, it undergoes creep. This is a time-dependent deformation that occurs even under relatively low stresses. Depending on the concrete quality, temperature, and humidity, the creep coefficient can reach as high as 2 to 4 when the concrete age is set to infinity [72]. Since the model's stiffness is unknown, this may have to be adjusted when the model is calibrated. As the documentation provided by the NPRA did not include specific information about the concrete density, a value of 2.4 tons/m^3 was used in the model. According to EC 2 [28], the Poisson's ratio should be set to 0 in the case of cracked concrete, and 0.2 in the case of uncracked concrete [28]. Following the condition assessment of the bridge, 0.2 was deemed a reasonable value. In Abaqus it is also necessary to create sections that contain information about one or multiple parts. For the parts containing concrete, a solid homogeneous section was created, and the assigned elastic material properties are presented in Table 10.

Table 10: Material properties of concrete

Concrete parameters	
Density	2.4E-9 [tons/mm^3]
Young's modulus	30 [GPa]
Poisson's ratio	0.2

The supports of the three slabs are constructed using massive stones that are dry stacked on top of each other. A thin layer of concrete has been smeared on the outside of these stones, which has eroded in certain areas. Determining the specific types of stones used in the supports is challenging and requires expertise in a different field. However, the Geological Surveys of Norway have mapped the country's bedrock, which provides valuable information. It is likely

that the stones were sourced locally, given the time the bridge was built. The bedrock surrounding the Øvre Kvamme bridge primarily consists of gabbro, gneiss, and granite [73]. The properties of natural stone can vary a lot depending on factors such as the type of stone, its origin, and geological history. It would be necessary to take core samples and conduct experimental tests in order to determine the exact material properties of the particular stones used in the bridge.

Defining the overall stiffness of the supports is complicated, as the stones are loosely placed on top of each other. Although the material properties of stones are generally superior to concrete, the structure's construction method implies that the stiffness is not very high. Natural stones exhibit a wide range of material properties, with a compressive strength ranging from 10 to 200 MPa. Similarly, the tensile strength can vary from 1 to 5 MPa and is generally 10 to 20% of the compressive strength. When experimental data are not available, a recommended estimation of the Young's modulus is 300-700*f_c [74]. Initially, a Young's modulus of 5 GPa was selected for the dry-stacked stone supports. The material properties of the supports are presented in Table 11.

Table 11: Material properties of supports

Support parameters	
Density	2.4E-9 [tons/mm^3]
Young's modulus	5 [GPa]
Poisson's ratio	0,2

The reinforcement bars are modelled as three-dimensional deformable wire parts in Abaqus. A wire element is sketched as a line and used to idealize a solid whose width and depth are small relative to its length [75]. Following the drawings, four different types of rebar had to be sketched. Among these are longitudinal and transverse reinforcement, stirrups at the slab ends and side edges, as well as stirrups in the parapets. Moreover, truss sections were created and assigned cross-sectional area and material properties. The reinforcement dimensions of the bridge are Ø12 and Ø25 according to the rebar bending schedules. The Ø25 dimension is used as longitudinal reinforcement at the bottom of the slabs, while Ø12 is used in the rest of the bridge. The Abaqus modeling incorporates a concrete cover of 30 and 40 mm, while the rebar spacing is between 85 and 300 mm depending on the type and direction of the rebar. A comprehensive description of the concrete covers and spacing employed in the Abaqus model can be seen in Table 12.

Table 12: Øvre Kvamme properties in Abaqus

Concrete cover [mm]	
Slab, top	30
Slab, bottom	40
Slab, sides and ends	40
Reinforcement spacing [mm]	
Longitudinal, bottom	85
Transverse, bottom	200
Longitudinal, top	300
Transverse, top	300
Stirrups, parapets	300
Stirrups, slab sides	300
Stirrups, slab ends	160

A systematic approach was used to ensure that the reinforcement bars were placed within the concrete as precisely as possible. The modeling of the reinforcement was carried out in a piecewise manner, using translation and rotation functions to position the rebars relative to the datum coordinate system. After placing the outermost rebars, a linear pattern function in Abaqus was utilized to expedite the process. Figure 54 shows the arrangement of all 1,020 reinforcement elements modelled within Abaqus. The reinforcement was modelled following the drawings provided by the NPRA and the results of the field investigation.

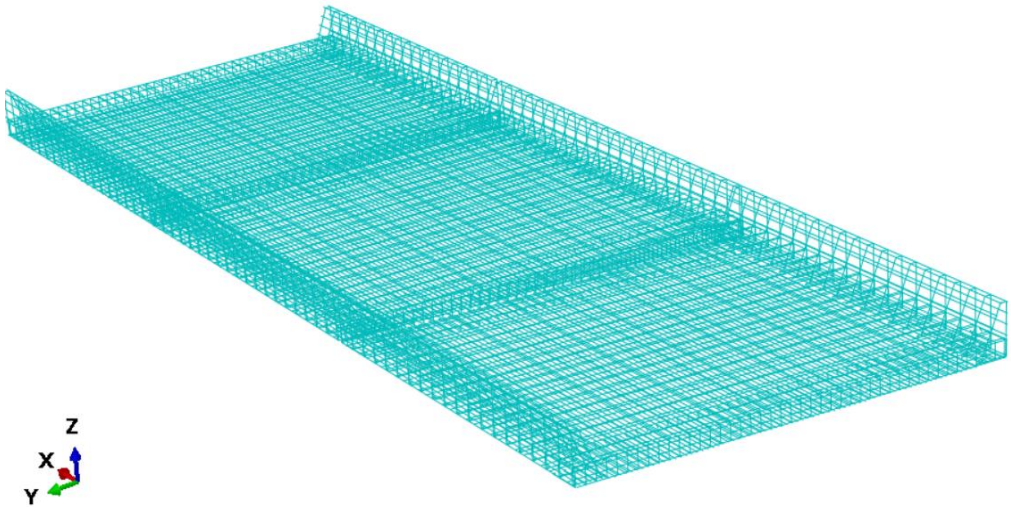

Figure 54: Reinforcement rebars of Øvre Kvamme

The reinforcing steel has been assigned a Young's modulus of 200 GPa and poisson's ratio of 0.3 [23]. The density of steel is determined based on the guidelines provided in "*V412 Bæreevneklassifisering av bruer, laster"* [76]. The stress-strain relationship of the reinforcement bars is assumed to be elastic-perfectly plastic with a yield stress of 400 N/mm^2

[8, 32]. Table 13 presents the defined elastic material properties of the reinforcing steel in Abaqus.

Table 13: Material properties of steel

Steel parameters	
Density	7.7E-9 [Tons/mm^3]
Young's modulus	200 [GPa]
Poisson's ratio	0.3

The implementation of corrosion and bond-slip in reinforcement bars within Abaqus can be a complex and time-consuming process. One effective approach is to define springs that transfer tensile forces between nodes in steel and concrete. While this method is relatively straightforward in a 2D model with a limited number of nodes, it becomes impractical when dealing with a large number of nodes that require manual assignment of springs and properties [77]. To account for visible corrosion identified during visual inspections, a 15% cross-sectional loss has been incorporated in the regions where corrosion was observed [78].

5.3.2 Load

Loads play a critical role in the simulations and are key to obtaining accurate results from the analyses. To accurately capture the response of the bridge, loads such as traffic and wind must be considered in a finite element analysis. Abaqus has the option to specify a wide variety of loads, such as concentrated, line, distributed, pressure, and thermal loads. It is also feasible to combine loads in various manners to simulate complex loading scenarios.

The self-weight of a structure is a type of permanent load that is characterized by the weight of the structure with all its permanent components. The bridge's self-weight is determined by the density of the various materials in the model. As previously stated, the density of the defined materials is 2.4, 2.4 and 7.7 tons/m^3 for concrete, rock, and steel reinforcement, respectively. The load itself is defined within the load module by creating load and further gravity load. Gravitational acceleration is defined as 9,810 mm/s^2 on the global y-axis with a downward-directed vector. Abaqus calculates the self-weight of each element in the bridge by considering its density and volume. The self-weight of the entire bridge is then obtained by accumulating the self-weight contributions from all the elements.

Vehicles mainly expose the bridges to vertical loads from vehicles' weight, but also cause horizontal forces due to breaking. These loads can be generated by both pedestrians, and vehicles of different sizes. Traffic loads are categorized into usage classes (Bk), axle loads and

total weights, special transport, motor tools and single transport [76]. Classification of bridges is based on the capacity of the weakest element, which in this case is the weakest slab. Today, Øvre Kvamme bridge is approved as Bk 10/60 and Sv 12/100 with centric one-way driving. This implies that a single vehicle can load the bridge with a maximum of 60 tons and 10 tons per axle for ordinary transport vehicles [76]. To evaluate the performance of the bridge, loads must be placed on the bridge following with the research project's purpose, which is to expand traffic lanes in both directions with Bk10/60 (ordinary usage), Sv 12/65 (motor tools) and Sv 12/100 (special transport) [31].

In the case of bridges shorter than or equal to 10 meters, a standardized brake load of 180 kN should be used, and for bridges longer than or equal to 40 meters, 360 kN [31]. Using interpolation, it has been determined that the braking load on the Øvre Kvamme bridge is 228 kN based on the length of the bridge, which is approximately 18 meters. Side loads are caused by skewed or asymmetrical braking or side impacts and act perpendicular to the longitudinal direction of the bridge. This load is equal to 25% of the brake load and is calculated to be 57 kN [76]. The various equivalent loads for class bk 10/60 are presented in Table 14 below and are divided into three main categories: bogie load, vehicle load and truck load [76].

Table 14: Load properties

Vertical loads		
Type of load	**Symbol**	**Class Bk 10/60**
Bogie load	A1	165 kN
	A2	120 kN
Vehicle load	A	80x5 kN
Truck load	A	63x9 kN
	P	6 kN/m
Horizontal loads		
Breaking load	B	228 kN
Side load	S	57 kN

In practice, design loads for short bridges will be determined by the axle, bogie, or triple bogie load. In contrast, the main structure for longer bridges is determined by the vehicle or truck load [79]. Hence, it has been considered most appropriate to check the bridge for bogie loads. A boogie load refers to the load exerted by two closely spaced axles on a vehicle. This load effect is represented by two distinctive concentrated loads, A1 and A2, with a spacing of 1.4

meters. The concentrated loads are multiplied by 1.3, which is a load factor for usage classes with two load fields [76]. Figure 55 shows the required width for two-way traffic with a guide edge.

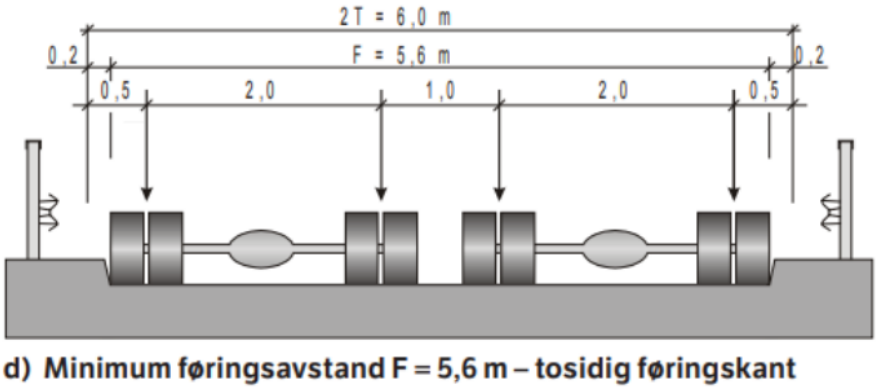

Figure 55: Required width for two-way traffic - Retrieved from [76]

Snow loads are not considered to occur at the same time as traffic loads on vehicle bridges. It is necessary to consider the load more thoroughly if the bridge is intended to be used as a storage area for snow or is not anticipated to be cleared for snow. Historically, earthquake loads have been an abnormal natural force in Norway, and the vast majority of older bridges are not designed to withstand them. In the case of evaluating the carrying capacity of bridges, it is generally not necessary to consider earthquake loads [31, 76].

In addition to the self-weight and traffic load of the bridge, it was also decided to incorporate the layer of asphalt. Based on the 3D scan and on-site measurements with a ruler, it has been determined that the thickness of the asphalt layer is 20 mm. This is defined as a distributed load with a density of 24 kN/m^3 on top of the concrete slabs in Abaqus [76].

5.3.3 Boundary conditions

The dry-stacked supports are fixed in all translational and rotational directions. This is accomplished by applying a fixed boundary condition to the bottom surface of the supports in Abaqus. Likewise, an interaction must be defined in the surfaces of the abutments directed towards the soil at both ends of the bridge. It is possible to consider these surfaces to be unrestrained if their stiffness is beyond the soil of unknown material. The supports of each end of the bridge were restrained longitudinally because it is assumed that deformation through the soil is quite limited.

Modeling the interaction between the reinforcement bars and the concrete is crucial for accurately predicting the behavior of the structure. One method to model the interaction

between steel reinforcement and concrete is to define an embedded region constraint [80]. The embedded constraint is defined by a set of nodes on two different types of parts. When defining this interaction, a host and an included region must be defined. The host region represents the primary material, while the included region represents the material that is embedded within the host region. This constraint was employed in the bridge model to ensure sufficient interaction between the reinforcing bars and the concrete. By embedding the steel reinforcement in the concrete sections, a perfect bond is assumed between the materials [16-17]. The model does therefore not include the effect of bond slip.

Abaqus offers several contact formulations, such as surface to surface, node to surface and edge to edge contact. The "find contact pairs" function was utilized to determine the elements of the bridge which are in contact with each other. Additionally, it is valuable for detecting modeling errors by highlighting unintended contact between elements. From the same menu, contact can be assigned to the desired regions that have been identified. Surface-to-surface contact was used for the interaction between the concrete slabs and the supports, as well as between the concrete slabs themselves. In the surface-to-surface contact characteristics, both normal and tangential behavior is specified. Tangential contact refers to sliding contact along or parallel to the contact surface, while normal contact refers to perpendicular sliding. This definition ensures that contact behavior is defined in all directions of the bridge. Normal behavior is set to "hard" contact, permitting separation after contact. For the tangential behavior, a penalty friction formulation is utilized with a friction coefficient of 0.8 [81-82].

5.3.4 Meshing

The meshing of an FEA model is one of the key components of a successful simulation. Mesh refers to the process of dividing a structure into smaller elements in a FEA software that can be simulated numerically. A mesh consists of discretized elements that together represent the shape of the geometry. Meshes should be balanced in terms of the number and size of elements. Having a mesh with too few elements may result in the analysis being unable to accurately simulate the behavior of the structure. On the contrary, if the mesh is dense, the simulation may become computationally costly and time-consuming.

For the first step, a very coarse mesh was used in order to quickly verify that everything else worked as it should without many errors and warnings. It was then easier to find the source of problems through trial and error since analyses were performed quickly. Following the correction of the errors, different mesh sizes were tested by doing a mesh sensitivity analysis to

see how much effect the mesh had on the results. In a mesh sensitivity study, the same model is simulated with different mesh densities in order to investigate how much the results differ between the densities. This is important to ensure that the mesh used in the final analyses is as accurate and reliable as possible. Typically, this is accomplished by starting with a very coarse mesh and comparing it with experimental data, theoretical data, or a model with a very dense mesh. Furthermore, the elements are reduced in size until a satisfactory result is achieved in terms of accuracy and computational efficiency.

Initially, the bridge slabs and supports elements were meshed using 8-noded linear brick with reduced integration (C3D8R). While this geometric order proved to be effective for certain mesh sizes, further experimentation revealed that the results were greatly overestimated. This issue was particularly noticeable when using a very coarse mesh size. The underlying problem was identified as shear locking, a phenomenon that can occur in numerical simulations. The shear locking issue was resolved using 20-noded quadratic brick elements (C3D20R). However, using higher order elements results in a considerable increase in the number of nodes being generated. Consequently, this led to a notable slowdown in the analyses, as the computational effort required became higher. In addition, the presence of shear locking was found to be at a mesh size of approximately 200 mm and coarser. It was therefore crucial to keep the final mesh size below this threshold to mitigate shear locking and maintain computational efficiency. Additionally, the student license in Abaqus is limited to a maximum of 250,000 nodes. Due to the model's size, this level is generated quite quickly with a dense mesh. Consequently, there is also a lower limit to the mesh size that can be defined without introducing errors to the simulation.

To mesh the reinforcement bars in Abaqus, truss elements (T3D2) were used. In contrast to other element types, such as solid or shell elements, the mesh controls for truss elements cannot be modified. This means that default meshing settings are automatically applied to the truss elements during the meshing process.

5.3.5 Material model

Using nonlinear analysis, it is possible to predict the structural response of reinforced concrete bridges and to identify possible failure modes. A number of nonlinear concrete modeling options are available in Abaqus, designed to simulate the complex behavior of concrete structures. Crushing in compression, cracking in tension, and yielding of the reinforcement bars are three major causes of nonlinear behavior in reinforced concrete [19]. Two of the most

commonly used options are concrete damage plasticity and concrete smeared cracking. After a thorough review of the literature findings presented in Section 2.3.2 and careful consideration of various factors, it was determined that the optimal material model for finite element analyses of the bridge is concrete damage plasticity. This decision was reached based on the observation that CDP most closely aligns with the unique properties and characteristics of the bridge and the objectives of this thesis.

For concrete damaged plasticity, concrete undergoes damage and plastic deformation when subjected to external loads. Damage is represented by a scalar variable ranging between 0 and 0.99, which describes the reduction in stiffness and strength [83]. Various loading conditions, including cyclic and dynamic loading, can be used with concrete damaged plasticity. It can also be applied to other materials such as rocks, mortar, and ceramics, making it suitable for the analysis of the supports of the bridge as well [84]. In order to develop the model, it is necessary to have concrete's compressive and tensile constitutive relationships, cracking and crushing damage parameters, as well as dilation angle, eccentricity, biaxial loading ratio, coefficient K and viscosity [85]. Based on values found in the literature, these parameters have been assigned, and are found in Table 15 [83, 86-87].

Table 15: CDP parameters used in Abaqus

Dilation angle	Eccentricity	fb0/fc0	K	Viscosity
31	0,1	1,16	0,67	0

An appropriate stress-strain ratio must be defined for the concrete in compression and tension in order to simulate compressive and tensile behavior. This study used formulas provided in Eurocode 2 to calculate the compressive stress-strain relationship since experimental data were not available. Yield stress, inelastic strain, cracking strain, and damage parameters must be defined in Abaqus. The same approach was used to determine the behavior of the supports. The stress-strain relationship for concrete in compression is given as follows [28]:

$$\sigma_c = \left[\frac{k\eta - \eta^2}{1 + (k-2)\eta}\right] f_{cm} \qquad \textit{Eq(2)}$$

where:

$$\eta = \frac{\varepsilon_c}{\varepsilon_{c1}} \qquad \textit{Eq(3)}$$

$$k = 1{,}05\, E_{cm} \frac{|\varepsilon_{c1}|}{f_{cm}} \qquad Eq(4)$$

$$\varepsilon_{c1} = 0{,}7\, {f_{cm}}^{0{,}31} \qquad Eq(5)$$

$$E_{cm} = 22 * (\frac{f_{cm}}{10})^{0{,}3} \qquad Eq(6)$$

σ_c and ε_c is the compressive stress and strain at any given location on the curve, f_{cm} is the compressive strength, ε_{c1} is the strain at maximum stress, and E_{cm} is the Young's modulus. The ultimate strain, ε_{cu1}, is set to 0.0035 according to table 3.1 in Eurocode 2 [28]. Figure 56 shows a schematic representation of the stress-strain relationship with the presented variables.

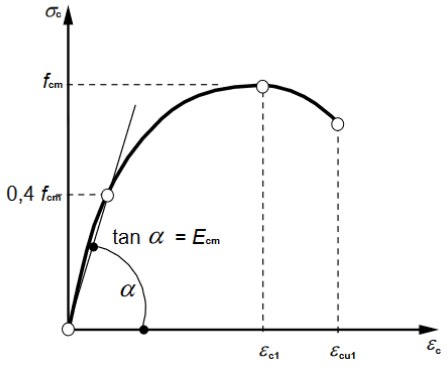

Figure 56: Stress-strain of concrete in compression – Retrieved from [28]

As mentioned previously, an input in the concrete damage plasticity model in Abaqus are inelastic strains, and these were calculated based on the total strain acquired. The elastic and inelastic strains for compression are calculated with the following formulas according to the Abaqus analysis user's manual [88]:

$$\varepsilon_c^{in} = \varepsilon_c - \varepsilon_{0c}^{el} \qquad Eq(7)$$

where:

$$\varepsilon_{0c}^{el} = \frac{\sigma_c}{E_0} \qquad Eq(8)$$

It has been determined that the concrete's tensile strength is 2.2 MPa for class B20 according to EC2 [28]. The relationship between stress and strain is assumed to be linear up to the tensile strength with a rate of increase equal to the Young's modulus. Several expressions exist in the literature that describe how concrete softens in tension following cracking. Among these tensile softening behaviors for concrete are linear, bilinear, and exponential [89]. The softening

behavior after the ultimate stress was assumed to be exponential but simplified by only calculating four points on the descending part of the curve, as shown in Figure 57 [90].

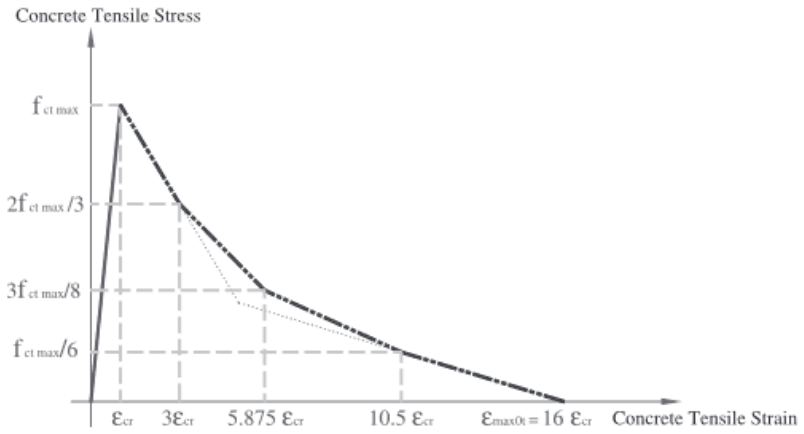

Figure 57: Stress-strain curve for concrete in tension – Retrieved from [90]

Similarly, as for compression, cracking strains are calculated for the tensile behavior. The cracking strains, ε_t^{ck}, are obtained by subtracting the elastic strain from the total tensile strain, ε_t, according to the following equations [88]:

$$\varepsilon_t^{ck} = \varepsilon_t - \varepsilon_{0t}^{el} \qquad Eq(9)$$

where:

$$\varepsilon_{0t}^{el} = \frac{\sigma_t}{E_0} \qquad Eq(10)$$

In addition to the compressive and tensile yield stress–inelastic strain behavior, it is also necessary to define the compressive and tensile damage parameters d_c and d_t, for every inelastic and cracking strain. The damage parameters provide insight into the extent of damage the material has sustained due to applied loads. It varies from 0, representing an undamaged material, to 1, indicating that the material has entirely lost its load-bearing capacity. These parameters are only calculated for the descending part of the stress-strain curves, as no damage develops in the elastic region. The formula used for the calculation of the compressive and tensile damage parameters are [87]:

$$d_c = \frac{f_{cm} - \sigma_c}{f_{cm}} \qquad Eq(11)$$

$$d_t = \frac{f_t - \sigma_t}{f_t} \qquad Eq(12)$$

See Appendix A, for a complete list of the calculations and parameters used.

5.4 Modal analyses and validation

Structural dynamics is a field of analysis within civil and mechanical engineering which focuses on the responses of structures under dynamic loads such as earthquakes, wind load, and human induced loads, such as vehicles. A dynamic load is considered to be a load that changes magnitude and direction over time. The discipline combines principles in order to predict and analyze the behavior of structures subjected to dynamic loads.

Nowadays, the majority of constructions operate under conditions responsive to excitations. Generally, most of the stresses that constructions are subjected to cannot be deemed entirely static. Except for the self-weight of structures, most loads applied to a structure can be classified as dynamic to some extent. Although some of these loads may be categorized as static due to their slow onset, they still have the potential to cause irresponsible excitations [91]. These excitations can result in undesirable responses that may cause unsafe operation of structures. A number of situations require the consideration of dynamic loadings, such as bridges, where moving vehicles and winds are powerful enough to cause the bridge or parts of it to be set in motion and vibrate [91].

Modal analysis is the study of the dynamic properties of a structure. The method involves identifying natural frequencies, mode shapes and damping ratios of the system. The natural frequency of a system is the frequency at which it oscillates in the absence of an external driving force. The mode shapes refers to the unique deformation pattern related to a particular natural frequency. The damping ratio is a unitless parameter that measures the energy dissipation of the system. A structure's dynamic behavior can be determined by identifying these three parameters. Overall, modal analysis is a powerful method for engineers and researchers to identify and understand the behavior of complex structures [92]. Two well-established techniques used to study the dynamic characteristics of structures are Experimental Modal Analysis (EMA) and OMA.

EMA is the oldest and most well-known technique performed in simulated controlled environments. EMA is a technique used to find the dynamic characteristics of a structure subjected to known excitations. EMA involves loading with a series of measured excitations

with tools such as impulse hammers or shakers. The reactions of the structure are then captured and processed utilizing mathematical algorithms to extract the modal parameters [93].

OMA on the other hand, is a technique used to determine the modal parameters of a structure while it is in operation. Rather than using artificial excitation, OMA uses ambient forces as the excitation source. The method is commonly referred to as output-only modal analysis because the excitations involved are unknown. The responses of the structures are often captured with sensors like accelerometers, which are placed in different locations of the structure [93] [94]. OMA is typically employed when the real structure differs from laboratory tests, when size and artificial excitation is impractical, when construction cannot be closed, or when ongoing health monitoring is required. Algorithms based on measurable response data can be utilized to derive modal parameters. However, processing these algorithms can be challenged and the obtained results may be misleading [93].

At the beginning of the 1990s, significant advances in the field led to the development of several OMA techniques. Generally, the techniques can be categorized into frequency domain and time domain methods. The most commonly used OMA techniques today include Peak Picking (PP), Frequency Domain Decomposition (FDD), time domain decomposition, natural excitation technique, auto-regressive moving average, and stochastic subspace identification [93]. When properly evaluated, the method serves as a valuable comprehensive tool that can give significant information about a structure under its operational conditions [94].

The concept behind modal analyses and validation can be displayed in Figure 58. In simple terms, the concept of model updating involves the continuous refinement of a FEM model by using experimental data. The goal is to adjust the FEM model until it accurately represents the real condition of the structure under investigation. This process continues until the FEM model aligns with the actual behavior of the structure within an acceptable range.

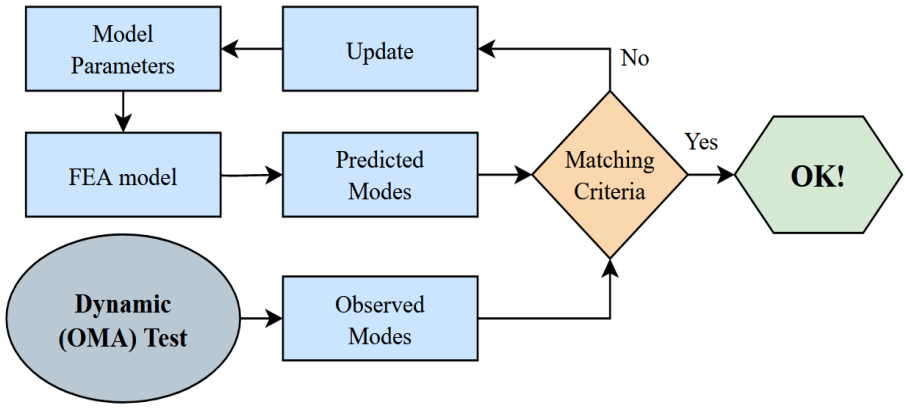

Figure 58: FEA model updating – Retrieved from [25]

5.4.1 Results from OMAway sensors

To evaluate and analyze the data collected by the sensors, it was necessary to extract it from the microSD memory cards within the sensor datalogger. This was achieved by inserting the memory card into a memory card adapter that is connected to a computer. The data was then transferred as text files to the computer. These text files were saved every 20 minutes at a sampling rate of 250 Hz, and as a result multiple files were saved per sensor throughout the recordings. The UnquakeOMAway software, which was previously mentioned in section 3.4.5, was used to import and process these text files. The files are combined within the software into one single 4-hour duration of data collected for each sensor. However, it was discovered that certain text files were corrupted and had no data. These files had to be removed in order for the UnquakeOMAway software to generate more refined charts.

The chart from the individual sensors from each setup was generated using the Fast Fourier Transform (FFT) technique, which allows for breaking down signals, and see which frequencies are present and at which intensity. FFT converts the signal representation from time domain to frequency domain, enabling the visualization of FFT amplitudes in the software [64]. The concept of FFT will not be further described in detail in this thesis however, it utilizes one of the most common OMA methods, including PP-method [93], as previously mentioned in Sub-chapter 5.4. The Peak Picking method is a simple OMA method used in modal analysis for output-only measurements as it identifies the natural frequencies by detecting the peaks in the FFT power spectrum, assuming that the modes are distinctly separated, and damping is minimal [93]. The peak-picking method has proved to be effective in identifying system modes with sufficient separation but may result inaccurate results if the modes are closely spaced due to its straightforward nature [93]. The PP method is utilized for obtaining mode frequencies from the FFT charts provided by the software.

Unfortunately, the results of the OMAway sensors revealed that the collected data was heavily corrupted and various factors, such as noise, bad weather conditions, and poor condition of the sensor equipment compromised the reliability of it. Figure 59 below displays the post-processed recorded data from sensor number 3, the reference. The local X-axis in Figure 59, a) corresponds to the global Z-axis, while the local Y-axis in Figure 59, b) corresponds to the global Y-axis of the bridge. The chart's X-axis represents the measured frequencies in Hz, and the Y-axis represents FFT amplitudes. For a better understanding of the corresponding global axis refer to Figure 49.

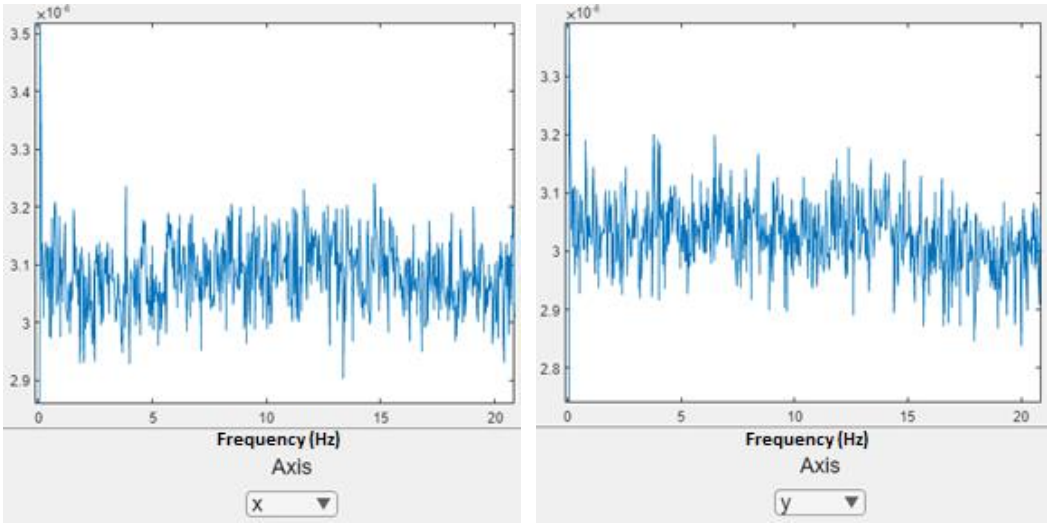

a) b)

Figure 59: FFT results from OMAway sensor 3

As observed in Figure 59, the frequencies have been significantly distorted due to the various sources mentioned earlier. The chart fails to exhibit a dependable frequency peak, rendering the readings obtained from the sensors unworkable and unsuitable for further use. However, there is one partially readable result from the OMAway sensors, which is sensor number 1 from the first sensor setup on the bridge. In Figure 60, a), the local X-axis result of sensor 1 from the first setup is presented which correspond to the global Z-axis of the Øvre Kvamme bridge, whereas the local Y-axis, b), refers to the global X-axis of the bridge.

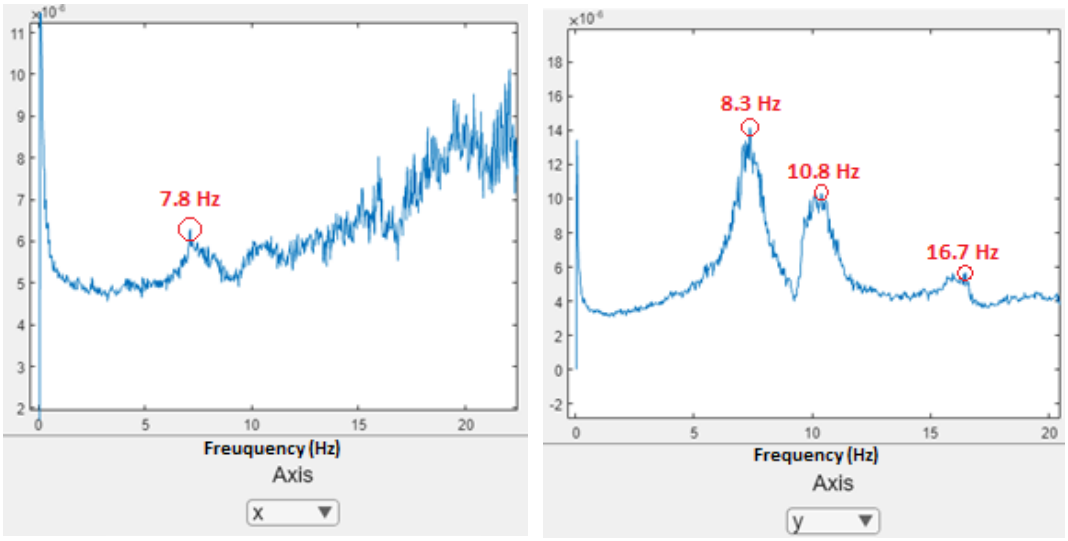

a) b)

Figure 60: FFT results from OMAway sensor 1

The experimental results retrieved from sensor 1 during the first setup were only reliable for the first three frequencies along the global X-axis, and only one frequency was detectable along the global Z-axis. The remaining data were too noisy, and therefore not sufficient to provide a

good foundation for further analysis. Moreover, the FFT amplitudes obtained were closely spaced, which could cause further unreliability when utilizing the PP-method, as previously mentioned. To address this issue, the FDD-method can be used to overcome the limitations of the PP-method as it provides more realistic natural frequencies [93]. However, due to time and scope limitations, utilizing FDD was not manageable. Nevertheless, even if FDD results were available, there would still be concerns about the accuracy of the data obtained as they would most likely be distorted due to the various influencing factors mentioned. Therefore, it is crucial to be cautious when using these natural frequency data for model updating in Abaqus, and a validation technique is furthermore required to ensure a more accurate FEM-model.

5.4.2 Model updating

The process of updating a finite element model using operational modal analysis sensor data typically involves adjusting various material and geometric properties of the model that influences the behavior of the structure, including the stiffness. By refining these properties to better align with the dynamic properties identified through OMA, the model can more accurately reflect the actual behavior of the structure. The process of model updating entails comparing the predicted behavior in the Abaqus model with the measured data obtained from OMA sensors.

Although the available sensor data was limited and of poor quality, it was decided to proceed with model updating to refine the finite element model of the bridge. The main motivation behind this choice was the significant uncertainty surrounding the actual stiffness of the bridge. Despite the difficulties posed by the incomplete sensor data, the focus shifted towards the data collected by the one sensor that was working properly. This sensor data served as the initial reference point for calibrating the model, aiming to increase the accuracy of the model.

The process of model updating was conducted iteratively, meaning that the model was updated multiple times until the predicted and observed data matched within a desired level of accuracy. In the case of the Øvre Kvamme bridge, the stiffness is influenced by several parameters such as material properties, moment of inertia, cross-sectional area, length, and boundary conditions. Since the size of the finite elements is predefined, the material properties are adjusted in Abaqus software to try to adapt the bridge's overall stiffness. The stiffness of a material is commonly characterized by its Young's modulus, which is a measure of its ability to resist deformation under stress. Hence, the Young's modulus was the parameter that was modified in the Abaqus software to improve the accuracy of the bridge's predicted stiffness.

To refine the finite element model of the bridge, the initial step involved conducting a frequency analysis in Abaqus. This analysis aimed to determine the first five natural frequencies and mode shapes of the structure. The natural frequencies obtained from the analysis are presented in Table 16.

Table 16: Mode shape for initial frequency analysis

Mode	Natural frequency (Hz)
1	33,545
2	40,042
3	42,350
4	48,771
5	53,194

To assess the accuracy of the finite element model, it was necessary to compare the results with the actual measurements. Ideally, the natural frequencies predicted by the model should be close to the measured values. However, upon comparison, it was found that there was a significant discrepancy between the predicted and measured natural frequencies. The frequencies obtained from the finite element analysis were found to be significantly higher than the actual measurements, indicating that the stiffness of the bridge is too high. This discovery was significant because the stiffness of a structure is critical and affects its behavior and performance. If the stiffness is overestimated, the predicted natural frequencies will be higher and the predicted mode shapes will be more rigid than the real ones. Given the significant difference between the predicted and measured natural frequencies, it was clear that the finite element model required more modification.

Due to the excessively high frequencies obtained in the Abaqus analysis, the overall stiffness had to be reduced. It was decided to investigate the effect of reducing the Young's modulus of the various components to mitigate this issue. It was attempted to reduce the Young's modulus of concrete, stones, and steel in various combinations to determine its effect on the frequencies.

The findings indicated that reducing the Young's modulus of steel had minimal impact, accounting for under 10% of the reduction in natural frequency. Therefore, no further reductions were made to steel. During the initial modeling phase, the support's material properties had already been considered low, and reducing the stiffness appeared implausible. However, when the Young's modulus of the concrete was reduced from the original 30 GPa to 20 GPa, a noticeable reduction of approximately 8 Hz was observed for mode 1. The decrease observed for modes 1 to 5 in the analysis is shown in Table 17.

Table 17: Mode shapes of reduced stiffness

Mode	Natural frequency (Hz)
1	25,805
2	29,597
3	30,819
4	32,508
5	40,392

Despite the previous attempts to modify the stiffness of the bridge, the measured sensor data remained significantly higher than in Abaqus. It was determined that further adjustments to the material parameters would not be appropriate to achieve the desired reduction. Instead, it was decided to alter the supports at both ends by removing the longitudinal restraint. This modification significantly reduced the overall stiffness of the bridge, bringing the natural frequencies closer to the sensor data. The mode shapes of modes 1 to 5 were plotted in Abaqus and are presented in Figure 61 from a) to e).

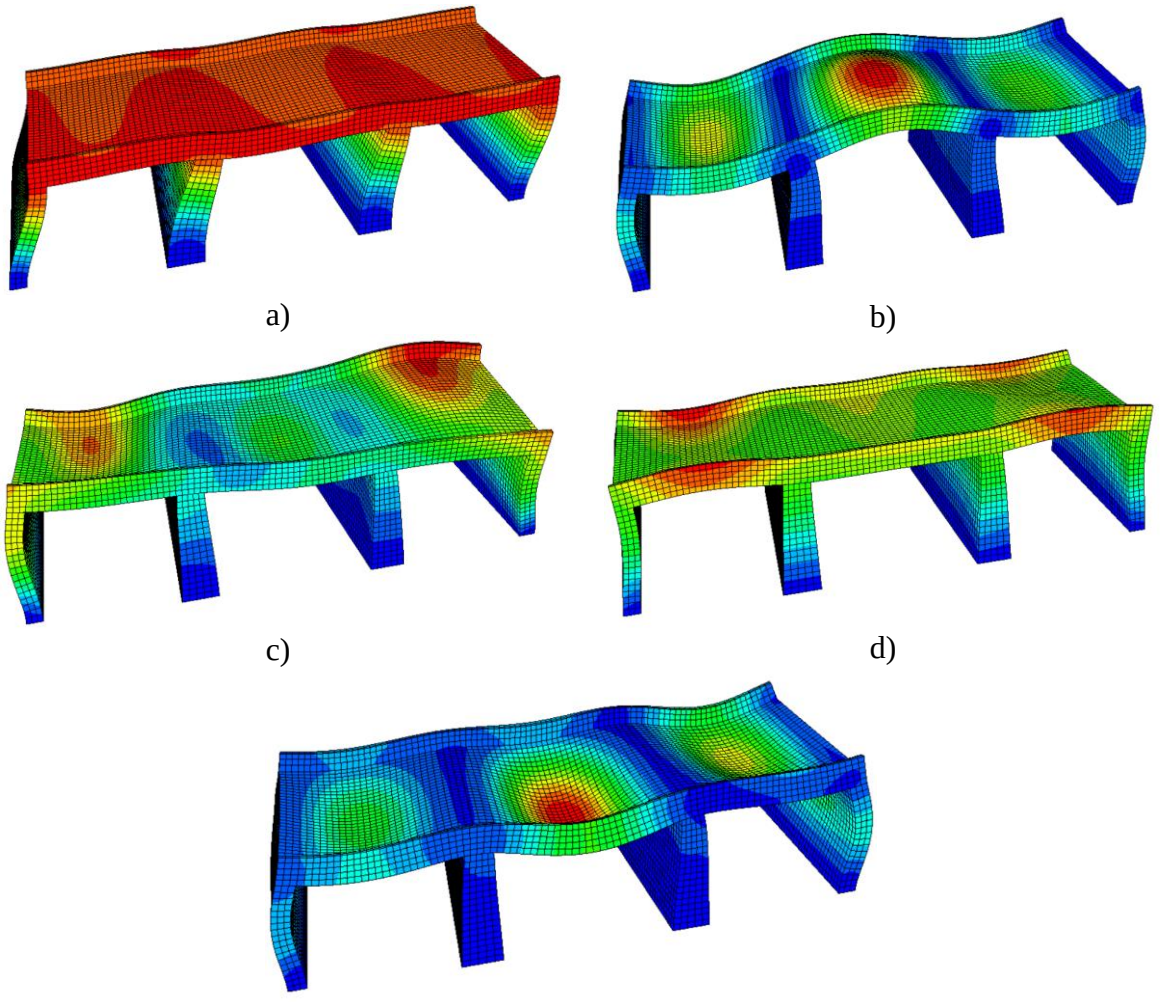

a) b) c) d) e)

Figure 61: Mode shapes w/o longitudinal constraints

These plots represent how the bridge would deform at specific frequencies. These specific frequencies for each mode are displayed in Table 18.

Table 18: Mode shapes values for w/o longitudinal constraints

Mode	Natural frequency (Hz)
1	11,012
2	26,620
3	29,183
4	30,115
5	31,270

These results yielded lower natural frequencies, especially for mode 1, but still were quite high compared to sensor results. At this point, various alternatives were explored to improve the accuracy of the model. Previous attempts to modify boundary conditions and Young's modulus had already been tested. To further investigate the behavior of the bridge, a simplified single span bridge with no reinforcement was analyzed. Additionally, it was tried to create all the parts in Abaqus to see if the imported geometry from Revit was the source of the error. Multiple types of contact definitions were tested, including general contact, surface-surface and cohesive interface with different properties. Unfortunately, none of these attempts were providing results in close proximity to the sensors, and the bridge still exhibited excessive stiffness. Given these results, it was deemed necessary to utilize another software to validate the accuracy of the model. This was done to determine if something was wrong with the model prior to performing comprehensive analyses on the bridge.

5.4.3 Model validation

As previously mentioned, the OMAway sensors demonstrated lack of consistency and reliability in their recorded data, highlighting the necessity of an additional validation method to improve the accuracy of the Abaqus model. In collaboration with a doctoral supervisor, a simplified ETABS model of the Øvre Kvamme RC bridge was created to validate the natural frequencies obtained from the sensors and in Abaqus.

ETABS is a finite element modeling software designed for the structural analysis and design of building systems [95]. While it shares some similarities with Abaqus, it is generally considered a more simplified FEM software than Abaqus. ETABS offers a range of capabilities for analyzing and designing structures [95]. The ETABS model developed for this thesis was specifically designed to replicate the essential characteristics of the Abaqus model, such as the

geometry, material properties, and boundary conditions. Figure 62 displays the simplified finite element model in ETABS.

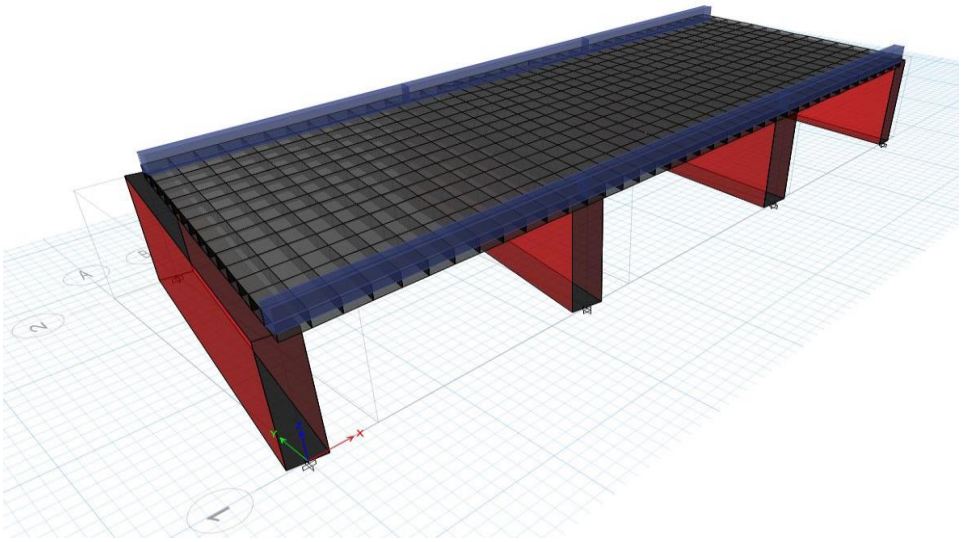

Figure 62: ETABS validation model - [95]

It is worth noting that the ETABS software does not have the capability to incorporate solid elements. Consequently, the key difference between the ETABS and Abaqus models lies in the choice of FEM element types. Specifically, the ETABS model is developed using shell elements, whereas the Abaqus FEM model utilizes solid elements. Additionally, the geometric representation of the bridge is intentionally kept simple in the ETABS model to expedite the analysis process. Considering these disparities between the models, it is important to acknowledge that the frequencies obtained from the simplified ETABS model will not yield very accurate results. Nevertheless, the results can provide a rough estimate of the expected frequencies that can be compared to the OMAway sensors and the Abaqus model. The first three mode shapes obtained in ETABS can be seen in Figure 63.

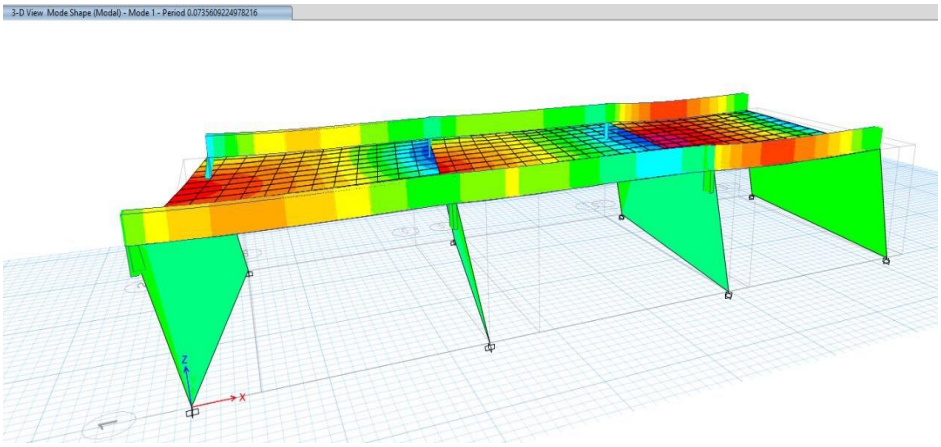

a)

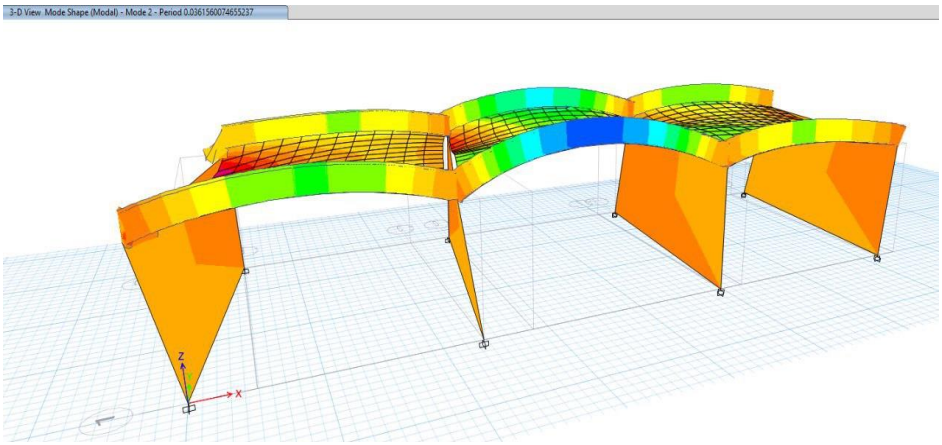

b)

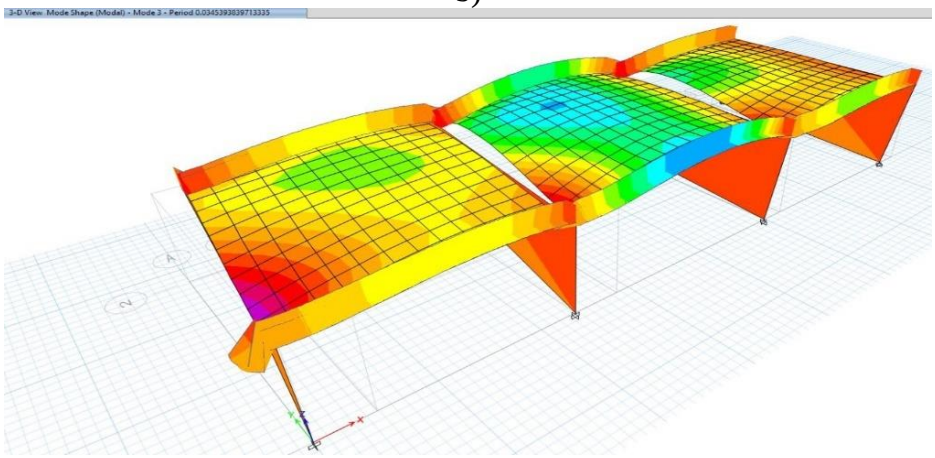

c)

Figure 63: a) Mode shape 1; b) Mode shape 2; c) Mode shape 3

Three mode shapes and natural frequencies were considered enough to ensure that the natural frequency aligns with the frequencies extracted from the Abaqus modal analysis results and the OMAway sensor. It is important to note, however, that ETABS does not provide frequencies in a direct manner as it rather provides periods. The following formula establishes the connection between frequency (measured in hertz) and period (measured in seconds).

$$f = \frac{1}{T} \qquad Eq(13)$$

where:

- f = Frequency (Hz)
- T = Period (s)

As demonstrated in the formula, frequency and period are inversely proportional to each other. Essentially, period denotes the duration for completing a single cycle of vibration, whereas frequency indicates the number of completed cycles per second. The period data extracted from the modal analysis of ETABS is displayed in Table 19, with the calculated natural frequencies.

Table 19: Results from modal analysis of the ETABS model

Mode	Period	Natural frequency (Hz)
1	0,0736	13,587
2	0,0362	27,624
3	0,0345	28,986

The first three mode shapes that were obtained from OMAway sensor 1, Abaqus, and the ETABS validation model are compared in Table 20.

Table 20: Comparison of collected natural frequencies from different sources

Mode shape	**Natural frequency (Hz)**		
	OMAway sensor 1	*Abaqus*	*ETABS*
1	8.3	11,012	13,587
2	10.8	26,620	27,624
3	16.7	29,183	28,986

When comparing the results of OMA and ETABS data, it can be observed from Table 20 that the natural frequencies differ between the two validation procedures. Specifically, the natural frequencies obtained from OMAway sensor show an initial value of approximately 8 Hz, compared to 13 Hz in ETABS. The substantial discrepancy between these two values indicates that the data obtained from the OMAway sensor is affected by noise and other potential variables, as described in section 5.4.1. The unrestrained and lower stiffness Abaqus FEM-model provides a value that falls between the two validation procedures. This ensures that the result of the data collected from Abaqus is feasible and showcases a more realistic FEM-model for Øvre Kvamme bridge for further FEA.

6 Finite element analyses

This chapter presents the results of the study, which utilized the finite element software Abaqus to analyze the behavior of the Øvre Kvamme RC bridge at its current condition. The FE-analyses conducted will include a pushover analysis and a vertical loading analysis. The results of the simulations presented will provide some insight into the behavior of the bridge at its current state.

6.1 Pushover analysis

Before performing a pushover analysis, a mesh sensitivity analysis is required to evaluate the effectiveness of mesh density on the simulation results. Analyzing the mesh refinement level is intended to determine the minimum level of refinement required to obtain accurate and reliable results. Mesh sensitivity analysis involves meshing the model with varying element sizes and running simulations for each mesh configuration. A comparison of the results is then performed to determine the extent to which the mesh density affects the solution. By identifying the optimal mesh density for a given level of accuracy, mesh sensitivity analysis can help refine the finite element model for accurate simulations and reduce computational time and resources. The conducted mesh sensitivity analysis of Øvre Kvamme bridge FEM-model is displayed in Figure 64. The figure presents a base shear-lateral displacement chart of various mesh sizes, including 250-, 200-, 150-, 125-, and 100 mm.

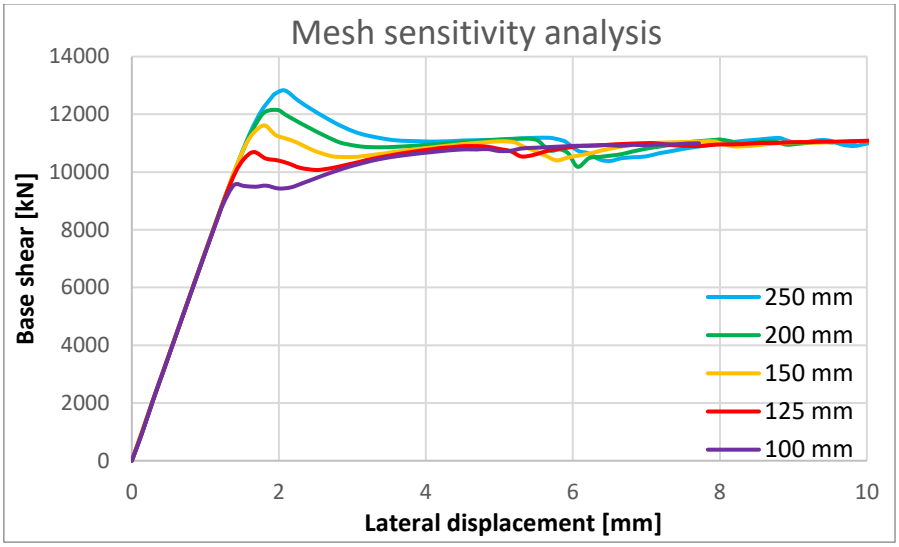

Figure 64: Mesh sensitivity analysis

The chart displays significant variances in the elastic yielding point across different mesh sizes, while the plasticity phase shows relatively consistent behavior. Typically, finer mesh sizes yield more accurate results, but at the cost of increased convergence time. Conversely, coarser meshes offer faster computations but sacrifice the precision of the outcomes. Given the time

constraints associated with the computationally intensive nature of FEAs in Abaqus, a mesh size of 150 mm is considered the most appropriate balance between efficiency and accuracy for subsequent analyses performed in Abaqus.

Pushover analysis is a non-linear static analysis technique that is used to simulate seismic deformations. Whenever a structural component has reached its maximum strength, its forces are redistributed to other components. A pushover analysis involves loading the construction until weak points or components are identified. As part of the analysis, the model is revised to reduce the impact of weak areas on the model's performance. Repeating this process will allow the distribution of weaknesses to be identified under seismic forces. Although the analysis is primarily aimed at assessing the seismic capacity of structures, it can also be used to retrofit structures [96]. Considering Norway's geographic location, seismic loads are generally not a problem. Thus, the objective of the analysis is not to determine the construction's vulnerabilities directly related to seismic loads but rather to assess the construction's resistance to vibrations induced from other sources.

Under the pushover analysis, the bridge was loaded laterally using a displacement-controlled loading approach. The purpose was to apply enough displacement causing damage in parts of the bridge to identify relevant areas for strengthening. A displacement of 15 mm was defined for slab surfaces on the bridge's sides. To prevent immediate damage and convergence difficulties, the parapet walls were partitioned so they were not loaded. A base shear force is calculated by adding the lateral reaction forces at the bottom of all four supports. The displacement is plotted for an arbitrary node in the middle of the bridge. The base shear-lateral displacement curve for the bridge model without strengthening is presented in Figure 65.

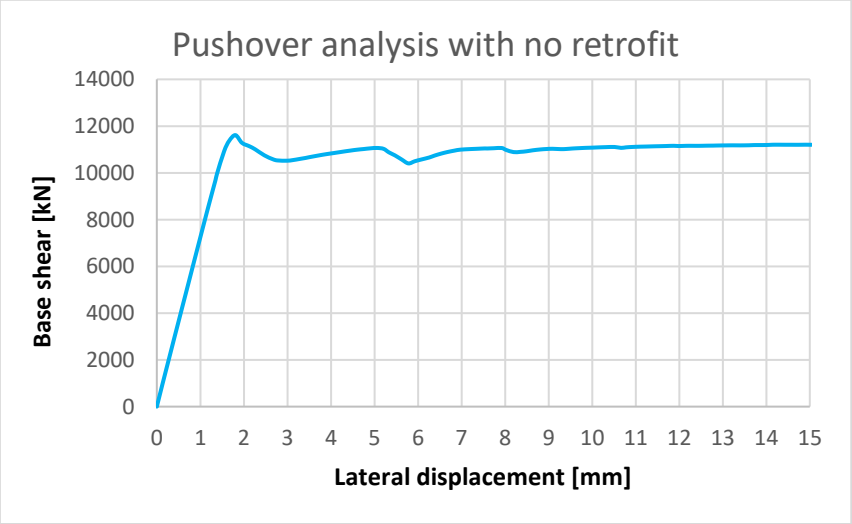

Figure 65: Base shear-lateral displacement for the Øvre Kvamme bridge w/o retrofitting

From the curve, it is observed that the deformation of the bridge is approximately linear until a displacement of 1.8 mm at a maximum load of 11,600 kN. At this point, the bridge started to develop permanent damage. Furthermore, there is a rapid increase in displacement without a significant increase in the applied load. This persists until another decline, leading to further spread of damage. Due to the bridge's design, with wide and sturdy supports, damage occurs in these areas. There is a comprehensive amount of corrosion on the concrete slabs of the bridge, which makes them particularly vulnerable. Hence, the analysis aims to identify weak components on the slabs rather than on the supports. As mentioned in section 5.3.1, the supports were assessed as having lower stiffness than the slabs due to the composition and lack of reinforcement. Hence, the bridge's response to lateral load have been identified to be dependent on the material properties and design of the supports.

6.2 Vertical load analysis

The second analysis involved subjecting the bridge slabs to vertical loads until failure, following a similar approach as the lateral analysis. Initially, a displacement-controlled loading procedure was attempted, but due to challenges, it was instead chosen to use a uniformly distributed load. By applying low displacements to the mid-spans, the results were characterized by immediate damage and strange crack patterns in the region of applied displacement. The force was defined as the pressure in Abaqus and applied to the three top surfaces of the slabs. A value of 0.2 N/mm^2 with a steady linear increase over the step time was chosen, equivalent to a force of 200 kN/m^2. This magnitude was deemed adequate since the reference model displayed significant damage over large areas during the analysis. Furthermore, the supports were modified to rigid to ensure minimal deformations, in order to capture the behavior of the slabs. This modification allowed a customized retrofitting strategy exclusively for the corroded concrete slabs. Figure 66, a), b), and c) presents the results of the vertical loading analysis without retrofit, illustrating the initiation of damage on the tensile side of each slab.

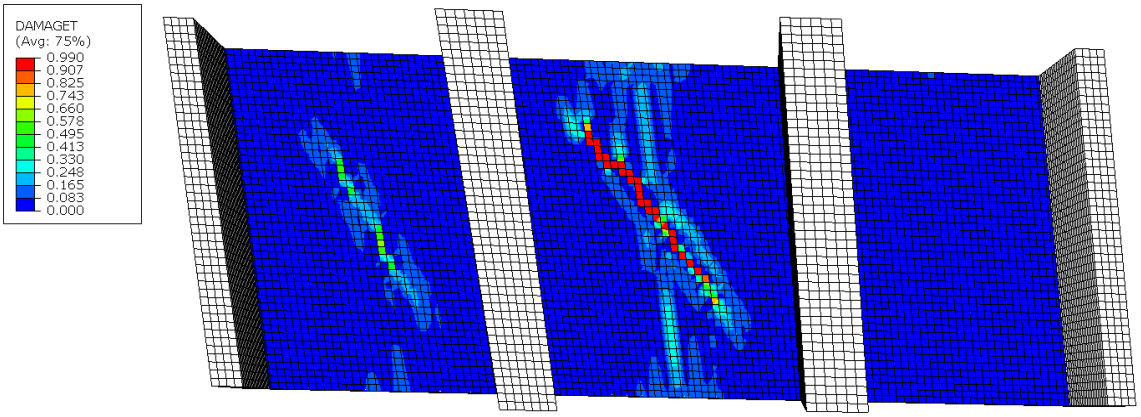

a)

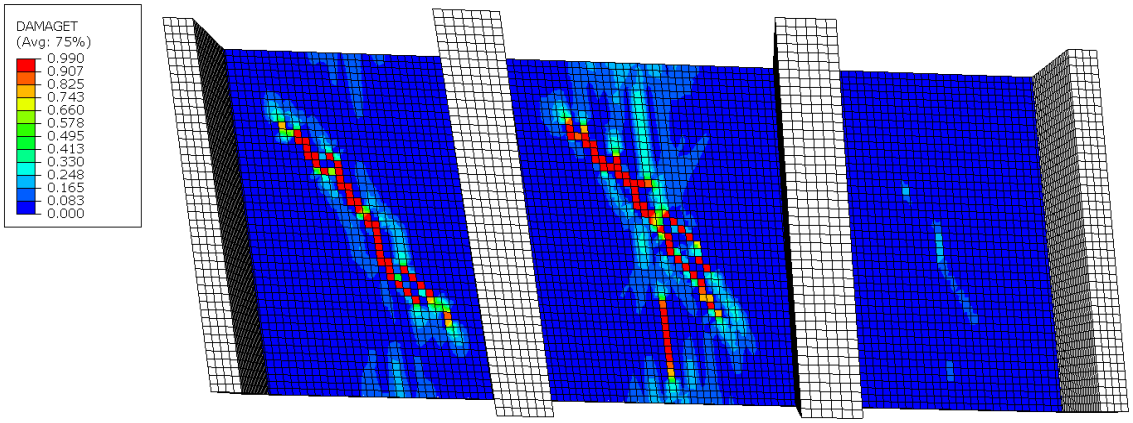

b)

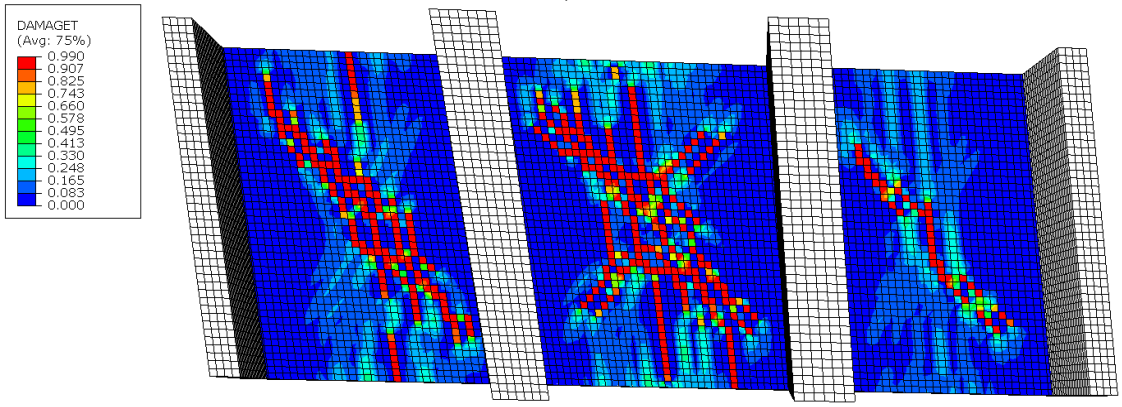

c)

Figure 66: Structural behavior of the Øvre Kvamme bridge w/o retrofitting

The results clearly show that the tensile damage emerges in the middle span first before the side slabs. This occurrence is due to the middle span being the longest in length and having the largest area among the three spans, resulting in a lower stiffness. The compressive damage has been excluded as no critical levels were observed during the analysis.

The analysis conducted on the entire bridge was very time-consuming, so efforts were made to simplify the model. Since the middle span appeared to be the weakest among the three, it was considered to be the most critical. The two side spans with belonging supports and reinforcement were temporarily removed to see if this greatly influenced the results. Moreover,

analyzing one slab and not the entire bridge as a whole simplifies the process of plotting graphs. The analysis of the whole bridge provides the reaction forces from all three spans collectively rather than individually. Loading each span individually as part of the whole bridge was considered as an alternative. However, due to time constraints, it was concluded to be impossible, considering the need to analyze the proposed strengthening models as well. Figure 67 a) and b) shows the first frame of tensile damage initiation from the analysis conducted solely on the mid-span and the belonging displacement distribution.

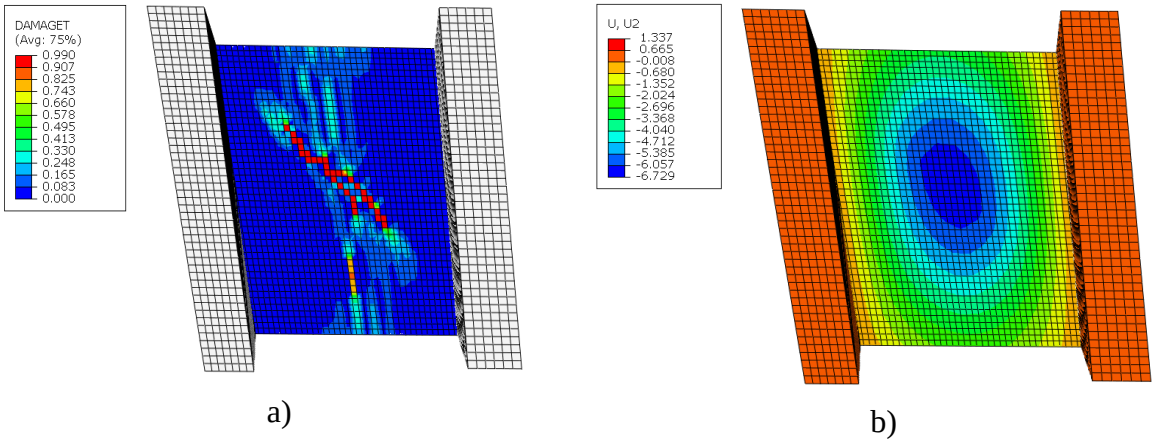

a) b)

Figure 67: a) Tensile damage initiation; b) vertical displacement distribution

This result exhibits a crack pattern quite similar to before, with crack initiation occurring at nearly the same step time, load, and displacement. The discrepancy between the two results is minimal, and it is challenging to distinguish them from each other. When analyzing the mid-span solely and the entire bridge model, the first crack appears at displacements of 6.7 and 6.4 mm with corresponding total loads of 3,932 kN and 3,846 kN, respectively. The minor discrepancy is likely due to frictional contact between the mid and side spans. On the model loaded individually, this resistance is not present, and the slab is able to flex freely. Given the minimal differences observed, it was decided to focus solely on the middle span and neglect these effects. It is assumed that the strengthening methods implemented in the middle span will be adequate for the two side spans.

The occurrence of cracking in concrete does not necessarily signify failure, and identifying the time frame of failure on the structure based on damage variables from the CDP variables alone is challenging. Therefore, the analysis result has been limited to 20 mm displacement, where it was observed that the reinforcement bars began to yield. The visualization of von Mises stress and AC yield in Abaqus are shown in Figure 68 a) and b).

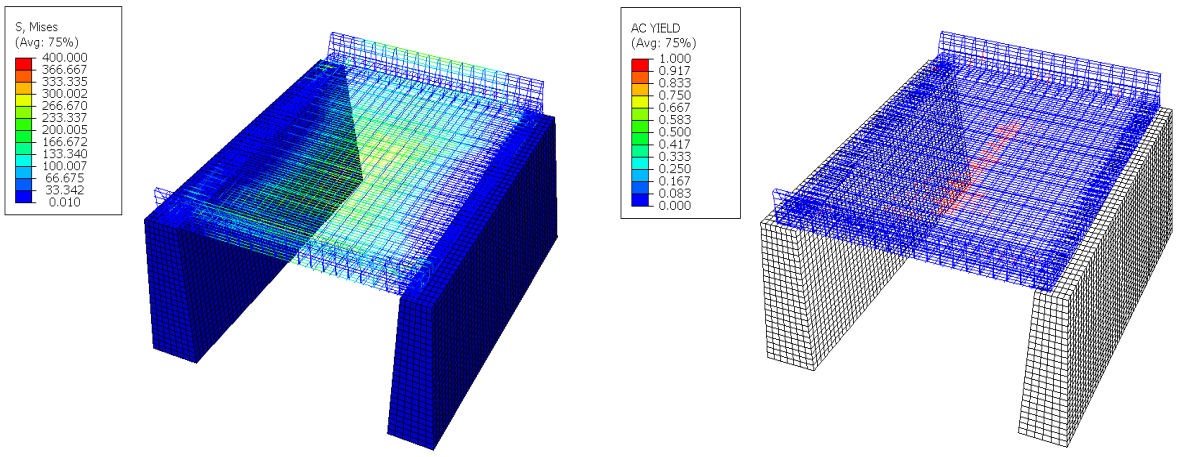

a) b)

Figure 68: a) Von Mises stress; b) AC yield, on the mid-span

From the figures, it is evident that the von Mises stress has reached a magnitude of 400 MPa, corresponding to the yield strength of the steel material used in the bridge. Additionally, a user-defined output variable exclusively for Abaqus, AC yield, demonstrates the activation of yielding. The AC yield ranges from 0 to 1, similar to the damage variables obtained for the concrete. At a displacement of 20 mm at mid-span, it is clear that the reinforcement has started to yield. Figure 69 shows the load-displacement curve of the middle span of the bridge. The graph initially contains a linear segment from the dead load of the bridge prior to the applied external load.

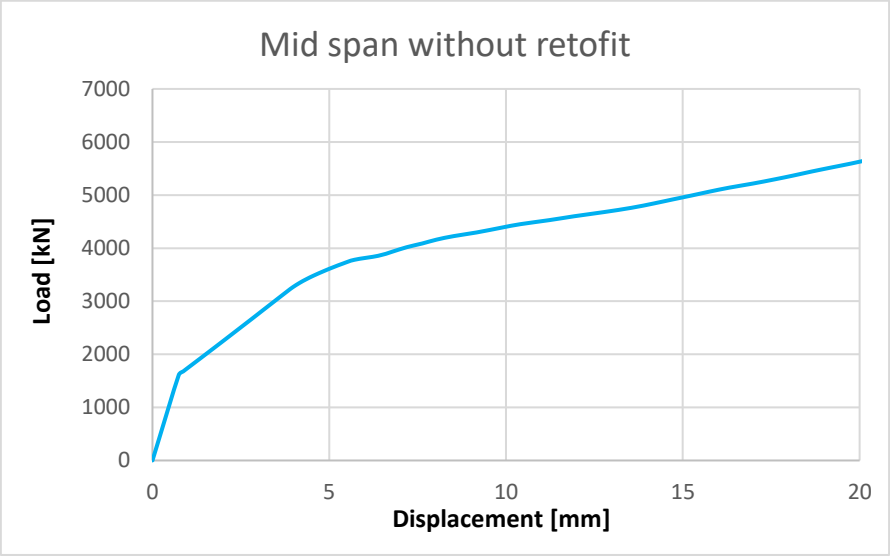

Figure 69: Load-displacement for mid-span without retrofitting

It is observed that the linear behavior of the bridge ceases at around 4.5 mm displacement at a load of 3,485 kN. Beyond this point, permanent damage is gradually evolving at the bottom surface of the slab. The Tensile Damage Parameter (DAMAGET) progressively increases from 0 to 0.99 at the small dip on the curve at 6.4 mm. Furthermore, the inelastic behavior continues,

and more regions are forming damage. Figure 70 a) and b) shows the extent of damage on the bottom surface of the middle span at a displacement of 10 and 20 mm subjected to a total force of 4,390 and 5,670 kN.

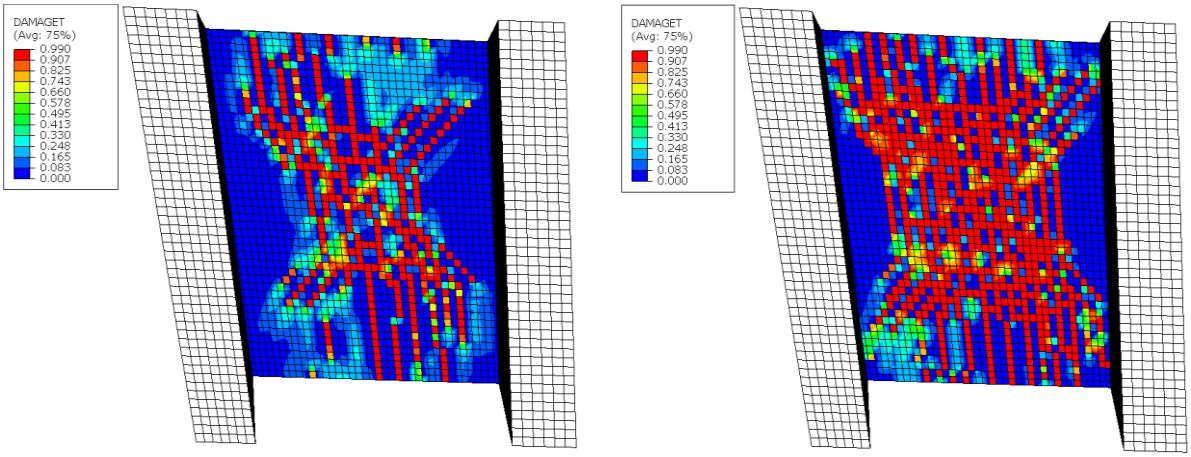

a) b)

Figure 70: Mid-span without retrofit at a) 10 mm; b) 20 mm

The damage is predominantly concentrated in the middle of the slab and has extended toward the side edges. The sides of the slab show less damage since the load is concentrated on the road, and not on the parapets. With a finer mesh, the position and pattern of damage could have been illustrated with greater accuracy. However, the existing level is a sufficient threshold to compare the subsequent analyses, including strengthening.

7 Rehabilitation and strengthening proposal for Øvre Kvamme bridge

Ensuring the safety and longevity of deteriorated RC bridges is a challenging yet critical task. To achieve effective outcomes and properly implement repair and strengthening techniques on Øvre Kvamme bridge, adherence to ISO 16311-3 [36] and 16311-4 [37] standards are imperative. ISO 16311-3 offers guidance on designing the repair and strengthening of existing RC structures, whereas ISO 16311-4 concentrates on the execution of repair and strengthening deteriorated RC structures. By utilizing these standards as a basis for proposing rehabilitation and strengthening methods, practical solutions can be guaranteed to solve the detected issues on Øvre Kvamme bridge from field investigation and FEA. In this thesis, UHPFRC and FRP composite materials are the strengthening methods selected for further structural analysis on Øvre Kvamme RC bridge.

ISO 16311-3 [36] states that concrete deterioration can be further prevented, maintained, and repaired using chemical, electrochemical, and physical methods. These methods can help prevent or stabilize the degradation of concrete and corrosion of steel [36]. Moreover, these mentioned methods are further described in detail as remedies throughout ISO 16311-3 [36] and the execution of it in ISO 16311-4 [37]. Additionally, the techniques and products applied on the existing structure could activate unwanted mechanisms affecting the structure's integrity. It is thus crucial to consider the impacts of individual techniques or products as well as the potential outcomes resulting from their interplay [36].

To achieve optimal results when strengthening Øvre Kvamme, a series of measures need to be implemented before applying composite materials like FRP and UHPFRC. Firstly, it is crucial to employ techniques and products for repair and strengthening that have a proven track record of success in similar projects, as specified in ISO 16311-3 [36]. Furthermore, from the literature review, it was discovered that the initial step in strengthening methods involves removing any damaged or loose concrete to ensure a satisfactory bonding surface between the old and new strengthening material, which is also emphasized in 16311-4 [37]. Bonding the new and old material is one of the most important factors for ensuring excellent results, particularly as a significant portion of the bottom surface of Øvre Kvamme bridge slabs has been affected by carbonation, as identified from the field investigation. Therefore, removing the degraded concrete surface is essential to ensure the robust structural integrity of the bridge with the suggested strengthening material.

Corrosion is a major concern on Øvre Kvamme bridge, and it is crucial to eliminate corroded areas from the existing reinforcement to prevent its propagation into the strengthening layer. Sandblasting is commonly used to remove corroded areas, and epoxy-coated reinforcement or cathodic protection can be utilized to protect the steel from future corrosion. To create a strong bond between the concrete and the composite material, a binder such as epoxy is necessary [97]. The surface to be strengthened is covered with epoxy before the new layer is applied, and a rough, often sandblasted, surface can further enhance the bond [97]. Furthermore, determining whether the cracks and the voids detected on the Øvre Kvamme bridge is a consequence of steel corrosion is crucial because the appropriate solution for addressing the cracks is contingent upon their underlying cause [36]. Cracks and voids in the structure must be repaired, and steps should be taken to prevent them from reappearing to avoid potential factors that could lead to further degradations in the RC structure.

ISO 16311-3 [36] introduces several remedies to address the mentioned issues on Øvre Kvamme bridge in a correct manner before installing strengthening composite materials on the structure [36]. A further detailed description of the execution of each remedy can be observed in ISO 16311-4 [37]. Some of these remedies include:

- Due to carbonated induced corrosion on the RC, it is important to remove areas that are affected by carbonation. The affected critical areas should be replaced with alkaline mortar/concrete. Minimizing the removal of concrete is vital for structural integrity.
- Decreasing the moisture inside the concrete will decrease the corrosion rate. This can be achieved with pore-filling impregnation or surface coating techniques and products.
- The anodic process can be halted by inducing re-passivation of the reinforcement, which can be achieved through the process of re-alkalization of carbonated-induced corrosion. This involves restoring a high pH level in carbonated concrete.
- To ensure strong bonding, it's crucial to clean and then roughen up the concrete surface thoroughly to remove any unwanted dust, loose materials, surface contaminants, or substances that may reduce its adhesive properties.

As per ISO 16311-3 [36] and 16311-4 [37], it should be emphasized that only experienced and trained personnel are authorized to implement these repair and strengthening techniques and each applied technique needs to be documented. The following sub-chapters will provide further details regarding the selected composite materials for strengthening Øvre Kvamme, including their materials properties and background.

7.1 Fiber reinforced polymers

Fiber Reinforced Polymers, also referred to as FRP, comprise a polymer matrix and thousands of continuous fibers, resulting in a composite material known for its strength, stiffness, and durability. A composite material involves blending two or more “parent” materials to produce a superior material that provides enhanced properties, surpassing those of its individual components [98]. The fibers in the composite material of FRP are typically made of materials such as carbon (CFRP), glass (GFRP), aramid, or basalt, while the polymer matrix is commonly composed of thermosetting or thermoplastics, materials such as epoxy, polymers, polyester, or vinylesters [22-23, 98-100]. GFRP was the first documented FRP material variant used, and it was embedded in polymeric resins that was initially developed in the petrochemical industry after World War II [101]. Although expensive at first, work began in the 1970s to lower the materials high cost, and it was later at the end of the 1980s when FRP materials were finding wider acceptance in construction of infrastructure [101].

Over the past few years, the construction industry has witnessed a surge in the popularity of FRP as a material of choice as seen from the literature review. The primary application of FRP in this sector involves the rehabilitation and strengthening of structures [23, 98]. A widely favored technique for reinforcing concrete slabs is bonding of FRP to the underside of concrete slabs (tension strengthening). This approach is becoming increasingly common as it effectively enhances the mechanical and durability properties of the structure providing numerous benefits, including increased ultimate flexural strength capacity, improved stiffness following cracking, and greater control over concrete cracks [21-22, 98-100]. The literature review findings indicate that the utilization of FRP techniques for reinforcing RC bridges allows for the preservation and upkeep of these structures following existing standards. Moreover, this reinforcement method can withstand the higher load levels necessary to sustain new national development plans, resulting in reduced expenses and retrofitting time [22-23, 98-99].

While providing numerous benefits, FRP also comes with certain downsides. One such disadvantage is its weak resistance to fire, which can lead to the release of toxic substances during combustion [22]. Additionally, the cost of materials is quite high, and the material itself is brittle due to the nature of the hardened polymer and the bond between concrete and the composite material. Strengthening concretes with FRP just increases the brittleness of the structure. Thus, achieving an excellent bond between new and existing materials is crucial to ensure optimal results. Furthermore, the anchoring and fastening process for the strengthening system involves drilling some FRP-material variants, which poses certain risks such as fiber

pull-out or breakage, matrix crack formation, thermal degradation, or delamination [22]. According to Ayesha et al. [22], the energy consumed during the production of a material is a significant determinant of its cost and sustainability. The production of FRP requires a considerably larger amount of energy than other conventional materials like steel and concrete, resulting in higher carbon emissions [22]. Despite this, the authors argue that when taking into account the entire service life, construction process, and maintenance requirements, FRP can still be considered cost- and environmentally friendly, even more than that of a steel-constructed structure [22].

Two methods can be used to install FRPs on existing structures: externally bonding with retrofitting laminates or near-surface mounted strips with or without adhesives and anchorage systems [22, 98]. For the purpose of this thesis, the most optimal technique for concrete bridge slab strengthening, as determined by the literature review, is retrofitting with external bonding. Externally bonding FRP with retrofitting on concrete bridge slabs improves the strength of the slab by 40-90% when the fibers of the FRP are oriented at zero degrees and bonded along the maximum bending zone [22]. The retrofitting can be carried out in various configurations, including side-bonding, U-wrapping, or full-wrapping, inclined or vertical, and can be achieved using mechanical anchoring, such as mechanical fasteners, spike anchors, straps, or with adhesives [22, 98]. Figure 71 displays some of the most common configurations of applying FRP on reinforced concrete structures.

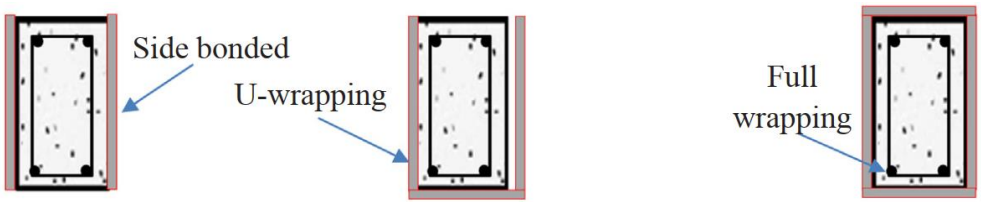

Figure 71: Configurations for FRP on RC structures - Retrieved from [98]

Before bonding the composite material, the deteriorated concrete surface must be cleaned, and major cracks should be filled with epoxy [25]. In addition, the surface where FRP sheets will be applied must be smooth and clean to ensure the best bonding between the existing and new material [98]. Furthermore, it is possible to add several layers on top of each other for additional benefits to the structure [22, 25]. Finally, in order to provide additional protection, it is recommended that a surface coating, such as a fire-resistant polymeric coating, be applied to the FRP material after the composite material has been applied to the existing structure [22, 98].

7.1.1 Material properties of CFRP

Even though FRP materials offers a wide range of benefits due to their excellent material properties, it is however, important to note that the properties of FRP materials are not consistent. This is due to the composite material being affected by various factors. One of the main factors that affect the properties of FRP is the size, type, and orientation of the fibers used [22]. Different fibers have different mechanical properties, and their orientation and size can impact the overall behavior of the material as evident by the findings from the literature review. For example, fibers that are aligned in the same direction as the applied load will have a higher stiffness and strength compared to fibers that are randomly oriented. In addition to fiber properties, the matrix used in FRP also affects the material properties. The matrix material provides a binding force that holds the fibers together and transfers the load between them [22].

Another factor that impacts the properties of FRP is surface texture, which affects the bonding between fibers and the matrix, and consequently, the material's overall strength and stiffness [22]. FRP's anisotropic nature results in substantially different mechanical properties in the longitudinal and transverse directions [22-23]. In the longitudinal direction (parallel to the fibers), the material is usually stronger and stiffer, while in the transverse direction, it is weaker and more flexible [22-23]. The fiber volume is additionally a large influencer on altering the material's behavior and properties, with a higher fiber volume typically resulting in a stronger and stiffer material and a lower fiber volume leading to increased flexibility. Typically, FRP materials contain a fiber volume of 50-70%, although this may vary depending on the application [98]. Figure 72 displays the material behavior of typical FRP materials compared to mild steel in a stress-strain curve. The figure illustrates CFRP exhibiting the most superior tensile properties compared to other types of FRP materials.

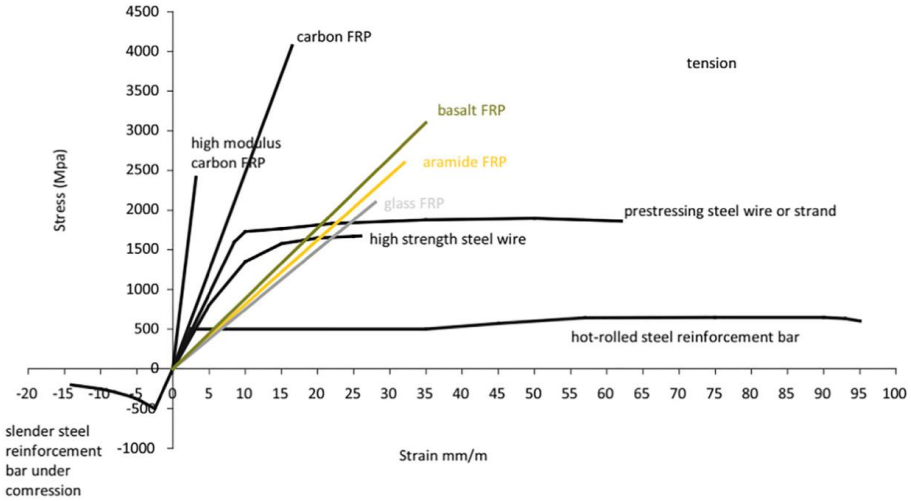

Figure 72: Stress-strain behavior of typical FRP materials - Retrieved from [22]

From the literature review findings in section 2.3.3, it was discovered that CFRP offers exceptional tensile and stiffness strength in proportion to its weight and size, which results in numerous advantages. This means that structures reinforced with CFRP can withstand heavy loads and stresses without adding unnecessary weight to the overall system. Importantly, it adds long-term material properties to the structure, particularly regarding fatigue behavior [22]. Furthermore, CFRP is also resistant to chemical attacks, making it an ideal material for harsh environments [22]. The composite material is easy to handle and transport, saving time and reducing costs during construction and installation [22]. This is particularly important when reinforcing existing structures, where time is often a critical factor [22-23]. As a result of the numerous benefits that have been attributed to CFRP as well as the superior mechanical properties showcased in the literature findings and Figure 72, the material has been selected as the preferred FRP material variant for further analysis as a strengthening solution for the Øvre Kvamme bridge. CFRP consists of a polymer resin matrix reinforced with carbon fibers, and the diameters of each fiber are approximately 5-10 μm [102]. Naser et al. [98] describe standard CFRP properties for plates and strips as an E-modulus of 155 GPa or higher, over 1.2 mm in thickness and 65-70% fiber volume. An illustration of the composite material structure can be seen in Figure 73.

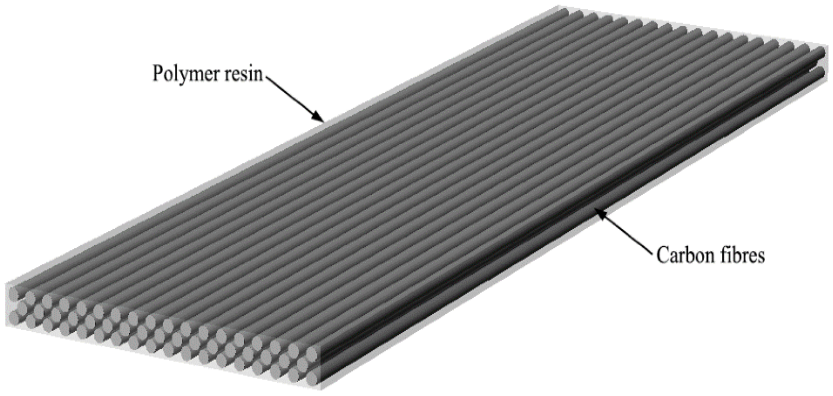

Figure 73: Structure of a CFRP matrix - Retrieved from [102]

7.2 Ultra-high performance fiber-reinforced concrete

Ultra-High Performance Fiber-Reinforced Concrete, also referred to as UHPFRC, was initially introduced and explored during the 1930s. The objective was to identify a more effective approach to improve the material properties of concrete to a greater extent [103]. It was in 1999 when Brühwiler introduced the idea of using UHPFRC to rehabilitate and strengthen existing bridges, ensuring their structural integrity throughout their entire lifespan and extend the

serviceability of the bridge [104]. Today the material is widely used in various rehabilitation and strengthening purposes, more commonly used on bridge elements and architectural building elements [97]. The composition of the material consists of aggregates, cement, water, additives, admixtures, and is reinforced with fibers [97, 103]. The most commonly used fibers in the material are steel, glass, carbon, plastic, or a combination of the mentioned fibers [103].

The difference between traditional concrete and UHPFRC, except for the addition of fibers, is based on the amount of binder and the size of the aggregates in the mix [103-104]. The material has a denser and more compact microstructure than regular concrete [97, 103]. The use of fine particles like silica fume, a low water-binder ratio, and a superplasticizer contribute to its low permeability. As a result, UHPFRC exhibits exceptional resistance to degradation processes such as carbon dioxide, chloride, sulfate, and corrosive liquids, as well as damage from thermal loads and freeze-thaw cycles compared to traditional concrete [97]. It was revealed from the literature review findings that UHPFRC exhibits outstanding durability and mechanical properties, including tensile strength over 7 MPa and compressive strength exceeding 150 MPa, while normal concrete is usually less than 50 MPa [20, 97, 103-104]. A large part of the enhanced properties is a result of the addition of fibers in the mixture, as it increases the ductility of the material both in compression and tension [97, 103]. As a result, this composite material is highly versatile and robust in contrast to traditional concrete.

Lionel & Philippe [26] characterized the material as having strong ductility and low permeability, making it a suitable substitute for conventional waterproofing membranes in structures. Bastien-Masse & Brühwiler [20] confirmed these findings, noting that the material offers superior bending and shear resistance to structural elements as well as increased load-bearing capacity. The utilization of UHPFRC on pre-existing structures can guarantee an improvement in both the durability and mechanical properties of the structures' health as discovered from the findings in section 2.3.3. The many benefits of UHPFRC make the material excellent for various applications and enables the material to be applied on complex structures [97].

UHPFRC is most commonly applied on the various deteriorated parts of bridges, including the bottom, top and sides of the bridge elements as an extra overlay on the existing structure surface layer [97]. Typically, the thickness of the applied UHPFRC layer ranges from 20 mm to 75 mm, and the scope and objectives of the strengthening procedure determine the insertion of additional reinforced rebars in the material. This was discovered during literature review

findings [20, 26, 97, 104]. Figure 74 displays three commonly used application methods of UHPFRC on existing concrete bridge decks [97]. The first two methods, a) and b), include utilizing a thin layer ranging from 20 to 30 mm of UHPFRC to protect the existing structure from water and other potentially harmful chemicals. Additionally, method b) also includes removing both the deteriorated existing concrete and its embedded rebars due to corrosion and replacing it with new rebars integrated into the UHPFRC, thus strengthening the reinforced structure in both durability and mechanical properties. Method c) the flexural strength is increased by applying a thicker UHPFRC layer ranging from 40 to 70 mm along with the installed rebars [97].

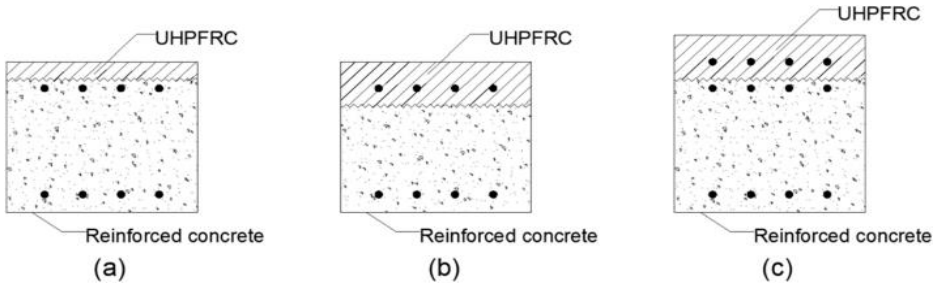

Figure 74: Application methods of UHPFRC – Retrieved from [97]

Huang et al. [97] explains that the bonding of UHPFRC on existing structures can be achieved with traditional concrete application methods, such as through cast in situ, adhesive bonding, or mechanical anchoring [97]. The choice of bonding method employed can lead to different levels of bond strength. Cast in situ is the most frequently utilized bonding technique for UHPFRC strengthened concrete structures because it is easy to use and straightforward with the addition of a fine concrete surface [97]. Huang et al. [97] revealed that when rebars were added in UHPFRC, epoxy bonding provided a greater capacity increase than mechanical anchorage. The selection of a particular application method depends on factors such as the extent and location of the damage on the bridge, as well as cost considerations since certain methods may require more man labor. Additionally, UHPFRC has a high material price and requires high-quality cement production, which makes it less environmentally friendly [97, 104]. Moreover, the material lacks standard design codes, which can make applying the composite material on existing structures more challenging than anticipated [97]. All these factors influence the selection of application methods and applied layer thickness of the material.

7.2.1 Material properties of UHPFRC

As mentioned in Sub-chapter 7.2, UHPFRC exhibits significantly superior mechanical properties compared to traditional concrete. With compressive strength values surpassing

150 MPa and tensile strength greater than 7 MPa as evident from the conducted literature review. The stress-strain behavior relationship of UHPFRC is highly impacted by the addition of fibers in the material mixture. The specific material properties change depending on several factors, including the type, geometry, orientation, stiffness, and volume fraction of fibers used in the mixture [103]. Furthermore, inserting fibers into the composite material will decrease the brittle behavior of the material, reducing the risk of sudden failure and instead improving the ductility properties [103]. This can be observed in Figure 75 and Figure 76. Figure 75 displays the stress-strain relationship regarding compressive stress on the composite material without fibers inserted in the mixture. The figure illustrates the typical mechanical characteristics of UHPFRC, which exhibits an E-modulus that falls within the range of circa 45 to 55 GPa.

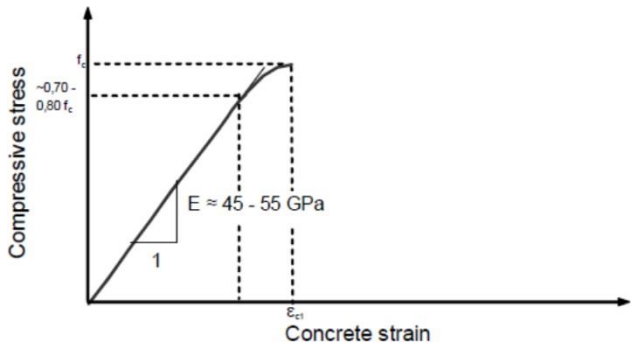

Figure 75: Stress-strain curve of UHPRC without fibers – Retrieved from [103]

It is observed that when the largest load is applied, the material begins to crack and then fails suddenly as one would expect from a brittle material. When fibers are applied into the material mixture, UHPFRC starts to deform before failure after the largest load is applied as shown in Figure 76. Adding fibers into the mixture enhances the ductile behavior of the composite material as mentioned.

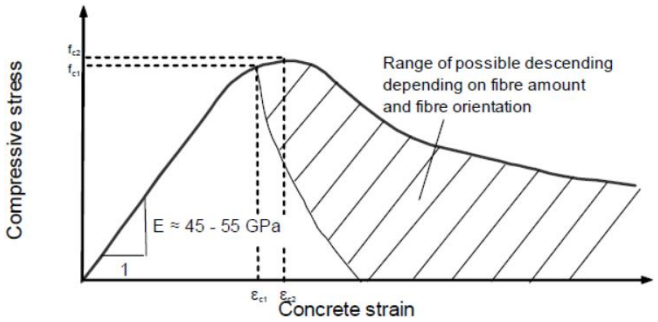

Figure 76: Stress-strain curve for UHPRC with fibers – Retrieved from [103]

The compressive strength of UHPFRC is often considered as its primary feature, but the flexural strength can be equally important, if not more [103]. Typically, the proportional limit for tensile stress is greater than 7 MPa. However, Mari & Jorun-Marie [103] suggest that by correctly incorporating fibers into the composite material mixture, it is possible to double the amount of

ultimate tensile strength [103], making the structure be more resistant to bending. Furthermore, in terms of tension behavior, UHPFRC can exhibit two distinct responses classified as either "strain-softening" or "strain-hardening" [20, 103]. When cracks begin to form at the yield stress load, the maximum tensile capacity of the structure can decrease if the fibers do not provide support. This concept is called strain-softening. On the other hand, if the fibers aid in preventing crack formation, the tensile capacity can increase, resulting in a strain-hardening response exhibited by the material. This concept can be observed in Figure 77 a), and b). Fiber type, geometry, and volume are all factors that decide the stress-strain response.

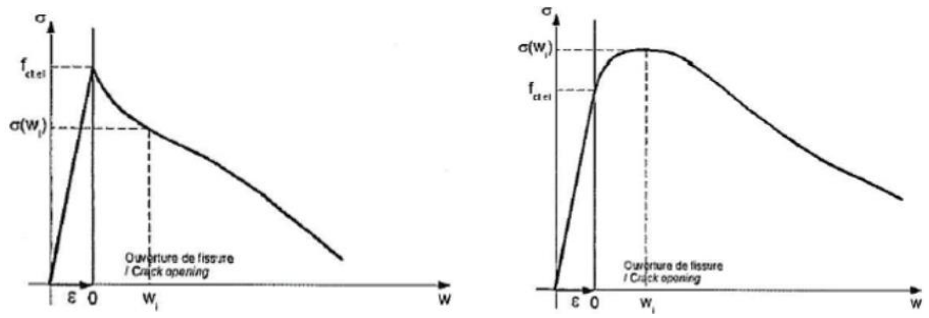

a) b)

Figure 77: a) strain-softening; b) strain-hardening response - Retrieved from [103]

Furthermore, it is common to enhance the material properties of UHPFRC even further when subjected to a thermal treatment [103]. The process of subjecting UHPFRC to a thermal treatment involves exposing the concrete element to high temperatures for a specific duration of time. This treatment offers several benefits to the concrete, making it a popular choice in the construction industry. One of the most significant benefits of thermal treatment is the improved strength of the concrete [103]. The exposure to high heat accelerates the chemical reactions that take place within the concrete, resulting in faster strengthening. As a result, the concrete gains increased compressive and tensile strength, making it more resistant to external forces and stress [103]. Another advantage of thermal treatment is the reduction in delayed shrinkage and creep effects. UHPFRC tends to shrink over time due to the evaporation of water, which can cause cracks and structural damage [103]. However, the heat treatment reduces the effects of delayed shrinkage and creep, thereby increasing the durability of the concrete. The exposure to high temperatures initiates the formation of more hydrates, which leads to the development of a denser and more compact microstructure [103].

7.3 Øvre Kvamme bridge strengthened with CFRP

In this thesis, the CFRP is created as a solid composite layup in Abaqus and the mesh is generated as SC8R continuum shell elements. The Øvre Kvamme RC bridge's tensile zone was retrofitted with CFRP plate and strip configurations for analysis and assessment. Using a mesh size of 150 mm, the CFRP plates resulted in a total of 1,620 elements, whereas the CFRP strips produced 867 elements. In addition, it was assumed perfect bonding between the materials and the bridge. Subsequently, the CFRP's material properties are implemented in two parts: the elastic criterion and the failure criterion. As the CFRP material is modelled as solid, the elastic properties are defined with the Engineering Constants, including Young's modulus (E), Poisson's ratio (ν) and Shear modulus (G) in all three directions (x=1, y=2, and z=3). The used elastic material properties of carbon fiber for the FEM model are retrieved from Zhenchao et al. [105] and are displayed in Table 21.

Table 21: Elastic material properties of carbon fiber

E_1	E_2	E_3	ν_{12}	ν_{13}	ν_{23}	G_{12}	G_{13}	G_{23}
[GPa]	[GPa]	[GPa]	-	-	-	[GPa]	[GPa]	[GPa]
230	15	15	0.21	0.21	0.307	9	9	5,03

The failure criterion, however, is implemented with the Hashin failure criterion. This criterion was developed by Zvi Hashin in 1980, which has emerged as one of the most utilized three-dimensional failure models for CFRP [106]. This criterion is recognized for its efficiency in capturing the complex failure behavior of CFRP by considering four different types of failures, including fiber tension, fiber compression, matrix tension, and matrix compression [106-107]. These failures are defined in Abaqus as HSNFTCRT, HSNFCCRT, HSNMTCRT, and HSNMCCRT, respectively. Each failure mode is characterized by a set of equations that describes the onset failure of the composite material. The equations *Eq(14-Eq(17*) are as follows [107-109]:

Fiber tens. ($\sigma_{11} \geq 0$): $$F_f^t = \left(\frac{\sigma_{11}}{X^T}\right)^2 + \alpha\left(\frac{\tau_{12}}{S^L}\right)^2 \quad \textit{Eq(14)}$$

Fiber comp. ($\sigma_{11} \leq 0$): $$F_f^c = \left(\frac{\sigma_{11}}{X^c}\right)^2 \quad \textit{Eq(15)}$$

Matrix tens. ($\sigma_{22} \geq 0$): $$F_m^t = \left(\frac{\sigma_{22}}{Y^T}\right)^2 + \left(\frac{\tau_{12}}{S^L}\right)^2 \quad \textit{Eq(16)}$$

Matrix comp. ($\sigma_{22} \leq 0$): $$F_m^c = \left(\frac{\sigma_{22}}{2S^T}\right)^2 + \left[\left(\frac{Y^c}{2S^T}\right)^2 - 1\right]\frac{\sigma_{22}}{Y^c} + \left(\frac{\tau_{12}}{S^L}\right)^2 \quad \textit{Eq(17)}$$

Where σ_{11}, σ_{12}, and τ_{12} represents factors of the equivalent stress tensor. While X^T, X^C, Y^T, Y^C, S^L, and S^T corresponds to the different type of strengths associated with longitudinal tensile, longitudinal compressive, transverse tensile, transverse compressive, longitudinal shear and transverse shear, respectively [107-109]. If the resulting values from the equations exceeds 1, failure occurs within the CFRP material [106]. The failure properties used in the FEM model are retrieved from Haichao et al. [107]. Table 22 displays the Hashin material properties of CFRP in Abaqus as well as its damage initiation parameters: G_X^T, G_X^C, G_Y^T, and G_Y^C, that presents the fracture energy of longitudinal tensile, longitudinal compressive, transverse tensile, and transverse compressive, respectively.

Table 22: Material properties of CFRP failure

X^T [MPa]	X^C [MPa]	Y^T [MPa]	Y^C [MPa]	S^L [MPa]	S^T [MPa]	G_X^T [kJ/m^2]	G_X^C [kJ/m^2]	G_Y^T [kJ/m^2]	G_Y^C [kJ/m^2]
1800	1250	50	150	93	50	40	40	0.25	0.75

It is important to address the fiber orientation when conducting FEA and NFEA of CFRP plies, as it can drastically change the mechanical properties and the overall performance of the composite material. The orientation of the fibers refers to the arrangement of the carbon fibers within the CFRP material, which can vary depending on specific applications and desired properties. Manufacturers typically customize the desired properties and fiber orientation of CFRP based on specific requirements and demands. The most commonly used fiber orientations in CFRP are longitudinal fibers (at 0°), transverse fibers (at 90°), and the in-between fibers (at ±45°) [110]. The different fiber orientations in the CFRP plies are presented in Figure 78.

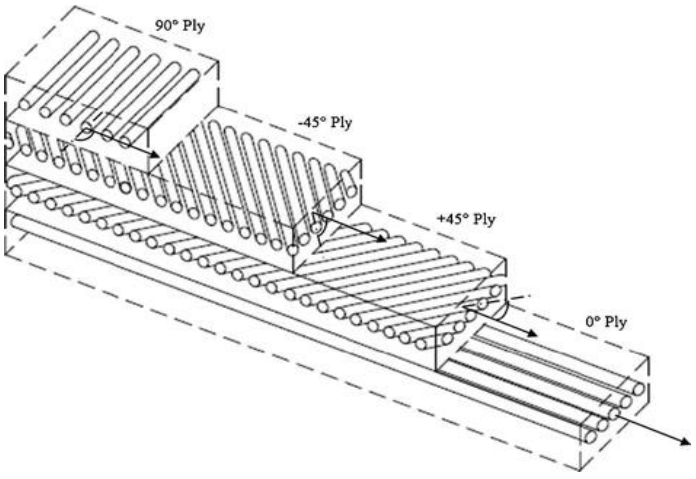

Figure 78: Different fiber orientations in CFRP laminate - Retrieved from [110]

It is important to establish a designated reference direction to properly incorporate the fiber orientations within each CFRP layer in Abaqus. This reference direction illustrates the

longitudinal orientation of the Øvre Kvamme bridge. Subsequently, various orientation types are employed to represent the fiber orientations at specific angles accurately. Figure 79 displays the difference in the fiber orientations at 0 and 90 degrees in Abaqus.

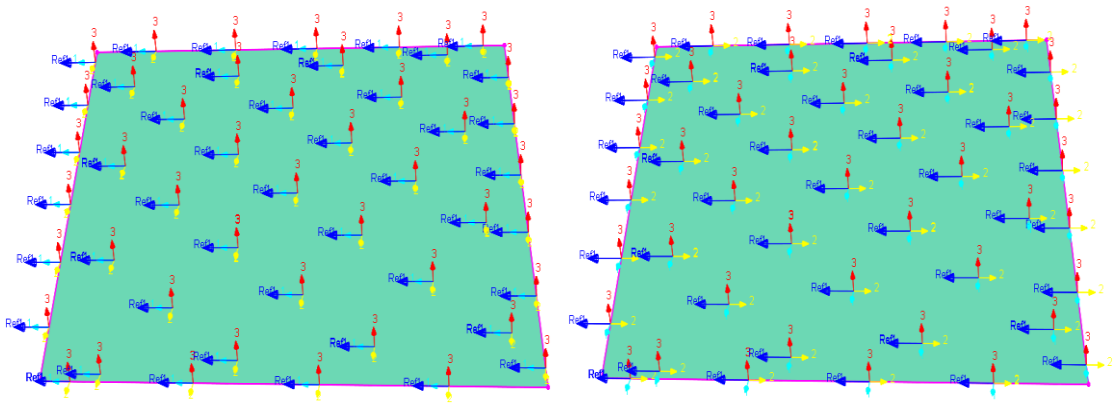

a) b)

Figure 79: a) Orientation at 0°; b) Orientation at 90°; of a CFRP plate in Abaqus

The dark blue arrow highlights the reference direction, while the light blue arrow showcases the assigned fiber orientation. The yellow and red arrows present other potential assigned fiber orientations if desired. Furthermore, it can be observed from the figure that the fiber orientation of 0 degrees is aligned perfectly with the reference direction, which could potentially indicate better mechanical properties.

Since CFRP consists of multiple plies, it is thus important to select the appropriate fiber orientations in each ply for the desired properties, resulting in different stacking sequences. Only two stacking sequences are investigated in the Øvre Kvamme model, the unidirectional laminate sequence, and the quasi-isotropic laminate sequence. The unidirectional sequence is characterized by having all the plies composed of a single fiber orientation. This approach allows for maximum strength and stiffness along a specific direction, as the fibers are aligned in a uniform manner. The investigated unidirectional sequence includes fiber orientations of 0°, 45°, and 90°. On the other hand, the quasi-isotropic laminate sequence involves incorporating different fiber orientations within each ply of the composite material. The aim is to achieve isotropic behavior, meaning that the CFRP mechanical properties are as similar as possible in all directions during different loading conditions. In the FEM model, the quasi-isotropic laminate sequence will incorporate all the mentioned fiber orientations. The fiber orientation techniques in CFRP for Øvre Kvamme bridge will be analyzed and assessed through four specific applications. Figure 80 shows the first crack initiation on the bridge's middle span (left), along with crack patterns at 10 mm displacement (right) using a) 0°, b) 45°, c) 90°, and d) Quasi-isotropic orientations on a 2 mm CFRP plate.

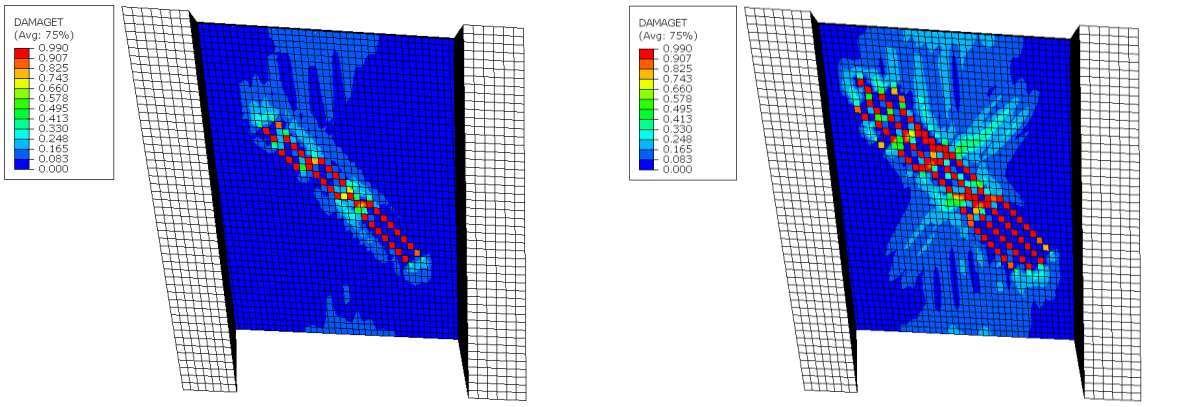

a)

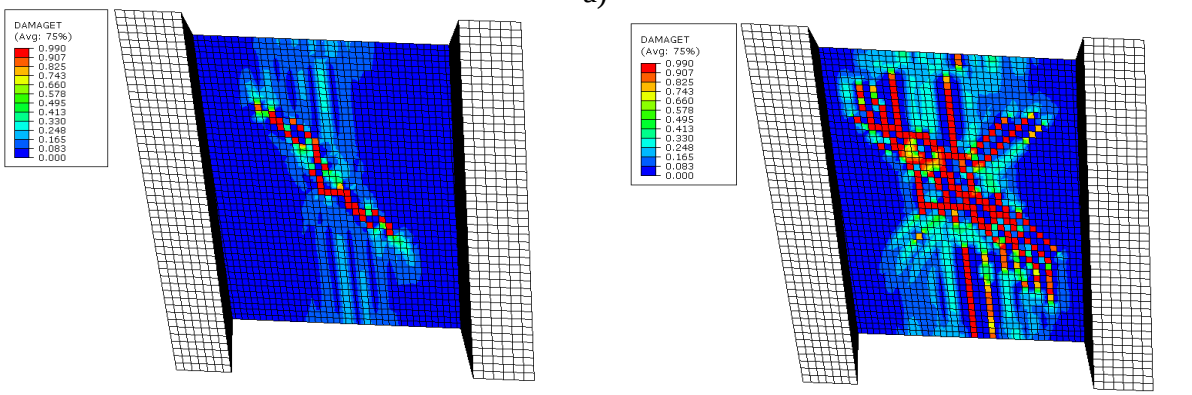

b)

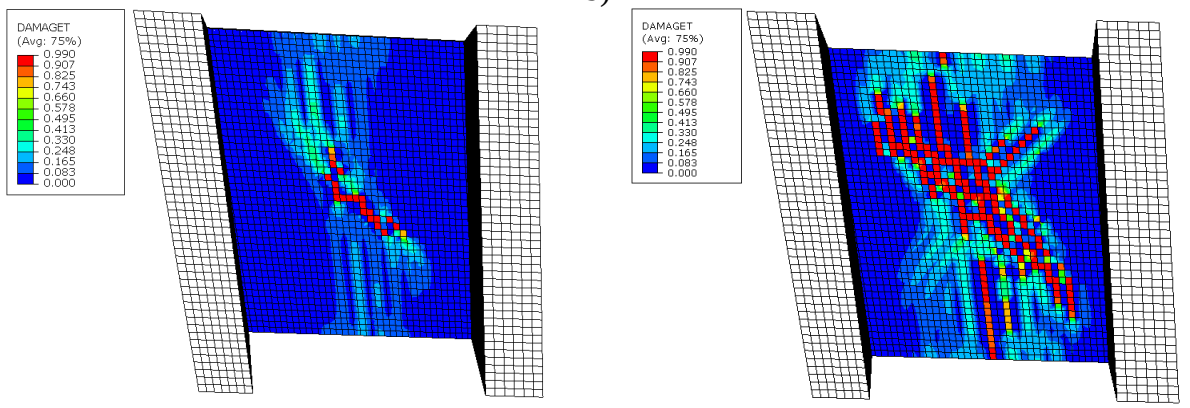

c)

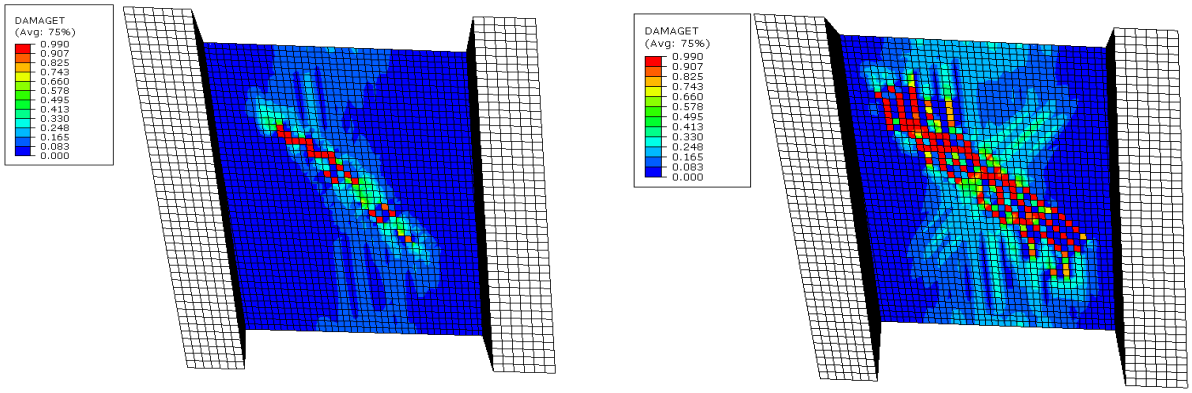

d)

Figure 80: a) 0°; b) 45°; c) 90°; and d) Quasi-isotropic, 2 mm CFRP plate

The FE-analysis conducted using Abaqus provided valuable results regarding the behavior of various fiber orientations of CFRP retrofitting. After analyzing the results, it can be observed that the crack pattern is most critical in the center of the bridge. Additionally, it is evident that while there are similarities in the initiation of the first crack among the various fiber orientations, there are also notable distinctions. The initiation of the first crack in the CFRP is influenced by the orientation of the fibers within the material as displayed in Figure 80. When the CFRP plate is loaded at approximately 4,050 kN, the first crack initiation is observed at a displacement of 6.744 mm for the 90° fiber orientation. Conversely, at 0° fiber orientation, the highest crack initiation displacement of 7.125 mm is observed. The findings indicate that when the fibers are aligned transversely (90°) to the RC slab, the material reaches its cracking point at a relatively low displacement. On the other hand, when the fibers are parallel to the longitudinal direction of the bridge (0°), the material can withstand greater deformations before cracking. The load at this point of crack initiation is found to be approximately 4,439 kN. Furthermore, in addition to the primarily flexural behavior that leads to diagonal cracks caused by shear forces, it is important to mention that there are also initiations of transverse cracks resulting from high tensile stresses at 45 and 90 degrees.

Furthermore, a notable disparity in the development of crack patterns at 10 mm displacement becomes evident when comparing the fiber orientations of 0° and quasi-isotropic with 45° and 90°. Even though the extent of crack propagation is considerably less in the 0° and quasi-isotropic sequence, the crack patterns of the fiber orientations are also different. Diagonal cracks predominate across all fiber orientations, but at 45 and 90 degrees, there are also large transverse cracks caused by high tensile stresses. Notably, a load of 5,139 kN was necessary to achieve a 10 mm displacement for a fiber orientation of 0 degrees, whereas only 4,607 kN was needed for 90 degrees, highlighting a substantial difference. Table 23 displays the notable loads and displacements observed of the different fiber orientations.

Table 23: Loads and displacement of different fiber orientation

Fiber orientation	Load at first crack	Displacement at first crack	Peak load	Load at 10 displacement	Crack pattern
0°	4,439 kN	7.125 mm	6,947 kN	5,139 kN	Diagonal
45°	4,090 kN	6.958 mm	5,890 kN	4,608 kN	Diagonal & transversely
90°	4,050 kN	6.774 mm	6,126 kN	4,607 kN	Diagonal & transversely
Quasi-isotropic	4,320 kN	7.109 mm	6,487 kN	4,829 kN	Diagonal

Figure 81 presents the structural behavior of different fiber orientations of a 2 mm CFRP plate installed on the tension zone of the mid-span. The figure covers the entire loading process until a displacement of 20 mm is reached.

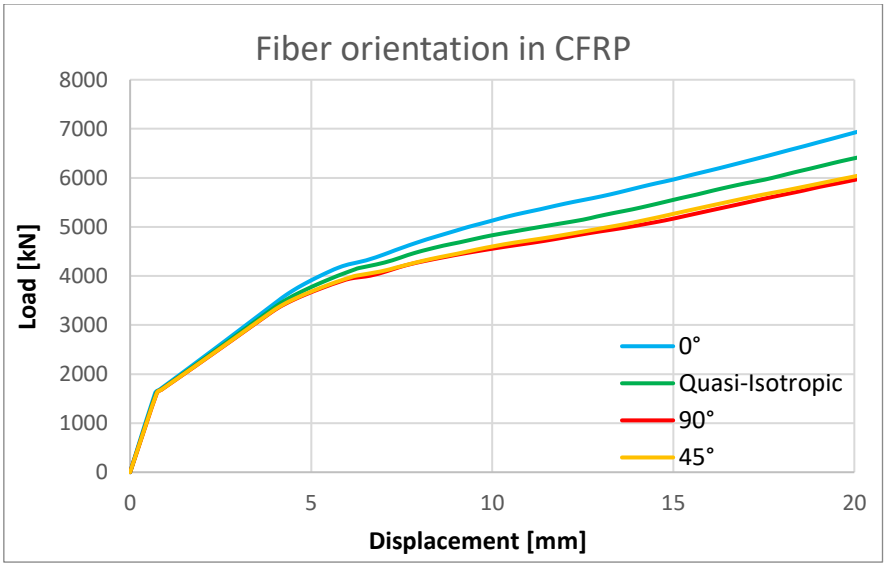

Figure 81: Load-displacement for fiber orientations in 2 mm CFRP plate

When examining the graphs and the extracted results, it becomes evident that the unidirectional fiber orientation of 0 degrees demonstrates the best resistance to flexural bending. This makes the fiber orientation of 0° the most effective option for Øvre Kvamme bridge when it is subjected to substantial vertical loading. In close consideration, the quasi-isotropic stacking sequence emerges as a secondary choice. Conversely, the unidirectional fiber orientations of 45 and 90 degrees demonstrate inferior performance, necessitating a lower load for the same displacement. It is important to note that no critical failure was observed in the CFRP plate itself. However, the concrete experienced complete failure during the analysis. These findings offer valuable insights into the influence of different stacking sequences and fiber orientations on the initiation of the first crack and subsequent behavior of the CFRP plate. The performance of the unidirectional fiber orientation of 0 degrees emphasizes its suitability for further analysis and exploration of CFRP types and thicknesses to strengthen the Øvre Kvamme RC bridge.

With the promising results observed for the fiber orientation of 0 degrees, a pushover analysis was performed to investigate further the effectiveness of retrofitting with 6 mm thick CFRP plate and strips. It is important to note that the CFRP strips were installed vertically and horizontally on the tension zone of the concrete slabs of Øvre Kvamme bridge. The strips were modelled with a width of 200 mm and a distance of 500 mm from each other throughout the bottom of the slabs. The base shear-lateral displacement curves extracted from Abaqus are displayed in Figure 82 below.

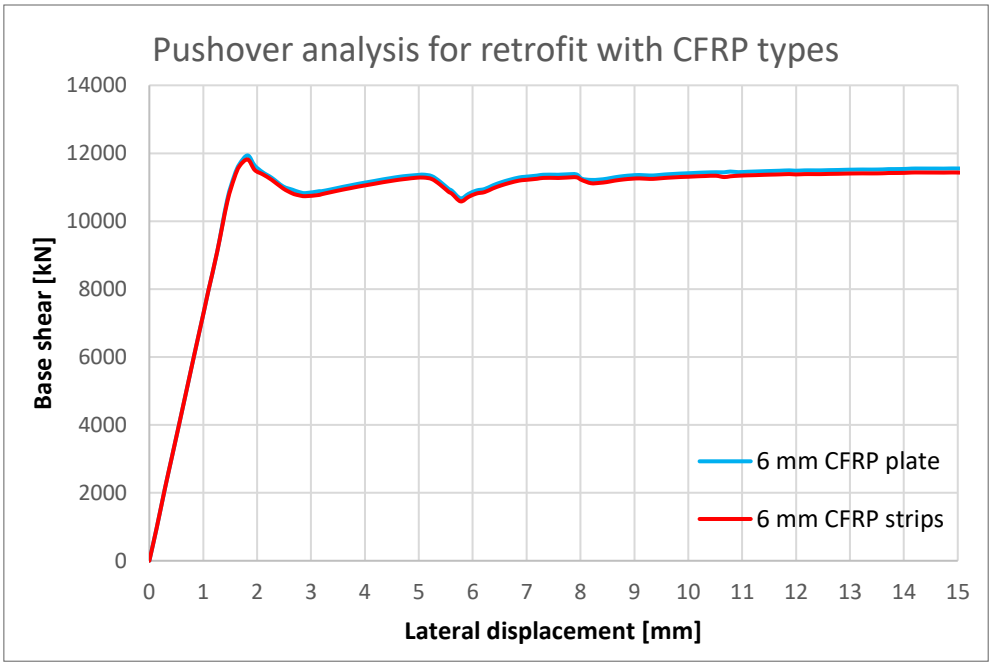

Figure 82: Base shear-lateral displacement for pushover analysis of CFRPs

The analyses of Øvre Kvamme bridge from the pushover analysis showcased a behavior resembling that of the RC bridge without retrofitting, although exhibiting slight improvement. The structure exhibits linear behavior up to a load of 11,816 kN, where the plastic behavior initiates, resulting in a decrease to around 10,582 kN. Subsequently, the structure behaves in a state of perfect plasticity, with a base shear value of approximately 11,600 kN observed at 8.4 mm displacement.

Furthermore, the effectiveness of different thicknesses of CFRP plate and strips retrofit configurations of Øvre Kvamme bridge was examined. The examined thickness for both of the CFRP types was selected to be 2-, 4-, and 6 mm. The influence of a thicker layer and the use of strips to cover the tensile side of the bridge was examined specifically on the tensile region of the middle span. The selection of CFRP strips over plate was deemed as a more ideal strategy for rehabilitation of the bridge, due to their higher flexibility and cost-efficiency. While CFRP plates offer significant advantages in terms of mechanical properties. Therefore, both options was explored and investigated as potential methods for strengthening the Øvre Kvamme RC bridge both in load-bearing capacity and durability.

Figure 83 displays the results of CFRP plates at a) 2 mm, b) 4 mm, and c) 6 mm; thicknesses at crack initiation and propagation at 10 mm displacement, when subjected to vertical loading with a fiber orientation of 0 degrees. It is important to note that the CFRP plates are hidden in order to assess the extent of damage to the concrete.

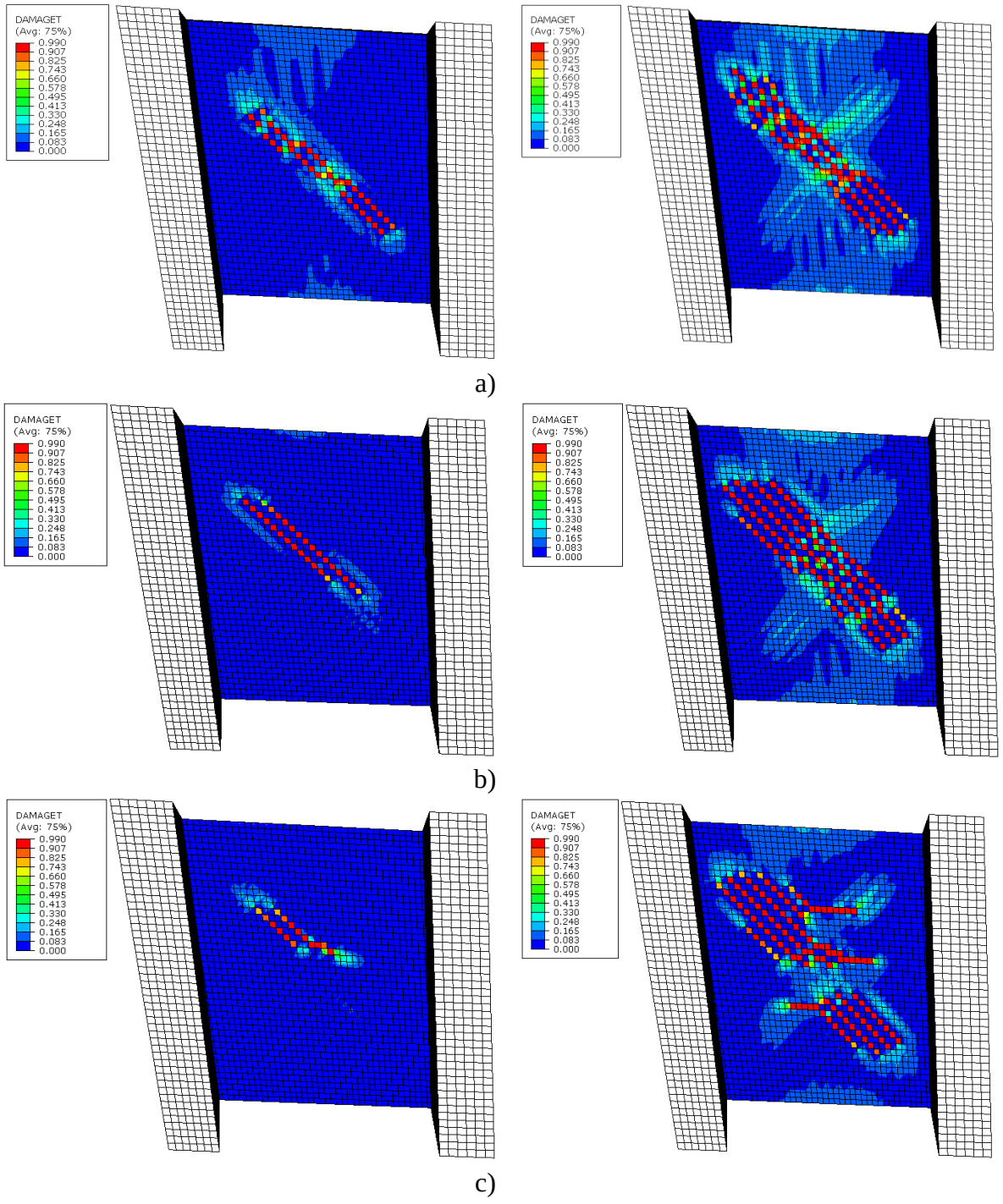

Figure 83: CFRP plate behavior at a) 2 mm; b) 4 mm; c) 6 mm thickness

When retrofitting Øvre Kvamme mid-span on the tension zone, the CFRP strips showcase a different behavior. The structural behavior and crack initiation is displayed in Figure 84 at a) 2 mm, b) 4 mm, and c) 6 mm thickness. The behavior is showcased for both the crack initiation and crack propagation at 10 mm displacement when subjected to vertical loading with a fiber orientation of 0 degrees.

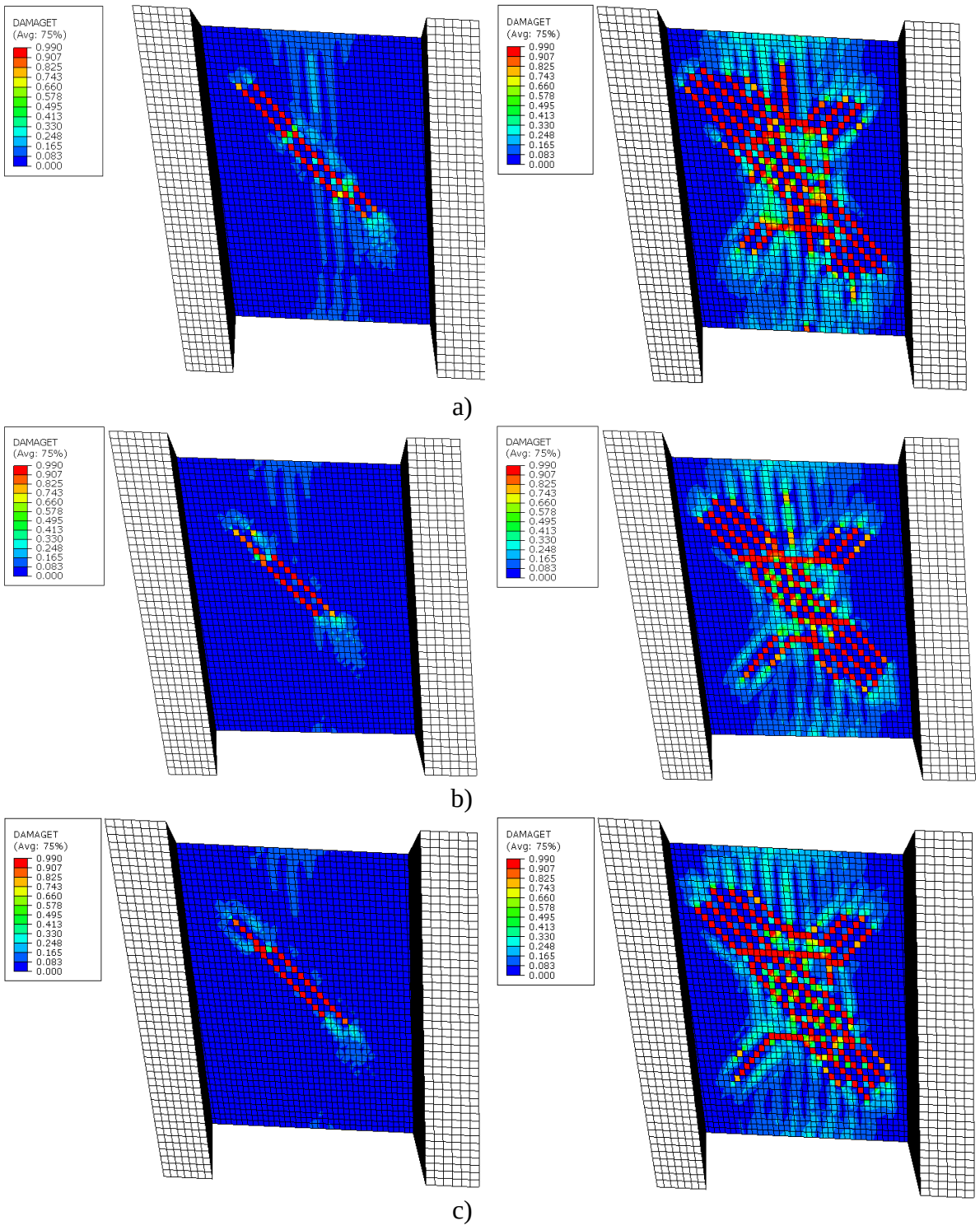

Figure 84: Behavior of CFRP strips with a) 2 mm; b) 4 mm; c) 6 mm thickness

The results obtained from the Hashin failure criteria exhibited a notable similarity between the CFRP strips and plates. However, CFRP failure was affecting the strips a lot more than the plate. Figure 85 shows the behavior of CFRP at 20 mm displacement when utilizing different thicknesses of strips. The figures to the left shows matrix tension damage (HSNMTCRT), while the right side shows fiber tension damage, (HSNFTCRT) at a) 2 mm, b) 4 mm, and c) 6 mm thickness. As mentioned previously, the CFRP material is permanently damaged when one of the parameters reaches a value of one.

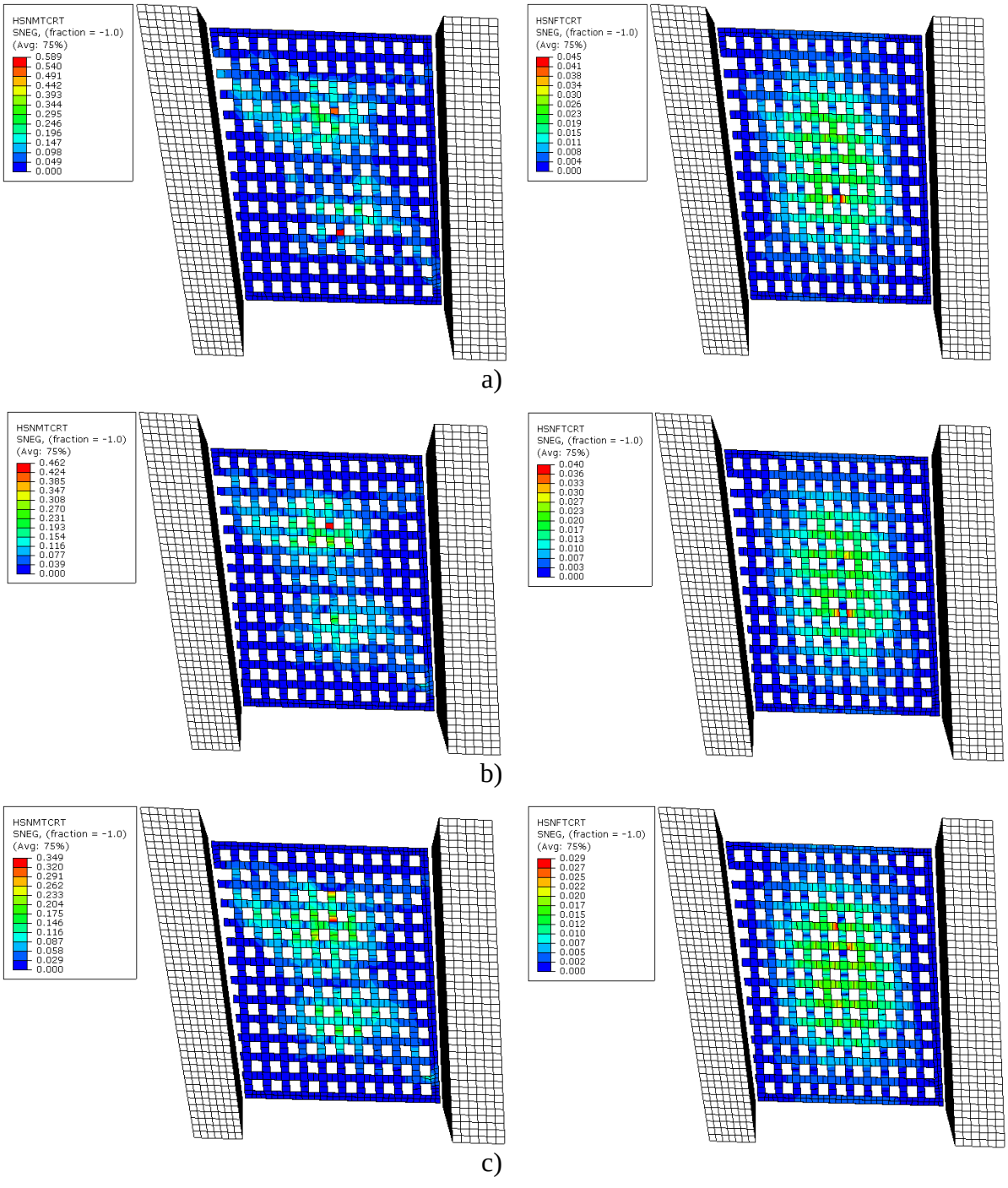

Figure 85: Hashin failure criteria for a) 2 mm; b) 4 mm c) 6 mm thick CFRP strips at 20 mm displacement

The structural behavior with the different configurations of CFRP plate and strips exhibits remarkable similarities during the two cracking stages. However, it was revealed that far less cracks developed on the concrete slab when retrofitting with CFRP plates compared to strips. The plates primarily only displayed diagonal cracks potentially due to shear force and excessive flexural stresses, while the strips displayed both diagonal and transverse cracks. The transverse cracks are likely a consequence of high tensile stresses. The results also confirm the expected outcome that as the thickness of the CFRP increases, the slabs become more capable of withstanding greater loads. Furthermore, it is important to note that while Hashin failure criteria did not indicate critical levels of damage at a displacement of 20 mm, it is crucial to acknowledge that failure will eventually occur as the load increases. The critical locations for potential matrix failure appear to correspond with fiber failure, although the matrix failures exhibit a more localized type of failure.

Figure 86 provides the load-displacement graphs of the various CFRP configurations at the maximum displacement of 20 mm. The different CFRP configurations are modelled on the bottom surface of the middle slab with a fiber orientation of 0 degrees.

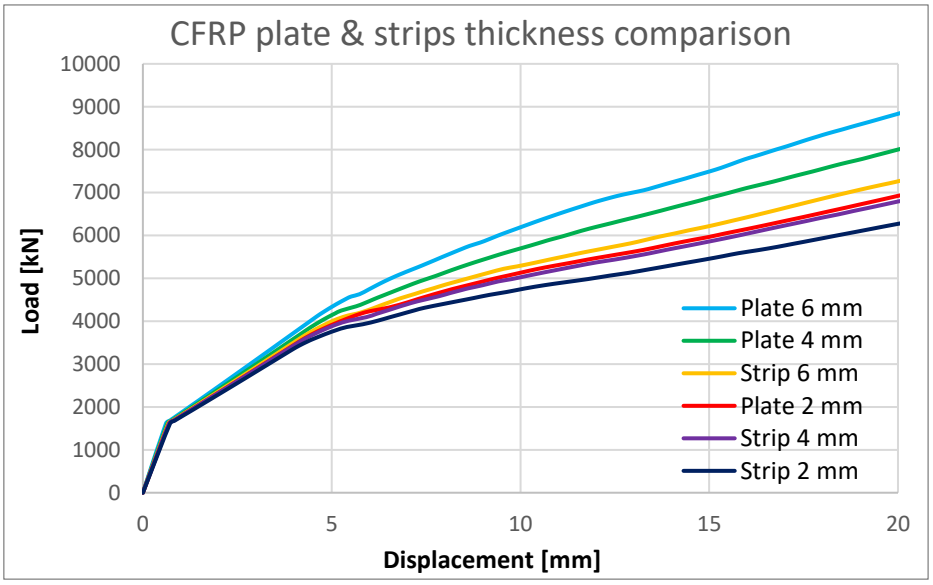

Figure 86: Load-displacement for CFRP plate & strips thicknesses

When examining results, it is apparent that the 6 mm CFRP plate is the optimal choice for improving the structural integrity of Øvre Kvamme bridge. Its performance can be attributed to the substantial thickness of the CFRP plate, which allows it to withstand a considerable amount of load without compromising its rigidity compared to the other investigated thickness and type. In contrast, the 2 mm CFRP strips demonstrate the least favorable performance among the tested configurations. This can be attributed to the smaller thickness and area of the 2 mm CFRP

strips compared to the other configurations. Interestingly, the 6 mm CFRP strip performed better than the 2 mm CFRP plate, showing promising results. It is noteworthy that none of the tested CFRP types and thicknesses exhibited failure. However, the Hashin failure criteria analysis provided valuable insights into the behavior of CFRP. It indicated that failure initiates in the matrix of the composite material before affecting the reinforcing carbon fibers.

Overall, the installation of CFRP plates with thicknesses of 2-, 4-, and 6 mm on the mid-span section of the Øvre Kvamme bridge yields significant improvements in its overall performance. Specifically, the application of 2-, 4-, and 6 mm CFRP plates results in approximately 9.6%, 18.6%, and 21.4% enhancements, respectively, compared to the CFRP strips with corresponding thicknesses. These findings highlight the effectiveness of CFRP plates in enhancing the load-bearing capacity and structural resilience of the bridge. Table 24, presented below, displays the summarized structural properties for the different CFRP retrofit configurations.

Table 24: Properties of different CFRP type and thicknesses

CFRP type (0 degrees)	Load at first crack	Displacement at first crack	Load at 10 mm displacement	Peak load	Crack pattern
Plate 2 mm	4,439 kN	7.125 mm	5,138 kN	6,947 kN	Diagonal
Plate 4 mm	4,560 kN	6.235 mm	5,764 kN	8,156 kN	Diagonal
Plate 6 mm	4,810 kN	6.075 mm	6,221 kN	8,986 kN	Diagonal
Strips 2 mm	4,158 kN	6.667 mm	4,762 kN	6,338 kN	Diagonal & transversely
Strips 4 mm	4,094 kN	5.966 mm	5,060 kN	6,875 kN	Diagonal & transversely
Strips 6 mm	4,174 kN	5.658 mm	5,362 kN	7,404 kN	Diagonal

7.4 Øvre Kvamme bridge strengthened with UHPFRC

UHPFRC was implemented as a 3D stress element of type C3D8R with a total of 1620 elements in Abaqus. In order to strengthen material Øvre Kvamme bridge, the model was modified, and UHPFRC incorporated to the bottom of the slab. The UHPFRC parts were modeled based on the coordinates of the existing bridge slabs, with careful consideration given to selecting coordinates of the section to avoid contact with the supports. To represent the behavior of the concrete in terms of plasticity and damage, the CDP model was also utilized. As the stress-strain behavior of UHPFRC is different compared to ordinary concrete, parameters found in the literature were used in the model [111]. The parameters can be found in Appendix A. To ensure

a perfect bond between the materials, similar to the installation of CFRP, the UHPFRC sections were connected to the existing concrete surface using a surface-based tie constraint in Abaqus. This tie constraint ensures that the translational and rotational motions are identical for the pair of surfaces.

Figure 87, presented below, illustrates the structural response of the bridge strengthened with 50 mm UHPFRC when subjected to lateral pushover load. The figure shows base shear along the y-axis and lateral displacement on the x-axis.

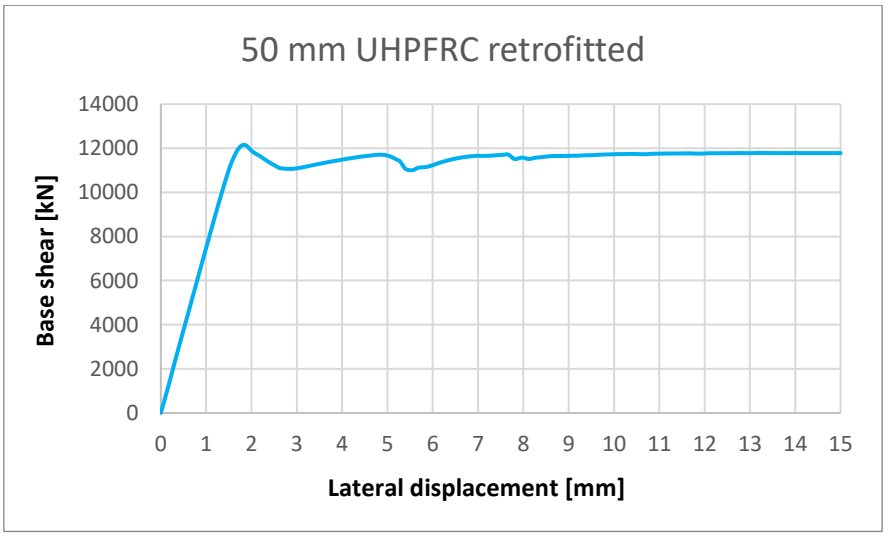

Figure 87: Base shear-lateral displacement for 30 mm UHPFRC retrofitted

Upon examining the outcomes derived from the pushover analysis displayed in Figure 87, it was evident that the retrofitted bridge exhibits similar behavior to the bridge model without retrofitting. However, it demonstrates its ability to withstand more lateral load. Under the influence of horizontal forces, the structure initially behaves linearly until it reaches an approximate lateral displacement of 1.8 mm at a maximum load of 12,146 kN. When reaching the maximum load, the structure enters a yielding elastic phase, exhibiting more plastic behavior until it gradually stabilizes at around 9 mm displacement. Once stability is achieved, the structure assumes a perfect plasticity behavior with a load of approximately 11,770 kN.

During the vertical loading analysis, various thicknesses of UHPFRC were investigated and compared to assess the effectiveness as a potential strengthening method. The chosen thicknesses used in the analyses were obtained from the comprehensive literature review and consist of a 20-50 mm layer attached to the bottom of the slab. Figure 88 illustrates the crack initiation to the left, and the tensile damage at a displacement of 10 mm to the right. Additionally, the figures are divided into a) 20 mm, b) 30 mm, c) 40 mm, and d) 50 mm.

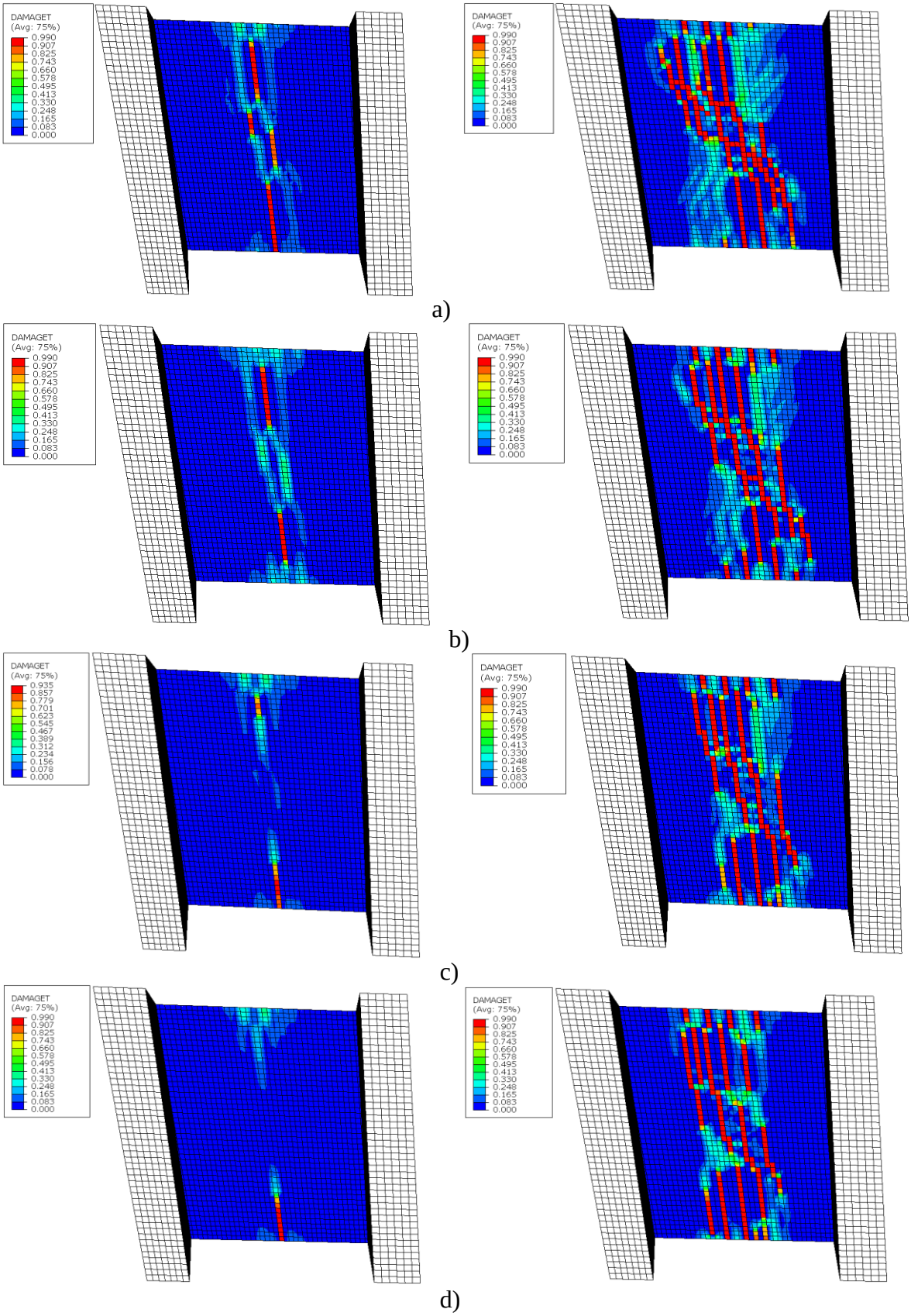

Figure 88: UHPFRC retrofitted with a) 20 mm; b) 30 mm; c) 40 mm; d) 50 mm

In Figure 89, the UHPFRC layer's condition is displayed for different strengthening configurations when exposed to a vertical load at a maximum displacement of 20 mm. Although the UHPFRC thickness configurations experience an equal amount of displacement, there are notable discrepancies in the magnitude of the applied load, which is significantly greater for the thicker sections. The figure showcases a) 20 mm, b) 30 mm, c) 40 mm, and d) 50 mm.

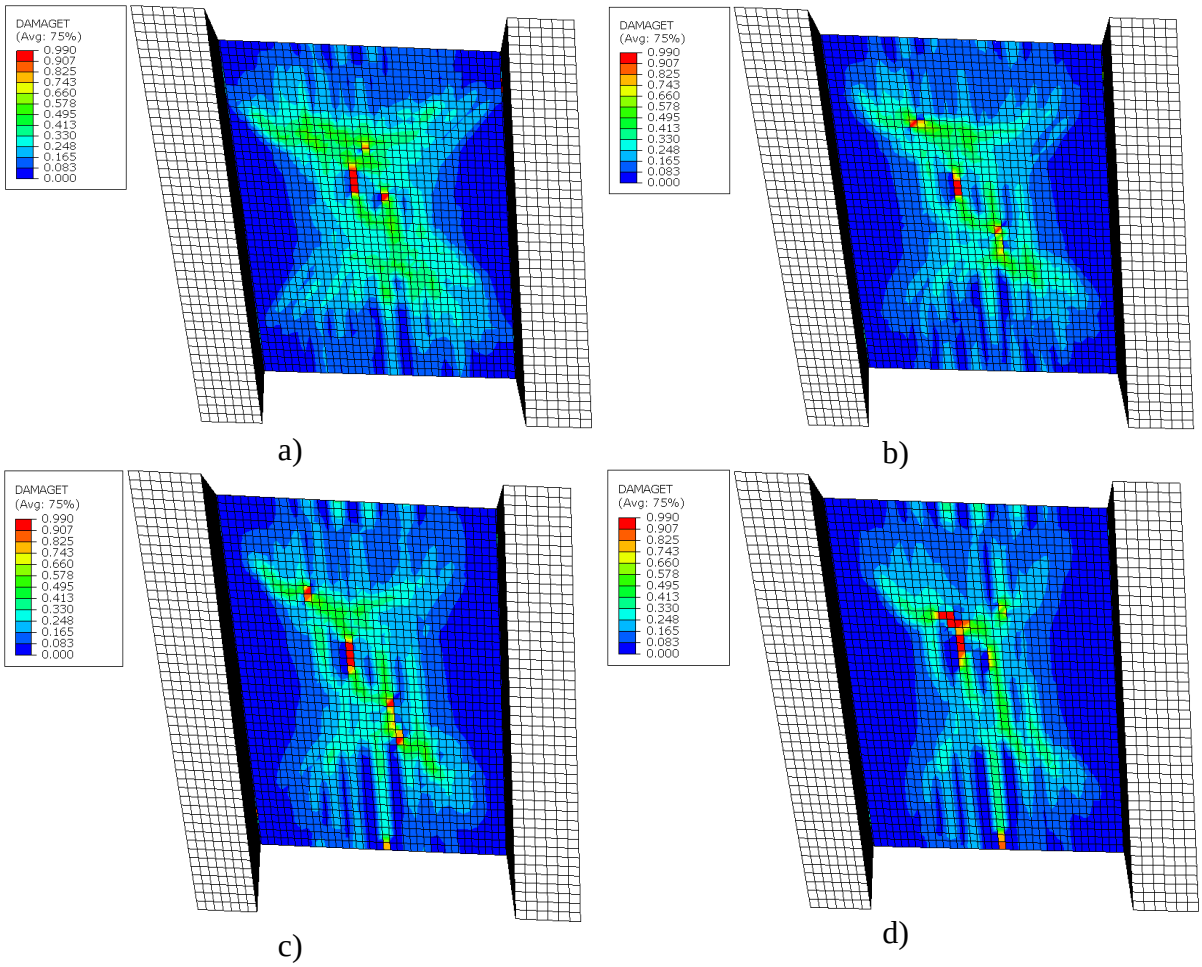

Figure 89: Condition of UHPFRC layer at a) 20 mm; b) 30 mm; c) 40 mm; d) 50 mm

By analyzing Figure 88, it can be observed a consistent structural behavior across the various thickness configurations when subjected to vertical loading. When the thickness of the composite layer is increased, the occurrence of cracks decreases at the same load. Furthermore, it can be observed that UHPFRC primarily results in transverse cracks in the tensile zone of the bridge slabs. Although it seems to exhibit potential diagonal cracks on the UHPFRC layer, as showcased in Figure 89. Overall, the condition of the UHPFRC appears to be in better shape than the underlying concrete, due to its higher flexural strength. However, some small cracks are observed in specific areas, as depicted in the figures.

The load-displacement graphs of every UHPFRC configuration are compared in Figure 90, and shows the effectiveness of increasing the thickness from 10 to 50 mm.

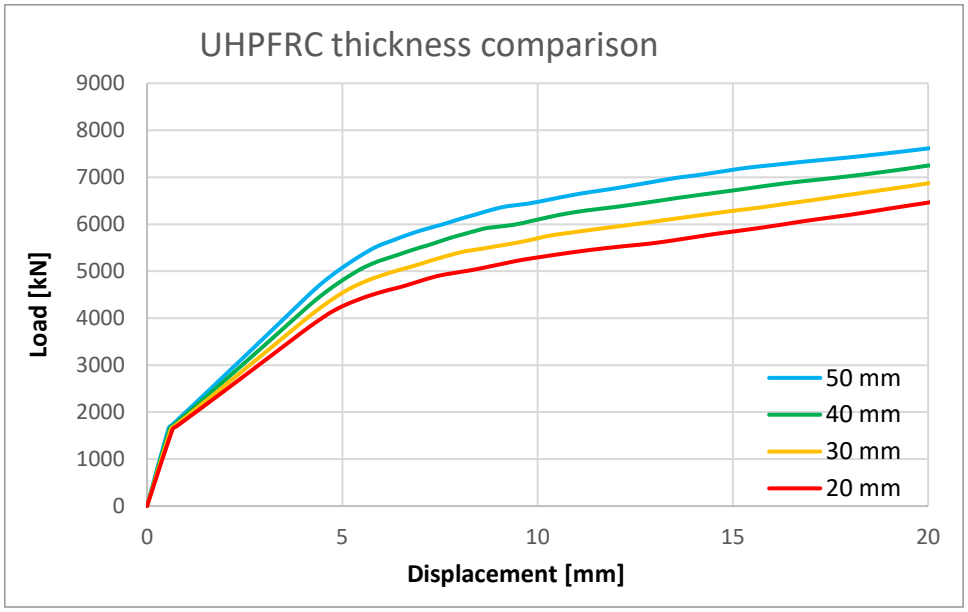

Figure 90: Load-displacement for Comparison of UHPFRC thicknesses at tensile zone

The graph demonstrates consistent patterns across various retrofitting thicknesses with UHPFRC, where thicker retrofits yield superior results. The behavior of the bridge appears to be consistent with the increasing trend of the vertical load. Notably, the highest load recorded is approximately 7,646 kN when implementing a 50 mm thick UHPFRC layer, while the lowest load stands at 6,504 kN with a 20 mm. Consequently, the optimal choice surpasses the least effective alternative by a significant margin of 17.6%. The properties of each UHPFRC thickness configuration applied to the tensile zone can be observed in Table 25.

Table 25: Properties of different UHPFRC retrofitting configurations

UHPFRC thickness	Load at first crack	Displacement at first crack	Load at 10 mm displacement	Peak load	Crack pattern
20 mm	4,643 kN	6.552 mm	5,312 kN	6,504 kN	Transverse
30 mm	5,089 kN	6.721 mm	5,695 kN	6,891 kN	Transverse
40 mm	5,450 kN	6.756 mm	6,074 kN	7,270 kN	Transverse
50 mm	5,660 kN	6.848 mm	6,483 kN	7,646 kN	Transverse

8 Results & discussions

The conducted field investigation on Øvre Kvamme bridge revealed that the structure had undergone significant deterioration, with corroded reinforcement being the primary cause and a critical factor influencing further degradation. Carbonation is identified as a major contributor to the corrosion process, with the sides of the bridge being the most severely affected areas. As a result, the load-bearing capacity in these regions is heavily reduced. Despite the high moisture level in the concrete, there is a significant difference in the recorded compressive strength between the investigation conducted by BruKon AS and the field investigation conducted on November 9th, 2022, indicating the expansion of carbonation during the testing periods. The performed field investigation also revealed a moderate probability of active corrosion beneath the concrete in areas with no visible signs. The bridge's condition has significantly weakened, affecting both its serviceability and load-bearing capacity, and urgent repair and strengthening are necessary to ensure its safe use in the future.

However, ensuring the safety and longevity of the deteriorated Øvre Kvamme bridge is challenging. To achieve effective results, adherence to standards and regulations is crucial. Measures such as removing damaged concrete, addressing corrosion, repairing cracks, and ensuring a strong bond between materials are essential when rehabilitating the bridge and strengthening it with the proposed materials. Several remedies can be recommended from standards and regulations, including replacing carbonation-affected areas, reducing moisture, re-alkalizing corrosion, and preparing the concrete surface for retrofitting. The implementation of these techniques should be carried out by experienced personnel, and proper documentation is crucial throughout the entire rehabilitation process.

Multiple methods and techniques were employed to develop a feasible finite element model of Øvre Kvamme bridge that can more accurately replicate the structural behavior of the actual conditions. This was necessary as the post-processed natural frequencies obtained from OMAway sensors displayed very low and unstable values. Thus, in order to achieve more similar frequencies from the FEM model to those obtained from the OMAway sensors, it was assumed that the supports had a higher stiffness than the surrounding soils. Furthermore, the stiffness of the concrete slabs had to be modified due to the significant degradation the bridge has experienced over time as evident from the field investigation. A numerical simulation was created to validate the acquired natural frequencies from the Abaqus model using ETABS. By refining the bridge's mode shapes using input from both OMAway sensors and the ETABS

validation model, it was ensured that the results from Abaqus were feasible, with a natural frequency of approximately 11 Hz.

The NFEA of the developed FEM-model revealed that the bridge's mid-span is the most critical among the three. The orientation of the fibers in the CFRP material greatly affects the first crack's initiation and propagation. Transverse alignment (90° orientation) leads to earlier cracking at lower displacements, while longitudinal alignment (0° orientation) allows for greater load resistance before the first crack occurs. Different fiber orientations result in distinct crack patterns, with diagonal cracks being most common due to shear forces and excessive flexural stresses. Additionally, transverse cracks appear at 45° and 90° fiber orientation due to high tensile stresses. Notably, the unidirectional fiber orientation at 0° demonstrates excellent resistance to flexural displacement and high load-bearing capacity. Therefore, it has proved to be the most effective choice for CFRP stacking sequence when strengthening the Øvre Kvamme bridge under significant vertical loads.

CFRP plates and strips have different crack patterns: plates exhibit diagonal, while strips lead to diagonal and transverse cracks. Thicker CFRP plates and strips need a much higher load to achieve the same equivalent displacements. Among the investigated thickness and configurations, the 6 mm CFRP plate stands out for its exceptional stiffness and improved structural integrity. Furthermore, the Hashin failure criteria revealed that failure in the CFRP material would start in the matrix before affecting the carbon fibers. However, even at a structural flexural displacement of 20 mm, the CFRP displayed no failure in the composite material and was able to withstand even greater displacement and loads.

Increasing the thickness of the UHPFRC layer relative to the applied load reduced the crack initiation. This behavior remained consistent even at higher loads and displacements. Transverse cracks mainly occurred in the bridge slabs tensile zone but with some diagonal cracks observed in the UHPFRC layer. However, the UHPFRC layer was in a better condition than the underlying concrete, but small cracks were present in certain areas. When the thickness of the UHPFRC layer was increased by 10 mm, a noticeable improvement of approximately 5-6% in load-bearing capacity was achieved. Consequently, retrofitting the Øvre Kvamme bridge with a 50 mm UHPFRC layer emerged as the most optimal choice among the various UHPFRC configurations investigated.

The purpose of the lateral pushover analyses was to examine the differences in the behavior when exposed to horizontal loads such as seismic, wind and breaking loads. Figure 91

demonstrates that strengthening the bridge slabs in tensile zone against lateral forces has limited effectiveness due to the differences in stiffness between the slabs and supports. Initially, the testing included evaluating all configurations of CFRP and UHPFRC used previously in the lateral pushover analysis. After comparing the results, minimal differences were observed between the non-retrofitted model and the models including the thinnest layers of CFRP and UHPFRC. Consequently, it was decided to only present the three most effective configurations compared to the non-retrofitted results. The remaining configurations naturally fall between the extremes, ordered by thickness and fiber orientation.

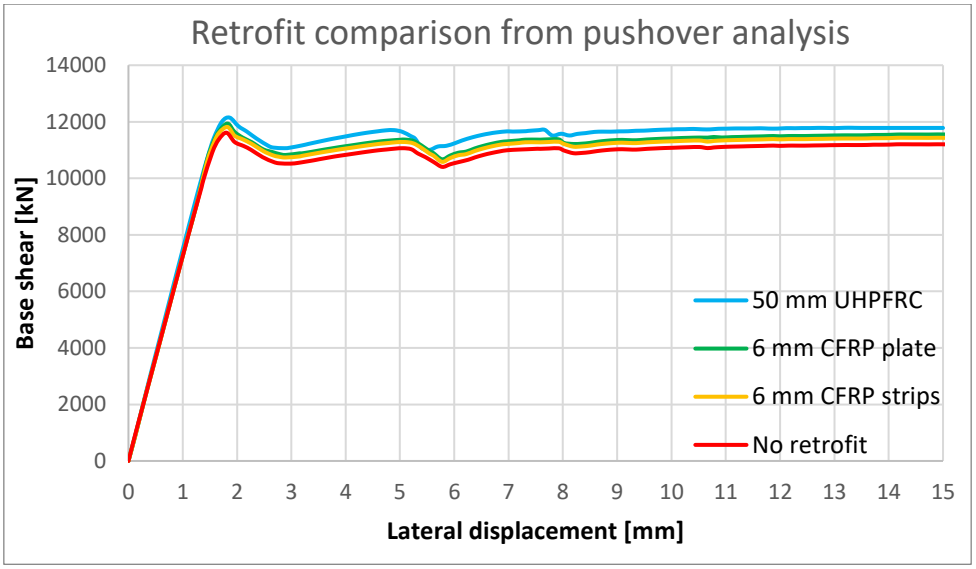

Figure 91: Base shear-lateral displacement for pushover comparison

The initial damage primarily develops at the bottom of the supports for every configuration and increases until local failure. Subsequently, it propagates upwards towards the slabs as the external load increases. The graphs further illustrate that the structure exhibits a linear response both with and without retrofitting until it reaches a yielding point of approximately 1.8 mm lateral displacement. Beyond this point, the structure enters a plastic deformation phase, where it will experience further deformation without any significant change in the applied load. It continues to deform plastically until it reaches around 9 mm displacement, at which point it exhibits perfect plastic behavior for the rest of the analyses. It is important to note that reinforcing slabs alone is not highly effective in providing resistance against lateral forces on the bridge. The stiffness of the structure heavily relies on the material properties of the supports. To enhance the bridge's overall resistance, it is necessary to explore methods for strengthening the supports. By strengthening the tensile zone of the structure with 50 mm UHPFRC, a small increase of 4.59% is obtained in ultimate load. The extracted results of the pushover analysis for each strengthening configuration are displayed in Table 26.

Table 26: Pushover results for different retrofit configurations

Strengthening method	Elastic yield load	Displacement at first crack	Load capacity improvement
No retrofit	11,613 kN	1.80 mm	-
CFRP strips, 6 mm	11,816 kN	1.81 mm	1.75%
CFRP plate, 6 mm	11,935 kN	1.82 mm	2.77%
UHPFRC, 50 mm	12,146 kN	1.86 mm	4.59%

When subjecting the Øvre Kvamme RC bridge to increasing vertical loads the differences between the reference model and the most suitable retrofitted configurations become more distinctive. Figure 92 presents the load-displacement curve, effectively demonstrating the response of the bridge under heavy vertical loading and highlighting the exceptional strength of CFRP.

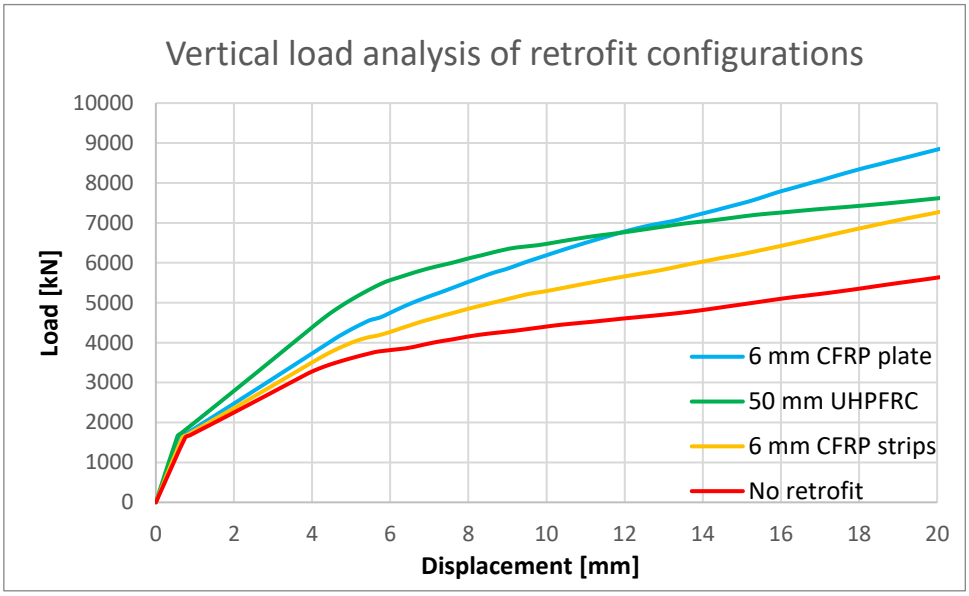

Figure 92: Load-displacement of retrofit configurations

Upon analyzing the results depicted in the chart, it can be observed that the UHPFRC configuration has a noteworthy higher initial stiffness compared to the CFRP retrofits. The 50 mm UHPFRC retrofit demonstrates a superior elastic and partially plastic stiffness, exhibiting its ability to withstand substantial forces. However, as the load increases to approximately 6,750 kN, it is revealed that the CFRP plate provides a higher resistance to flexural bending and can endure even greater loads than UHPFRC. Under the influence of heavy load, CFRP undergoes intense hardening during its plasticity phase as observed from the chart. This

signifies its remarkable ability to bear substantial loading before eventually experiencing sudden failure due to its brittle characteristics.

Additionally, significant observations arise when examining the propagation of cracks in each retrofit configuration during vertical analysis. The findings reveal the contrasting vulnerabilities exhibited by CFRP and UHPFRC in their respective applications. It becomes evident from the findings that CFRP is more vulnerable to shear forces and excessive flexural stress on the bridge compared to retrofitting with UHPFRC. The properties of CFRP materials render them more prone to these types of structural forces when the fiber orientation is at 0 degrees on the tensile zone of the Øvre Kvamme bridge. The increased vulnerability to shear forces can be attributed to the relatively lower shear strength and limited resistance offered by CFRP in comparison to UHPFRC.

On the other hand, UHPFRC retrofitting showcases mechanical weakness with its resistance to high tensile stresses. UHPFRC, owing to its unique concrete composition and properties, possesses excellent compressive strength and durability. However, it exhibits relatively lower tensile strength compared to CFRP. Consequently, UHPFRC retrofitting becomes more vulnerable to tensile stresses and strains, which can initiate and propagate cracks under certain loading conditions, as observed from the conducted NFEA. It is thus crucial to consider these concrete characteristics when assessing the retrofitting effectiveness of UHPFRC.

Overall, the 6 mm CFRP plate exhibits an increase in load-bearing capacity of the bridge by 58.48% compared to the bridge's current condition, whereas retrofitting the Øvre Kvamme bridge with 6 mm CFRP strips, and 50 mm UHPFRC displays 30.58% and 34.85% increment respectively. The highlighted results from the vertical loading analysis is displayed in Table 27.

Table 27: Results from vertical loading analysis

Retrofit configuration	Load at first crack	Displacement at first crack	Peak load	Load capacity improvement	Crack pattern
No retrofit	3,485 kN	4.566 mm	5,670 kN	-	Diagonal
6 mm CFRP strips	4,174 kN	5.658 mm	7,404 kN	30.58%	Diagonal
50 mm UHPFRC	5,660 kN	6.848 mm	7,646 kN	34.85%	Transverse
6 mm CFRP plate	4,810 kN	6.075 mm	8,986 kN	58.48%	Diagonal

In the final finite element analysis, the most effective strengthening methods were compared to the reference model under more realistic loading conditions to satisfy the usage class bk 10/60 requirements. Figure 93 compares the performance of three different strengthening configurations with the reference model without retrofitting. The first linear segment represents the self-weight of the bridge and the following segment is the vertical load as previously mentioned.

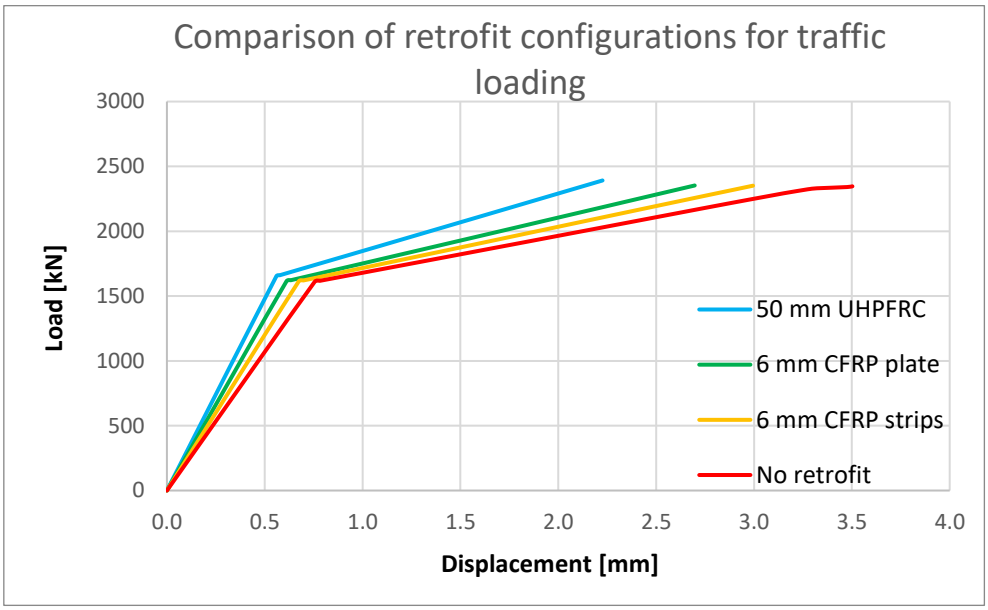

Figure 93: Load-displacement for vertical loading comparison

The various retrofit configurations signify a slightly higher load after the first segment due to increased self-weight from UHPFRC and CFRP. Additionally, it is apparent that the three strengthening approaches significantly increase the stiffness of the bridge. The reference model reached the plastic region at a displacement of 3.28 mm, and as a result, developed permanent damage towards the end of the simulation. Low load-bearing capacity was expected as the bridge was narrowed to one-way traffic due to the extensive damage. It is evident that the bridge must be strengthened to fulfil the current requirements and facilitate the reopening of traffic in both directions. All the results, which include strengthening, indicate solely elastic behavior, which is advantageous as it avoids permanent deformations. Nevertheless, both solutions utilizing CFRP show displacements that are relatively close to the reference of 3.52 mm.

Furthermore, when strengthening Øvre Kvamme to withstand traffic load with the various retrofitting configurations, it is observed from the analyses that the bridge remains healthy and free from the initiation of cracks or any other forms of structural degradation. Table 28 presents

the variations in the results across different measures, including the magnitude of the gravity load, crack displacement, max displacement, and a percentage increase in flexural stiffness.

Table 28: Properties for traffic loading analysis

Retrofit configurations	**Gravity load**	**Displacement at first crack**	**Max displacement**	**Displacement improvement**
No retrofit	1,617 kN	3.28 mm	3.51 mm	-
CFRP strips, 6 mm	1,638 kN	-	2.99 mm	14.81%
CFRP plate, 6 mm	1,640 kN	-	2.69 mm	23.36%
UHPFRC, 50 mm	1,678 kN	-	2.23 mm	36.47%

Based on displacement on mid-span, CFRP strips and plate increase the bridge's strength 14.81% and 23.36%, respectively. Among the three options, the bridge exhibited the highest strength and lowest displacement with 50 mm UHPFRC. Based on the previous vertical analyses, it was observed that the CFRP plate outperformed UHPFRC prior to failure. It can therefore be anticipated that if the load is significantly increased, CFRP will be superior.

9 Conclusion

The comprehensive structural assessment of the Øvre Kvamme bridge has provided valuable insights into its condition and identified potential areas for improvement. Detailed data on the bridge's current state were obtained through the examination of existing documentation, as well as a visual inspection and the utilization of advanced tools such as the 3D laser scanner, profometer, Schmidt's hammer, electrical resistivity meter, and sensors. Additionally, the development of finite element models in Abaqus and subsequent analyses allowed simulating various load cases and evaluate the effectiveness of different strengthening techniques.

- The field investigation revealed substantial deterioration, primarily due to corroded reinforcement, with carbonation playing a major role. As a result, the bridge's sides are severely affected, resulting in lowered load-bearing capacity. It also revealed a moderate probability of ongoing corrosion within the concrete. Given its impact on serviceability and load-bearing capacity, it is imperative to take necessary actions on the bridge.
- Significant deviations from existing documents and drawings were observed through profometer measurements on the longitudinal reinforcement at the bottom of the slabs.
- Conducting a 3D laser scan and processing it using various software proved to be an efficient method for capturing highly accurate geometric properties, which were utilized in the finite element analysis software Abaqus.
- Different configurations of CFRP and UHPFRC with varying thickness and fiber orientation were subjected to lateral, vertical, and traffic loads to assess their effectiveness in strengthening the bridge. As anticipated, increasing the thickness of the materials resulted in significant improvement in flexural strength. Furthermore, it was determined that fiber orientation at 0 degrees yielded the most favorable outcomes.
- Strengthening the concrete slabs concerning pushover analysis proved to not be practical as the lateral stiffness predominantly relies on the supports.
- Implementing CFRP plate, UHPFRC, or CFRP strips on the tensile zone of the bridge enhanced the ultimate load-bearing capacity by 58.48%, 34.85%, and 30.58% respectively.
- In terms of Bk10/60 traffic load, 50 mm UHPFRC proved to be the best option with an increased load-bearing capacity of 36.47%. The CFRP plates and strips demonstrated improvements of 23.36% and 14.81%, respectively.

9.1 Future work

Investing additional time and resources in this study would provide a more detailed and comprehensive understanding of the Øvre Kvamme RC bridge. Given the extensive scope of the study, multiple areas can be further explored and expanded upon to improve the analysis of the bridge's condition. These areas include:

- Conducting a thorough evaluation of the long-term effects of proposed repairs and strengthening techniques on the bridge. This assessment would provide valuable insights into the effectiveness and durability of the chosen strengthening approach, justifying the investment in rehabilitation.
- Evaluating the specific increase in the bridge's lifespan resulting from implementing a strengthening method. This assessment would offer essential information about the effectiveness and longevity of the chosen approach, further justifying the investment in rehabilitation.
- Assessing the long-term environmental and cost-efficiency aspects of proposed bridge repairs and strengthening through a comprehensive cost- and LCA analysis. This can involve exploring alternative materials, construction methods, and maintenance strategies to minimize the ecological footprint and overall costs associated with bridge maintenance over extended periods.
- Enhancing FEM-analyses and modal analysis by utilizing advanced measurement technologies and tools like high-resolution sensors, NDT- and DT instruments. Access to better instruments would ensure more accurate and precise measurements, thus improving the reliability of the obtained data for analysis.
- Conducting laboratory testing to obtain more precise material properties for FEM simulations and a more accurate condition assessment. This could involve performing tests on bridge components or extracting samples from the structure to determine their mechanical properties under different conditions more accurately. Obtaining correct material properties would enhance the reliability of the performed analysis.
- Exploring additional types of FEA and NFEA applicable to bridge analysis, such as torsional, buckling, and dynamic analyses. Incorporating these techniques alongside the conducted FE-analyses would provide a comprehensive understanding of the bridge's behavior and other potential failure modes.

References

[1] B. Richard, S. Epaillard, C. Cremona, L. Elfgren and L. Adelaide, "Nonlinear finite element analysis of a 50 years old reinforced concrete trough bridge," *Engineering Structures,* vol. 32, no. 12, pp. 3899-3910, 8 October 2010. Available: https://www.sciencedirect.com/science/article/pii/S0141029610003391. doi: https://doi.org/10.1016/j.engstruct.2010.09.003.

[2] J. Tørset, "BRIDGES in NORWAY," Norges teknisk-naturvitenskapelige universitet, Trondheim, 2003.Available: https://www.konstruksjon.com/manuel/gammel/bridges.htm.

[3] T. Omar and M. L. Nehdi, "Condition Assessment of Reinforced Concrete Bridges: Current Practice and Research Challenges," *Infrastructures,* vol. 3, no. 3, p. 36, 2018. Available: https://www.mdpi.com/2412-3811/3/3/36. doi: https://doi.org/10.3390/infrastructures3030036.

[4] M. Alsharqawi, T. Zayed and S. A. Dabous, "Common practices in assessing conditions of concrete bridges," *MATEC Web Conf.,* vol. 120, 2017. Available: https://www.matec-conferences.org/articles/matecconf/abs/2017/34/matecconf_ascm2017_02016/matecconf_ascm2017_02016.html. doi: https://doi.org/10.1051/matecconf/201712002016.

[5] Y. Yardim, E. Periku and M. A. Koroglu, "Assessment of Reinforced Concrete Bridge Deficiencies Under Service Loads," *The baltic journal of road and bridge engineering,* vol. 17, no. 1, pp. 167-188, 2021. Available: https://bjrbe-journals.rtu.lv/article/view/bjrbe.2022-17.556. doi: https://doi.org/10.7250/bjrbe.2022-17.556.

[6] J. K. Wight, Reinforced Concrete - Mechanics and Design: Seventh Edition, Michigan: Pearson, 2016.

[7] W. Lin and T. Yoda, Chapter Fourteen - Repair, Strengthening, and Replacement, W. Lin and T. Yoda, Eds., Butterworth-Heinemann, 2017, pp. 245-271. doi: https://doi.org/10.1016/B978-0-12-804432-2.00014-1..Available: https://www.sciencedirect.com/science/article/pii/B9780128044322000141.

[8] H.-T. Hu, F.-M. Lin and Y.-Y. Jan, "Nonlinear finite element analysis of reinforced concrete beams strengthened by fiber-reinforced plastics," *Composite Structures,* vol. 63, no. 3-4, pp. 271-281, 2004. Available: https://www.sciencedirect.com/science/article/pii/S0263822303001740. doi: https://doi.org/10.1016/S0263-8223(03)00174-0.

[9] V. Jagota, A. P. S. Sethi and K. Kumar, "Finite element method: an overview," *Walailak Journal of Science and Technology (WJST),* vol. 10, no. 1, pp. 1-8, 2013. Available:

https://www.researchgate.net/publication/287331381_Finite_Element_Method_An_Overview. doi: 10.2004/wjst.v10i1.499.

[10] W. K. Liu, S. Li and H. S. Park, "Eighty years of the finite element method: Birth, evolution, and future," *Archives of Computational Methods in Engineering,* vol. 29, no. 6, pp. 4431-4453, 2022. Available: https://link.springer.com/article/10.1007/s11831-022-09740-9. doi: 10.1007/s11831-022-09740-9.

[11] M. J. Grant and A. Booth, "A typology of reviews: an analysis of 14 review types and associated methodologies," *Health Information & Libraries Journal,* vol. 26, no. 2, pp. 91-108, 2009. Available: https://onlinelibrary.wiley.com/doi/10.1111/j.1471-1842.2009.00848.x. doi: https://doi.org/10.1111/j.1471-1842.2009.00848.x.

[12] M. J. Page, D. Moher, P. M. Bossuyt, I. Boutron, T. C. Hoffmann, C. D. Mulrow, L. Shamseer, J. M. Tetzlaff, E. A. Akl, S. E. Brennan, R. Chou, J. Glanville, J. M. Grimshaw, A. Hrobjartsson, M. M. Lalu, T. Li, E. W. Loder, E. Mayo-Wilson, S. McDonald, L. A. McGuinnes, L. A. Stewart, J. Thomas, A. C. Tricco, V. A. Welch, P. Whiting and J. E. McKenzie, "Creating a PRISMA flow diagram: PRISMA 2020," 1 September 2020. [Online]. Available: https://guides.lib.unc.edu/prisma. [Accessed 20 3 2023].

[13] N. J. van Eck and L. Waltman, "VOSviewer Manual," University of Leiden, Zuid-Holland, 2019.Available: https://www.vosviewer.com/documentation/Manual_VOSviewer_1.6.13.pdf.

[14] G. Zanardo, H. Hao, Y. Xia and A. J. Deeks, "Stiffness Assessment through Modal Analysis of an RC Slab Bridge before and after Strengthening," *Journal of Bridge Engineering,* vol. 11, no. 5, pp. 1-13, 1 September 2006. Available: https://ascelibrary.org/doi/10.1061/%28ASCE%291084-0702%282006%2911%3A5%28590%29. doi: https://doi.org/10.1061/(ASCE)1084-0702(2006)11:5(590).

[15] G. B. Wijaya and N. Pacuribot, "Condition Assessment of the Deteriorated Reinforced Concrete Bridge," *Civil Engineering Dimension,* vol. 19, no. 2, pp. 111-120, 2017. Available: https://ced.petra.ac.id/index.php/civ/article/view/20327. doi: https://doi.org/10.9744/ced.19.2.111-120.

[16] M. R. Abandah and M. A. Issa, "Influence of reinforcement parameters on punching shear capacity of laterally restrained FRP-reinforced concrete bridge deck slabs," *Structures,* vol. 41, pp. 434-446, 2022. Available: https://www.sciencedirect.com/science/article/abs/pii/S2352012422003368?via%3Dihub. doi: https://doi.org/10.1016/j.istruc.2022.04.074.

[17] A. M. Puurula, O. Enochsson, G. Sas, T. Blanksvard, U. Ohlsson, L. Bernspång, B. Taljsten and L. Elfgren, "Loading to failure and 3D nonlinear FE modelling of a strengthened RC bridge," *Structure and Infrastructure Engineering,* vol. 10, no. 12, pp. 1606-1619, 2014. Available:

https://www.tandfonline.com/doi/abs/10.1080/15732479.2013.836546. doi: http://dx.doi.org/10.1080/15732479.2013.836546.

[18] M. R. Biggs, F. W. Barton, J. P. Gomez, P. J. Massarelli and W. T. McKeel, "FINITE ELEMENT MODELING AND ANALYSIS OF REINFORCED-CONCRETE BRIDGE DECKS," Virginia Transportation Research Council, Charlottesville, 2000.

[19] S. Roy, "NONLINEAR FINITE ELEMENT ANALYSIS OF REINFORCED CONCRETE BRIDGE DECK/BRIDGE APPROACH SLAB USING ABAQUS," UMI, Kansas City, 2005.

[20] M. Bastien-Masse and E. Bruhwiler, "Ultra high performance fiber reinforced concrete for strengthening and protecting bridge deck slabs," *Bridge Maintenance, Safety, Management and Life Extension*, pp. 2176-2182, 2014. Available: https://www.researchgate.net/publication/300272724_Ultra_high_performance_fiber_reinforced_concrete_for_strengthening_and_protecting_bridge_deck_slabs. doi: 10.1201/b17063-333. .

[21] M. Zabihi-Samani, M. Shayanfar, A. Safiey and A. Najari, "Simulation of the Behavior of Corrosion Damaged Reinforced Concrete Beams With/without CFRP Retrofit," *Civil Engineering Journal*, vol. 4, no. 5, pp. 958-970, 2018. Available: https://www.civilejournal.org/index.php/cej/article/view/690. doi: 10.28991/cej-0309148.

[22] A. Siddika, A. A. M. Md., W. Ferdous and R. Alyousef, "Performances, challenges and opportunities in strengthening reinforced concrete structures by using FRPs – A state-of-the-art review," *Engineering Failure Analysis*, vol. 111, 2020. Available: https://www.sciencedirect.com/science/article/abs/pii/S1350630719311884?via%3Dihub. doi: https://doi.org/10.1016/j.engfailanal.2020.104480..

[23] F. A. Fathelbab, M. S. Ramadan and A. Al-tantawy, "Strengthening of RC bridge slabs using CFRP sheets," *Alexandria Engineering Journal*, vol. 53, no. 4, pp. 843-854, 2014. Available: https://www.sciencedirect.com/science/article/pii/S1110016814001008. doi: https://doi.org/10.1016/j.aej.2014.09.010.

[24] Dassault Systemes, "Getting Started With Abaqus/CAE," Simulia, 3 July 2015. [Online]. Available: http://130.149.89.49:2080/v2016/books/gsa/default.htm. [Accessed 24 3 2023].

[25] N. Haritos and A. Hira, "Repair and strengthening of RC flat slab bridges using CFRPs," *Composite Structures*, vol. 66, no. 1-4, pp. 555-562, 2004. Available: https://www.sciencedirect.com/science/article/abs/pii/S0263822304001795?via%3Dihub. doi: 10.1016/j.compstruct.2004.05.003.

[26] L. Moreillon and P. Menetrey, "REHABILITATION AND STRENGTHENING OF EXISTING RC STRUCTURES WITH UHPFRC: VARIOUS APPLICATIONS,"

Symposium, pp. 127-136, 2013. Available: https://www.rilem.net/publication/publication/422?id_papier=8843.

[27] Standards Norway, "Eurocode 2 — Design of concrete structures — Part 1-1: General rules and rules for buildings," Standards Norway, Oslo, 2004.Available: https://www.standard.no/en/webshop/ProductCatalog/ProductPresentation/?ProductID=1365301.

[28] Standard Norge, "Eurocode 2 — Design of concrete structures — Part 1-1: General rules and rules for buildings," Standard Norge, Oslo, 2021.Available: https://www.standard.no/no/Nettbutikk/produktkatalogen/Produktpresentasjon/?ProductID=1365301.

[29] Standard Norge, "Eurocode 2: Design of concrete structures - Concrete bridges - Design and detailing rules," Standard Norge, Oslo, 2005.Available: https://www.standard.no/en/webshop/ProductCatalog/ProductPresentation/?ProductID=416511.

[30] Norwegian Public Road Administration, Handbook N400: Bridge design, Oslo: Norwegian Public Road Administration, 2023. doi: https://www.vegvesen.no/globalassets/fag/handboker/hb-n400-bruprosjektering.pdf.Available: https://www.vegvesen.no/fag/publikasjoner/handboker/vegnormalene/n400/.

[31] Norwegian Public Road Administration, Håndbok V412: Load-bearing capacity classification of bridges, loads, Oslo: Norwegian Public Road Administration, 2021. doi: https://www.vegvesen.no/globalassets/fag/handboker/hb-v412-bareevneklassifisering.pdf.Available: https://vegvesen.brage.unit.no/vegvesen-xmlui/handle/11250/3057110.

[32] Norwegian Public Road Administration, Handbook V413: Load-bearing capacity classification of bridges, materials, Oslo: Norwegian Public Road Administration, 2023. Available: https://viewers.vegnorm.vegvesen.no/product/859963/nb.

[33] Norwegian Public Road Administration, "Handbook V441: Bridge inspection," Norwegian Public Road Administration, Oslo, 2019.Available: https://vegvesen.brage.unit.no/vegvesen-xmlui/handle/11250/3057144.

[34] International Organization for Standardization, "Maintenance and repair of concrete structures — Part 1: General principles," International Organization for Standardization, Switzerland, 2014.Available: https://www.standard.no/no/Nettbutikk/produktkatalogen/Produktpresentasjon/?ProductID=698845.

[35] International Organization for Standardization, "Maintenance and repair of concrete structures - Part 2: Assessment of existing concrete structures," International Organization for Standardization, Switzerland, 2014.Available:

https://www.standard.no/no/Nettbutikk/produktkatalogen/Produktpresentasjon/?ProductID=698846.

[36] International Organization for Standardization, "Maintenance and repair of concrete structures - Part 3: Design of repairs and prevention," International Organization for Standardization, Switzerland, 2014.Available: https://www.standard.no/no/Nettbutikk/produktkatalogen/Produktpresentasjon/?ProductID=698847.

[37] International Organization for Standardization, "Maintenance and repair of concrete structures — Part 4: Execution of repairs and prevention," International Organization for Standardization, Switzerland, 2014.Available: https://www.standard.no/no/Nettbutikk/produktkatalogen/Produktpresentasjon/?ProductID=698848.

[38] Proceq SA, "Browse our document database," Proceq, 2017. [Online]. Available: https://www.screeningeagle.com/en/download/. [Accessed 20 3 2023].

[39] Proceq SA, "Profometer: Operating Instructions," Proceq SA, Schwerzenbach, 2017.Available: https://www.screeningeagle.com/en/products/category/concrete/rebar-diameter-cover. doi: https://media.screeningeagle.com/asset/Downloads/Profometer_Operating%20Instructions_English_high.pdf.

[40] Proceq SA, "Operating instructions - SilverSchmidt & Hammerlink," Proceq SA, Schwerzenbach, 2017.Available: https://media.screeningeagle.com/asset/Downloads/SilverSchmidt_Operating%20Instructions_English_high.pdf.

[41] Proceq SA, "Operating Instructions - Concrete Durability Testing," Proceq SA, Schwerzenbach, 2017.Available: https://www.screeningeagle.com/en/products/resipod. doi: https://media.screeningeagle.com/asset/Downloads/Resipod%20Family_Operating%20Instructions_English_high.pdf.

[42] HDS Software Product Management, "Leica Cyclone REGISTER 360 PLUS - 3D Laser Scanning Point Cloud Registration Software," Leica Geosystems, 12 November 2020. [Online]. Available: https://leica-geosystems.com/products/laser-scanners/software/leica-cyclone/leica-cyclone-register-360. [Accessed 13 March 2023].

[43] S. P. Zotkin., E. V. Ignatova and I. A. Zotkina, "The Organization of Autodesk Revit Software Interaction with Applications for Structural Analysis," *Procedia Engineering,* vol. 153, pp. 915-919, 2016. Available: https://www.sciencedirect.com/science/article/pii/S1877705816323736. doi: https://doi.org/10.1016/j.proeng.2016.08.225..

[44] A. Khennane, Introduction to Finite Element Analysis using MATHLAB and ABAQUS, New York: Taylor & Francis Group, 2013. Available:

https://books.google.no/books?hl=no&lr=&id=IHXfSNYXRD8C&oi=fnd&pg=PP1&dq=abaqus+&ots=cvu73lhp4C&sig=pFpuFAyKmj2UePB1EfrjPE5EEkU&redir_esc=y#v=onepage&q=abaqus&f=false.

[45] Dassault Systèmes, "Abaqus 2016 Online Documentation," Simulia, 5 July 2015. [Online]. Available: http://130.149.89.49:2080/v2016/books/usi/default.htm. [Accessed 21 3 2023].

[46] UnQuake, "OMAway Solution," UnQuake, Dafni, 2019.Available: https://unquake.co/.

[47] A. M. Selberg, "Spesialinspeksjon Kvamme Øvre bru," BruKon AS, Lærdal, 2022.

[48] C. Kuchekar and U. Deshpande, "Visual Inspection of concrete bridge," *INTERNATIONAL JOURNAL OF INNOVATIONS IN ENGINEERING RESEARCH AND TECHNOLOG*, vol. 4, no. 3, pp. 125-127, 2017. Available: https://www.neliti.com/publications/427218/visual-inspection-of-concrete-bridge.

[49] N. M. Sutan and H. Sinin, "Efflorescence Phenomenon on Concrete Structures," *Advanced Materials Research*, vol. 626, pp. 747-750, 2012. Available: https://www.scientific.net/AMR.626.747. doi: https://doi.org/10.4028/www.scientific.net/AMR.626.747.

[50] Portland Cement Association, "Types and causes of concrete deterioration," Portland Cement Association, Skokie, 2002.

[51] A. Gheitasi and D. K. Harris, "Performance Assessment of Steel-Concrete Composite Bridges with Subsurface Deck Delamination," *Structures*, vol. 17, pp. 8-20, 2015. Available: https://www.researchgate.net/publication/271019878_Performance_Assessment_of_Steel-Concrete_Composite_Bridges_with_Subsurface_Deck_Delamination. doi: 10.1016/j.istruc.2014.12.001.

[52] TeamCivil, "Surface Scaling and Spalling of Concrete," Civil Engineering Forum, 7 May 2017. [Online]. Available: https://www.civilengineeringforum.me/surface-scaling-spalling-concrete/. [Accessed 31 March 2023].

[53] RCI Interface, "Technical Article - Assessment and repair of concrete structures," 1 July 2008. [Online]. Available: https://galeassociates.org/knowledge/technical-articles/. [Accessed 30 March 2023].

[54] H. R. Kumavat, N. R. Chandak and I. T. Patil, "Factors influencing the performance of rebound hammer used for non-destructive testing of concrete members: A review," *Case Studies in Construction Materials*, vol. 14, pp. 1-12, 2021. Available: https://www.sciencedirect.com/science/article/pii/S2214509521000061. doi: https://doi.org/10.1016/j.cscm.2021.e00491.

[55] G. Mishra, "Rebound Hammer Test on Concrete - Principle, Procedure, Advantages &," The Constructor, 2 July 2018. [Online]. Available:

https://theconstructor.org/concrete/rebound-hammer-test-concrete-ndt/2837/. [Accessed 2023 April 1].

[56] F. Schick, "Rebound Hammer," Technische Universitat Munchen, 13 June 2019. [Online]. Available: https://wiki.tum.de/display/zfp/Rebound+hammer. [Accessed 1 April 2023].

[57] D. Corbett and G. Tronca, "Non-Destructive Testing of Steel Fibre Reinforced Concrete," *Materials Science and Engineering,* vol. 246, pp. 1-9, 2017. Available: https://iopscience.iop.org/article/10.1088/1757-899X/246/1/012016/meta. doi: 10.1088/1757-899X/246/1/012016.

[58] K. Tesic, A. Baricevic and M. Serdar, "Comparison of cover meter and ground penetrating radar performance in structural health assessment: case studies," *Gradevinar,* vol. 73, pp. 1131-1144, 2021. Available: http://www.casopis-gradjevinar.hr/archive/article/3323. doi: https://doi.org/10.14256/JCE.3323.2021.

[59] P. Azarsa and R. Gupta, "Electrical Resistivity of Concrete for Durability Evaluation: A Review," *Advances in Materials Science and Engineering,* vol. 2017, pp. 1-31, 2017. Available: https://www.hindawi.com/journals/amse/2017/8453095/. doi: https://doi.org/10.1155/2017/8453095.

[60] E. Kaartinen, K. Dunphy and A. Sadhu, "LiDAR-Based Structural Health Monitoring: Applications in Civil Infrastructure Systems," *Sensors,* vol. 22, pp. 1-32, 2022. Available: https://www.mdpi.com/1424-8220/22/12/4610. doi: https://doi.org/10.3390/s22124610.

[61] Leica Geosystems AG, "Leica BLK360 - User Manual," Leica Geosystems AG, Heinrich-Wild-Strasse, 2021.Available: https://shop.leica-geosystems.com/leica-blk/blk360/blk360-manuals-and-support-documents. doi: https://shop.leica-geosystems.com/sites/default/files/2022-01/853811_Leica_BLK360_UM_v4.0.0_en.pdf.

[62] Leica Geosystems AG, "Leica BLK360 Imaging Laser Scanner," Leica Geosystems AG, 2023. [Online]. Available: https://leica-geosystems.com/products/laser-scanners/scanners/blk360. [Accessed 4 April 2023].

[63] A. Dlesk, K. Vach, J. Sedina and K. Pavelka, "COMPARISON OF LEICA BLK360 AND LEICA BLK2GO ON CHOSEN TEST OBJECTS," *The International Archives of the Photogrammetry, Remote Sensing and Spatial Information Sciences,* Vols. XLVI-5/W1-2022, pp. 77-82, 2022. Available: https://isprs-archives.copernicus.org/articles/XLVI-5-W1-2022/77/2022/. doi: https://doi.org/10.5194/isprs-archives-XLVI-5-W1-2022-77-2022.

[64] Unquake, "OMAway Solution - Manual Rev. 04," Unquake, Attica, 2018.

[65] C. Obbink-Huizer, "Units in Abaqus," Simuleon, 25 2 2019. [Online]. Available: https://info.simuleon.com/blog/units-in-abaqus.

[66] V. Preetha, S. Hariharan, P. Santhoshkumar, S. Suseendran and P. Gowtham, "Effect of linear and non-linear behavior of steel beam sections," *Materials Today: Proceedings,* vol. 45, no. 2, pp. 1012-1016, 2021. Available: https://www.sciencedirect.com/science/article/pii/S2214785320318496. doi: https://doi.org/10.1016/j.matpr.2020.03.074.

[67] Charles Camp, "CIVL 1101 - Civil Engineering Measurements," University of Memphis, 16 December 2022. [Online]. Available: http://www.ce.memphis.edu/1101/. [Accessed 2 April 2023].

[68] H. M. Kh, M. Ozakca and T. Ekmekyapar, "A Review on Nonlinear Finite Element Analysis of Reinforced Concrete Beams Retrofitted with Fiber Reinforced Polymers," *Advanced Research in Applied Mechanics,* vol. 22, no. 1, pp. 13-48, 2016. Available: https://www.researchgate.net/publication/315716360_A_Review_on_Nonlinear_Finite_Element_Analysis_of_Reinforced_Concrete_Beams_Retrofitted_with_Fiber_Reinforced_Polymers.

[69] M. Abedini and C. Zhang, "Performance Assessment of Concrete and Steel Material Models in LS-DYNA for Enhanced Numerical Simulation, A State of the Art Review," *Computational Methods in Engineering,* vol. 28, pp. 2921-2942, 2020. Available: https://link.springer.com/article/10.1007/s11831-020-09483-5. doi: https://doi.org/10.1007/s11831-020-09483-5.

[70] G. Markeset and V. Plevris, "Educational challenges in computer-based Finite Element Analysis and design of structures," *Journal of Computer Science,* vol. 14, pp. 1351-1362, 2018. Available: https://www.researchgate.net/publication/328873108_Educational_Challenges_in_Computer-based_Finite_Element_Analysis_and_Design_of_Structures. doi: 10.3844/jcssp.2018.1351.1362.

[71] Dassault systems, "Abaqus Analysis User's Guide," Simulia, 5 July 2015. [Online]. Available: http://130.149.89.49:2080/v2016/books/usb/default.htm. [Accessed 2 April 2023].

[72] A. Ghali, R. Favre and M. Elbadry, Concrete structures: Stresses and deformations: Analysis and design for sustainability, CRC Press, 2020, pp. 2-3.Available: https://books.google.no/books?hl=no&lr=&id=DgoHEAAAQBAJ&oi=fnd&pg=PP1&dq=creep+coefficient+of+concrete+infinite+time&ots=F_czpPF_az&sig=EoC5eUBpST1c44-D81gs4MR7SGc&redir_esc=y#v=onepage&q&f=false.

[73] Norges geologiske undersøkelse, "Berggrunn - Nasjonal berggrunnsdatabase," Norges geologiske undersøkelse, [Online]. Available: https://geo.ngu.no/kart/berggrunn_mobil/.

[74] B. Ghiassi, A. T. Vermelfoort and P. B. Lourenço, "Chapter 7 - Masonry mechanical properties," in *Numerical Modeling of Masonry and Historical Structures,* B. Ghiassi and G. Milani, Eds., Woodhead Publishing, 2019, pp. 239-261. doi:

https://doi.org/10.1016/B978-0-08-102439-3.00007-5.Available: https://www.sciencedirect.com/science/article/pii/B9780081024393000075.

[75] Simulia, "Abaqus Manual," [Online]. Available: https://classes.engineering.wustl.edu/2009/spring/mase5513/abaqus/docs/v6.6/books/usi/default.htm?startat=pt03ch11s09s03.html.

[76] Vegdirektoratet, "V412 Bæreevneklassifisering av bruer, laster," 24 February 2023. [Online]. Available: https://viewers.vegnorm.vegvesen.no/product/859962/nb.

[77] M. A. Al-Huri, M. A. Al-Osta and S. Ahmad, "Finite Element Modelling of Corrosion-Damaged RC Beams Strengthened Using the UHPC Layers," *Materials,* vol. 15, no. 21, p. 7606, 2022. Available: https://www.mdpi.com/1996-1944/15/21/7606. doi: https://doi.org/10.3390/ma15217606.

[78] J. Liu, X. Luo and Q. Chen, "Degradation of Steel Rebar Tensile Properties Affected by Longitudinal Non-Uniform Corrosion," *Materials,* vol. 16, no. 7, p. 2917, 2023. Available: https://www.mdpi.com/1996-1944/16/7/2917. doi: https://doi.org/10.3390/ma16072917.

[79] Vegdirektoratet, "Bruklassifisering [Håndbok R412]," 2014. [Online]. Available: https://vegvesen.brage.unit.no/vegvesen-xmlui/handle/11250/2768075.

[80] H. Sinaei, M. Shariati, A. H. Abna, M. Aghaei and A. Shariati, "Evaluation of reinforced concrete beam behaviour using finite element analysis by ABAQUS," *Scientific Research and Essays,* vol. 7, no. 21, pp. 2002-2009, 2012. Available: https://www.researchgate.net/publication/301841036_Evaluation_of_reinforced_concrete_beam_behavior_using_finite_element_analysis_by_ABAQUS.

[81] F.-x. Ding, W.-j. Wang, D.-r. Lu and X.-m. Liu, "Study on the behavior of concrete-filled square double-skin steel tubular stub columns under axial loading,," *Structures,* vol. 23, pp. 665-676, 2020. Available: https://www.sciencedirect.com/science/article/pii/S2352012419302188. doi: https://doi.org/10.1016/j.istruc.2019.12.008.

[82] M. E. Mohamad, I. S. Ibrahim, R. Abdullah, A. B. Abd. Rahman, A. B. H. Kueh and J. Usman, "Friction and cohesion coefficients of composite concrete-to-concrete bond," *Cement and Concrete Composites,* vol. 56, pp. 1-14, 2015. Available: https://www.sciencedirect.com/science/article/pii/S0958946514001954. doi: https://doi.org/10.1016/j.cemconcomp.2014.10.003.

[83] M. Hafezolghorani, F. Hejazi, R. Vaghei, M. S. B. Jaafar and K. Karimzade, "Simplified damage plasticity model for concrete," *Structural Engineering International,* vol. 27, no. 1, pp. 68-78, 2017.

[84] Simulia, "4.5.2 Damaged plasticity model for concrete and other quasi-brittle materials," Simulia, [Online]. Available:

https://classes.engineering.wustl.edu/2009/spring/mase5513/abaqus/docs/v6.6/books/stm/default.htm?startat=ch04s05ath120.html.

[85] Y. Dere and M. A. Koroglu, "Nonlinear FE modeling of reinforced concrete," *International Journal of Structural and Civil Engineering Research,* vol. 6, no. 1, pp. 71-74, 2017. Available: https://d1wqtxts1xzle7.cloudfront.net/88273138/20170216025855706-libre.pdf?1657028460=&response-content-disposition=inline%3B+filename%3DNonlinear_FE_Modeling_of_Reinforced_Conc.pdf&Expires=1680882759&Signature=dzBuXAyd-adZxVWzFOQqzRBbJhF8Teg7SicPdNCn5b0P.

[86] C.-L. T, L.-M. H and T. Sang-To, "A nonlinear concrete damaged plasticity model for simulation reinforced concrete structures using ABAQUS," *Frattura ed Integrità Strutturale,* vol. 59, pp. 232-242, 2022.

[87] R. Shamass, X. Zhou and G. Alfano, "Finite-element analysis of shear-off failure of keyed dry joints in precast concrete segmental bridges," *Journal of Bridge Engineering,* vol. 20, no. 6, p. 04014084, 2015.

[88] Simulia, "18.5.3 Concrete damaged plasticity," Simulia, [Online]. Available: https://classes.engineering.wustl.edu/2009/spring/mase5513/abaqus/docs/v6.6/books/usb/default.htm?startat=pt05ch18s05abm36.html.

[89] S. Gopinath, J. Rajasankar, N. R. Iyer, T. S. Krishnamoorthy, B. H. Bharatkumar and N. Lakshmanan, "A strain-based constitutive model for concrete under tension in nonlinear finite element analysis of RC flexural members," *Structural Durability & Health Monitoring,* vol. 5, no. 4, p. 311, 2009.

[90] S. M. Allam, M. S. Shoukry, G. E. Rashad and A. S. Hassan, "Evaluation of tension stiffening effect on the crack width calculation of flexural RC members," *Alexandria Engineering Journal,* vol. 52, no. 2, pp. 163-173, 2013. Available: https://www.sciencedirect.com/science/article/pii/S1110016813000045. doi: https://doi.org/10.1016/j.aej.2012.12.005.

[91] J. Tedesco, W. G. McDougal and C. A. Ross, "Structural dynamics," *STRUCTURAL ENGINEERING AND GEOMECHANICS,* vol. II, 2000. Available: https://www.eolss.net/sample-chapters/c05/E6-139-13.pdf.

[92] Z.-F. Fu and J. He, Modal analysis, Elsevier, 2001, p. 2. doi: https://doi.org/10.1016/B978-0-7506-5079-3.X5000-1.Available: https://www.sciencedirect.com/book/9780750650793/modal-analysis.

[93] F. B. Zahid, Z. C. Ong and S. Y. Khoo, "A review of operational modal analysis techniques for in-service modal identification," *Journal of the Brazilian Society of Mechanical Sciences and Engineering,* vol. 42, pp. 1-18, 2020. Available: https://www.researchgate.net/publication/342749983_A_review_of_operational_moda

l_analysis_techniques_for_in-service_modal_identification. doi: http://dx.doi.org/10.1007/s40430-020-02470-8.

[94] R. Brincker and C. Ventura, Introduction to operational modal analysis, John Wiley & Sons, 2015, pp. 6-7.Available: https://books.google.no/books?hl=no&lr=&id=ZonmCQAAQBAJ&oi=fnd&pg=PR11&dq=Introduction+to+operational+modal+analysis&ots=gZp6P8xtsC&sig=khCoAXr9NAGXRgrd4MFkPBl37tI&redir_esc=y#v=onepage&q&f=false.

[95] Computers & Structures, Inc., "User's Guide to ETABS 2016," Computers & Structures, Inc., USA, 2016.Available: https://wiki.csiamerica.com/display/doc/ETABS+Training+manuals. doi: https://ottegroup.com/wp-content/uploads/2021/02/ETABS2016-Users-Guide.pdf.

[96] M. A. Khan, "Chapter Ten - Seismic Design for Buildings," in *Earthquake-Resistant Structures*, Boston, Butterworth-Heinemann, 2013, pp. 283-315. doi: https://doi.org/10.1016/B978-1-85617-501-2.00010-9.Available: https://www.sciencedirect.com/science/article/pii/B9781856175012000109.

[97] Y. Huang, S. Grünewald, E. Schlangen and M. Lukovic, "Strengthening of concrete structures with ultra high performance fiber reinforced concrete (UHPFRC): A critical review," *Construction and Building Materials,* vol. 336, pp. 1-20, 2022. Available: https://www.sciencedirect.com/science/article/pii/S0950061822010753. doi: https://doi.org/10.1016/j.conbuildmat.2022.127398.

[98] M. Z. Naser, R. A. Hawileh and J. A. Abdalla, "Fiber-reinforced polymer composites in strengthening reinforced concrete structures: A critical review," *Engineering Structures,* vol. 198, pp. 1-20, 2019. Available: https://www.sciencedirect.com/science/article/pii/S0141029618310113?via%3Dihub. doi: https://doi.org/10.1016/j.engstruct.2019.109542.

[99] A. M. Ceci, J. R. Casas and M. Ghosn, "Statistical analysis of existing models for flexural strengthening of concrete bridge beams using FRP sheets," *Construction and Building Materials,* vol. 27, no. 1, pp. 490-520, 2012. Available: https://www.sciencedirect.com/science/article/abs/pii/S0950061811003680?via%3Dihub. doi: 10.1016/j.conbuildmat.2011.07.014.

[100] P. Kotes and P. Kotula, "Modeling and strengthening of RC bridges by means of CFRP," *Proceedings of the 6th International conference on FRAMCOS,* pp. 1-8, 2007. Available: https://www.researchgate.net/publication/288799270_Modeling_and_strengthening_of_RC_bridges_by_means_of_CFRP.

[101] C. E. Bakis, L. C. Bank, V. L. Brown, E. Cosenza, J. F. Davalos, J. J. Lesko, A. Machida, S. H. Rizkalla and T. Triantafillou, "Fiber-Reinforced Polymer Composites for Construction—State-of-the-Art Review," *Journal of Composites for Construction,* vol. 6, no. 2, pp. 73-87, 2002. Available: https://www.researchgate.net/publication/234095053_Fiber-

Reinforced_Polymer_Composites_for_Construction-State-of-the-Art_Review. doi: https://ascelibrary.org/doi/10.1061/%28ASCE%291090-0268%282002%296%3A2%2873%29.

[102] Y. Liu, B. Zwingmann and M. Schlaich, "Carbon Fiber Reinforced Polymer for Cable Structures—A Review," *Polymers,* vol. 7, no. 10, pp. 2078-2099, 2015. Available: https://www.mdpi.com/2073-4360/7/10/1501. doi: https://doi.org/10.3390/polym7101501.

[103] M. B. Eide and J.-M. Hisdal, "Ultra High Performance Fibre Reinforced Concrete (UHPFRC) - State of the art," SINTEF Building and Infrastructure, Oslo, 2012. doi: https://www.sintefbok.no/book/download/1068/vinfopubutgivelsercoincoin_project_reportscoin_report_no_44nettcoin-no44pdf.

[104] A. Hajiesmaeili, F. Pittau, E. Denarie and G. Habert, "Life Cycle Analysis of Strengthening Existing RC Structures with R-PE-UHPFRC," *Sustainability,* vol. 11, pp. 1-13, 2019. Available: https://www.mdpi.com/2071-1050/11/24/6923. doi: https://doi.org/10.3390/su11246923.

[105] Z. Qi, Y. Liu and W. Chen, "An approach to predict the mechanical properties of CFRP based on cross-scale simulation," *Composite Structures,* vol. 210, pp. 339-347, 2019. Available: https://www.sciencedirect.com/science/article/pii/S0263822318336675?casa_token=tXUfF3wNUZUAAAAA:eVIqEiqfP3WMc3m05KePOcZQ7x7pYSpXXa19MAf8Gf0USZ2ld-pWudGNvU-_40lEvWCiMPKaKxY. doi: https://doi.org/10.1016/j.compstruct.2018.11.056.

[106] G.-D. Wang and S. K. Melly, "Three-Dimensional finite element modeling of drilling CFRP composites using Abaqus/CAE: a review," *The International Journal of Advanced Manufacturing Technology,* vol. 94, pp. 599-614, 2018. Available: https://link.springer.com/article/10.1007/s00170-017-0754-7. doi: https://doi.org/10.1007/s00170-017-0754-7.

[107] H. Hu, Q. Wei, B. Liu, Y. Liu, N. Hu, Q. Ma and C. Wang, "Progressive Damage Behaviour Analysis and Comparison with 2D/3D Hashin Failure Models on Carbon Fibre–Reinforced Aluminium Laminates," *Polymers,* vol. 14, no. 14, pp. 2946-2971, 2022. Available: https://www.mdpi.com/2073-4360/14/14/2946. doi: https://doi.org/10.3390/polym14142946.

[108] K. A.-D. Bsisu, H. H. Hussein and S. M. Sargand, "The Use of Hashin Damage Criteria, CFRP–Concrete Interface and Concrete Damage Plasticity Models in 3D Finite Element Modeling of Retrofitted Reinforced Concrete Beams with CFRP Sheets," *Arabian Journal for Science and Engineering,* vol. 42, pp. 1171-1184, 2018. Available: https://link.springer.com/article/10.1007/s13369-016-2356-3. doi: 10.1007/s13369-016-2356-3.

[109] M. Vishwas, S. Joledarashi and S. Kulkarni, "Comparative study of damage behavior of synthetic and natural fiber-reinforced brittle composite and natural fiber-reinforced

flexible composite subjected to low-velocity impact," *Transactions B: Mechanical Engineering*, vol. 27, no. 1, pp. 241-349, 2020. Available: http://scientiairanica.sharif.edu/article_21099.html. doi: 10.24200/sci.2018.51294.2100.

[110] G. R. Ahmadzadeh, A. Shirazi and A. Varvani-Farahani, "Damage Assessment of CFRP [90/±45/0] Composite Laminates over Fatigue Cycles," *Appl Compos Mater*, vol. 18, pp. 559-569, 2011. Available: https://link.springer.com/article/10.1007/s10443-011-9216-9#citeas. doi: https://doi.org/10.1007/s10443-011-9216-9.

[111] D. Hashim , F. Hejazi and Y. Voo, "Simplified Constitutive and Damage Plasticity Models for UHPFRC with Different Types of Fiber," *International Journal of Concrete Structures and Materials*, vol. 14. Available: https://www.researchgate.net/publication/343347357_Simplified_Constitutive_and_Damage_Plasticity_Models_for_UHPFRC_with_Different_Types_of_Fiber. doi: 10.1186/s40069-020-00418-9.

Appendix A

Compressive behavior of concrete

ε, total	σc	εc1	n	E	fcm	k	dc	εel	εin	εpl
0	0	0.002	0	20000	28	1.5	0	0.00000	0.00000	0.00000
0.00042	8.475084	0.002	0.21	20000	28	1.5	0	0.00042	0.00000	0.00000
0.0006	11.85882	0.002	0.3	20000	28	1.5	0	0.00059	0.00001	0.00001
0.0008	15.4	0.002	0.4	20000	28	1.5	0	0.00077	0.00003	0.00003
0.001	18.66667	0.002	0.5	20000	28	1.5	0	0.00093	0.00007	0.00007
0.0012	21.6	0.002	0.6	20000	28	1.5	0	0.00108	0.00012	0.00012
0.0014	24.12308	0.002	0.7	20000	28	1.5	0	0.00121	0.00019	0.00019
0.0016	26.13333	0.002	0.8	20000	28	1.5	0	0.00131	0.00029	0.00029
0.0018	27.49091	0.002	0.9	20000	28	1.5	0	0.00137	0.00043	0.00043
0.002	28	0.002	1	20000	28	1.5	0	0.00140	0.00060	0.00060
0.0022	27.37778	0.002	1.1	20000	28	1.5	0.0222	0.00137	0.00083	0.00080
0.0024	25.2	0.002	1.2	20000	28	1.5	0.1000	0.00126	0.00114	0.00100
0.0026	20.8	0.002	1.3	20000	28	1.5	0.2571	0.00104	0.00156	0.00120
0.0028	13.06667	0.002	1.4	20000	28	1.5	0.5333	0.00065	0.00215	0.00140
0.0029	7.381818	0.002	1.45	20000	28	1.5	0.7364	0.00037	0.00253	0.00150

Tensile behavior of concrete

ε,total	σt	E	dc	εel	εck	εpl
0	0	20000	0		0	
0.0001	2	20000	0	0.0001	0	0
0.0003	1.333333	20000	0.333333	6.67E-05	0.000233333	0.0002
0.0005875	0.75	20000	0.625	3.75E-05	0.00055	0.0004875
0.00105	0.333333	20000	0.833333	1.67E-05	0.001033333	0.00095
0.0016	0.01	20000	0.9925	5E-07	0.0015995	0.001533333

Compressive behavior of the supports of Øvre Kvamme bridge

ε, total	σc	E	dc	εin
0	0	5000	0	0.00000
0.000451	4	5000	0	0.00000
0.000586	5	5000	0	0.00013
0.000735	6	5000	0	0.00028
0.000905	7	5000	0	0.00045
0.001106	8	5000	0	0.00065
0.001368	9	5000	0	0.00092
0.002000	10	5000	0	0.00155
0.002632	9	5000	0.1	0.00218
0.002894	8	5000	0.2	0.00244
0.003095	7	5000	0.3	0.00264

Tensile behavior of the supports of Øvre Kvamme bridge

ε,total	σt	E	dc	εel	εck	εpl
0	0	5000	0		0	
0.0003	1.5	5000	0	0.0003	0	0
0.0009	1	5000	0.333333	0.0002	0.0007	0.0006
0.001763	0.5625	5000	0.625	0.000113	0.00165	0.001463
0.00315	0.25	5000	0.833333	0.00005	0.0031	0.00285
0.0048	0.01	5000	0.99	0.000002	0.004798	0.0046

Concrete damage plasticity parameters UHPFRC [111]

Material's parameters	**UHPFRC (T2)**	**Plasticity parameters**	
		Dilation angle	33
Concrete elasticity		Eccentricity	0.1
E (GPa)	30	*fb0/fc0*	1.16
N	0.2	*K*	0.67
		Viscosity parameter	0
Concrete compressive behavior		**Concrete compression damage**	
Yield stress (MPa)	**Inelastic strain**	**Damage parameter C**	**Inelastic strain**
0	0	0	0
20.9	0.000242	0	0.000242
40.8	0.000708	0	0.000708
61.9	0.000893	0	0.000893
71.9	0.00101	0	0.00101
80.9	0.001147	0	0.001147
90.9	0.001328	0	0.001328
109.8	0.00345	0	0.00345
133.6	0.0039	0	0.0039
35.1	0.00435	0.73728	0.435
21.6	0.0046168	0.838421	0.0046168
16.2	0.0046255	0.878816	0.0046255
10.8	0.0046284	0.919211	0.0046284
5.4	0.0046371	0.959605	0.0046371
2.7	0.0046429	0.979803	0.0046429
Concrete tensile behavior		**Concrete tension damage**	
Yield stress (MPa)	**Cracking strain**	**Damage parameter T**	**Cracking strain**
7.75	0	0	0
0.00601	0.004665	0.999224	0.004665

Appendix B

Ferdigbrutegning

208

ØVRE KVAMME II	bru	E veg	16 HP2 nr.	208 Byggenr.	1927 Bygd år

Arkiv nr.

Fylke	Herred	Kilometrering (beliggende)
SOGN OG FJORDANE	LÆRDAL	6.115 km for LÆRDALS – ØYRI

Brusystem: FRITT OPPLAGT PLATE I 3 SPENN

Konstruksjon (materialer): ARMERT BETONG

Brudekke: ARMERT BETONG Slitedekke: BETONG

Underbygning (materialer): BETONG

Fundamentering: PÅ FAST GRUNN

~~Spennvidde~~/Fri lengde: Lt = 4,96 + 5,73 + 5,07

Kurveutv; b = m | Gangbaner G = m | Føringsavst. F = 6,00 m

Fri bredde over føring	Fri bredde over rekkv.	Fri høyde over pl.	Fri høyde ℄ bru	Fritt seilløp
m	m	m	m	m

Konstruert for lastkl.: 2 / 1920
Konstruert for akseltrykk: tonn

Endringer av lastkl./akseltr.: 1/1930 10 t 19?
FORSTERET MIDTSPENN

Overbygning:
Konstruert av: SOGN OG FJORDANE VEGVESEN
Bygd av: "

Underbygning:
Konstruert av: SOGN OG FJORDANE VEGVESEN
Bygd av: "

Tverrsnitt M = 1:100

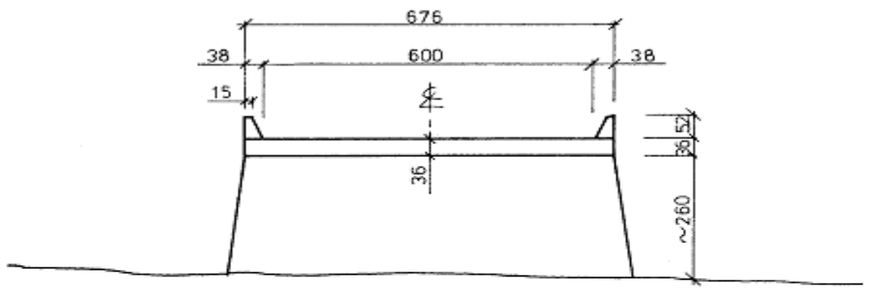

Oppriss M = 1:200

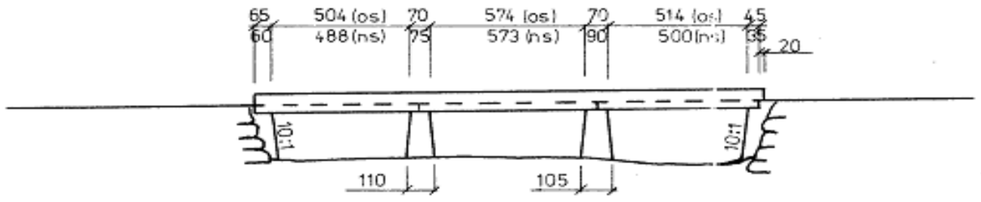

Grunnriss M = 1:200

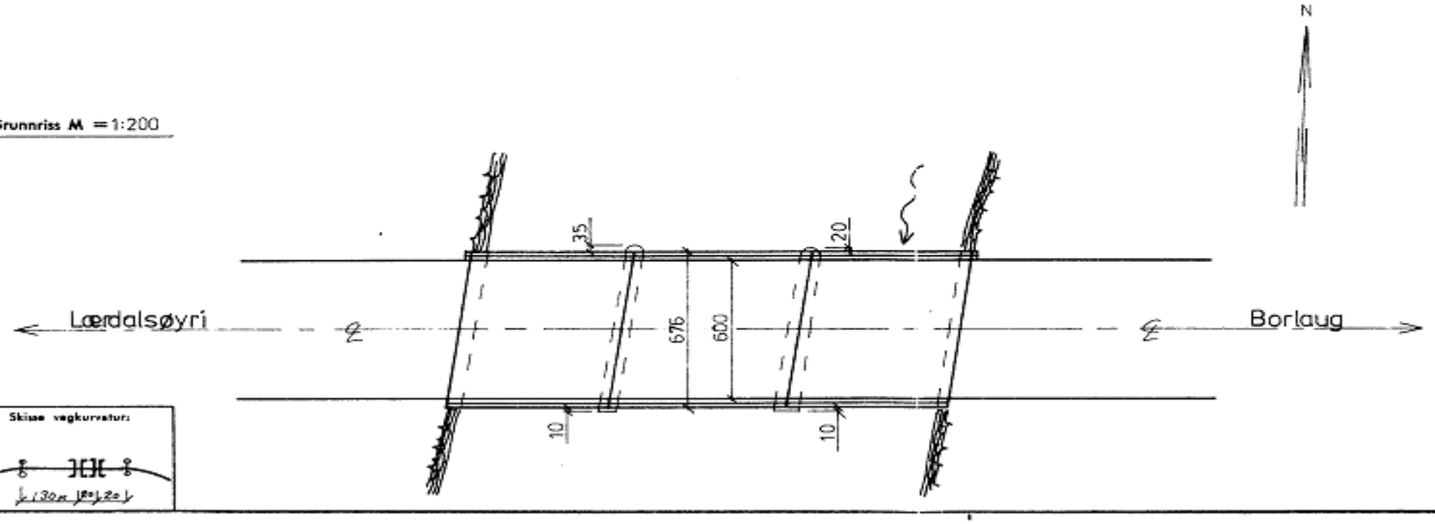

Skisse vegkurvatur:

Forsterket/Utv.:

Tegnet den 17/12 1974
av: OAK

Blankett nr. 25

STATENS VEGVESEN

Appendix C

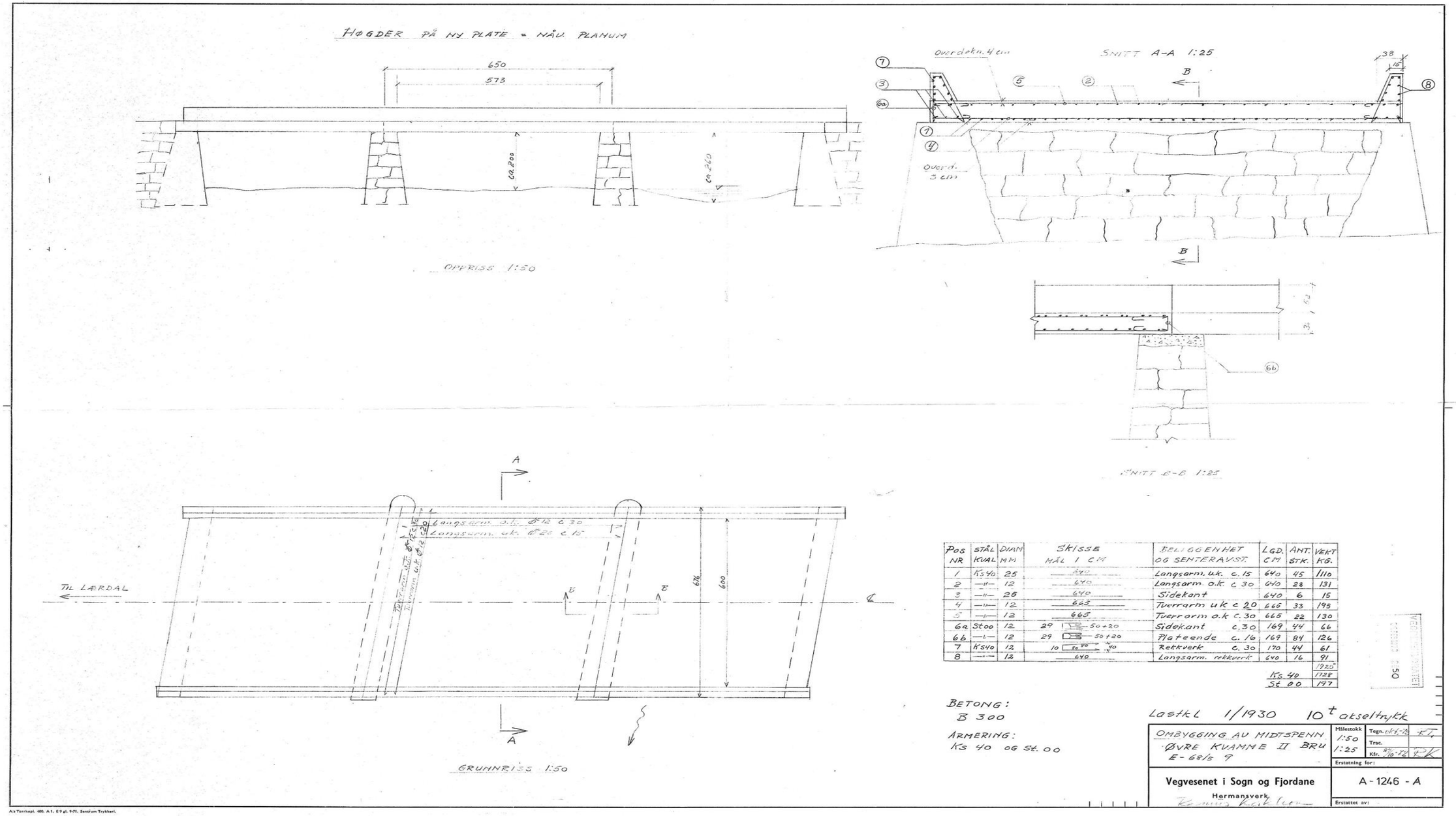

Pos NR	STÅL KVAL	DIAM MM	SKISSE MÅL I CM	BELIGGENHET OG SENTERAVST.	LGD. C.M	ANT. STK.	VEKT KG.
1	Ks40	25	640	Langsarm. u.k. c. 15	640	45	1110
2	—"—	12	640	Langsarm. o.k. c. 30	640	28	131
3	—"—	25	640	Sidekant	640	6	15
4	—"—	12	665	Tverrarm u.k c. 20	665	33	195
5	—"—	12	665	Tverrarm o.k c. 30	665	22	130
6a	St00	12	29 — 50+20	Sidekant c. 30	169	44	66
6b	—"—	12	29 — 50+20	Plateende c. 16	169	84	126
7	Ks40	12	10 — 50 — 40	Rekverk c. 30	170	44	61
8	—"—	12	640	Langsarm. rekkverk	640	16	91
							1920
				Ks 40			1728
				St 00			197

BETONG:
B 300

ARMERING:
Ks 40 og St. 00

Lastkl 1/1930 10 t akseltrykk

OMBYGGING AV MIDTSPENN
ØVRE KVAMME II BRU
E-68/s 9

Målestokk 1:50 1:25
Tegn. okt-72 K.T.
Trac.
Kfr. 27/10-72 K.T.

Erstatning for: A-1246-A

Vegvesenet i Sogn og Fjordane
Hermansverk

Erstattet av:

Appendix D

DOI	Title	Authors	Date	Country	Type of research	FEM software used	Research question	Methodology	Result & findings	Conclusion
https://doi.org/10.7250/bjrbe.2022-17.556	Assessment of Reinforced Concrete Bridge Deficiencies Under Service Loads	Yavuz Yardim, Erion Periku, Mehmet Alpaslan Koroglu	11. May 2022	Latvia	Article	-	Identify and evaluate the distresses on existing RC bridges in Albania	104 RC bridges were visually inspected and assessed, as well as an interview survey from each bridges design & construction people	The visual inspection and examination showcased that the critical RC bridges in Albania were in very bad physical conditions. This was due to increased traffic load, the aging of bridges, lack of maintenance & repair, not ideal environment conditions and lastly, lack of proper project designs.	It is extremely critical to conduct inspections and maintenance every now and then on RC bridges. Being first and early before the deterioration becomes a problem is vital for the structures health and durability. A maintenance plan schedule is a MUST for bridges. To perform a good visual inspection, the use of NDT's will be extremely helpful.
10.1051/matecconf/201712002016	Common practices in assessing conditions of concrete bridges	Mohamed Alsharqawi, Tarek Zayed, Salah Abu Dabous	9. Aug. 2017	UAE	Article	-	Limitation for common practices for condition assessment	Reviewing of common practices for condition assessment of RC bridges and also a study of 6 NDT tools and a comparison	Of all the six NDT tools, Ground Penetrating Radar - GPR was revealed to be the most efficient tool to use when on a visual inspection to assess the RC bridges.	When conducting a visual inspection, it is very important to understand to a preliminary analysis of the bridge and plan out what NDT's will be suitable for the RC bridge. GPR proved to show extremely good results from all the NDT tools.
10.3390/infrastructures3030036	Condition assessment of reinforced concrete bridges	Tarek Omar, Moncef L. Nehdi	14. Sep. 2018	Canada	Article	-	Advantages and limitations of condition assessment methods for RC bridges	Overview and a review of five assessment categories. Visual inspection, Load testing, NDT&E, Structural health monitoring and FEM	Each assessment categories has its own advantages and limitations; it is important to know which one is required and which ones are not required when assessing.	When condition assessing, it is important to understand what types of method of assessment is required before starting the work and the appropriate tools/softwares in order to get a more correct assessment. Maximizing the advantages and minimizing the disadvantages is the goal when assessing.
10.9744/ced.19.2.111-120	Condition assessment of the deteriorated reinforced concrete bridge	Gunawan Budi Wijaya, Narciso Pacuribot	1. Sep. 2017	Indonesia	Article	-	Evaluation of condition and causes of deteriorations revealed in RC bridge	Field investigation with visual inspection and a set of NDT tools. Also, lab testing of extracted concrete core and powder samples	From the lab and NDT tests, it was revealed that the columns of the reinforced concrete bridge to be the construction part in most bad condition	Destructive test such as extracting core & powder samples from the deteriorated RC bridge can make assumption and results a lot more precise and accurate and thus will result in a better overall assessment
10.1051/matecconf/201819901004	Fiber Reinforced Concrete for repairing and strengthening RC structures: some recent advancements	Giovanni A. Plizarri	31. Oct. 2018	Italy	Article	DIANA	Assessment of Fiber materials as a reinforcement for concrete structures	Review of two experimental research studies regarding Fiber materials as reinforcement for concrete	UHPFRC can increase both horizontal and vertical bearing capacity, it can also enhance the resistance towards cracking of the structure which results in a higher service life of the RC bridge	Ultra High-Performance Fibre Reinforce Concrete (UHPFRC) revealed great strengthening values for the concrete structure, both resistance towards mechanical issues but also extended the durability for the existing structure
10.1080/1573247080 2214930	Life cycle evaluation of deteriorated structural performance of neutralized reinforced concrete bridges	Yu-Chi Sung, Chao-Hsun Huang, Kuang-Yen Liu, Chuan-Huei Wang, Chin-Kuo Su, Kuo-Chun Chang	16. Jul. 2008	Taiwan	Article	-	Can performance degradation curve of an existing RC bridge be predicted for bridge management system	Data and test result gathered from 21 different RC bridges in Taiwan were examined to extract the necessary parameters for a regression analyses	due to neutralization, the resistance of the bending moment of the superstructure was seen decreased as service life increased due to deterioration of materials. Increasing the thickness of concrete cover is the most economical and effective method of mitigating the possible damages from the neutralization of a RC bridge	With correct use of nonlinear regression analysis, one can calculate the service life of an existing bridge as well as extend the service life.
10.3390/su11246923	Life cycle analysis of strengthening existing RC structures	Amir Hajiesmaeili, Francesco Pittau, Emmanuel Denarie, Guillaume Habert	5. Dec. 2019	Switzer-land	Article	-	Comparison of environmental impacts for PE-UHPFRC compared to UHPFRC	Life Cycle Assessment (LCA) on an existing bridge using PE-UHPFRC compared to conventional UHPFRC	LCA results revealed a 55% and 29% decrease of environmental impacts of strengthening method when using PE-UHPFRC compared to replacing the existing bridge with a new bridge, and the conventional UHPFRC method.	PE-UHPFRC proved to be a strong match for strengthening existing RC structures with both good mechanical and environmental results.

DOI	Title	Authors	Date	Country	Type of research	FEM software used	Research question	Methodology	Result & findings	Conclusion
10.1016/j.strusafe.2015.03.004	Limit state design criteria for FRP strengthening of RC bridge components	Naiyu Wang, Bruce R. Ellingwood	16. May. 2015	USA	Article	-	Strength design criteria for bonded FRP system as a strengthening tool for RC bridges	Literature review, reliability analysis and an analytical study	To get a value of 3.5 target reliability in design of FRP strengthening of RC bridge beams, a θfrp = 0.85 must be applied to the moment capacity by the FRP strengthening. Also, excessive use of FRP can lead to damages	FRP strengthening is the most effective when it takes 25-30% of the overall moment capacity of the strengthened RC beam. Thus, it is important to not use too many FRP layers as it can lead to cracking of concrete.
10.1016/j.engstruct.2016.03.065	Modeling of degradation processes in concrete	Martina Somodikova, David Lehky, Jiri Dolezel, Drahomir Novak	23. Apr. 2016	Czech Republic	Article	-	Modeling of degradation process in RC structures	Advanced reliability analysis in combination with NFEA-analysis	This paper reveals that the estimated load-bearing capacity value is very dependent on the probability density function of the limit state function. Probabilistic approach shows values that are less conservative compared to deterministic approach, which are used by the code standards	Probabilistic assessment methods in combination with non-linear finite element model analysis has been found out to be highly effective and practical tool for the evaluation of the load-bearing capacity and reliability of existing RC structures.
/10.1016/j.engstruct.2010.09.003	Nonlinear finite element analysis of a 50 years old reinforced concrete trough bridge	Benjamin Richard, Sebastien Epaillard, Christian Cremona, Lennart Elfgren, Lucas Adelaide	8. Oct. 2010	Sweden	Article	ATENA	Assessment and strengthening of a RC bridge for larger traffic loads and a longer service life	Performing a Nonlinear Finite Element model-method in combination with load test for an analysis of the bridge In question	The numerical results of the proposed methods seems to be very similar to the experimental measurements	Finite element study is a very effective method for structural analyses when it comes to deteriorated structures. One should make a model without any corrosion and compare it to the same model with corrosion for great results regarding the damage done and also the pacing of growth of the deteriorations.
-	Rehabilitation and strengthening of existing RC structures with UHPFRC	Lionel Moreillon, Philippe Menetrey	3. Oct. 2013	France	Article	-	Performance and challenges of using Ultra-High-Performance Fiber Reinforce on RC structures	Traditional analytical analysis of different application methods of UHPF-reinforcement.	Ultra High-Performance Fiber Reinforced Concrete (UHPFRC) reveals to be a great passive reinforcement for structures such as bridges to increase the shear and flexural strength.	by Applying Ultra-High Performance Fiber layers as a strengthening method on reinforced concrete, it can result in greater mechanical strength and a longer service life. This method is also great economically and waterproofing the structure
10.1051/matecconf/20168306001	Satistical analysis of reinforced concrete bridge defects for optimum maintenance planning and budgeting	A. Abdul-Ameer, K. Alhefeiti	Jan. 2016	UAE	Article	-	Performance of calculating mean service life with statistical analysis	Statistical analysis method on over 400 reinforced concrete bridges to gather data	It was revealed that most RC bridges that was reviewed, starts to see hairline cracks when the average age of the building is around 20.2 years. And the cracks accelerate past 25 years of age. Spalling usually happens at a much older state in respect to its age.	The age of RC structures is seen to show some of the same deterioration types at around the same time as specified in the report. This can be used for a better system towards bridge maintenance management
10.1016/j.asoc.2011.01.004	Service life of the reinforced concrete bridge deck in corrosive environments	Jafar Sobhani, Ali Akbar Ramezanianpour	11. Jan. 2011	Iran	Article	-	Performance of self-developed soft computing system for calculation of service life	Comparison between performance of self-developed soft computing system compared to traditional probabilistic method on estimation of remaining service life of a RC bridge	The self-developed soft computing system has proven to be accessible for service life design and life cycle prediction purposes. Additionally, the proposed soft computing system predicted a longer service life than the traditional probabilistic method.	The proposed method of estimating life cycle and service life estimation with using soft computing method is practically feasible
10.1016/j.conbuildmat.2011.07.014	Statistical analysis of existing models for flexural strengthening of concrete	Alfredo M. Ceci, Joan R. Casas, Michel Ghosn	23. Aug. 2011	Italy	Article	-	Statistical analysis of models for resisting debonding of FRP sheets. End debonding and crack induced debonding modes of failure are studied for beams in flexure.	Two experimental databases were assembled to study the debonding failure of FRP. One database for end debonding, and one for crack induced debonding.	The objective of many models are not to predict load of failure, but to provide safe lower bounds on failure loads for design purposes. Prevent rather than predict.	Many models are overpredicting the load carrying capacity of FRP strengthened beams. Important to calibrate design for FRP debonding. Few models take into consideration the difference in behavior due to installation process. Multiple studies ignore the effect of the FRP interface and did not consider the adhesive. Although the debonding initiates at the surface.

DOI	Title	Authors	Date	Country	Type of research	FEM software used	Research question	Methodology	Result & findings	Conclusion
10.1061/(ASCE)1084-0702(2006)11:5(590)	Stiffness assessment through model analysis of an RC slab bridge before and after strengthening	Giovanna Zanardo, Hong Hao, Yong Xia, Andrew J. Deeks	1. Sep. 2006	Australia	Article	SAP2000	Bridge in Australia assessed to evaluate its condition before and after strengthening with CFRP.	Assessment through analytical results with field observations and dynamic testing. Vibration based assessment was conducted prior and after strengthening. In particular, change of structural properties and stiffness. Experimental and analytical model were used to determine frequencies before and after strengthening.	Experimentally determined modal properties and updated numerical models indicates a change of up to 10% on modal frequencies. This change indicates an increase in structural stiffness.	Dynamic measurements provide valuable support to understanding changes in structural behavior prior and after strengthened with CFRP.
10.1016/B978-1-78242-446-8.00018-5	Strengthening of existing structures	D. Bournas	19. Feb. 2016	UK	Book	-	-	-	-	Introduces some cases that conducted different methods of repair and strengthening for RC-structures. For example, reinforcing the structure with e.g., composite materials such as TRM, FRP, and other mean of repair techniques like mortar repairment and epoxy resins.
10.1016/j.aej.2014.09.010	Strengthening of RC bridge slabs using CFRP sheets	Fahmy A. Fathelbab, Mostafa S. Ramadan, Ayman Al-Tantawy	16. Sept. 2014	Egypt	Article	ANSYS	Strengthening of reinforced concrete bridge slabs due to excessive loads using externally bonded FRP sheets.	FEM program ANSYS was used to perform a structural linear and non-linear analysis for strengthened slab models using several schemes of FRP sheets.	Strengthening of RC structures and bridges using FRP allows keeping these structures under nowadays standards. Strengthening with CFRP sheets increase slab mechanical properties like strength, ductility, toughness, cracking behavior, and failure mode.	Increasing CFRP sheet width increases capacity and toughness. Increasing number of CFRP plies and decreasing spacing between also increase capacity and toughness.
10.1201/b17063-333	Ultra-high performance fiber reinforced concrete for strengthening and protecting bridge deck slabs	Malena Bastien-Masse, Eugen Bruhwiler	May. 2014	Switzer-land	Article	-	Investigation on ultra-high performance fiber reinforced concrete as strengthening of concrete bridge slabs	Proposes to add a UHPFRC layer of 25 to 75 mm on top of the slabs with or without reinforcement. Experimental studies were conducted on different composite beams and slabs, to study the behavior and failure modes. under various different types of loading. Also, two analytical models were used.	UHPFRC has excellent mechanical properties with compressive strength higher than 150 MPa and tensile strength higher than 10 MPa. It also have low permeability which can serve as a waterproofing layer protecting from water and chlorides.	A layer of UHPFRC over an RC section significantly increases the load-bearing capacity.
10.1016/j.engfailanal.2020.104480	Performances & challenges in FRP strengthening of RC bridges	Ayesha Siddika, Md. Abdullah Al Mamun, Wahid Ferdous, Rayed Alyousef	5. Mar. 2020	Bangla-desh	Article	-	Performance, challenges, and future opportunities of FRP strengthened RC structures under different loading scenarios.	Literature review	FRP leads to satisfactory performances under static, dynamic, and extreme environmental conditions.	RC structures are commonly strengthened with FRPs due to their high strength. Different wrapping techniques are reliable for shear, impact, fatigue, ductility, and durability. Debonding and rapture are common failure mode. FRP improves failure mode from brittle to more flexible. However, the brittleness of FRP should still be investigated and reduced. Negative sides are risk of fire, accidental damage, high energy consumption and carbon emissions, and high costs. No standard specifications available for strengthening with FRP.

DOI	Title	Authors	Date	Country	Type of research	FEM software used	Research question	Methodology	Result & findings	Conclusion
-	Bond Behavior of Naturally Corroded Reinforcement in Concrete Structures	Eyrun Gestdottir, Tomas Gudmundsson	2012	Sweden	Thesis	DIANA, FX+	Investigation of naturally corroded reinforcement in concrete to gain a more comprehensive understanding of the structural effects	Several naturally corroded specimens were tested with four-point bending tests with indirect supports. Additionally, investigation of the behavior using non-linear 2D plane stress FE model	The results of the experiments indicate that a higher level of corrosions leads to a decreased ultimate load, while a longer available anchorage length leads to an increased ultimate load.	2D analysis revealed great results regarding maximum load and deflections but was not reliable in terms of studying the free end slip and crack patterns.
10.28991/cej-0309148	Simulation of the Behavior of Corrosion Damaged Reinforced Concrete Beams with/without CFRP Retrofit	Masoud Zabihi-Samani, Mohsenali Shayanfar, Amir Safiey, Amir Najari	5. May 2018	Iran	Article	Abaqus, SAP2000	What is the influence of different levels of corrosion on the structural behavior of reinforced concrete beams, and how effective is carbon fiber reinforced polymer (CFRP) retrofit in compensating for the loss of shear and flexural capacity due to corrosion?	Numerical simulation with ABAQUS and SAP 2000 to investigate the influence of different levels of corrosion (20% & 40%) on the structural behavior of RC beams and the effectiveness of CRRP	The use of CFRP retrofitting can compensate effectively for the loss of shear and flexural capacity due to corrosion in RC beams. CFRP revealed great results in mechanical strength and stiffness of the corroded beam.	Important to not overuse CFRP strips on structures, recommended to not get higher than 40% capacity gain. Installing U-shaped CFRP strips on both side on the lower end of the beam revealed to be the most optimal solution for the installment of CFRP.
10.3390/s22228884	Finite Element Model Updating of RC Bridge Structure with Static Load Testing: A Case Study of Vietnamese ThiThac Bridge in Coastal and Marine Environment	Duc Cong Nguyen, Marek Salamak, Andrzej Katunin, Micheal Gerges	Nov. 2022	Poland	Article	MATLAB, SOFISTIK	Is it possible to enhance the accuracy of the FEM model of an existing bridge using GA-optimization based on measured field static load testing to determine the health state and load capacity	Experimental field static load testing, optimization techniques, and modal updating of the bridge FEM-model	The proposed methods revealed accurate prediction of the load limits of the existing bridge structure. These methods are viable for large bridges and complex structures with a reliable FE analysis software.	Performing field tests and extracting the data to calibrate the Finite element model can provide excellent results if used correctly. The output of the structural analysis is only as good as the input of it; thus, it is important to carefully understand what data and how to input it in a reliable FE-analysis software.
10.1016/j.istruc.2022.04.074.	Influence of reinforcement parameters on punching shear capacity of laterally restrained FRP-reinforced concrete bridge deck slabs	R. Abandah Mohammed, A. Issa Mohsen	Jul. 2022	USA	Article	Abaqus	Effect of reinforcement parameters on the punching shear capacity of laterally restrained FRP-reinforced concrete bridge decks and is it possible to create an empirical formula to calculate punching shear capacity	A combination of numerical parametric study and a statistical approach to analyze the collected data from 16 specimens to then conduct three experiments to develop an empirical formula	The developed formula managed to provide more accurate and real-scenario behavior results versus the existing models. The developed formula had smaller margin of errors and higher accuracy, additionally it was revealed that bar spacing has more influence on punching shear strength than bar area.	The most important to note here is that it was revealed that bar spacing has more influence on punching shear strength than bar area, furthermore, increasing the transverse reinforcement will enhance the serviceability of the bridge deck. Another thing to note is that the reinforcement ratio ρ to predict punching shear capacity is not accurate, due to topic of bar spacing and bar area.
10.1016/j.engstruct.2019.110078	Reinforced concrete bridge exposed to extreme maritime environmental conditions and mechanical damage: Measurements and numerical simulation	Marija Kuster Maric, Josko Ozbolt, Gojko Balabanic	Feb. 2020	Croatia	Article	-	Can a recently developed 3D chemo-hygro-thermo-mechanical model be used to realistically predict the service life of reinforced concrete structures exposed to chlorides and mechanical damages	A combination of experimental and numerical modeling approach. It was conducted a field measurements to collect data for further use in the 3D model.	The numerical simulations provided accurate results with class exposure of XS1 and XS3, and thus it was concluded that the recently developed 3D model to simulate chloride transport in concrete was found to be accurate in predicting the service life of reinforced concrete structures exposed to chlorides and mechanical damages.	The study reveals that micro-climate parameters, including cracks in concrete, wind direction and speed have a considerable impact on the chloride content in the concrete structure.

DOI	Title	Authors	Date	Country	Type of research	FEM software used	Research question	Methodology	Result & findings	Conclusion
10.1080/157324 79.2013 .836546	Loading to failure and 3D nonlinear FE modelling of a strengthened RC bridge	Arto M. Puurula, Ola Enochsson, Gabriel Sas, Thomas Blanksvard, Ulf Ohlsson, Lars Bernspång, Bjorn Taljsten, Lennart Elfgren	Dec. 2014	Sweden	Article	Abaqus	Comparing calculation results with actual behavior using "Sustainable Bridges" method	A full-scale test to load the bridge to failure while being monitored and recorded then performing structural analyses with FEM	The behavior of the bridge during experimental testing with loading to failure, can be closely predicted using the developed 3D nonlinear FE model up to bond failure. The 3D NFE-model was not accurate once the bond failed. The failure was caused by shear, torsion and bending.	The behavior of the bridge during increasing load can be closely predicted with the developed 3D nonlinear FE model up to the load when the bond failure occurred. The method developed in the study can be used to get a close estimation of the load-carrying capacity of bridges, such as for a train load.
10.1177 /14759 21720 930990	Dynamic nonlinearities for identification of the breathing crack type damage in reinforced concrete bridges	Srinivas Voggu, Saptarshi Sasmal	Jan. 2021	India	Article	-	How to evaluate nonlinear dynamic features in order to detect and identify breathing-crack type damage in RC structures	Experimental approach with static loads at different levels to simulate the damage scenarios, and then measuring the vibration responses using accelerometers.	It was revealed that the breathing crack mechanism displays a weak nonlinearity, which produces sub- and super-harmonics in the vibration responses.	The study suggests that the nonlinear features extracted from the vibration signals can provide valuable information regarding the damage scenario in concrete structures, more specifically breathing crack damage mechanism.
-	FE modeling and analysis of RC bridge decks	R. Micheal Biggs, Furman W. Barton, Joe P. Gomez, Peter J. Massarelli, Wallace T. McKeel	1. Sep. 2000	USA	Article	Abaqus	FEM-analysis of a RC-bridge girder decks	Using ABAQUS software to simulate their RC-model in order to perform a FEM analysis	All studies of reinforced concrete use one of three possible strategies for precise presentation of the reinforcing steel.	RC- structures can be modelled with many modeling characteristics in Abaqus and it can calculate a more precise behavior of steel+concrete interaction which is difficult to obtain through standard experimentations
10.1016 /S0263- 8223(03)00174-0	NFEA RC beams strengthened by FRP	Hsuan-Teh Hu, Fu-Ming Lin, Yih-Yuan Jan	29. Jul. 2003	Taiwan	Article	Abaqus	NFEA on RC concrete beams strengthened by FRP	Numerical analyses with Abaqus software	The use of FRP on the bottom of the RC-beam as a strengthening mechanic proved higher values than FRP on the sides of the beam	Correct placement and use of FRP can drastically strengthen the RC beam. The behavior of the RC-beam strengthened by FRP at the bottom is influenced by the ratio of steel/rebars compared to its length. Increasing the bending resistance of the RC beam is more critical than to increase the transverse shear resistance
-	NFEA RC bridge deck/bridge	Sujata Roy	5. Oct. 2005	USA	Thesis	Abaqus	NEFA on RC bridge on the approach slab by using Abaqus	Running simulations in Abaqus to present a NFEA analysis	For a FEM analysis, Tension stiffness must be added to present the interaction behavior of the two material, concrete & steel in the post cracked stage.	Abaqus is a great tool to showcase behavior of RC and works nicely with correct parameters to present a NFEA.
-	Modellering av etteroppspente betongbruer med korrosjonskadet spennarmering	Håvard Rodahl Kvale, Trond Jørgen Opheim	5. Jun. 2019	Norway	Thesis	Abaqus	How corrosion effects RC structures in an analytical & numerical aspect	3 damage types will be simulated and analyzed as well as conducting numerical calculations	Corrosion has led to reduced bond, area and cable break which has resulted in heavy damages on the RC	Abaqus can present great analysis with corrosion if used correctly with the correct parameters

DOI	Title	Authors	Date	Country	Type of research	FEM software used	Research question	Methodology	Result & findings	Conclusion
-	Dimensjonering av betongbruer i bruksgrensetilstand	Synne Aasrum Midtgarden	18. Dec. 2015	Norway	Thesis	BABE v1.0, Abaqus	Evaluation of calculation methods for SLS design of RC bridges	Simulating the model in ABAQUS and numerical calculating in PTC Mathcad Prime	Using Abaqus as a primary simulation software showcased good results for analysis, while BABE did not provide good results	BABE-software did not prove precise results while ABAQUS proved to be a strong modeling method
-	Kapasitetskontroll av korrosjonsskadet betongelementbru	Audun Fossum, Halvard Henjum Halsnes, Valon Hyseni	11. Jun. 2017	Norway	Thesis	Abaqus, Robot	Capacity control on corrosive effected RC bridge	Hand- & software numerical calculations with respect to Standard codes regulations as well as 3D simulation of the model	Fortunately, the bridge in question in the report was not greatly affected by corrosion, thus the bridges mechanical strength was still sufficient, but maintenance on the bridge was highly recommended	Corrosion infected bridges can result in high catastrophes if left un-unchecked. Thus, using software programs such as Robot and Abaqus can greatly provide information regarding the state of the bridge with correct parameters and values used
10.1139/cice-2011-0263	A methodology for evaluating the effects of spalling on the structural capacity of reinforced concrete bridge girders	Jeffrey Luckai, Maria Anna Polak, Scott Walbridge	4. Jan. 2014	Canada	Article	MATLAB, AutoCAD	How to evaluate effects of spalling on structural capacity of RC bridge girders	Use of graphical spalling surveys, rebar layout information, existing information on used material and geometrical properties as basis for flexural and shear analysis of damaged RC-bridge girders	If the spalling is more than 30% of the span for fc=20 MPa, or 70% of the span for fc equal or larger than 30 MPa, then this method is not suitable	The proposed methodology for evaluation of deterioration on structural capacity of RC-bridge girders showcased a strong accurate result and is a viable tool for assessing spalled bridge girders. This methodology is great for rapid assessment of rehabilitation projects.
10.1515/corrrev-2018-0046	Field test of a reinforced concrete bridge under marine environmental corrosion	Haijun Zhou, Siyu Chen, Yanliang Du, Zhiyao Lin, Xuebing Liang, Jun Liu, Feng Xing	10. Jun. 2020	China	Article	-	Investigation of extracted corroded and demolished RC bridge samples for mechanical properties	Experimental testing of 29 samples of corroded steel bars and 12 corroded stirrups extracted from a specific corroded bridge due to marine environment	The samples extracted from the deteriorated RC bridge provided strong results and showcased that the marine environment had caused more damage to the bridge than expected. The corrosion had greatly reduced the ductility index	Very important to follow guidelines and requirements from standard codes to apply a correct concrete quality when near marine environment to resist corrosion for decades
10.1061/(ASCE)BE.1943-5592.0001742	Model-Based interpretation of measurements for Fatigue Evaluation of Existing Reinforced Concrete Bridges	Imane Bayane, Sai G. S. Pai, Ian F. C. Smith, Eugen Bruhwiler	Aug-21	USA	Article	MATLAB, ANSYS	Can onsite Acoustic Emissions and strain measurements be accurately interpreted using calibrated physics-based models to evaluate fatigue safety of non-accessible elements in RC-bridge slabs?	Performing various NDT's and modal update the FE model using load-tests results and Error-Domain Model Falsification (EDMF)	The safety of the slab-girder connection was assessed as secure by analyzing the monitoring data, despite a disparity between the current condition and the design assumptions. This supports the increasing evidence that the majority of structural elements surpass design specifications in terms of safety.	The utilization of physics-based models and data interpretation techniques like EDMF can result in improved precision in identifying structural parameters and making predictions about the safety and performance of structural elements that are not directly measurable.